INVESTIGATIONS INTO UREASE MATURATION AND METAL ION SELECTIVITY

By

Eric Lee Carter

A DISSERTATION

Submitted to
Michigan State University
in partial fulfillment of the requirements
for the degree of

DOCTOR OF PHILOSOPHY

Microbiology and Molecular Genetics

2011

ABSTRACT

INVESTIGATIONS INTO UREASE MATURATION AND METAL ION SELECTIVITY

By

Eric Lee Carter

This dissertation consists of three projects that dissect the nature of urease maturation and metal ion selectivity. The first project examines the role of the UreD accessory protein during *in vivo* maturation of the nickel-containing urease from *Klebsiella aerogenes*. A translational fusion of the maltose binding protein with UreD (MBP-UreD) was generated and found to be soluble. The UreD domain of MBP-UreD bound nickel and zinc ions, formed complexes with $(UreABC)_3$, UreF, UreG, UreF plus UreG, and $(UreABC)_3$–UreF–UreG *in vivo*, and formed a complex with the UreF domain of the UreE-UreF fusion *in vitro*. MBP-UreD was shown to be a functional form of UreD as *malE-ureD* partially complemented for a Δ*ureD* urease cluster.

The second project revealed several roles for the *K. aerogenes* urease structural subunit UreB during urease maturation. UreB was purified as a monomer and shown to spontaneously bind to isolated $(UreAC)_3$**,** forming $(UreABC^*)_3$, while an N-terminal deletion mutant of UreB lacking the first 19 residues did not form the apoprotein complex. $(UreABC^*)_3$ shared similar *in vitro* activation properties as urease apoprotein preformed *in vivo*, whereas exposure of a mixture of $(UreAC)_3$ and UreBΔ1-19 to activation conditions led to negligible levels of active enzyme. Activity assays and metal analyses of various *in vitro* activated species demonstrated that UreB facilitates efficient incorporation of Ni^{2+} into the active site and protects the metal from chelators. Additional studies revealed that UreB interfaced with accessory proteins, and the N-

terminus was critical for this process. Finally, UreB enhanced the stability of UreC against proteolytic cleavage by trypsin.

The third project characterized a unique urease from *Helicobacter mustelae*, UreA2B2, which was shown to exhibit O_2-labile activity in whole cells. UreA2B2 was purified aerobically from its native host and found to contain ~ 2 iron per active site, or ~1 iron and 0.7 zinc when purified under anaerobic conditions. Anaerobically purified UreA2B2 was active, though highly O_2-labile, with its activity enhanced by EDTA and inhibited by acetohydroxamic acid or nickel ions. The inactive, oxidized enzyme was slowly reactivated by incubation with dithionite to levels approaching the wild-type enzyme accompanied by bleaching of its UV-visible spectrum, where the chromophore was consistent with μ-oxo bridged diferric atoms. Resonance Raman spectroscopy of this sample revealed bands at ~500 cm^{-1} and ~780 cm^{-1} that are characteristic of a Fe(III)-O-Fe(III) metallocenter. The ~500 cm^{-1} feature was sensitive to bulk solvent exchange with $H_2{}^{18}O$ or deuterium oxide, and both features were downshifted in the presence of urea. Protein purified aerobically from recombinant *Escherichia coli* grown in rich medium contained ~1 equivalent of iron and negligible levels of other metals, while *E. coli* cultured in minimal medium generated apoprotein with ~0.2 equivalents of iron and 0.0-0.2 zinc. Temperature-dependent circular dichroism measurements indicated that iron enhanced the thermal stability of UreA2B2. The apoprotein form of the enzyme was activated to levels representing ~20% of wild-type activity with ferrous ions and bicarbonate under anaerobic conditions. Lastly, the crystal structure of UreA2B2 was determined at 3.0 Å revealing an active site architecture nearly identical to that for nickel ureases. Numerous amino acid residue substitutions around the active site suggest that metal specificity for iron likely arises during the metal loading process.

I dedicate this dissertation to my family for their unwavering support.

ACKNOWLEDGEMENTS

I would like to thank my mentor, Robert Hausinger for his guidance, encouragement, and providing numerous opportunities to advance my career including authorship of a critical review and assistance with several fellowships. Thank you to my friends and colleagues, Tim Miles, Scott Mulrooney, Tina Müller, Lee Macomber, Jodi Boer, William Kittleman, Piotr Gryzska, and Adam Cornish for insightful scientific discussions throughout graduate school. I had the opportunity to train several gifted undergraduates including Rachel Morr, Scott Taber, and Christopher Towns; these individuals worked hard and certainly deserve recognition for their efforts. I would like to thank Dr. Eric Hegg for the use of his anaerobic chamber. Lastly, a special thanks to the Rudolph Hugh, DuVall, and Barnett Rosenberg fellowships for generously supporting my graduate school endeavor.

TABLE OF CONTENTS

LIST OF TABLES

LIST OF FIGURES

LIST OF ABBREVIATIONS

β-ME, 2-mercaptoethanol

CD, circular dichroism

CHES, 2-(cyclohexylamino)ethanesulfonic acid

EDTA, ethylenediaminetetraacetic acid

EPR, electron paramagnetic resonance spectroscopy

EXAFS, extended X-ray absorption fine structure

HEPES, 4-(2-hydroxyethyl)piperazine-1-ethanesulfonic acid

ICP-AES, inductively coupled plasma-atomic emission spectroscopy

IPTG, isopropyl β-D-1-thiogalactopyranoside

MALDI-MS, matrix-assisted laser desorption ionization mass spectrometry

MBP, maltose binding protein

MCD, magnetic circular dichroism

MES, 2-(N-morpholino)ethanesulfonic acid

MWCO, molecular weight cut-off

PCR, polymerase chain reaction

TAPS, N-tris(hydroxymethyl)methyl-3-aminopropanesulfonic acid

TCEP, tris(2-carboxyethyl)phosphine hydrochloride

Tris, 2-amino-2-(hydroxymethyl)-1,3-propanediol or (tris(hydroxymethyl)aminomethane)

SDS-PAGE, sodium dodecyl sulfate-polyacrylamide gel electrophoresis

U, μmol of urea degraded min^{-1}

XANES, X-ray absorption near edge structure

CHAPTER 1

Introduction

Urease is a urea-hydrolyzing enzyme found in fungi, plants, bacteria, and Archaea. Of historical significance, urease was the first enzyme to be crystallized (31), a feat that resulted in the awarding of a Nobel Prize to James Sumner in 1946. Since that time several crystal structures of ureases from different organisms have been reported, each showing a highly conserved tertiary structure with various quaternary arrangements (Figure 1.1) (4). Urease was also the premier enzyme shown to contain nickel (7), a cofactor that is essential for its activity. Nickel ion delivery and incorporation into the nascent urease active site requires the concerted effort of several accessory proteins, a process that has served as a paradigm for understanding the *in vivo* maturation of metalloproteins (4). Of medical concern, the enzyme is a virulence factor employed by uropathogens and the gastric-ulcer causing bacterial genus *Helicobacter* (19). Additionally, agriculture is impacted by plant ureases that are essential during seed-germination (32) and by soil-borne microbes that produce urease which degrade urea-based fertilizers (18). A wealth of literature focused on these topics and other aspects of urease biology has left us with a solid understanding of the principles of *in vivo* maturation, catalysis, and the physiological impact of urease on different systems (4, 14, 19). Nonetheless, at the time I began my studies several major questions still existed that required detailed investigation; these questions were partially addressed in this dissertation.

What is the molecular mechanism of nickel transfer by accessory proteins to the nascent urease active site, and what is the role of each accessory/structural protein during this process? Most of our current understanding of urease maturation *in vivo* comes from studies utilizing the heterologous expression of *Klebsiella aerogenes* urease genes in *Escherichia coli*. Collectively, *K. aerogenes* urease, composed of the UreA, UreB, and UreC subunits, requires four accessory proteins, UreD, UreE, UreF, and UreG, to effectively incorporate two nickel atoms and a

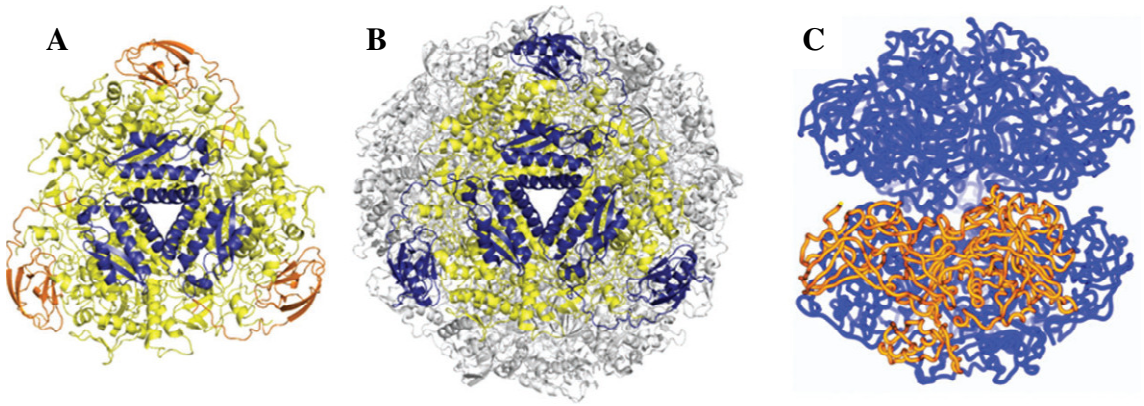

Figure 1.1: The structures of three well-characterized ureases. (A) *K. aerogenes* urease (PDB access code 1fwj) with UreA depicted in blue, UreB in orange, and UreC in yellow, together forming a $(UreABC)_3$ structure. (B) *Helicobacter pylori* urease (1e9z) with UreA (corresponding to a fusion of the two small subunits in the *K. aerogenes* enzyme) depicted in blue and UreB (analogous to UreC in the *K. aerogenes* protein) shown in yellow for one $(UreAB)_3$ unit, with three more $(UreAB)_3$ units shown in gray included in the biologically relevant $[(UreAB)_3]_4$ structure. (C) Jack bean urease with one subunit (comparable to a fusion of all three *K. aerogenes* subunits) shown in gold in the otherwise blue hexameric protein (two trimers interacting in a face-to-face manner and shown after a 90 degree rotation compared to the other ureases). For interpretation of the references to color in this and all other figures, the reader is referred to the electronic version of this dissertation.

molecule of carbon dioxide in the form of a carboxylated lysine into the nascent active site of the apoprotein (4). The current model of activation, depicted in Figure 1.2, begins with the urease apoprotein UreABC binding to the UreD accessory protein. As of 2010, UreD remained essentially uncharacterized because the protein was insoluble when overproduced without other urease components. Despite the lack of biochemical information regarding UreD, clues to the role of this accessory protein had been revealed through several studies. A systematic deletion analysis of urease accessory genes demonstrated that *ureD* is critical for the production of urease holoenzyme; i.e., cells containing a Δ*ureD* urease cluster produced enzyme containing only trace levels of nickel, an indication that UreD is essential for the efficient incorporation of Ni^{2+} into the apoprotein (15). UreD also has been isolated in several protein complexes pertinent to urease

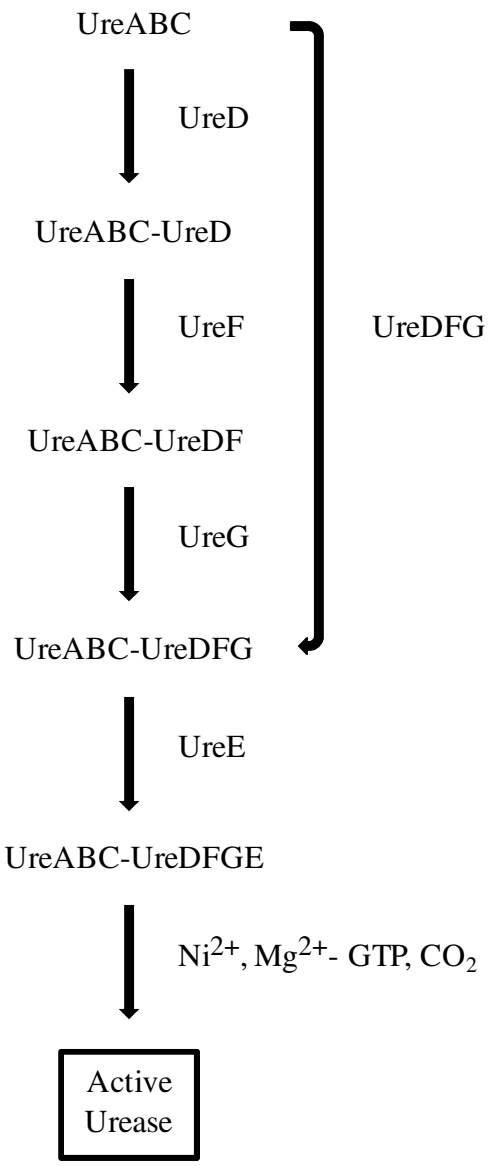

Figure 1.2: Schematic representation of the *in vivo* urease maturation process.

activation, all of which have been described (Figure 1.2). Of significance, it was shown that ~25% of the nascent active sites in the purified UreABC–UreD complex are activated in a solution containing nickel and bicarbonate (a CO_2 donor) whereas apoprotein alone is only activated to ~15% of wild-type levels (24, 25). These data suggest that UreD is a urease-specific

molecular chaperone that increases the competence of the structural subunits to accept and properly incorporate nickel ions and carbon dioxide. Furthermore, UreD may play a direct role in nickel transfer to urease apoprotein via specific metal binding sites on the protein as shown by the ability of the UreABC–UreD complex to bind ~3 equivalents of nickel versus ~2 equivalents for UreABC when these species were treated with the metal and analyzed by atomic absorption spectroscopy (24). These hypotheses were the basis for studies described in Chapter 2.

Subsequent to UreABC–UreD formation, this complex associates with UreF. Similar to UreD, UreF is insoluble when overproduced alone, although two soluble forms of UreF have been described. A translational fusion between UreF and the maltose binding protein (MBP-UreF) was soluble, but not examined for its properties or its interactions with urease apoprotein (13). On the other hand, a soluble fusion between UreE and UreF (UreE-UreF) was found to be monomeric and competent to bind UreABC–UreD *in vitro*. Additional studies demonstrated the formation of a UreABC–UreD–UreE-UreF–UreG complex *in vivo*. Furthermore, covalent attachment of UreE to UreF did not preclude the function of the latter protein during urease apoprotein activation *in vivo* (11). In addition to this study, the UreABC–UreD–UreF (abbreviated UreABC–UreDF) complex has been purified and activated *in vitro* by incubation with nickel ions and bicarbonate to ~30% of the specific activity of wild-type enzyme (21), similar to the UreABC–UreD complex. However, UreABC–UreDF is unique in that lower concentrations of bicarbonate were required for its activation and it was resistant to nickel inactivation, indicating that UreF may play some role in regulating the sequential incorporation of carbon dioxide and nickel into the active site (or it may modulate the chaperone activity of UreD to perform these actions). Nonetheless, despite reconciling the protein:protein interaction network of UreF with other urease-related proteins, and revealing some details of UreF

participation during *in vitro* activation, the role of UreF during urease maturation remains unknown. One group has suggested that UreF is structurally homologous to GTPase activating proteins (27), although this conclusion was based on computational methods that were unsupported by experimental evidence.

Following the proposed model, UreABC-UreDF binds UreG to form a pre-activation complex. UreG is a soluble protein that has been purified and characterized from several organisms including *K. aerogenes* (2, 20) , *Bacillus pasteurii* (22, 35), *Mycobacterium tuberculosis* (34), and *Helicobacter pylori* (17, 36). *B. pasteurii* UreG binds two zinc and four nickel ions per dimer (35), *H. pylori* UreG binds 0.5 zinc and two nickel ions per monomer (36), and the *K. aerogenes* protein binds one nickel and one zinc per monomer (2). Despite some variability in metal-binding properties, the fact that UreG from multiple organisms binds nickel suggests that this protein directly engages in the nickel transfer event, however experimental evidence is needed to support this claim. The *ureG* sequences reveal a nucleotide-binding motif (P-loop) consistent with a GTPase role for UreG during urease maturation. Whereas the rates of GTP hydrolysis by various isolated UreG species are very low or zero (34-36), the more important question is whether GTP hydrolysis is coupled to nickel incorporation or a different maturation event such as inducing conformational changes in the activation complex to favor nickel transfer or specificity, or the dissociation of accessory proteins subsequent to the production of holoprotein. Currently, UreG has not been structurally characterized by X-ray crystallographic methods, perhaps due to its intrinsically disordered behavior (22); however, the structure of a homologous protein, HypB, a hydrogenase maturation factor, has been determined from *Methanocaldococcus jannaschii*. The dimeric protein contains a dinuclear Zn site at the subunit interface in addition to its GTP binding sites (8).

The UreABC–UreD–UreF–UreG (simplified as UreABC–UreDFG) complex was produced *in vitro* by mixing purified UreG with UreABC–UreDF. When incubated in buffer containing nickel and bicarbonate over ~50% of the nascent active sites were activated (29). More importantly, the inclusion of GTP to the assay, but not other nucleotide tri-phosphates, resulted in a significant increase in activity with physiologically relevant bicarbonate levels when compared to a similar reaction without GTP. Hydrolysis of GTP was required as shown by the lack of stimulation when using a non-hydrolyzable analogue. The site of GTP action was determined to be UreG as shown by studies using UreG with a mutation in the P-loop incorporated into the UreABC-UreDFG complex; that species had little competence for activation with GTP (29). In addition to the UreABC–UreDFG complex, UreG has been found in an insoluble urease-free complex consisting of UreD and UreF, termed UreD–UreF–UreG or UreDFG. This heterotrimer was isolated from cells expressing *ureD*, *ureF*, and *ureG* without *ureE* or the structural subunit genes. Upon detergent solubilization, the complex was purified by using a combination of anion-exchange chromatography followed by a detergent removal step. Intriguingly the purified wild-type complex was able to bind to an ATP-linked agarose resin while the UreDFG complex composed of a P-loop variant of UreG was unable to bind, indicating that an intact P-loop is necessary for nucleotide binding (20). The presence of this complex suggests that UreDFG may be a physiologically relevant species that exists in the cell as a preformed metallochaperone primed for direct binding and activation of urease apoprotein rather than the sequential binding of UreD, UreF, and UreG to urease (Figure 1.2).

Finally, the pre-activation complex composed of UreABC–UreDFG interacts with the metallochaperone, UreE. This protein from *K. aerogenes* has been well studied, both in its full-length form and as the H144* UreE truncated form, and is known to bind nickel (six atoms per

dimer with a K_d of 9.6 ± 1.3 μM for full-length or two atoms per dimer that show cooperatively for binding to H144* UreE) (3, 6, 9, 16, 28). Significantly, incubation of UreABC–DFG with UreE and physiologically relevant levels of bicarbonate, nickel, and Mg^{2+}-GTP resulted in the formation of urease holoprotein with wild-type specific activity. Thus, UreE presumably facilitates the nickel transfer event. Intriguingly, recent studies have demonstrated a metal-dependent association between UreE and UreG, indicating these proteins likely play a cooperative role during nickel passage (1, 2). The nickel and zinc binding properties of UreD, as described in Chapter 2 of this dissertation make for a compelling argument that UreD also may participate in the nickel trafficking cascade, likely shuttling the metal from UreG to the appropriate ligands in the apoprotein. Although purely speculative, this model takes into account all experimental evidence obtained to date.

Another puzzling aspect of the maturation process is the role of the urease structural subunits. Most bacterial ureases consist of two small subunits, UreA and UreB, and a large subunit, UreC, which harbors the active site. While the role of UreA is unknown, UreB has been shown to be more functionally dynamic. Chemical cross-linking and small angle X-ray scattering studies have demonstrated that the UreD and UreF accessory proteins bind to the apoprotein at the vertices of the triangular structure (i.e., $[UreABC]_3$), making contacts with UreB and UreC (5, 26). Additionally, UreD and UreF are proposed to induce a conformational change that shifts the position of UreB so as to allow greater access to the nascent active site, which is normally covered by UreB as observed in the crystal structure (5). In support of this finding, computational methods demonstrated that the main domain of UreB could pivot around a flexible region in its N-terminus while remaining anchored to UreC (26). Collectively these

results support the notion that UreB participates in the activation process, but an exact function for the protein remained elusive. The studies described in Chapter 3 of this dissertation establish several roles for UreB (or its equivalent subunit in other ureases) during urease maturation.

What is the basis of metal ion selectivity in urease and do nickel-independent forms of the enzyme exist in nature? Until 2008, there was a general consensus that all ureases utilized nickel as the catalytic cofactor. Studies had shown that nickel was the preferred metal ion for the *in vitro* activation of urease apoprotein; that zinc, copper, and cobalt inhibited this process (24); and that copper and cobalt occupy the metallocenter and generate inactive enzyme (33). Substituting manganese for nickel in the activation assay led to enzyme possessing 2% of wild-type activity (24). Comparing the pH dependence of activity for the manganese urease versus nickel enzyme demonstrated moderate perturbations in pK_a values suggesting that metal substitutions likely affect the protonation state of the catalytic water (33). Moreover, these data lead to speculation that accessory proteins play a critical role not only in promoting efficient nickel delivery to the apoprotein, but also in metal ion selectivity by either rejecting access to non-productive metals, or catalyzing expulsion of metals that are misincorporated. Additional evidence that *Bacillus subtilis* synthesized a nickel-containing urease in the absence of accessory proteins supported the idea that this enzyme strictly utilizes nickel regardless of source (12). However, in 2008 the dogma was questioned due to urease findings related to *Helicobacter mustelae*, a micro-aerophilic gastric pathogen of ferrets. The complete genome sequence of this microorganism contained two urease structural gene clusters: one cluster included *ureA* and *ureB* flanked by the typical urease accessory genes while the second cluster was composed of *ureA2* and *ureB2* with no discernable accessory genes in their vicinity (23) (Note: ureases of *Helicobacter* species are

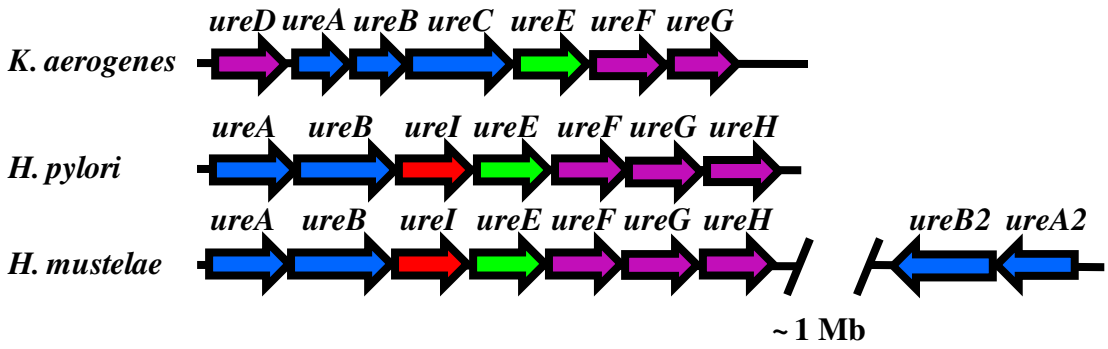

Figure 1.3: Organization of representative urease gene clusters. The urease gene cluster of *K. aerogenes* (*ureDABCEFG*) is compared to the gene organization found in *H. pylori* and *H. mustelae*. In *Helicobacter* species urease is produced from two structural subunit encoding genes (see main text for more details) and the *ure* locus contains a proton-gated urea channel (*ureI*). In addition, *ureH* is analogous to *ureD* from other bacteria. Genes encoding urease subunits are shown in blue, the *ureE* gene encoding a metallochaperone is green, other urease accessory genes are purple, and *ureI* genes are red. The sizes of the arrows do not accurately reflect the sizes of the genes.

composed of only two subunits, UreA, which is a fusion of the two small subunits from most other bacteria, and UreB, which is analogous to UreC). These findings were in contrast to the typical arrangement exemplified by *K. aerogenes* and *H. pylori*, which both have one *ure* locus (Figure 1.3). Significantly, a Dutch group demonstrated that expression of *ureAB* was induced by nickel while *ureA2B2* was repressed by nickel and induced by iron. A *H. mustelae* mutant strain (*nikR ureB ureG*; where *nikR* encodes a nickel responsive regulator) retained ureolytic behavior, indicating that the UreA2B2 species is a functional urease and its activity is not dependent on the conventional urease accessory protein, UreG. Moreover, a mutant strain that constitutively expressed *ureA2B2* was ureolytic, but lost this activity upon cell lysis, suggesting that UreA2B2 activity may be oxygen-labile (30). Taken together, these data led the authors to hypothesize that UreA2B2 may be a nickel-independent enzyme that uses iron as the essential metal cofactor. In addition, the results suggested a novel maturation pathway may be involved to activate the UreA2B2 species *in vivo*. These ideas laid the foundation for the studies described in Chapters 4

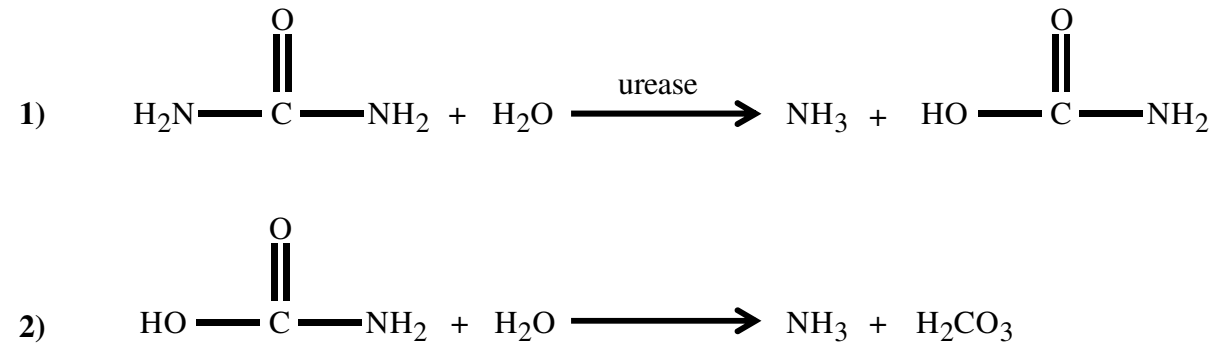

Figure 1.4: The hydrolysis of urea catalyzed by urease. Step 1 of the reaction is the hydrolytic degradation of urea by urease into a molecule of ammonia and carbamic acid. Step 2 is the spontaneous breakdown of carbamic acid into another molecule of ammonia and carbonic acid.

and 5, which demonstrate that UreA2B2 is an oxygen-labile, iron-containing urease. This work reinforces the question, what factors are responsible for metal ion selectivity in ureases and what role do the accessory proteins play?

What is the chemical mechanism of urea hydrolysis catalyzed by urease? Urea is an incredibly stable molecule with a half-life of 3.6 years in aqueous solution (10). The catalytic proficiency of urease has been estimated to be $>10^{14}$ when comparing the enzymatic hydrolysis of urea (Figure 1.4) with the uncatalyzed elimination reaction that results in the formation of ammonia and cyanic acid. Thus, urease is highly adept at degrading urea, but it requires a complex binuclear metallocenter to perform the reaction. In fact, it is this complexity that has curbed attempts to describe a unified catalytic mechanism. Of several proposed mechanisms (4) (Figure 1.5), the most compelling has the metal bridging hydroxide acting as a nucleophile, attacking urea (poised by an interaction of the urea carbonyl with the five coordinate Ni) to form a tetrahedral intermediate that breaks down to carbamate and a molecule of ammonia, with His320 (*K. aerogenes* numbering; refer to Figure 3.1 for reference) acting as a general acid.

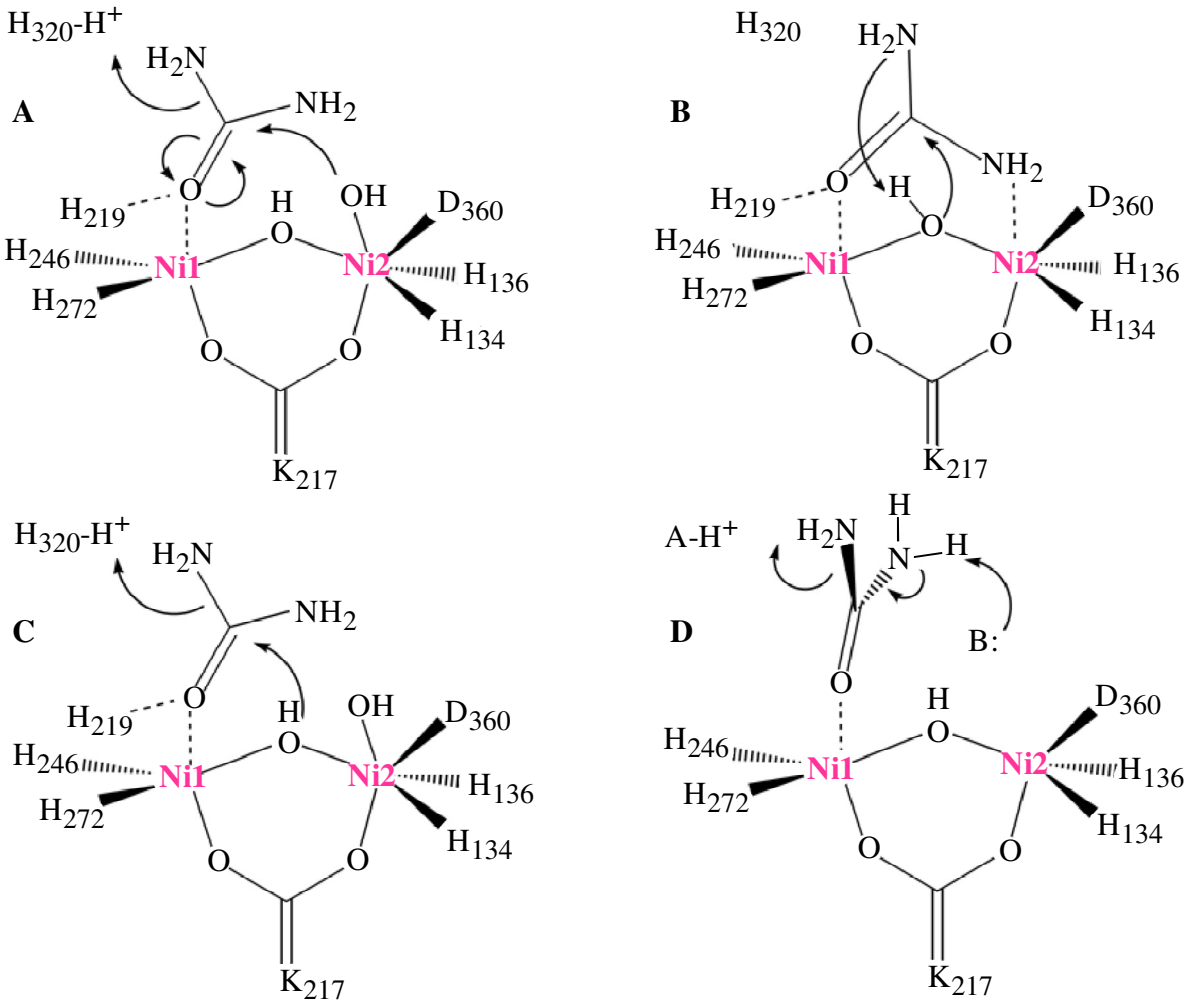

Figure 1.5: Proposals for the urease catalytic mechanism. (A) The hydroxyl group bound to Ni2 attacks urea, whose carbonyl group is polarized by coordination to Ni1, forming a tetrahedral intermediate that releases ammonia with His320 (*K. aerogenes* numbering) acting as a general acid. (B) The bridging hydroxyl group attacks urea, bound with its carbonyl group coordinated to Ni1 and an amine interacting with Ni2, and the hydroxyl proton transfers to the released ammonia. (C) A merged mechanism in which the bridging water attacks the substrate, but with His320 acting as a general acid. (D) Elimination mechanism to form a cyanic acid intermediate that subsequently becomes hydrated (not depicted) to form carbamate. In all mechanisms, the carbamate spontaneously decomposes.

Although this model takes into account several lines of experimental evidence, including kinetic analysis of active site variants, inhibition studies, and crystallographic data, there is very little descriptive spectroscopic data available because Ni^{2+} is essentially spectroscopically silent. The

discovery of an iron-containing urease, UreA2B2 (as outlined in Chapters 4 and 5), affords a unique opportunity to use new spectroscopic approaches to investigate the metallocenter including resonance Raman spectroscopy, electron paramagnetic resonance, and Mössbauer spectroscopy that can yield detailed information about the chemical environment of iron atoms. Future studies utilizing these techniques could provide the necessary evidence to produce a more accurate reaction mechanism. Ultimately, understanding the chemical basis of urea hydrolysis can lead to the development of urease inhibitors that mimic the enzyme transition state.

BIBLIOGRAPHY

BIBLIOGRAPHY

1. **Bellucci, M., B. Zambelli, F. Musiani, P. Turano, and S. Ciurli.** 2009. *Helicobacter pylori* UreE, a urease accessory protein: Specific Ni^{2+} and Zn^{2+} binding properties and interaction with its cognate UreG. Biochemical Journal **422:**91-100.

2. **Boer, J. L., S. Quiroz-Valenzuela, K. L. Anderson, and R. P. Hausinger.** 2010. Mutagenesis of *Klebsiella aerogenes* UreG to probe nickel binding and interactions with other urease-related proteins. Biochemistry **49:**5859-5869.

3. **Brayman, T. G., and R. P. Hausinger.** 1996. Purification, characterization, and functional analysis of a truncated *Klebsiella aerogenes* UreE urease accessory protein lacking the histidine-rich carboxyl terminus. Journal of Bacteriology **178:**5410-5416.

4. **Carter, E. L., N. Flugga, J. L. Boer, S. B. Mulrooney, and R. P. Hausinger.** 2009. Interplay of metal ions and urease. Metallomics **1:**207-221.

5. **Chang, Z., J. Kuchar, and R. P. Hausinger.** 2004. Chemical crosslinking and mass spectrometric identification of sites of interaction for UreD, UreF, and urease. Journal of Biological Chemistry **279:**15305-15313.

6. **Colpas, G. J., T. G. Brayman, L.-J. Ming, and R. P. Hausinger.** 1999. Identification of metal-binding residues in the *Klebsiella aerogenes* urease nickel metallochaperone, UreE. Biochemistry **38:**4078-4088.

7. **Dixon, N. E., C. Gazzola, R. L. Blakeley, and B. Zerner.** 1975. Jack bean urease (EC 3.5.1.5). A metalloenzyme. A simple biological role for nickel? Journal of the American Chemical Society **97:**4131-4133.

8. **Gasper, R., A. Scrima, and A. Wittinghofer.** 2006. Structural insights into HypB, a GTP-binding protein that regulates metal binding. Journal of Biological Chemistry **281:**27492-27502.

9. **Grossoehme, N. E., S. B. Mulrooney, R. P. Hausinger, and D. E. Wilcox.** 2007. Thermodynamics of Ni^{2+}, Cu^{2+}, and Zn^{2+} binding to urease metallochaperone UreE. Biochemistry **46:**10506-10516.

10. **Karplus, P. A., M. A. Pearson, and R. P. Hausinger.** 1997. 70 years of crystalline urease: What have we learned? Accounts of Chemical Research **30:**330-337.

11. **Kim, J. K., and R. P. Hausinger.** 2006. The UreEF fusion protein provides a soluble and functional form of the UreF urease accessory protein. Journal of Bacteriology **188:**8413-8420.

12. **Kim, J. K., S. B. Mulrooney, and R. P. Hausinger.** 2005. Biosynthesis of active *Bacillus subtilis* urease in the absence of known urease accessory proteins. Journal of Bacteriology **187:**7150-7154.

13. **Kim, K. Y., C. H. Yang, and M. H. Lee.** 1999. Expression of the recombinant *Klebsiella aerogenes* UreF protein as a MalE fusion. Archives of Pharmaceutical Research **22:**274-278.

14. **Krajewska, B.** 2009. Ureases I. Functional, catalytic and kinetic properties: A review. Journal of Molecular Catalysis B: Enzymatic **59:**9-21.

15. **Lee, M. H., S. B. Mulrooney, M. J. Renner, Y. Markowicz, and R. P. Hausinger.** 1992. *Klebsiella aerogenes* urease gene cluster: Sequence of *ureD* and demonstration that four accessory genes (*ureD*, *ureE*, *ureF*, and *ureG*) are involved in nickel metallocenter biosynthesis. Journal of Bacteriology **174:**4324-4330.

16. **Lee, M. H., H. S. Pankratz, S. Wang, R. A. Scott, M. G. Finnegan, M. K. Johnson, J. A. Ippolito, D. W. Christianson, and R. P. Hausinger.** 1993. Purification and characterization of *Klebsiella aerogenes* UreE protein: A nickel-binding protein that functions in urease metallocenter assembly. Protein Science **2:**1042-1052.

17. **Mehta, N., S. Benoit, and R. J. Maier.** 2003. Roles of conserved nucleotide-binding domains in accessory proteins, HypB and UreG, in the maturation of nickel-enzymes required for efficient *Helicobacter pylori* colonization. Microbial Pathogenesis **35:**229-234.

18. **Mobley, H. L. T., and R. P. Hausinger.** 1989. Microbial ureases: Significance, regulation, and molecular characterization. Microbiological Reviews **53:**85-108.

19. **Mobley, H. L. T., M. D. Island, and R. P. Hausinger.** 1995. Molecular biology of microbial ureases. Microbiological Reviews **59:**451-480.

20. **Moncrief, M. B. C., and R. P. Hausinger.** 1997. Characterization of UreG, identification of a UreD-UreF-UreG complex, and evidence suggesting that a nucleotide-binding site in UreG is required for in vivo metallocenter assembly of *Klebsiella aerogenes* urease. Journal of Bacteriology **179:**4081-4086.

21. **Moncrief, M. B. C., and R. P. Hausinger.** 1996. Purification and activation properties of UreD-UreF-urease apoprotein complexes. Journal of Bacteriology **178:**5417-5421.

22. **Neyroz, P., B. Zambelli, and S. Ciurli.** 2006. Intrinsically disordered structure of *Bacillus pasteurii* UreG as revealed by steady-state and time-resolved fluorescence spectroscopy. Biochemistry **45:**8918-8930.

23. **O'Toole, P. W., W. J. Snelling, C. Canchaya, B. M. Forde, K. R. Hardie, C. Josenhans, R. L. J. Graham, G. McMullan, J. Parkhill, E. Belda, and S. D. Bentley.** 2010. Comparative genomics and proteomics of *Helicobacter mustelae*, an ulcerative and carcinogenic gastric pathogen. BMC Genomics **11:**164.

24. **Park, I.-S., and R. P. Hausinger.** 1996. Metal ion interactions with urease and UreD-urease apoproteins. Biochemistry **35:**5345-5352.

25. **Park, I.-S., and R. P. Hausinger.** 1995. Requirement of carbon dioxide for *in vitro* assembly of the urease nickel metallocenter. Science **267:**1156-1158.

26. **Quiroz-Valenzuela, S., S. C. K. Sukuru, R. P. Hausinger, L. A. Kuhn, and W. T. Heller.** 2008. The structure of urease activation complexes examined by flexibility analysis, mutagenesis, and small-angle X-ray scattering. Archives of Biochemistry and Biophysics **480:**51-57.

27. **Salomone-Stagni, M., B. Zambelli, F. Musiani, and S. Ciurli.** 2007. A model-based proposal for the role of UreF as a GTPase-activating protein in the urease active site biosynthesis. Proteins **68:**749-761.

28. **Song, H. K., S. B. Mulrooney, R. Huber, and R. P. Hausinger.** 2001. Crystal structure of *Klebsiella aerogenes* UreE, a nickel-binding metallochaperone for urease activation. Journal of Biological Chemistry **276:**49359-49364.

29. **Soriano, A., and R. P. Hausinger.** 1999. GTP-dependent activation of urease apoprotein in complex with the UreD, UreF, and UreG accessory proteins. Proceedings of the National Academy of Sciences, United States of America **96:**11140-11144.

30. **Stoof, J., S. Breijer, R. G. J. Pot, D. van der Neut, E. J. Kuipers, and A. H. M. van Vliet.** 2008. Inverse nickel-responsive regulation of two urease enzymes in the gastric pathogen *Helicobacter mustelae*. Environmental Microbiology **10:**2586-2597.

31. **Sumner, J. B.** 1926. The isolation and crystallization of the enzyme urease. Journal of Biological Chemistry **69:**435-441.

32. **Witte, C.-P.** 2011. Urea metabolism in plants. Plant Science **180:**431-438.

33. **Yamaguchi, K., N. J. Cosper, C. Stalhanske, R. A. Scott, M. A. Pearson, P. A. Karplus, and R. P. Hausinger.** 1999. Characterization of metal-substituted *Klebsiella aerogenes* urease. Journal of Biological Inorganic Chemistry **4:**468-477.

34. **Zambelli, B., F. Musiani, M. Savini, P. Tucker, and S. Ciurli.** 2007. Biochemical studies on *Mycobacterium tuberculosis* UreG and comparative modeling reveal structural and functional conservation among the bacterial UreG family. Biochemistry **46:**3171-3182.

35. **Zambelli, B., M. Stola, F. Musiani, K. De Vriendt, B. Samyn, B. Devreese, J. Van Beeumen, A. Dikiy, D. A. Bryant, and S. Ciurli.** 2005. UreG, a chaperone in the urease assembly process, is an intrinsically unstructured GTPase that specifically binds Zn^{2+}. Journal of Biological Chemistry **280:**4684-4695.

36. **Zambelli, B., P. Turano, F. Musiani, P. Neyroz, and S. Ciurli.** 2009. Zn^{2+}-linked dimerization of UreG from *Helicobacter pylori*, a chaperone involved in nickel trafficking and urease activation. Proteins **74:**222-239.

CHAPTER 2

Characterization of *Klebsiella aerogenes* Urease Accessory Protein UreD in Fusion with the Maltose Binding Protein

This work was published in the *Journal of Bacteriology*, 2010, 192 (9), pp 2294-2304, with the authors listed as Eric L. Carter and Robert P. Hausinger

ABSTRACT

Assembly of the *Klebsiella aerogenes* urease metallocenter requires four accessory proteins, UreD, UreE, UreF, and UreG, to effectively deliver and incorporate two Ni^{2+} ions into the nascent active site of the urease apoprotein (UreABC). Each accessory protein has been purified and characterized with the exception of UreD, due to its insolubility when overproduced in recombinant cells. In this study, a translational fusion was made between the maltose binding protein (MBP) and UreD, with the resulting MBP-UreD found to be soluble in *Escherichia coli* cell extracts and able to complement a Δ*ureD*-urease cluster in this host microorganism. MBP-UreD was purified as a large multimer (>670 kDa) that bound approximately 2.5 Ni^{2+} (K_d ~ 50 μM) per UreD protomer according to equilibrium dialysis measurements. Zn^{2+} directly competes with 10-fold higher affinity (~4 Zn^{2+} per protomer, K_d = 5 μM) for the Ni^{2+} binding sites. MBP pull-down experiments demonstrated that the UreD domain of MBP-UreD formed *in vivo* complexes with UreF, UreG, UreF plus UreG, or UreABC when these proteins were overproduced in the same *E. coli* cells. In addition, a UreABC— (MBP-UreD) —UreF—UreG complex was observed in cells producing all urease components. Comparative *in vitro* binding experiments with purified proteins demonstrated an approximate 1:1 binding ratio between the UreD domain of MBP-UreD and the UreF domain of the UreE-UreF fusion, only weak or transient interaction between MBP-UreD and UreG, and no binding with UreABC. These studies are the first to describe the properties of purified UreD and they extend our understanding of its binding partners, both *in vitro* and in the cell.

INTRODUCTION

A requirement for accessory proteins in metalloenzyme maturation is a common theme in microbiology, with examples including the auxiliary proteins critical for synthesis of FeMoco in bacterial nitrogenase, the creation of [NiFe] and [FeFe] metalloclusters in microbial hydrogenases, and the delivery and incorporation of Ni^{2+} into the dinuclear active site of urease (16, 21, 27). Urease catalyses the hydrolysis of urea to two molecules of ammonia and carbonic acid, a reaction dependent on the Ni^{2+}-containing active site of the holoenzyme (3). The accessory proteins involved in activation of urease have been the focus of intensive research as this enzyme can act as a virulence factor in infectious microorganisms including *Helicobacter pylori* (26) and uropathogenic *Proteus mirabilis* (9).The best studied urease maturation system is that of *Klebsiella aerogenes* for which the urease apoprotein and holoprotein structures are known (10, 11) and several accessory protein components and their complexes with urease have been extensively characterized (3).

K. aerogenes urease, encoded by the *ureDABCEFG* gene cluster, uses four accessory proteins, UreD, UreE, UreF, and UreG, to form the metallocenter in the UreABC apoenzyme (17). UreE is proposed to function as a metallochaperone that delivers Ni^{2+} to the nascent active site (18). This protein has been structurally characterized (29), shown by equilibrium dialysis methods to bind about six Ni^{2+} per homo-dimer with a K_d of 9.6 ± 1.3 μM (18), and further characterized by isothermal titration calorimetry, mutagenesis, and spectroscopic approaches (4-6, 8). UreD and UreF are insoluble when overproduced alone, leading to difficulty in characterizing these proteins. Recently, however, a UreE-UreF translational fusion (subsequently abbreviated UreEF) was constructed, resulting in a functional and soluble form of UreF (12).

Significant levels of urease activation take place in cells expressing the entire urease cluster with the *ureEF* fusion replacing the individual genes. Pull-down assays using the UreE domain of UreEF revealed the *in vivo* presence of a UreABC—UreD— UreEF —UreG complex in cells expressing all urease components. Moreover, the UreEF fusion protein associates with UreABC—UreD as shown by a similar *in vitro* pull-down experiment (12). UreG contains a conserved P-loop motif compatible with its role in GTP binding and hydrolysis during urease activation (19, 31). The protein is present as the free monomer, but UreG also associates with UreABC—UreD—UreF (abbreviated UreABC—UreDF) to form the UreABC—UreD—UreF—UreG complex (hereafter called UreABC—UreDFG) which interacts with UreE and allows for urease activation to wild-type levels in a GTP-dependent manner (30).

UreD, the focus of the work described here, is the least characterized of the urease accessory proteins. Nevertheless, some clues to its role during urease apoenzyme maturation have been revealed. Extracts of *Escherichia coli* cells containing a Δ*ureD*-urease cluster contain negligible amounts of urease activity (<1 U mg^{-1}) when compared to extracts from cells containing the wild-type gene cluster (~200 U mg^{-1}) (17). A UreD—urease apoprotein complex is known (23), and urease within UreABC—UreD can be partially activated *in vitro* in the presence of Ni^{2+} and bicarbonate (needed to form a carbamylated-Lys residue that bridges the dinuclear center) to a greater level than UreABC alone (24). UreABC—UreDF and UreABC—UreDFG complexes also have been identified and found to have enhanced activation properties compared to the UreD—urease apoprotein complex (20, 31). In addition, UreD is found in an insoluble UreD—UreF—UreG (or UreDFG) complex that was hypothesized to function as a unit during urease activation (19).

Despite our knowledge of several UreD-containing urease complexes, the role of this protein during *in vivo* urease maturation remains unknown. The major bottleneck in carrying out a thorough biochemical analysis of the protein is its insolubility of UreD when *ureD* is overexpressed alone. To circumvent this problem a translational fusion was constructed between UreD and the maltose binding protein (MBP). The linked species provides a functional and soluble form of UreD that provides us with the first analysis of this critical urease accessory protein.

MATERIALS AND METHODS

Plasmid construction. Molecular biology techniques were performed by using standard protocols (28), with primers obtained from Integrated DNA Technologies (Coralville, Iowa). All plasmids associated with this study are outlined in Appendix A and their correct construction was confirmed by sequence analysis. *E. coli* DH5α (Invitrogen) was used as the host for all cloning procedures described below.

For purification and pull-down studies of MBP-UreD, cells containing pEC002 were used for protein overproduction. This plasmid was constructed by PCR amplification of *ureD* using pKK17 (5) as a template, a forward primer (5'-TATA*GGATCC*GTGTTACCACCACTCAAA-AAAGGCTG-3') with an engineered 5'-BamHI restriction site (shown in italics), and a reverse primer with a 5'-HindIII restriction site (5'-TATA*AAGCTT*TTAAGTCAGCCAGATTCGGGG-AAG-3'). After amplification the isolated BamHI-HindIII *ureD* fragment was digested and ligated into the similarly digested pMal-c2x vector (New England Biolabs). The resulting pEC002 encoded an in-frame translational fusion of *ureD* with *malE*, the open reading frame of MBP. A modified pMal-c2x vector also was used for overproduction of the UreD-free MBP by inserting a stop codon (using forward primer 5'-CGGGATCGAGGGAAGG**TGA**TCAGAATT-

CGGATCC-3' and reverse primer 5'-GGATCCGAATTCTGA**TCA**CCTTCCCTCGATCCCG-3', where the mutations are in bold) after the bases encoding the C-terminal Arg residue. This plasmid is denoted pMBP2*.

For one-step purification of UreG, we used a C-terminal *Strep*-tag fusion that was constructed by inserting the wild-type *ureG* into SacII-PstI-digested pASK-IBA3plus (IBA GmbH, Göttingen, Germany) to produce pIBA3+G (25) .

To test the ability of the *malE-ureD* fusion to complement a Δ*ureD*-urease cluster, pEC006 and pEC013 were constructed. pEC006 consists of *ureABCEFG* inserted into the *tac* promoter-based expression vector pACT3 (7). Briefly, *ureABC* was PCR amplified by using pKK17 as a template, a forward primer with a 5'-KpnI restriction site (5'-GATCG*GGTACC*-TAAGAGAACGTTATGGAACTGACCC-3'), and a reverse primer with a 5'-XbaI restriction site (5'-GATCG*TCTAGA*TTAAAACAGAAAATATCGTTGCGC-3'). The isolated KpnI-XbaI *ureABC* fragment was digested and ligated into similarly digested pACT3, resulting in pEC004. Utilizing a unique BamHI restriction site within *ureC*, pKK17 was digested with BamHI and HindIII resulting in a fragment containing the 3' end segment of *ureC* with full length *ureE*, *ureF*, and *ureG*. This fragment was ligated into similarly digested pEC004, resulting in pEC006. pEC013 consists of pKK17 with *malE-ureD* replacing wild-type *ureD* within the urease cluster. *malE-ureD* was PCR amplified by using pEC002 as a template, a forward primer with a 5'-EcoRI restriction site (5'-GATCG*GAATTC*ATGAAAATCGAAGAAGGTAAACTGGTAA-3'), and a reverse primer identical to the one used for construction of pEC002. The isolated *malE-ureD* fragment was partially digested with EcoRI and SbfI (*ureD* contains a unique SbfI restriction site) and a resulting ~1.7 kb band was isolated via gel extraction and ligated to pKK17 digested with the same enzymes, resulting in pEC013.

Plasmids pEC005, pEC007, pEC008, and pEC009 were constructed to carry out co-expression studies involving *ureE*, *ureF*, and *ureG*. Plasmid pEC005 consists of the *ureFG* genes PCR amplified by using pKK17 as a template, a forward primer (5'-GATCG*GGTACC*AGGAG-GTCTAGCATGTCGACAGCGGAACAACG-3') with both a 5'-KpnI restriction site and an engineered ribosomal binding site (underlined), and a reverse primer with a 5'-XbaI restriction site (5'-GATCG*TCTAGA*CTATTTGCCAAGCATGCCTTTGTCT-3'). The isolated KpnI-XbaI *ureFG* fragment was digested and ligated into similarly digested pACT3. Plasmid pEC008 contains only *ureF* that was PCR amplified from the pKK17 template by using the same forward primer utilized for *ureFG* amplification and a reverse primer (5'- GATCG*TCTAGA*CTAGGAA-CGGAATAATCGAGAGTA-3') specific for *ureF* with a 5'-XbaI restriction site. This KpnI-XbaI *ureF* fragment was ligated into similarly digested pACT3. Finally, pEC007 and pEC009 containing *ureE* and *ureG*, respectively, were constructed in the same manner as pEC008; however, gene-specific primers for *ureE* and *ureG* amplification used forward primers (5'-GATCG*GGTACC*AGGAGAGCGGATGCTTTATTTAAC-3' and 5'- GATCG*GGTACC*AGG-AGAAGCCATGAACTCTTATAA-3', respectively) with a 5'-KpnI restriction site and reverse primers (5'-GATCG*TCTAGA*CTAGTGGCTGTGAGCGTGGTGGTC-3' and the same as used for pEC005) with a 5'-XbaI restriction site. The forward primers in these reactions did not contain the engineered ribosomal binding site described for pEC008.

Protein purification. MBP-UreD was purified from *E. coli* BL21-Gold(DE3) cells (Stratagene) transformed with pEC002 and grown with shaking in lysogeny broth (LB) supplemented with 300 μg ml^{-1} ampicillin at 30 °C until the cells reached an optical density at 600 nm ($O.D._{600}$) of ~0.5. The cultures were induced with 0.5 mM isopropyl β-D-thiogalacto-pyranoside (IPTG; Calbiochem), incubated at 25 °C for 12-16 h, and harvested by centrifugation.

Cell pellets were resuspended in 20 mM Tris-HCl, pH 7.5, 1 mM EDTA, and 1 mM β-mercaptoethanol (TEB) buffer with 500 mM NaCl and disrupted by sonication (Branson Sonifier, 5 cycles of 2 min each, power level 4, 50% duty cycle with cooling in an ice water/ethanol mixture). Cell extracts were obtained by centrifugation at 100,000 *g* for 1 h at 4 °C. Extracts were diluted at least 1:1 with TEB buffer containing 500 mM NaCl before loading onto amylose resin (New England Biolabs) that had been pre-equilibrated with the same buffer. The column (30 ml bed volume) was washed with the same buffer until the A_{280} reached baseline, at which point the bound proteins were eluted with TEB buffer containing 500 mM NaCl plus 10 mM maltose. The eluted fractions were collected, pooled, and dialyzed against TEB buffer containing 15 mM NaCl overnight. Subsequent to dialysis the MBP-UreD solution was loaded onto a Q-Sepharose column (2.5 cm X 14 cm, GE Healthcare) pre-equilibrated with TEB buffer containing 20 mM NaCl. The column was washed with at least 2.5 bed volumes of buffer before a linear gradient was applied from 20 mM NaCl to 1 M NaCl in TEB. Fractions containing MBP-UreD were verified by sodium dodecyl sulfate-polyacrylamide gel electrophoresis (SDS-PAGE) before pooling. Depending on downstream applications, the purified MBP-UreD was concentrated by using a 10,000 molecular weight cutoff Amicon Ultra centrifugal filter device (Millipore) and dialyzed against either TEB buffer with 25 mM NaCl for pull-down experiments or with 50 mM Tris-HCl, pH 7.5, containing 100 mM NaCl for equilibrium dialysis experiments.

Purified MBP (unlinked to UreD) was obtained by three methods: (1) direct purchase from New England Biolabs; (2) Factor Xa (New England Biolabs) proteolytic digest of MBP-UreD with a subsequent purification step using DEAE-Sepharose according to the manufacturer's instructions (GE Healthcare); (3) amylose resin purification of MBP

overproduced in *E. coli* BL21-Gold(DE3) harboring pMBP2*. The MBP is identical in sequence regardless of which source was used.

The UreEF fusion protein was initially purified by using Ni^{2+}-Sepharose High Performance media (GE Healthcare) as previously described (12). Purified UreEF was dialyzed against TEB buffer containing 25 mM NaCl overnight and subjected to gel-filtration chromatography by using a 1.5 cm X 69 cm Superdex 75 column (GE Healthcare) pre-equilibrated with TEB buffer plus 25 mM NaCl. The eluted fractions were analyzed by SDS-PAGE and those containing pure UreEF were pooled.

The C-terminus *Strep*-tagged UreG protein ($UreG_{Str}$) was purified from *E. coli* DH5α transformed with pIBA3+G, grown with shaking in LB supplemented with 300 μg ml^{-1} ampicillin at 37 °C until the cells reached $O.D._{600}$ ~0.5, induced with 200 ng ml^{-1} anhydrotetracycline, and incubated overnight before harvesting. Cell pellets were resuspended in 100 mM Tris-HCl, pH 8.0, 150 mM NaCl, and 1 mM EDTA then disrupted with sonication. Soluble cell-free extracts were obtained by centrifugation at 100,000 *g* for 1 h at 4 °C. Purification of $UreG_{Str}$ followed the manufacturer's instructions (IBA GmbH, Germany).

UreE was purified from *E. coli* BL21-Gold(DE3) cells transformed with pEC007, grown with shaking in LB supplemented with 50 μg ml^{-1} chloramphenicol at 37 °C until the cells reached $O.D._{600}$ of ~0.5, induced with 0.5 mM IPTG, and incubated overnight until the cells were harvested. The UreE purification procedure was the same as that used for the purification of the UreE H144* variant, as previously described (2).

Both holoprotein and apoprotein forms of urease were purified from *E. coli* BL21-Gold(DE3) cells transformed with pKK17. For purification of holoenzyme, cells were grown with shaking in LB supplemented with 300 μg ml^{-1} ampicillin and 1 mM $NiCl_2$ at 37 °C until the cells reached $O.D._{600}$ ~0.5 at which point the culture was induced with 0.1 mM IPTG and allowed to incubate overnight until harvesting the cells. Cell pellets were resuspended in PEB buffer (20 mM Na-phosphate buffer pH 7.4, 1 mM EDTA, 1 mM β-mercaptoethanol) and disrupted by sonication. Soluble cell-free extracts were obtained by centrifugation at 100,000 *g* for 1 h at 4 °C and applied to a 2.5 cm X 10 cm DEAE-Sepharose column pre-equilibrated with PEB buffer. A linear gradient from 0 M to 1 M KCl in PEB buffer was applied and fractions containing urease were pooled, adjusted to 1.5 M KCl, and applied to a phenyl-Sepharose (GE Healthcare) column (2.5 cm X 9 cm) pre-equilibrated with PEB buffer containing 1.5 M KCl. The column was washed with equilibration buffer and bound proteins were step-eluted with PEB buffer containing no KCl. Fractions containing pure urease were pooled and dialyzed against TEB buffer containing 25 mM NaCl. Urease apoprotein was purified in an identical manner as the holoenzyme; however, this protein was purified from cultures grown without the addition of $NiCl_2$ to the medium. Prior studies have demonstrated that urease activity is nearly undetectable under these conditions, presumably because the metal-binding components in the medium prevent uptake and incorporation of the metal (22).

Gel filtration analysis of MBP-UreD. To assess the native size of MBP-UreD, a sample was chromatographed on a column of Sephacryl S300-HR (1.5 x 65 cm, GE Healthcare) equilibrated in 50 mM Tris-HCl, pH 7.5, containing 100 mM NaCl while monitoring the absorbance at 280 nm. Gel filtration standards (Bio-Rad) were used for calibration of the

column. The effects of metal ions on the elution position of MBP-UreD were examined by repeating the analyses after equilibration of the column in 50 mM Tris-HCl, pH 7.5, containing 100 mM NaCl and 100 μM of either $NiCl_2$ or $ZnCl_2$.

Analysis for metal content. The metal content of purified MBP-UreD was assessed by inductively coupled plasma atomic emission spectroscopy (Chemical Analysis Laboratory at the Univ. Georgia, Athens, GA). Control buffer samples were analyzed for comparison.

Equilibrium dialysis. One method for assessing the metal-binding properties of MBP-UreD made use of the metallochromogenic indicator 4-(2-pyridylazo)resorcinol (PAR, Sigma). Purified MBP-UreD (9.6 μM for Ni^{2+} experiments, 7.1 μM for Zn^{2+} experiments) and MBP (19.6 μM) were extensively dialyzed against 50 mM Tris-HCl, pH 7.5, containing 100 mM NaCl prior to equilibrium dialysis. Protein samples (300 μl) at the designated concentrations were dialyzed against the same buffer containing various concentrations of $NiCl_2$ or $ZnCl_2$ (500 μl) by using a Rapid Equilibrium Dialysis device (Pierce Biotechnology, Rockford Il.). The device was shaken at 200 or 300 rpm for 4 h at 37 °C, then 200 μl aliquots from each side of the membrane were assayed for [Ni^{2+}] or [Zn^{2+}] by mixing with 800 μl of PAR solution (100 μM in 50 mM Tris-HCl, pH 7.5, 100 mM NaCl; prepared from 5 mM PAR aqueous stock solution titrated to pH 8.0 with 1 M KOH). The concentration of the PAR:metal complex was quantified by measuring the absorption at 500 nm for the aliquot from the protein-containing chamber and subtracting that for the protein-free aliquot, and comparing to standard curves that were developed by using Ni and Zn atomic absorption standards (Sigma). The data were analyzed directly or corrected for the metal ions bound to MBP and fit to the following equation for a single type of binding site (Sigma Plot, Systat Software, Inc.) where *Y* is the number of moles of

metal ion bound per mole of protomer, B_{max} is the maximal number of moles of metal ion bound per mole of protomer, [M] is the concentration of free metal ion, and K_d is the dissociation constant.

Equation 2.1:

$$Y = (B_{max}[M])/(K_d + [M])$$

A second approach for assessing Ni^{2+} binding to MBP-UreD and MBP as well as for examining the competition between Ni^{2+} and Zn^{2+} for the former protein made use of radiolabeled $^{63}NiCl_2$ (1,445 mCi/mmol; Du Pont NEN Research Products Inc., Wilmington, DE). MBP-UreD and MBP (approximately 10 µM and 30 µM, respectively) were dialyzed against the indicated concentrations of $^{63}NiCl_2$ and unlabeled $ZnCl_2$ using the Rapid Equilibrium Dialysis device as described above. After shaking at 300 rpm for 4 h at 37 °C, 200 µl samples were mixed with 10 ml of Safety-Solve scintillation fluid (Research Products International Corp.) and analyzed with a Beckman-Coulter LS6500 liquid scintillation counter. The data were fit as above (where [M] is the concentration of free Ni^{2+}) or using the competitive inhibition equation (where K_i is the inhibition constant of Zn^{2+}).

Equation 2.2:

$$Y = (B_{max}[Ni])/\{K_d(1 + [Zn]/K_i) + [Ni]\}$$

Polyacrylamide gel electrophoresis and Western blot analysis. SDS-PAGE was performed by using buffers previously described (14), 12% or 12.5% polyacrylamide running gels, and 4.5% or 5.0% stacking gels. Native PAGE was performed by using buffers without

SDS, 6% polyacrylamide running gels, and 3% stacking gels. Protein bands were visualized with Coomassie brilliant blue stain or the gels were electroblotted onto Immobilon-P polyvinylidene fluoride membranes (Millipore) and blotted with anti-*K. aerogenes* urease antibodies (25). Reactive protein bands were visualized with anti-rabbit IgG alkaline-phosphatase conjugated antibodies and BCIP®/NBT liquid substrate (containing 5-bromo-4-chloro-3-indolyl phosphate and nitroblue tetrazolium, Sigma). Protein band intensities were measured by using gel-scanning software, AlphaEaseFC (Alpha Innotech Corp., San Leandro, California) and ratios between bands were calculated using integrated density values (area under the curve); protein molecular mass was not accounted for unless indicated otherwise. The calculated molecular mass of UreA (11.1 kDa), UreB (11.7 kDa), UreE (17.6 kDa), UreG (21.9 kDa), $UreG_{Str}$ (23.2 kDa), UreF (25.2 kDa), UreEF (42.8 kDa), UreD (29.8 kDa), MBP-LacZα (50.8 kDa), UreC (60.3 kDa), and MBP-UreD (72.9 kDa) generally migrate during electrophoresis as expected with the exception of UreG which behaves as if it was larger than UreF.

Urease activity and protein assays. Urease activity was measured by quantifying the amount of ammonia released during urea hydrolysis by the formation of indophenol which was monitored at 625 nm (33). One unit of activity is defined as the amount of enzyme necessary to hydrolyze 1 μmol of urea per min at 37 °C. Standard assay buffer consisted of 50 mM HEPES, pH 7.8, and 50 mM urea. Protein concentrations were determined by using a standard protein assay (Bio-Rad) with bovine serum albumin as the standard.

In vivo *interactions and complementation experiments*. *E. coli* BL21-Gold(DE3) cells were transformed by following the manufacturer's instructions (Stratagene). Double transformants were generated by making the singly-transformed cells competent using $CaCl_2$, followed by a standard heat shock transformation protocol as previously described (28).

Transformants were maintained on LB agar plates containing ampicillin (100 µg ml^{-1}) or chloramphenicol (50 µg ml^{-1}), for single transformants, or both antibiotics for double transformants. Pre-cultures for *in vivo* pull-down experiments or complementation studies consisted of 5 ml of LB supplemented with 300 µg ml^{-1} ampicillin, 50 µg ml^{-1} chloramphenicol, or both antibiotics in the case of double transformants. These cultures were incubated overnight at 37 °C in a shaking incubator and subcultured 1:100 into 25 ml of LB supplemented with the same antibiotics plus 1 mM $NiCl_2$ in the case of complementation studies. The 25 ml cultures were incubated at 37 °C with shaking until the cells reached $O.D._{600}$ ~0.5 at which point they were induced with 0.5 mM IPTG for pull-down experiments or 0.1 mM IPTG for complementation studies. After induction, the cultures were incubated for an additional 12-16 h before harvesting. Cell pellets were resuspended in 1 ml of TEB buffer containing 25 mM NaCl or 1 ml of 50 mM HEPES, pH 7.8, for pull-down experiments or complementation studies, respectively. In both cases, the cell slurries were supplemented with 1 mM phenylmethanesulfonyl fluoride (Sigma) before disruption by sonication. Subsequently, the disrupted cultures were centrifuged at 16,000 *g* for 20 min in a table-top microcentrifuge, the soluble cell-free extracts were kept, and the pellets were discarded. For complementation assays, soluble cell-free extracts obtained after sonication and centrifugation were directly assayed for urease activity. For some experiments, soluble cell-free extracts were mixed from two different types of recombinant cells that overproduced different individual proteins; in this case 800 µl of each preparation was mixed and incubated at room temperature for 1 h before the pull-down analysis.

For *in vivo* pull-down assays the soluble cell-free extracts derived from the recombinant *E. coli* cells were mixed with 200 µl bed volume of amylose resin that had been washed with water and equilibrated in TEB buffer containing 25 mM NaCl. The cell-free extract/amylose resin slurry was incubated at room temperature for 1 h with gentle rocking before washing the amylose resin 5 times with 1 ml TEB buffer containing 25 mM NaCl. After the final wash, the resin was pelleted and resuspended in 500 µl TEB buffer plus 25 mM NaCl containing 10 mM maltose. This slurry was briefly vortexed and the resin was pelleted for 1 min at 1,200 *g*. The remaining supernatant was removed and analyzed by using SDS-PAGE.

In vitro *interaction experiments*. Purified proteins were dialyzed against TEB buffer containing 25 mM NaCl before each experiment. Depending on the particular experiment, MBP-UreD or MBP (2 µM) was mixed with UreEF, UreE, UreG$_{Str}$, urease apoprotein, or holoenzyme (10 µM) in 250 µl, 500 µl, or 1 ml solutions by using TEB buffer plus 25 mM NaCl to adjust the volume. When necessary the salt concentrations of the mixtures were adjusted to 1 M NaCl by using buffer containing 3 M NaCl. Additionally, in selected experiments soluble cell-free extracts of *E. coli* MG1655 (used as a standard wild-type cell) were prepared in TEB buffer with 25 mM NaCl identical to those described in the prior section and added at 1/6 the assay volume. After mixing, the protein solutions were incubated (room temperature, 37 °C, or 42 °C) for 1 h and amylose resin (1/5 the solution volume; previously washed and equilibrated in the buffer) was added to the mixture. The slurry was gently rocked for 1 h at room temperature then micro-centrifuged for 1 min to separate the amylose resin from the discarded supernatant. The resin was washed five times with one reaction volume of TEB buffer containing either 25 mM or 1 M NaCl, then resuspended in half the original reaction volume with TEB buffer containing 10 mM

maltose. The maltose-containing slurry was briefly vortexed and the resin was pelleted for 1 min at 1,200 *g*. The remaining supernatant was removed and analyzed by using SDS-PAGE.

RESULTS

Purification and properties of the MBP-UreD fusion protein. In order to generate a form of UreD that would be useful for biochemical analysis, an in-frame translational fusion between UreD and the MBP was created. The soluble MBP-UreD was purified to near homogeneity by sequential chromatography using amylose and Q-Sepharose resins and shown to exist as a large multimer (>670-kDa) according to gel filtration chromatography. Whereas MBP-UreD was highly soluble, the addition of Factor Xa to purified MBP-UreD at room temperature for 3 h liberated UreD which was found to be not suitable for further study. Chromatography of the Factor Xa digest on DEAE-Sepharose led to irreversible interaction of UreD with the chromatographic resin. Furthermore, visible protein precipitation was observed after >6 h of digestion with Factor Xa, attributed to UreD instability. Thus, further studies focused on the intact form of MBP-UreD.

To determine whether structural or tightly-bound metal ions were present in MBP-UreD, the metal content of purified protein was determined by using inductively coupled plasma atomic emission spectroscopy. This analysis showed that no metals were associated with MBP-UreD that had been purified in the presence of 1 mM EDTA (a chelator commonly added to urease purification buffers and shown not to remove the enzyme-bound Ni^{2+}). Although the protein as purified was free of metal ions, it was of interest to assess the ability of the UreD domain of MBP-UreD to reversibly bind metals. In particular, we focused on Ni^{2+} because of its obvious relevance to urease activation and Zn^{2+} because this metal is known to bind to UreE (2, 8) and

UreG (35, 36) accessory proteins. Inclusion of 100 μM $NiCl_2$ or $ZnCl_2$ had no effect on the protein behavior as assessed by gel filtration chromatography.

In one approach to assess metal ion binding, MBP-UreD was subjected to equilibrium dialysis against varying [$NiCl_2$] or [$ZnCl_2$] and the concentrations of protein-bound metal versus free metal were determined by using the metallochromic indicator PAR. The MBP-UreD data (Figure 2.1, panel A) could be fit by assuming a single type of binding site with a maximum (B_{max}) of 2.1 ± 0.1 Ni^{2+} per protomer and a dissociation constant (K_d) of 33.8 ± 4.1 μM; however, significant binding of Ni^{2+} to MBP was observed over this metal ion concentration range. To correct for the non-specific Ni^{2+} binding to MBP, a linear fit to the MBP data was subtracted from the MBP-UreD data and the resulting points analyzed to yield a B_{max} of 1.6 ± 0.1 Ni^{2+} per UreD protomer with a K_d of 24.3 ± 3.1 μM. Although the error ranges are quite small, we note that the greatest Ni^{2+} concentration tested was only 5-fold the apparent K_d so the data do not approximate saturation. By contrast, the Zn^{2+} data (Figure 2.1, panel B) did approach saturation and binding to MBP was less significant; thus, a B_{max} of 4.1 ± 0.2 Zn^{2+} per protomer with a K_d of 4.7 ± 0.7 μM was confidently established.

As an alternative approach to measure Ni^{2+} interactions with MBP-UreD, varied concentrations of radiolabeled $^{63}NiCl_2$ were used during equilibrium dialysis studies (Figure 2.1, panel C). Direct fitting of the data by assuming a single type of binding site yielded a B_{max} of 3.1 ± 0.1 Ni^{2+} per MBP-UreD protomer and a K_d of 62.0 ± 5.8 μM; however, correction of these

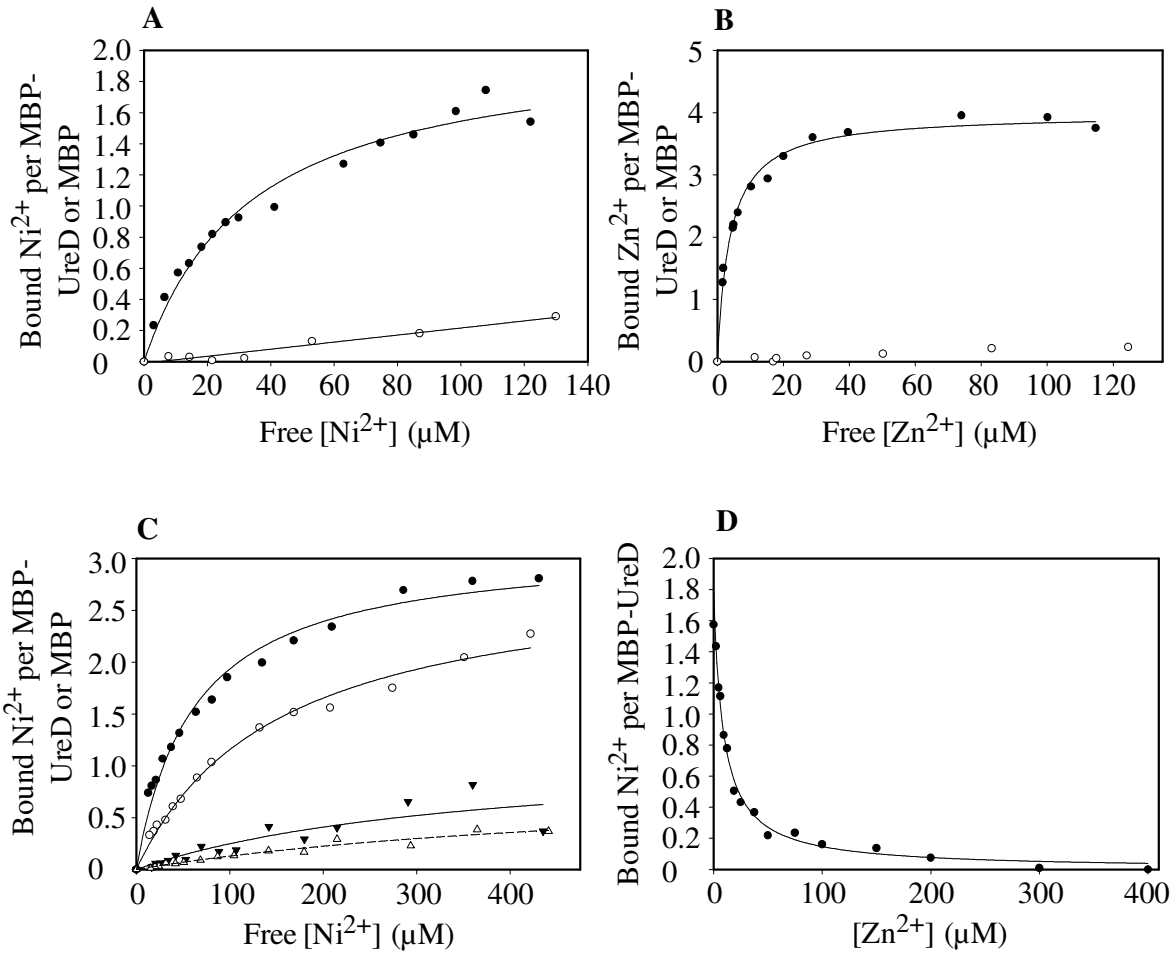

Figure 2.1: Equilibrium dialysis of MBP-UreD and MBP with $NiCl_2$, $^{63}NiCl_2$, and $ZnCl_2$. (A) MBP-UreD (closed circles) or MBP (open circles) were dialyzed against varied concentrations of $NiCl_2$ and the amounts of bound Ni^{2+} per protomer were determined by using the metallochromic indicator PAR. Data were fit by assuming saturation behavior at a single type of binding site for MBP-UreD or by using a linear equation for MBP. (B) Analogous results obtained for dialysis of MBP-UreD (closed circles) or MBP (open circles) against $ZnCl_2$. The MBP-UreD data were fit as above. (C) MBP-UreD was dialyzed against varying concentrations of $NiCl_2$ containing radioactive ^{63}Ni along with 0 μM (closed circles), 12.5 μM (open circles), and 125 μM (closed triangles) $ZnCl_2$. Concentrations of free and bound Ni^{2+} were determined by scintillation counting. Also shown are control data for MBP with varied concentrations of $^{63}NiCl_2$ (open triangles). Each data set was fit by assuming saturation behavior at a single type of binding site. (D) MBP-UreD was dialyzed against 100 μM $^{63}NiCl_2$ and the indicated concentrations of $ZnCl_2$. Data were fit by using a competitive inhibition equation.

data for the Ni^{2+} bound to MBP provided a B_{max} of 2.7 ± 0.1 Ni^{2+} per UreD protomer and K_d of 50.0 ± 4.4 μM. These data include Ni^{2+} concentrations that more closely approach saturation than were obtained in the PAR experiments and are considered to be more reliable.

The use of ^{63}Ni in equilibrium dialysis experiments also allowed for investigation of the competition between Ni^{2+} and Zn^{2+}. MBP-UreD was dialyzed against varying concentrations of $^{63}NiCl_2$ with set $ZnCl_2$ concentrations of either 12.5 μM or 125 μM (Figure 2.1, panel C). The data from the experiment containing 12.5 μM Zn^{2+} were corrected for non-specific Ni^{2+} binding to MBP in the same manner as done with the Zn^{2+}-free sample. These data were fit to a competitive inhibition equation using B_{max} and K_d values as described above, providing a Zn^{2+} K_i of 5.0 ± 0.3 μM, in close agreement to the K_d measured for Zn^{2+} by using PAR. At 125 μM Zn^{2+} nearly all of the Ni^{2+} binding sites were occupied by Zn^{2+}. A reciprocal experiment was performed in which MBP-UreD was dialyzed against varying concentrations of $ZnCl_2$ with a set concentration of 100 μM $^{63}NiCl_2$ (Figure 2.1, panel D). The data were well fit by using the competitive inhibition equation, with B_{max} and K_d calculated above, yielding a Zn^{2+} K_i of 3.0 ± 0.2 μM. These data clearly demonstrate that the UreD domain of MBP-UreD reversibly binds both Ni^{2+} and Zn^{2+}, and that Zn^{2+} exhibits high affinity for the Ni^{2+} binding sites.

malE-ureD *replacement or complementation of a* ΔureD *urease cluster*. To assess the ability of the UreD domain of MBP-UreD to function during *in vivo* urease maturation it was

Plasmid Derivative	Specific Activity (U mg^{-1} protein)
pKK17 (wild-type urease cluster)	171.2 ± 22.0
pEC002 (*malE-ureD*) + pEC006 (Δ*ureD*-urease cluster)	15.1 ± 2.4
pMal-c2x (*malE-lacZα*) + pEC006 (Δ*ureD*-urease cluster)	<0.1
pEC013 (urease cluster with *malE-ureD* replacing *ureD*)	56.2 ± 4.2

Table 2.1: Urease specific activity in soluble cell-free extracts of *E. coli* BL21-Gold(DE3) harboring the indicated plasmids. Data are represented as the average ± standard deviation for triplicate biological samples.

necessary to show that *malE-ureD* could complement a Δ*ureD* urease gene cluster, or functionally replace *ureD* within the urease cluster. *E. coli* BL21-Gold(DE3) cells were either co-transformed with pEC002, coding for the MBP-UreD fusion, and pEC006, a *tac*-based expression vector for overproduction of a Δ*ureD* urease cluster, or singly transformed with pEC013 encoding an intact urease cluster with *malE-ureD* replacing wild-type *ureD.* For comparison and control, the same cells were transformed with pKK17 (with the wild-type urease gene cluster from *K. aerogenes*) or pMal-c2x plus pEC006 (where pMal-c2x overproduces a MBP-LacZα fusion so UreD would not be present). Soluble cell-free extracts of cells harboring pEC002 and pEC006 possessed about 10% of the urease activity measured for extracts of cells containing the wild-type urease cluster (Table 2.1). Analogous extract preparations from cells containing pEC013 exhibited a specific activity of 56.2 ± 4.2 U mg^{-1} or 33% of wild-type activity. The reduction in activity compared to cells with pKK17 is likely due to the requirement for dual plasmids or to steric hindrance introduced by the 42-kDa fusion protein. In contrast to

these positive results, extracts of cells harboring pMal-c2x and pEC006 were inactive, demonstrating that the UreD domain of MBP-UreD was responsible for complementation and that MBP-UreD provides a functional form of UreD.

MBP-UreD interactions with other urease components in vivo. To map the cellular protein-protein interaction network of UreD with other urease components, *E. coli* BL21-Gold(DE3) cells were co-transformed with pEC002 (encoding MBP-UreD) and a series of other expression vectors encoding various urease-related proteins. The soluble extracts of these cells were examined directly by using SDS-PAGE or applied to amylose resin and the subsequently bound proteins were eluted with buffer containing 10 mM maltose and analyzed by electrophoresis (Figure 2.2). As controls, analogous experiments made use of cells co-transformed with pMal-c2x instead of pEC002. In all cases, the MBP-LacZα control experiments (where UreD was absent) demonstrated negligible co-purification of urease components during amylose chromatography. This finding confirmed that the UreD domain of the MBP-UreD fusion was responsible for the observed protein-protein interactions, rather than MBP itself.

The results depicted in Figure 2.2 reveal the cellular interactions of MBP-UreD. The initial soluble extracts of all cells (odd numbered lanes) contained a prominent band just below the position of UreF; this band most likely is attributed to chloramphenicol acetyltransferase and contributes little, if at all, to the intensity of the UreF band in samples bound to and released from the amylose resin (even numbered lanes). The pull-down analysis of soluble extracts from cells co-transformed with pEC004 (encoding UreA, UreB, and UreC) confirm the co-purification of UreABC with MBP-UreD (Panel A, lane 2). The band corresponding to UreC was unclear on this gel due to its overlap with MBP-UreD; however, the presence of UreC was substantiated by

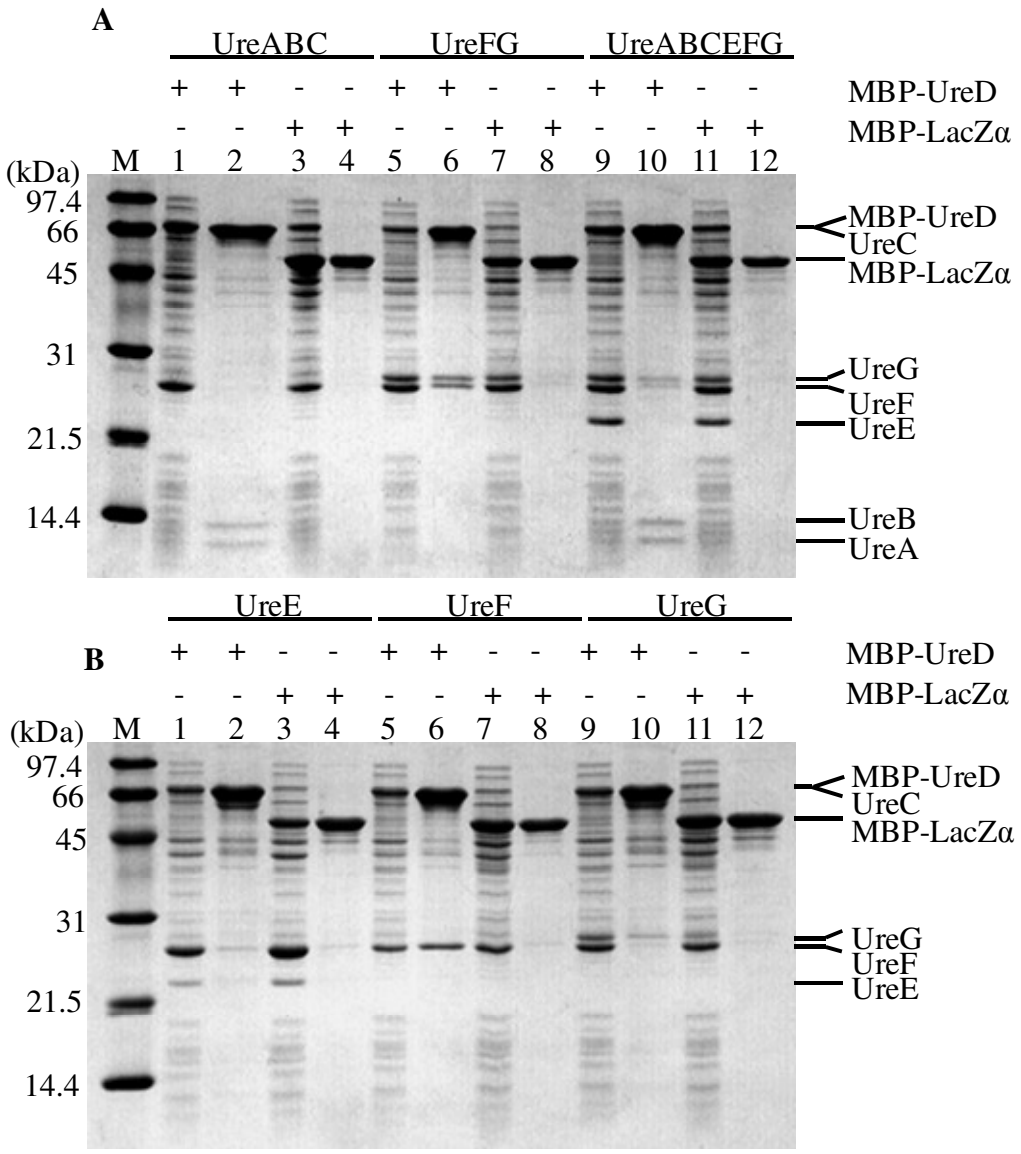

Figure 2.2: Interactions of MBP-UreD with other urease components *in vivo*. *E. coli* BL21-Gold(DE3) cells were co-transformed with either pEC002 (encoding MBP-UreD) or pMal-c2x (encoding MBP-LacZα) along with pEC004, pEC005, pEC006, pEC007, pEC008, or pEC009 (encoding UreABC, UreFG, UreABCEFG, UreE, UreF, or UreG, respectively). Soluble cell-free extracts were analyzed directly by SDS-PAGE (odd numbered lanes) or subjected to amylose resin chromatography with the proteins eluted by maltose addition and analyzed by SDS-PAGE (even numbered lanes). (A) MBP-UreD interactions with multiple urease components. (B) MBP-UreD interactions with single urease components. M = molecular mass markers.

immunoblot analysis using anti-urease antibodies (data not shown). Pull-down examination of soluble extracts from cells co-transformed with pEC005 (encoding UreF and UreG) showed that

both UreF and UreG co-purify with MBP-UreD (Panel A, lane 6). For pEC006 (encoding the Δ*ureD*-urease cluster), UreABC, UreF, and UreG all co-purified with MBP-UreD (Panel A, lane 10), but UreE was not detected. A pull-down of soluble extracts from cells with pEC007 (encoding UreE) indicated that UreE does not co-purify with MBP-UreD (Panel B, lane 2). The same analysis for pEC008 (encoding UreF) confirmed that UreF co-purified with MBP-UreD (Panel B, lane 6). Lastly, pull-down studies involving pEC009 (encoding UreG) demonstrated co-purification of UreG with MBP-UreD (Panel B, lane 10). Densitometric analyses of the SDS-PAGE gels in Figure 2.2 revealed a UreG:MBP-UreD ratio of only 0.07:1 for co-purification of UreG with MBP-UreD, compared to a UreF:MBP-UreD ratio of 0.42:1 when UreF was overproduced alone with MBP-UreD, or a UreF:UreG:MBP-UreD ratio of 0.16:0.19:1 when UreF and UreG were both overproduced with MBP-UreD. The ratios reflect the upper limit of the amount of bound UreF since we cannot completely rule out contamination of these samples with trace amounts of the chloramphenicol acetyltransferase.

In order to further investigate the interaction between UreD and urease apoprotein, soluble cell-free extracts of *E. coli* BL21-Gold(DE3) pEC002 (containing MBP-UreD) and *E. coli* BL21-Gold(DE3) pEC004 (containing UreABC) were mixed, incubated at room temperature for 1 h, and subjected to amylose resin pull-down analysis (Figure 2.3, panel A). Lanes 1 and 2 depict soluble cell-free extracts of the two strains prior to mixing. Lane 3 shows the proteins eluted from amylose resin by maltose addition, clearly demonstrating that MBP-UreD and UreABC from separate cells can interact to form a complex by mixing the soluble extracts under these conditions.

MBP-UreD interactions with other urease components in vitro. The protein-protein interactions identified above by *in vivo* pull-down analyses were compared to the interactions

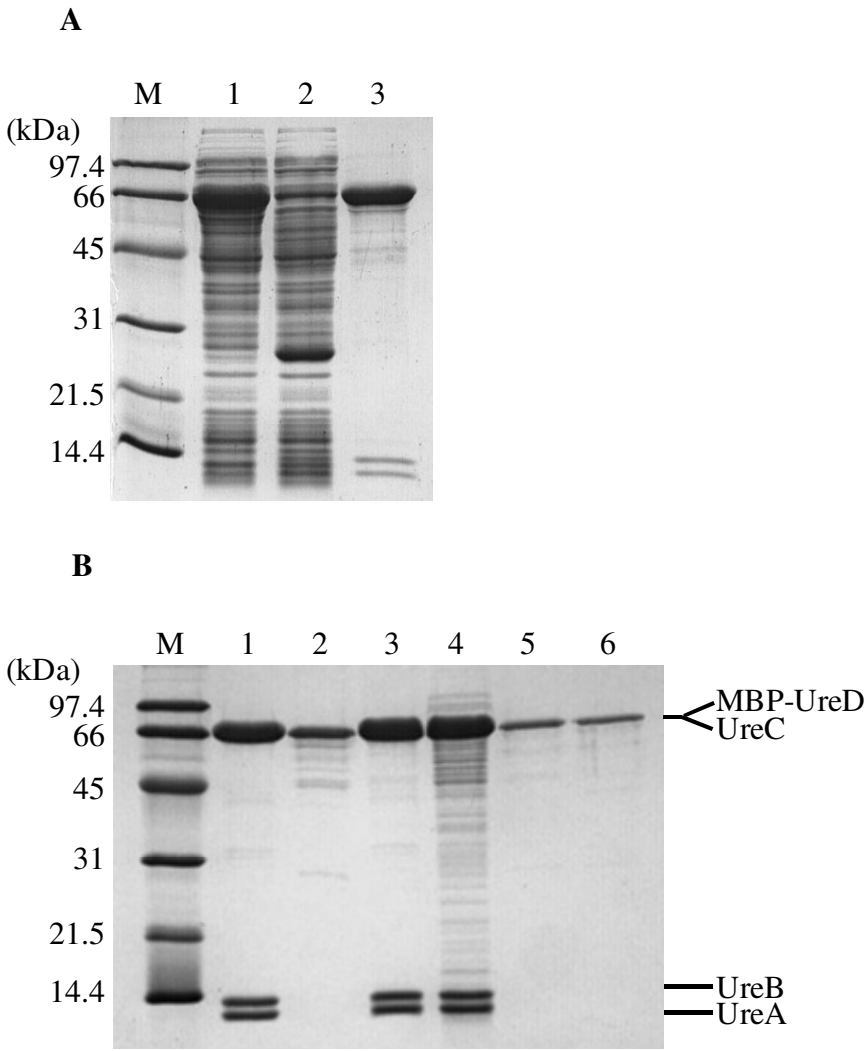

Figure 2.3: Interactions of MBP-UreD with urease apoprotein. (A) *In vivo* complex formation. Soluble cell-free extracts of IPTG-induced *E. coli* BL21-Gold(DE3) pEC002 (encoding MBP-UreD) and *E. coli* BL21-Gold(DE3) pEC004 (encoding UreABC) were mixed, incubated at room temperature for 1 h, and chromatographed on amylose resin. Bound proteins were eluted in buffer containing 10 mM maltose and visualized by SDS-PAGE. Lanes: M, molecular mass markers; 1, pEC002 cell-free extracts; 2, pEC004 cell-free extracts; 3, co-elution of UreABC with MBP-UreD from the amylose resin. (B) *In vitro* interactions. Purified MBP-UreD (2 µM) was mixed with isolated urease apoprotein (10 µM) in TEB buffer with 25 mM NaCl and, where indicated, cell-free extracts of *E. coli* MG1655. Reactions were incubated at room temperature for 1 h before the mix was subjected to amylose resin chromatography. Bound proteins were eluted with buffer containing 10 mM maltose. Lanes: M, molecular mass markers; 1, purified urease apoprotein; 2, purified MBP-UreD; 3, MBP-UreD plus urease apoprotein; 4, MBP-UreD plus urease apoprotein along with *E. coli* MG1655 cell-free extracts; 5, eluted fraction from lane 3; 6, eluted fraction from lane 4.

observed when using purified proteins (Figure 2.3, panel B and Figure 2.4). Thus, MBP-UreD or MBP was mixed with various purified urease-related proteins and subjected to amylose resin pull-down experiments as already described. The quality of the samples are illustrated for urease apoprotein (Figure 2.3, panel B, lane 1), MBP (Figure 2.4, panel A, lane 1), MBP-UreD (Figure 2.3, panel B, lane 2 and Figure 2.4, panel A, lane 2), UreEF (Figure 2.4, panel A, lane 3), $UreG_{Str}$ (*Strep*-tagged UreG; Figure 2.4, panel A, lane 4), and UreE (Figure 2.4, panel B, lane 2).

Whereas a complex between MBP-UreD and urease apoprotein was formed when soluble cell-free extracts containing these separate components were mixed (Figure 2.3, panel A), purified MBP-UreD did not bind to isolated urease apoprotein (Figure 2.3, panel B). Samples examined prior to (lane 3) and after (lane 5) the pull-down analysis confirmed the absence of interaction. The same experiments were repeated in the presence of soluble extracts from wild-type *E. coli* MG1655 cells to assess whether any soluble intracellular constituents were responsible for the complex formation observed *in vivo*, but even after incubation for 1 h, we observed no complex between urease apoprotein and MBP-UreD (Figure 2.3, panel B, lanes 4 and 6). Furthermore, incubation of MBP-UreD with urease apoprotein or holoenzyme at 37 °C or 42 °C failed to produce an interaction between the two species according to pull-down analysis (data not shown).

When MBP-UreD was incubated with the UreEF fusion protein at 37 °C (Figure 2.4, panel A, lane 5), only a weak interaction (a UreEF:MBP-UreD ratio of 0.21:1 by densitometry) was detected. An identical experiment performed at 42 °C resulted in a significant enhancement of interaction (UreEF:MBP-UreD ratio of 1.17:1) indicating that higher temperature increases the affinity of MBP-UreD for UreEF (Figure 2.4, panel A, lane 6). When the same sample at

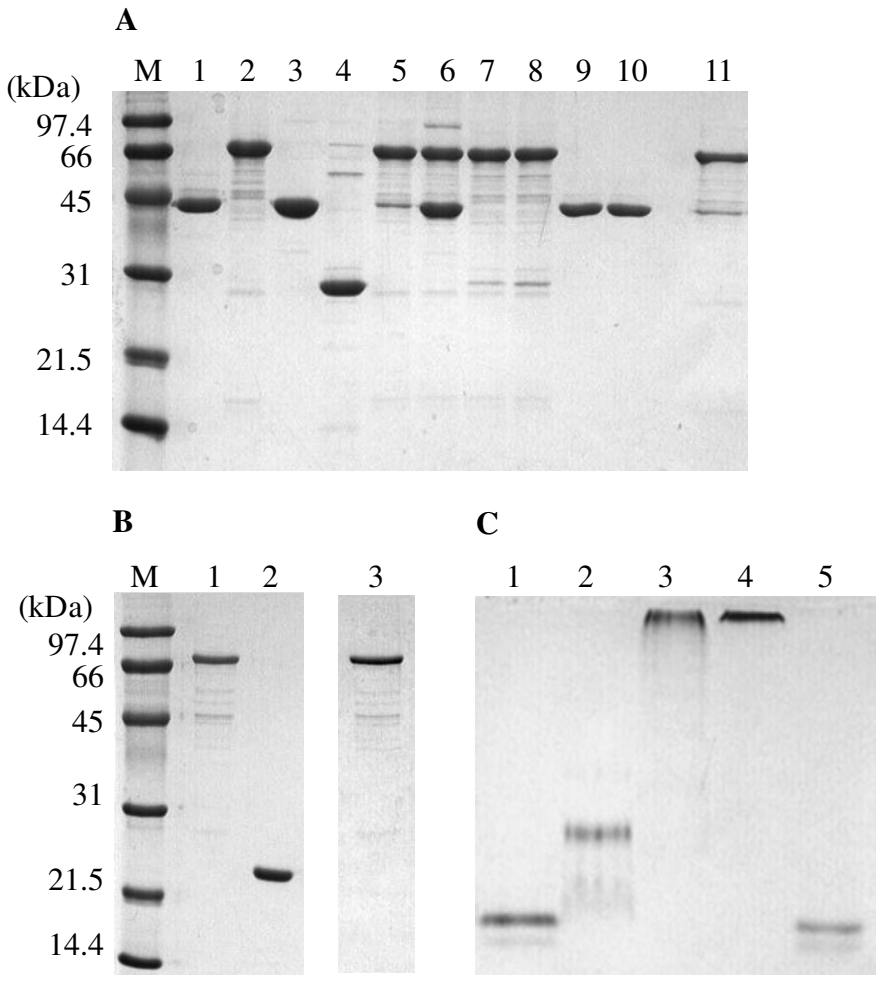

Figure 2.4: Interactions of MBP-UreD with other urease components *in vitro*. Purified MBP-UreD and MBP (2 μM) were tested for their abilities to form complexes with UreEF, UreE, or $UreG_{Str}$, (10 μM) in TEB buffer containing 25 mM NaCl (unless indicated otherwise). (A) SDS-PAGE analysis of purified components (lanes 1-4) and selected protein mixtures that were incubated at the indicated temperature and subjected to amylose resin chromatography with the fractions eluted by maltose analyzed (lanes 5-11). Lanes: M, molecular mass markers; 1, MBP; 2, MBP-UreD; 3, UreEF; 4, $UreG_{Str}$; 5, MBP-UreD and UreEF at 37 °C; 6, MBP-UreD and UreEF at 42 °C; 7, MBP-UreD and $UreG_{Str}$ at 37 °C; 8, MBP-UreD and $UreG_{Str}$ at 42 °C; 9, MBP and UreEF at 42 °C; 10, MBP and $UreG_{Str}$ at 42 °C; 11, MBP-UreD and UreEF at 42 °C in the presence of 1 M NaCl. (B) SDS-PAGE analysis of MBP-UreD interactions with UreE. Lanes: M, molecular mass markers; 1, MBP-UreD; 2, UreE; 3, maltose elution of chromatographed mixture of MBP-UreD and UreE incubated at 42 °C. (C) Native-PAGE analysis of the interaction of MBP and MBP-UreD with UreEF. Lanes: 1, MBP; 2, UreEF; 3, MBP-UreD; 4, maltose elution of chromatographed mixture MBP-UreD and UreEF incubated at 42 °C; 5, elution of MBP and UreEF incubated at 42 °C.

42 °C was examined in buffer containing 1 M NaCl, the UreEF:MBP-UreD ratio dropped (to 0.19:1) indicating that the interaction between these two species is sensitive to high ionic strength (Figure 2.4, panel A, lane 11). A similar set of experiments performed using $UreG_{Str}$ indicated a weak interaction whether incubated at 37 °C (UreG:MBP-UreD ratio of 0.10:1; Figure 2.4, panel A, lane 7) or 42 °C (UreG:MBP-UreD ratio of 0.18:1; Figure 2.4, panel A, lane 8). The addition of 1 M NaCl to this protein mixture had no effect on complex formation (data not shown). To confirm that the UreD domain of MBP-UreD was responsible for the interaction with UreEF, an analogous pull-down experiment was carried out with purified MBP and UreEF. Because the UreEF and MBP bands overlap on SDS-PAGE (Figure 2.4, panel A, lane 9), the interaction between these species was examined by utilizing native PAGE (Figure 2.4, panel C). This analysis confirmed that MBP and UreEF do not form a complex. To test whether the UreE domain of UreEF was responsible for the complex formation between UreEF and MBP-UreD, purified UreE (Figure 2.4, panel B, lane 2) was mixed with MBP-UreD and examined; no interaction between UreE and MBP-UreD was detected (Figure 2.4, panel B, lane 3). When MBP-UreD was mixed with both UreEF and $UreG_{Str}$ at 42 °C, no increase in the affinity of MBP-UreD for $UreG_{Str}$ was noted; however, an approximately 1:1 complex between MBP-UreD and UreEF was present (data not shown). Therefore, a clear interaction between UreD and UreF was confirmed both *in vitro* and *in vivo*.

DISCUSSION

In this study we investigated the properties of a translational fusion between MBP and UreD, where the resulting MBP-UreD is the first soluble form of UreD to be described. The

fusion protein is stable and readily purified via sequential chromatography on amylose and Q-Sepharose resins, whereas the free UreD liberated by Factor Xa digestion was highly unstable and precipitated during chromatography or storage. In a similar way, digestion of a MBP-UreF fusion produced an unstable UreF (13). These results highlight the usefulness of the MBP domain for increasing the solubility of normally insoluble urease accessory proteins.

While MBP-UreD purified in the presence of EDTA was free of metal ions, it was shown that the UreD domain of this protein could bind reversibly either Ni^{2+} or Zn^{2+}, similar to the case for UreE (2, 8) and UreG (35, 36) from various microorganisms. All metal binding data were reasonably well fit by assuming a single type of binding site, although distinct sites with similar binding parameters are likely. For Ni^{2+}, the PAR and radioactive ^{63}Ni methods provided different results indicating 1.6 or 2.7 Ni^{2+} bound per UreD protomer with K_d of 24 or 50 μM, respectively. We suggest the latter set of data is more reliable because of its greater range of Ni^{2+} concentrations, and thus conclude that UreD binds approximately 2.5 Ni^{2+} per protomer. A non-integer number of bound Ni^{2+} can be explained by a binding site at the interface of two protomers in the quaternary structure. The PAR-derived data indicate the ability to bind 4 Zn^{2+} per protomer with a K_d of 5 μM, in excellent agreement with the Zn^{2+} K_i measured in two studies examining competition with $^{63}Ni^{2+}$ binding. Thus, we conclude that Zn^{2+} competes with 10-fold higher affinity for the Ni^{2+} binding sites on UreD and binds to at least one additional site. It is important to note, however, that the metal binding properties of UreD may differ dramatically when in complex with urease. For example, increased Ni^{2+} specificity could

potentially be present in the UreABC—UreD complex. Furthermore, activation of urease apoprotein within the UreABC—UreDFG complex by Ni^{2+}, CO_2, GTP, and UreE takes place even in the presence of Ni^{2+}-chelating agents; this linking of nucleotide hydrolysis to metallocenter assembly indicates that the process cannot simply be viewed from a thermodynamic perspective. Our finding that UreD binds metal ions suggests its involvement in Ni^{2+} translocation to the urease active site.

In order to show that MBP-UreD could function during *in vivo* urease maturation, complementation studies were performed either by transforming *E. coli* cells with the plasmid encoding the fusion protein and a second vector carrying a Δ*ureD* urease cluster or by using a single plasmid encoding a urease cluster with *malE-ureD* replacing wild-type *ureD*. Co-transformed cells exhibited the capacity to activate urease apoprotein, but only to ~10 % of the activity found in cells carrying the wild-type urease gene cluster; this low percentage of complementation coincides with that in a previous study in which *E. coli* extracts from co-transformed cells (with plasmids producing the *K. aerogenes* wild-type *ureD* or a *K. aerogenes* urease cluster with a partial *ureD* deletion) yielded a specific activity of 17.2 U mg^{-1} or 8.7% of that for extracts of cells containing the wild-type urease cluster (198.4 U mg^{-1}) (17). Thus we conclude that MBP-UreD behaves similarly to wild-type UreD during analogous *in vivo* complementation assays. *E. coli* soluble extracts from cells transformed with a single plasmid encoding an intact urease cluster with the *ureD* fusion replacing wild-type *ureD* yielded a specific activity corresponding to 33% of wild-type activity. Although this value is higher than that obtained with the co-transformant system, it still does not meet wild-type levels indicating

that the MBP domain likely hinders UreD functionality. Nevertheless, these results provide strong support that MBP-UreD is at least a partially functional form of UreD.

Utilizing the MBP domain of MBP-UreD as a convenient affinity tag for amylose binding, a series of pull-down studies were performed to map the *in vivo* protein-protein interaction network of UreD with other urease components. When overproduced in the same cell, the UreD domain of MBP-UreD was shown to interact with the structural subunits UreABC in the absence of other accessory proteins. This interaction was expected as a UreABC—UreD complex has been purified and characterized (23). When MBP-UreD was overproduced with a Δ-*ureD* cluster, a pull-down study showed that UreABC— (MBP-UreD) —UreFG was formed within the cell. The wild-type version of this complex, UreABC—UreDFG has been purified and shown to be highly competent for *in vitro* reconstitution with Ni^{2+} and bicarbonate (31). Also of interest was the demonstration that the UreD domain of MBP-UreD interacts with both UreF and UreG in the cell to form a soluble MBP-UreDFG complex. A previous study reported the purification of an insoluble UreDFG complex by using an ATP-linked column matrix (19), where the nucleotide binding is attributed to the UreG component of the heterotrimer (a UreDFG complex containing a mutation in the P-loop motif of UreG did not bind this resin). The UreDFG heterotrimer complex has been hypothesized to represent a physiologically relevant species that serves as a pre-formed molecular chaperone (19). Preparing this complex with soluble MBP-UreD, now shown to be feasible by the experiments described here, may allow further exploration of the function of this species during urease *in vivo* maturation.

In addition to its simultaneous interactions with multiple urease components in the cell, the UreD domain of MBP-UreD also formed individual complexes *in vivo* with UreF or UreG, but not UreE. These data are in agreement with previous yeast two-hybrid studies in which a

UreD—UreF interaction was seen in *Proteus mirabilis* (9) and a UreH (UreD orthologue) — UreF interaction was observed in *H. pylori* (32). Densitometry analysis demonstrated that MBP-UreD bound approximately six times more UreF than UreG in these individual complexes; whereas, UreF and UreG are stoichiometric within the MBP-UreD—UreFG complex when these proteins were synthesized in the cell. The amount of UreG that co-eluted with MBP-UreD increased 2.7 fold when compared to the similar pull-down study without concomitant production of UreF. These data suggest that UreF within MBP-UreDF provides a cooperative binding surface that increases the affinity for UreG. Related to this result, a previous study focusing on the interactions of the UreEF fusion protein with other urease components demonstrated a weak or transient interaction between the UreF domain of that fusion protein and UreG. Together these data indicate that UreD and UreF likely interact prior to UreG binding when forming the UreDFG complex, rather than UreG binding individually first with UreD or UreF.

To further investigate the interactions between the UreD domain of MBP-UreD and other urease proteins, purified components were mixed and monitored for their interactions by using a similar pull-down system. Surprisingly, isolated MBP-UreD did not form a complex with purified urease apoprotein even though a complex was formed when paired cell extracts containing the two proteins were mixed. Furthermore, the addition of cell extracts to the mixture of purified proteins failed to stimulate complex formation. These results demonstrate that concomitant folding is not a pre-requisite for these two species to interact; however, they suggest that the purification process somehow renders MBP-UreD or urease apoprotein incompetent to bind each another. For MBP-UreD and UreEF, a direct ~1:1 stoichiometric complex was observed when the two species were incubated at 42 °C prior to the pull-down experiment. If the

ratio of UreEF to MBP-UreD is recalculated by dividing the integrated density value for each protein band (Figure 2.4, panel A, lane 6) by the molecular mass of that protein, the new ratio becomes 3.8:1. Similar samples on different gels yielded ratios between 0.72-1.5:1 indicating a high level of variability among replicates. Nevertheless, the positive effect of increasing temperature on the stoichiometry of UreEF to MBP-UreD was observed in several experiments. Of note, the crystal structure of truncated UreF from *H. pylori* indicates the protein exists as a dimer (15); thus, UreEF:MBP-UreD ratios approaching 2:1 could reflect dimeric UreEF binding to MBP-UreD. The interaction was shown to exist between the UreD domain of MBP-UreD and the UreF domain of UreEF, since purified MBP did not interact with UreEF and UreE did not interact with MBP-UreD under identical conditions. Additionally, the inclusion of 1 M NaCl to the pull-down assay resulted in a sub-stoichiometric complex indicating that UreD and UreF may bind one another via electrostatic interactions. By contrast, only a weak or transient interaction was seen between the UreD domain of MBP-UreD and UreG; furthermore, this interaction was not enhanced by the addition of UreEF. The distinction between these results and the *in vivo* pull-down investigations, where UreF increased the interaction between UreG and MBP-UreD, may be due to steric interference by the UreE domain of UreEF, to the need for an unidentified cellular component that was not present in the *in vitro* assay, or to an unidentified change in one of the proteins during purification.

In conclusion, our studies with MBP-UreD have uncovered the previously unknown metal-binding capability of UreD and revealed new aspects of its interactions with other urease components. Consistent with previous studies that characterized urease apoprotein alone and in complex with UreD, UreDF, and UreDFG (20, 23, 31), we show here that MBP-UreD can form such complexes *in vivo* and, in a subset of these cases, *in vitro* as well. The different urease

apoprotein complexes each have distinct activation properties. Of particular significance, the importance of UreD is shown by the finding that ~30% of the nascent active sites in purified UreABC—UreD can form active enzyme, whereas only ~15% of UreABC alone is activated in solutions containing Ni^{2+} and bicarbonate ions (24). These data suggest that UreD plays an important role in apoprotein activation, but that role remains enigmatic. The metal-binding capacity of MBP-UreD leads us to hypothesize that these binding sites contribute to UreD's function during the activation process. Two other urease accessory proteins, UreG and UreE, are known to bind various metal ions. For example, UreG from *Bacillus pasteurii* binds two Zn^{2+} or four Ni^{2+} per dimer, and that from *H. pylori* binds 0.5 Zn^{2+} or 2 Ni^{2+} per monomer (35, 36). Similarly, UreE from *K. aerogenes*, *B. pasteurii*, and *H. pylori* are known to bind both $Ni^{2+}$and Zn^{2+} (1, 2, 34). Taking together our equilibrium dialysis of MBP-UreD and the protein-protein interaction network we have clarified, we speculate that the accessory proteins work together to carry out sequential transfers of Ni^{2+} from UreE to UreG to UreD to the urease active site (Figure 2.6). Regardless of the physiological relevance of this model for sequential metal binding, the present results provide clear support for the hypothesis that UreD directly participates in Ni^{2+} transfer to urease apoprotein during *in vivo* maturation.

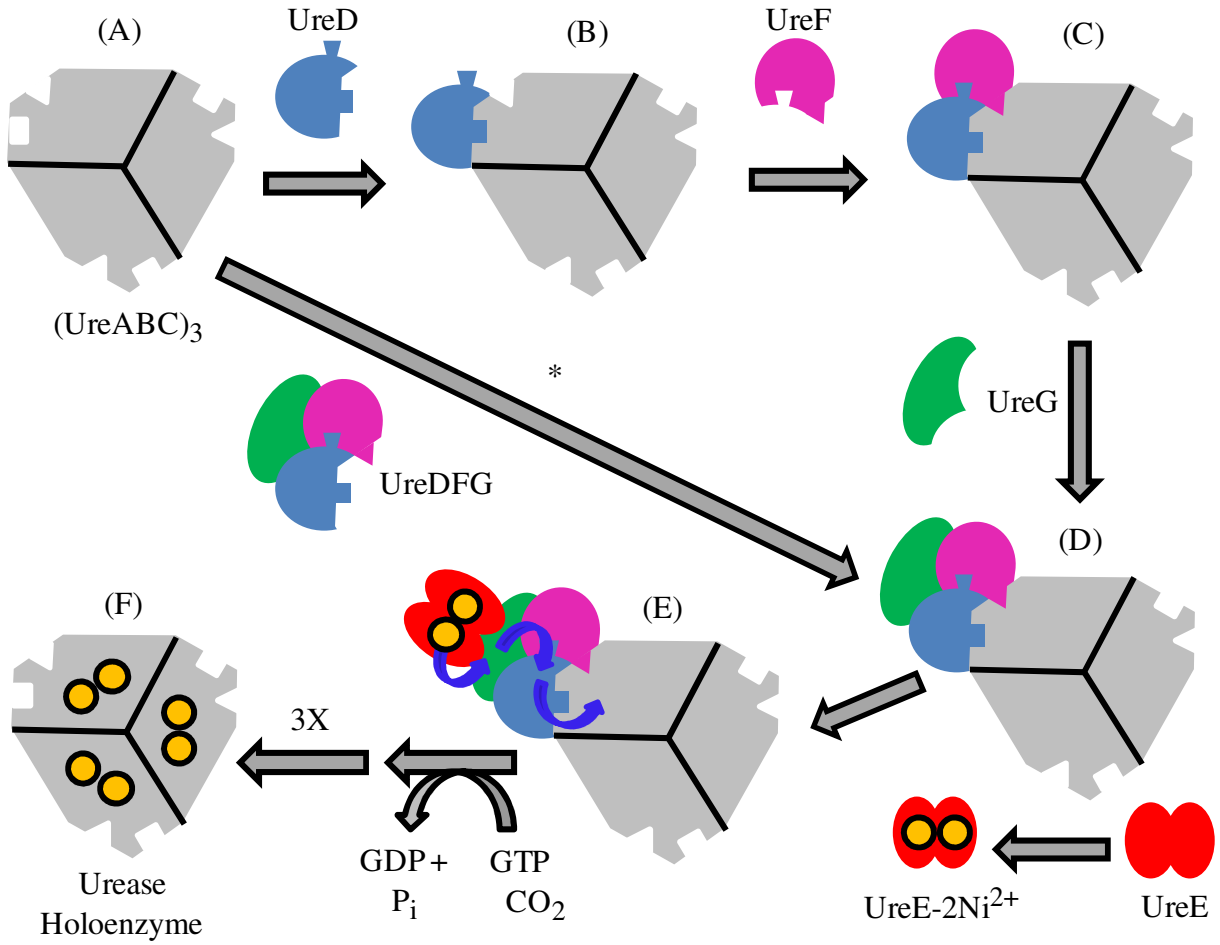

Figure 2.6: Working model of urease activation. The urease apoprotein trimer-of-trimers (A) sequentially binds UreD, UreF, and UreG to form UreABC—UreD (B), UreABC—UreDF (C), and UreABC—UreDFG (D). Alternatively, UreDFG may exist as a pre-formed molecular chaperone that directly binds the urease apoprotein as indicated by the asterisk. Urease apoprotein binds to UreD and, less well, to UreF; UreD and UreF bind each other; and UreG binds to these proteins with no direct interactions to urease. The UreE metallochaperone delivers Ni^{2+} via an interaction with UreG (E). *In vivo*, urease activation requires CO_2 to carboxylate a nascent active site lysine along with GTP which is bound and hydrolyzed by UreG in the activation complex. Coupled to this process, we propose the directed transfer of Ni^{2+} from UreE to UreG to UreD and finally into the urease apoprotein to generate active enzyme (F).

BIBLIOGRAPHY

BIBLIOGRAPHY

1. **Benoit, S., and R. J. Maier.** 2003. Dependence of *Helicobacter pylori* urease activity on the nickel-sequestering ability of the UreE accessory protein. Journal of Bacteriology **185:**4787-4795.

2. **Brayman, T. G., and R. P. Hausinger.** 1996. Purification, characterization, and functional analysis of a truncated *Klebsiella aerogenes* UreE urease accessory protein lacking the histidine-rich carboxyl terminus. Journal of Bacteriology **178:**5410-5416.

3. **Carter, E. L., N. Flugga, J. L. Boer, S. B. Mulrooney, and R. P. Hausinger.** 2009. Interplay of metal ions and urease. Metallomics **1:**207-221.

4. **Colpas, G. J., T. G. Brayman, J. McCracken, M. A. Pressler, G. T. Babcock, L.-J. Ming, C. M. Colangelo, R. A. Scott, and R. P. Hausinger.** 1998. Spectroscopic characterization of metal binding by *Klebsiella aerogenes* UreE urease accessory protein. Journal of Biological Inorganic Chemistry **3:**150-160.

5. **Colpas, G. J., T. G. Brayman, L.-J. Ming, and R. P. Hausinger.** 1999. Identification of metal-binding residues in the *Klebsiella aerogenes* urease nickel metallochaperone, UreE. Biochemistry **38:**4078-4088.

6. **Colpas, G. J., and R. P. Hausinger.** 2000. *In vivo* and *in vitro* kinetics of metal transfer by the *Klebsiella aerogenes* urease nickel metallochaperone, UreE. Journal of Biological Chemistry **275:**10731-10737.

7. **Dykxhoorn, D. M., R. St. Pierre, and T. Linn.** 1996. A set of compatible *tac* promoter expression vectors. Gene **177:**133-136.

8. **Grossoehme, N. E., S. B. Mulrooney, R. P. Hausinger, and D. E. Wilcox.** 2007. Thermodynamics of Ni^{2+}, Cu^{2+}, and Zn^{2+} binding to urease metallochaperone UreE. Biochemistry **46:**10506-10516.

9. **Heimer, S. R., and H. L. Mobley.** 2001. Interaction of *Proteus mirabilis* urease apoprotein and accessory proteins identified with yeast two-hybrid technology. Journal of Bacteriology **183:**1423-1433.

10. **Jabri, E., M. B. Carr, R. P. Hausinger, and P. A. Karplus.** 1995. The crystal structure of urease from *Klebsiella aerogenes*. Science **268:**998-1004.

11. **Jabri, E., and P. A. Karplus.** 1996. Structures of the *Klebsiella aerogenes* urease apoprotein and two active-site mutants. Biochemistry **35:**10616-10626.

12. **Kim, J. K., and R. P. Hausinger.** 2006. The UreEF fusion protein provides a soluble and functional form of the UreF urease accessory protein. Journal of Bacteriology **188:**8413-8420.

13. **Kim, K. Y., C. H. Yang, and M. H. Lee.** 1999. Expression of the recombinant *Klebsiella aerogenes* UreF protein as a MalE fusion. Archives of Pharmaceutical Research **22:**274-278.

14. **Laemmli, U. K.** 1970. Cleavage of structural proteins during the assembly of the head of bacteriophage T4. Nature (London) **227:**680-685.

15. **Lam, R., V. Romanov, K. Johns, K. Battaile, J. Wu-Brown, J. L. Guthrie, R. P. Hausinger, E. Pai, and N. Y. Chirgadze.** 2010. Structure of a truncated urease accessory protein UreF from *Helicobacter pylori*. Proteins **78:**2839-2848.

16. **Leach, M. R., and D. B. Zamble.** 2007. Metallocenter assembly of the hydrogenase enzymes. Current Opinion in Chemical Biology **11:**159-165.

17. **Lee, M. H., S. B. Mulrooney, M. J. Renner, Y. Markowicz, and R. P. Hausinger.** 1992. *Klebsiella aerogenes* urease gene cluster: Sequence of *ureD* and demonstration that four accessory genes (*ureD*, *ureE*, *ureF*, and *ureG*) are involved in nickel metallocenter biosynthesis. Journal of Bacteriology **174:**4324-4330.

18. **Lee, M. H., H. S. Pankratz, S. Wang, R. A. Scott, M. G. Finnegan, M. K. Johnson, J. A. Ippolito, D. W. Christianson, and R. P. Hausinger.** 1993. Purification and characterization of *Klebsiella aerogenes* UreE protein: A nickel-binding protein that functions in urease metallocenter assembly. Protein Science **2:**1042-1052.

19. **Moncrief, M. B. C., and R. P. Hausinger.** 1997. Characterization of UreG, identification of a UreD-UreF-UreG complex, and evidence suggesting that a nucleotide-binding site in UreG is required for in vivo metallocenter assembly of *Klebsiella aerogenes* urease. Journal of Bacteriology **179:**4081-4086.

20. **Moncrief, M. B. C., and R. P. Hausinger.** 1996. Purification and activation properties of UreD-UreF-urease apoprotein complexes. Journal of Bacteriology **178:**5417-5421.

21. **Mulrooney, S. B., and R. P. Hausinger.** 2003. Nickel uptake and utilization by microorganisms. FEMS Microbiology Reviews **27:**239-261.

22. **Mulrooney, S. B., H. S. Pankratz, and R. P. Hausinger.** 1989. Regulation of gene expression and cellular localization of cloned *Klebsiella aerogenes* (*K. pneumoniae*) urease. Journal of General Microbiology **135:**1769-1776.

23. **Park, I.-S., M. B. Carr, and R. P. Hausinger.** 1994. *In vitro* activation of urease apoprotein and role of UreD as a chaperone required for nickel metallocenter assembly. Proceedings of the National Academy of Sciences, United States of America **91:**3233-3237.

24. **Park, I.-S., and R. P. Hausinger.** 1995. Requirement of carbon dioxide for *in vitro* assembly of the urease nickel metallocenter. Science **267:**1156-1158.

25. **Quiroz-Valenzuela, S.** 2008. New insights in the urease activation process obtained by characterization of apourease complexes and the UreG accessory protein of *Klebsiella aerogenes*. Thesis. Michigan State University.

26. **Rain, J.-C., L. Selig, H. de Reuse, V. Battaglia, C. Reverdy, S. Simon, G. Lenzen, F. Petel, J. Wojcik, V. Schächter, Y. Chemama, A. Labigne, and P. Legrain.** 2001. The protein-protein interaction map of *Helicobacter pylori*. Nature **409:**211--215.

27. **Rubio, L. M., and P. W. Ludden.** 2005. Maturation of nitrogenase: A biochemical puzzle. Journal of Bacteriology **187:**405-414.

28. **Sambrook, J., E. F. Fritsch, and T. Maniatis.** 1989. Molecular cloning: A laboratory manual, 2nd ed, vol. Cold Spring Harbor Laboratory, Cold Spring Harbor, NY.

29. **Song, H. K., S. B. Mulrooney, R. Huber, and R. P. Hausinger.** 2001. Crystal structure of *Klebsiella aerogenes* UreE, a nickel-binding metallochaperone for urease activation. Journal of Biological Chemistry **276:**49359-49364.

30. **Soriano, A., G. J. Colpas, and R. P. Hausinger.** 2000. UreE stimulation of GTP-dependent urease activation in the UreD-UreF-UreG-urease apoprotein complex. Biochemistry **39:**12435-12440.

31. **Soriano, A., and R. P. Hausinger.** 1999. GTP-dependent activation of urease apoprotein in complex with the UreD, UreF, and UreG accessory proteins. Proceedings of the National Academy of Sciences, United States of America **96:**11140-11144.

32. **Voland, P., D. L. Weeks, E. A. Marcus, C. Prinz, G. Sachs, and D. Scott.** 2003. Interactions among the seven *Helicobacter pylori* proteins encoded by the urease gene cluster. Liver Physiology **284:**G96-G106.

33. **Weatherburn, M. W.** 1967. Phenol-hypochlorite reaction for determination of ammonia. Analytical Chemistry **39:**971-974.

34. **Won, H.-S., Y.-H. Lee, J.-H. Kim, I. S. Shin, M. H. Lee, and B.-J. Lee.** 2004. Structural characterization of the nickel-binding properties of *Bacillus pasteurii* UreE in solution. Journal of Biological Chemistry **279:**17466-17472.

35. **Zambelli, B., M. Stola, F. Musiani, K. De Vriendt, B. Samyn, B. Devreese, J. Van Beeumen, A. Dikiy, D. A. Bryant, and S. Ciurli.** 2005. UreG, a chaperone in the urease assembly process, is an intrinsically unstructured GTPase that specifically binds Zn^{2+}. Journal of Biological Chemistry **280:**4684-4695.

36. **Zambelli, B., P. Turano, F. Musiani, P. Neyroz, and S. Ciurli.** 2009. Zn^{2+}-linked dimerization of UreG from *Helicobacter pylori*, a chaperone involved in nickel trafficking and urease activation. Proteins **74:**222-239.

CHAPTER 3

The Function of UreB in *Klebsiella aerogenes* Urease

This work was published in the journal *Biochemistry*, 2011, 50 (43), pp 9296–9308, with the authors listed as Eric L. Carter, Jodi L. Boer, Mark A. Farrugia, Nicholas Flugga, Christopher L. Towns, and Robert P. Hausinger

E.L.C. designed and performed the majority of the research and wrote the initial draft of paper; J.L.B. performed metal content studies; M.A.F performed the *in vitro* pull-down experiment; N.F. generated plasmid constructs; and C.L.T. assisted with the research

ABSTRACT

Urease from *Klebsiella aerogenes* is composed of three subunits (UreA, UreB, and UreC) which assemble into a $(UreABC)_3$ quaternary structure. UreC harbors the dinuclear nickel active site, whereas the functions of UreA and UreB remain unknown. UreD and UreF accessory proteins previously were suggested to reposition UreB and increase exposure of the nascent urease active site, thus facilitating metallocenter assembly. In this study, cells were engineered to separately produce $(UreAC)_3$ or UreB, and the purified proteins were characterized. Monomeric UreB spontaneously binds to the trimeric heterodimer of UreA plus UreC to form $(UreABC^*)_3$ apoprotein, as shown by gel filtration chromatography, integration of electrophoretic gel band intensities, and mass spectrometry. Similar to authentic urease apoprotein, active enzyme is produced by incubation of $(UreABC^*)_3$ with Ni^{2+} and bicarbonate. Conversely, UreBΔ1-19, lacking the 19 residue potential hinge and tether to UreC, does not form a complex with $(UreAC)_3$ and yields negligible levels of active enzyme when incubated under activation conditions with $(UreAC)_3$. Comparison of activities and nickel contents for $(UreAC)_3$, $(UreABC^*)_3$, and $(UreABC)_3$ samples treated with Ni^{2+} and bicarbonate and then desalted indicates that UreB facilitates efficient incorporation of the metal into the active site and protects the bound metal from chelation. Amylose resin pull-down studies reveal that MBP-UreD (a fusion of maltose binding protein with UreD) forms complexes with $(UreABC)_3$, $(UreAC)_3$, and UreB *in vivo*, but not *in vitro*. By contrast, MBP-UreD does not form an *in vivo* complex with UreBΔ1-19. The soluble MBP-UreD—UreF—UreG complex binds *in vitro* to

$(UreABC)_3$, but not to $(UreAC)_3$ or UreB. Together these data demonstrate that UreB facilitates the interaction of urease with accessory proteins during metallocenter assembly, with the N-terminal hinge and tether region being specifically required for this process. In addition to its role in urease activation, UreB enhances the stability of UreC against proteolytic cleavage.

INTRODUCTION

Urease hydrolyses urea to ammonia and carbamic acid, with the latter compound spontaneously decomposing to form a second molecule of ammonia and carbonic acid (5, 42). Of medical importance, the human gastric ulcer-causing bacterium *Helicobacter pylori* employs urease as an essential virulence factor during colonization of stomach tissue, and uropathogens commonly produce urease that is directly related to stone formation and pyelonephritis (20). This enzyme is also important in agriculture as seed germination is accompanied by release of urea that must be decomposed via plant urease for subsequent nitrogen assimilation, and urease produced by soil-borne microbes catalyzes the spurious degradation of urea-containing fertilizers (19, 40). Furthermore, urease has historical and basic research significance: it was the first enzyme to be crystallized (34) and the first shown to contain nickel (10), a cofactor essential for its activity.

The *in vivo* maturation of urease requires the concerted effort of several accessory proteins, a process that has served as a paradigm for metallocenter assembly (5, 42). In the best-studied model system, that involving the expression of *Klebsiella aerogenes* urease genes (*ureDABCEFG*) in *Escherichia coli*, the metallochaperone UreE (18) delivers Ni^{2+} to an activation complex consisting of the $(UreABC)_3$ urease apoprotein along with UreD, a molecular

chaperone that is thought alter urease apoprotein conformation and also binds metal (6, 23), UreF, a putative GTPase activating protein (15, 17, 30), and UreG, a Ni^{2+} and Zn^{2+}-binding GTPase (4, 21). In a process that is not well understood, CO_2 forms a Lys-carbamate bridging ligand at the nascent active site, GTP is hydrolyzed by UreG, Ni^{2+} is transferred from UreE (possibly via UreG and UreD) to the appropriate ligands in $(UreABC)_3$, and the accessory proteins dissociate, providing the fully active holoprotein. Additional studies hint that a UreD—UreF—UreG heterotrimeric complex interacts with urease apoprotein, rather than the sequential binding of the individual accessory proteins (5, 6, 21).

Various forms of the urease apoprotein are partially activated *in vitro* by incubation with excess bicarbonate (as a CO_2 donor) and Ni^{2+} ions. Whereas $(UreABC)_3$ is activated under optimized conditions to levels representing ~16% of the fully active enzyme [i.e., ~400 U (mg of protein)$^{-1}$ versus 2500 U (mg of protein)$^{-1}$, respectively, where U represents units of μmol urea degraded min^{-1} at 37 °C], the $(UreABC)_3$—UreD, $(UreABC)_3$—UreD—UreF, and $(UreABC)_3$—UreD—UreF—UreG complexes are activated to ~25%, ~30%, and ~50%, respectively of this level (22, 24, 25, 33). Furthermore, incubation of $(UreABC)_3$—UreD—UreF—UreG with UreE, Mg^{2+}-GTP, and physiologically relevant levels of Ni^{2+} and bicarbonate lead to wild-type levels of activity (32). These results illustrate the importance of accessory proteins, Mg^{2+}-GTP, and CO_2 in the efficient assembly of the urease active site.

Crystal structures of urease from *K. aerogenes* (14, 26), *Bacillus pasteurii* (2, 3), *H. pylori* (12), and jack bean (*Canavalia ensiformis*) (1) have been solved, each revealing highly

similar tertiary structures and essentially identical active sites containing a dinuclear nickel metallocenter bridged by a Lys-carbamate and a solvent molecule [the *K. aerogenes* structure is shown in (Figure 3.1)]. A related urease from *Helicobacter mustelae* has been structurally characterized and shown to contain a dinuclear iron metallocenter (7). In *K. aerogenes* urease, the 60.3-kDa UreC subunit harbors the active site while the UreA and UreB small subunits (11.1 kDa and 11.7 kDa, respectively) have no obvious role in catalysis, but contribute to the overall $(UreABC)_3$ quaternary structure. The function of each subunit (or protein domain for ureases where the subunits are fused) is likely the same for ureases from different organisms.

Studies focused on the interaction of accessory proteins with *K. aerogenes* urease have provided potential insights into a role for UreB during urease activation. In a chemical cross-linking investigation, amine group-specific reagents were used to treat several urease apoprotein complexes, followed by mass spectrometric analysis of tryptic peptides (8). In particular, a cross-link was detected in the $(UreABC)_3$—UreD—UreF complex between UreB Lys76 and UreC Lys382—residues which are distant from each other in the enzyme crystal structure. This finding was interpreted as indicating a UreD—UreF-induced conformational change in UreB, where the shift in its position allows greater access to the buried active site by CO_2 and Ni^{2+} (e.g., note the increased accessibility of the nickel atoms after removal of UreB from the crystal structure in Figure 3.1, panel D). The UreB-shift hypothesis was supported by ProFlex computational analysis that identified increased flexibility of UreB residues 11-19 (28). This region was predicted to be a hinge that potentially allowed UreB's main domain, which exhibited

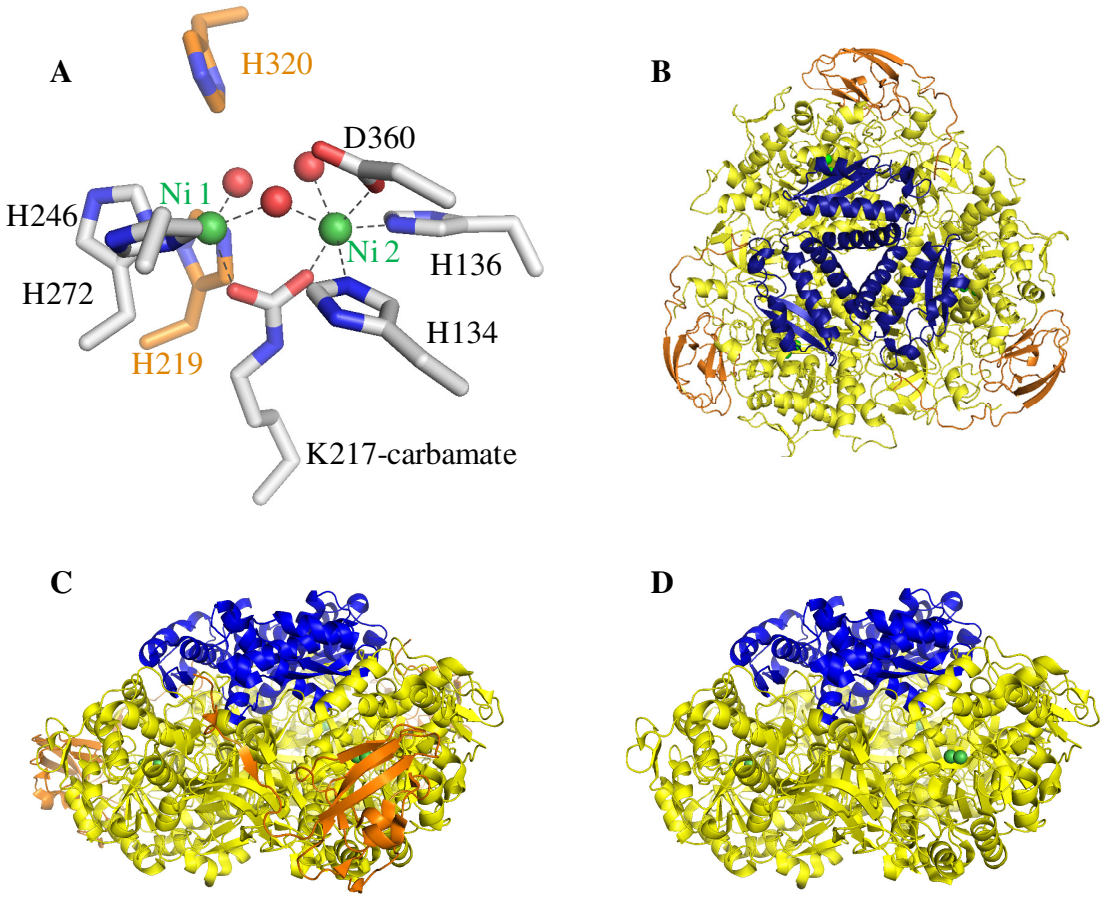

Figure 3.1: Structure of *K. aerogenes* urease. (A) Dinuclear nickel active site of urease. The two nickel atoms (green) are bridged by a Lys-carbamate and a hydroxyl group. Ni 1 also is coordinated by two His and a terminal solvent, while Ni 2 also has 2 His, an Asp, and a terminal water. Waters are red, metal-binding side chains are depicted with white carbons, and two nearby His residues that function in catalysis are shown with orange carbons. (B and C) Two views of the $(UreABC)_3$ cartoon structure with UreA in blue, UreB in orange, UreC in yellow, and nickel atoms in green. (D) Same view as panel C, but with the UreB subunits removed. Figures were prepared using PYMOL and PDB access code 1FWJ.

only weak interactions with UreC, to move while remaining anchored via residues 2-8. Additional structural evidence for UreB's role is derived from small-angle X-ray scattering of $(UreABC)_3$—UreD and $(UreABC)_3$—UreD—UreF; modeling of the data indicate UreD and UreF are positioned near UreB at the vertices of the triangular apoprotein (28). Together, these results point to UreB playing a crucial role during the *in vivo* activation of urease apoprotein.

In this study, *K. aerogenes* UreB and the complex of UreA plus UreC [demonstrated to be $(UreAC)_3$] were purified individually and shown to be capable of forming a stoichiometric complex *in vitro*. The resulting $(UreABC^*)_3$ apoprotein shares similar *in vitro* activation properties to authentic apoprotein purified from the cell. Additionally, metal analyses and activity assays of various activated species demonstrate that UreB is required for the efficient incorporation of Ni^{2+} into the active site and stabilizes the site against metal chelation. I also examine the protein-protein interaction network of UreB with other urease components *in vivo* and *in vitro* and show that UreB is partially responsible for the interaction of $(UreABC)_3$ with accessory proteins. Furthermore, I show that a UreB truncation mutant lacking the proposed hinge and tether region (i.e. N-terminal residues 1-19) is unable to associate with $(UreAC)_3$ or a soluble form of UreD. These results highlight the importance of UreB, especially its N-terminus, for interfacing with urease accessory proteins. Together, these data implicate UreB as a key player in facilitating the interaction of accessory proteins with urease apoprotein and directing the efficient incorporation of Ni^{2+} into the nascent active site. In addition, we show that UreB stabilizes urease against proteolytic cleavage.

MATERIALS AND METHODS

Plasmid construction. Standard molecular biology techniques were employed for construction of the plasmids described below and summarized in Appendix A (31). Polymerase chain reaction (PCR) was carried out with oligonucleotide primers purchased from IDT DNA (Coralville, IA) and *Pfu*Turbo® Hotstart PCR Master Mix (Stratagene, USA). *Escherichia coli*

DH5α (Invitrogen) was the host bacterial strain for cloning manipulations, and plasmids were verified by sequence analysis (Davis Sequencing, Davis, CA).

For the overproduction of UreB, pUreB was constructed by PCR amplification using a forward primer (5'-GGAGATATACCA*CATATG*ATCC-3') containing an NdeI restriction site (in italics), a reverse primer (5'-TGATGC*AAGCTT*CTATTACTCATCG-3') containing a HindIII restriction site, and pKK17 as a template (9). The resultant amplicon coding for full-length *ureB* (followed by successive ochre and amber stop codons for increased transcriptional termination efficiency) was digested with NdeI and HindIII, with the resultant *ureB*-containing fragment ligated into similarly digested pET-42b (Merck, Darmstadt, Germany).

To assess the function of the putative hinge and tether region of UreB encompassing the N-terminal residues 1-19, pUreBΔ1-19 was constructed by PCR amplification using a forward primer (5'-AGCTACGAG*CATATG*GCAACCTGTCGCGTGGTCGTTGAGAACCACGG-CGATC-3') containing an NdeI restriction site, a reverse primer (5'-TATA*GGATCC*CTATT-ACTCATCGTTTACCTCCAGAGGGCCCATGACC-3') containing a BamHI restriction site (plus tandem ochre and amber stop codons), and pUreB as a template. The resultant amplicon was digested with NdeI and BamHI, and the desired fragment ligated into similarly digested pET-42b. pUreBΔ1-19 encodes a Met residue followed by UreB residues 20-106.

To produce urease lacking UreB, the pUreAC vector was constructed coding for *ureA* and *ureC*. The *ureA* gene was amplified by using a forward primer (5'-AGTCAGAG*CCATG-G*AACTGACCCCCCGAC-3') containing an NcoI restriction site, a reverse primer (5'-AGTCA-GAG*CTTAAG*TCAGATAATCGGGTTGTGAACG-3') containing an AflII restriction site, and pKK17 as template. Similarly, *ureC* was amplified by using a forward primer (5'-AGCTACG-AG*CATATG*AGTAATATTTCACGC-3') containing an NdeI restriction site, a reverse primer

(5'-AGTCAGAG*TTAATTAA*AACAGAAAATATCGTTG-3') containing a PacI restriction site, and pKK17 as template. The resulting amplicons were digested with their respective restriction endonucleases and the appropriate fragments were stepwise ligated into similarly digested pETDuet-1 (Merck, Darmstadt, Germany).

For studies focusing on the interaction of UreD with $(UreAC)_3$, UreB, and UreBΔ1-19, pCDF-MBP-UreD was constructed by amplifying the *malE-ureD* transcriptional fusion from pEC002 (6), using a forward primer (5'-GCATA*GGTACC*ATGAAAATCG-3') containing a KpnI restriction site and a reverse primer (5'- TATA*AAGCTT*TTAAGTCAGCCAGATTCGGG-GAAG -3') containing a HindIII restriction site. The resultant amplicon was digested with KpnI and HindIII, and the desired fragment was ligated into similarly digested pCDF-1b (Merck, Darmstadt, Germany). pCDF-MBP-UreD encodes full-length MBP-UreD with an N-terminal His_6 tag.

Urease activity and protein assays. Urease activity was determined by measuring the rate of ammonia production, monitored by its conversion to indophenol with quantification at 625 nm (37). Aliquots of a reaction mixture consisting of 50 mM 4-(2-hydroxyethyl)piperazine-1-ethanesulfonic acid (HEPES), pH 7.8, 50 mM urea, 0.5 mM ethylenediaminetetraacetic acid (EDTA), and protein were removed at selected times and mixed with an alkaline solution of phenol and sodium nitroprusside. Protein concentrations were determined by using the Protein Assay reagent (Bio-Rad) with bovine serum albumin as a standard.

Polyacrylamide gel electrophoresis and Western blot analysis. Sodium dodecyl sulfate-polyacrylamide gel electrophoresis (SDS-PAGE) was performed by using standard buffers (16) and 12% polyacrylamide running gels with 4% stacking gels. Proteins were visualized with Coomassie brilliant blue stain. For Western blot analysis, SDS-PAGE gels were electroblotted

onto Immobilon-P polyvinylidene difluoride membranes (Millipore) and blotted with anti-*K. aerogenes* urease antibodies (27). Reactive protein bands were visualized with anti-rabbit IgG alkaline phosphatase-conjugated antibodies and 5-bromo-4-chloro-3-indolylphosphate/nitroblue tetrazolium liquid substrate (Sigma). Whereas the antibodies react strongly with UreB and UreC, they react only weakly with UreA. Gel scanning was carried out by using AlphaEaseFC software (Alpha Innotech Corp., San Leandro, California) and assuming the following molecular masses: UreA, 11.1 kDa; UreB, 11.7 kDa; UreBΔ1-19, 9.8 kDa; UreC, 60.3 kDa. Molecular mass markers for Coomassie-stained gels and Western blots were purchased from Bio-Rad.

Protein purification. UreB was purified from *E. coli* BL21-Gold(DE3) cells (Stratagene, USA) harboring pUreB and grown in Lennox Broth (LB; Fisher Scientific) supplemented with 50 μg ml^{-1} of kanamycin with shaking at 37 °C until the cells reached an optical density at 600 nm ($O.D._{600}$) of ~0.5. Protein production was induced by the addition of 0.5 mM isopropyl β-D-1-thiogalactopyranoside (IPTG). The cultures were incubated overnight and harvested by centrifugation. Cell pellets were suspended in PEB buffer [20 mM Na-phosphate, pH 7.4, 1 mM EDTA, and 1 mM 2-mercaptoethanol (β-ME)] and disrupted by sonication using a Branson Sonifier (3-4 cycles, 2 min per cycle, 50% duty cycle, power level 3-5, and cooling in an ice water-ethanol bath between cycles). Soluble cell-free extracts were obtained by centrifuging the cell lysate for 45-60 min at 120,000 *g* and applied to DEAE-Sepharose (2.5 cm x 13 cm; GE Healthcare) equilibrated in PEB. Unbound species were allowed to flow through before starting a linear gradient from 0-1 M KCl in PEB over ~6 column volumes. UreB eluted in the latter portion of the flow-through fractions and the beginning of the linear gradient. Fractions containing UreB were verified by SDS-PAGE, pooled, and concentrated to ~1 ml by using both an Amicon ultrafiltration stir cell equipped with a 10,000 molecular weight cut-off (MWCO)

membrane and a 10,000 MWCO Amicon centrifugal filter device (Millipore). The sample was loaded onto a preparative Superdex-75 (GE Healthcare) column (1.5 cm x 68 cm) equilibrated in PEB. Fractions containing UreB were identified by SDS-PAGE, pooled, and buffer exchanged either by dialysis or by repeated concentration/dilution into HT buffer [50 mM HEPES, pH 7.8, and 1 mM tris(2-carboxyethyl)phosphine hydrochloride (TCEP)] before snap-freezing in liquid N_2 prior to storage at -80 °C. Protein stored in this manner was stable for at least a month.

UreBΔ1-19 was purified from *E. coli* BL21-Gold(DE3) harboring pUreBΔ1-19 by a process similar to that for UreB. In this case, however, the cells were supplemented with 1 mM IPTG and grown for an additional 3 h prior to harvesting by centrifugation.

UreAC [shown to be $(UreAC)_3$] was purified from *E. coli* BL21-Gold(DE3) harboring pUreAC and grown in LB supplemented with 300 μg ml^{-1} of ampicillin with shaking at 37 °C until the cells reached $O.D._{600}$ of ~0.5. Protein production was induced by the addition of 1 mM IPTG, the cultures were incubated under the same conditions for 3 h, and cells were harvested by centrifugation. Cell pellets were suspended in PEB buffer, and a soluble cell-free extract was prepared and chromatographed on DEAE-Sepharose as described above for the purification of UreB. $(UreAC)_3$ eluted at approximately the midpoint of the KCl gradient, similar to the anion-exchange chromatographic behavior of fully assembled urease, $(UreABC)_3$ (35). Fractions containing $(UreAC)_3$ were identified by SDS-PAGE, pooled, and adjusted to 1.5 M KCl by dialysis. The sample was filtered and applied to phenyl-Sepharose CL-4B (2.5 cm x 13 cm; GE Healthcare) equilibrated in PEB containing 1.5 M KCl. Unbound species were eliminated by washing with equilibration buffer before step eluting the bound $(UreAC)_3$ with PEB. Fractions

containing $(UreAC)_3$ were identified by SDS-PAGE, pooled, buffer exchanged into HT, and stored similarly to UreB. These samples also were stable for at least one month at -80 °C.

Urease apoprotein was purified from *E. coli* cells harboring pKAU22Δ*ureD-1* that were grown in LB supplemented with 300 μg ml^{-1} of ampicillin with shaking at 37 °C overnight before harvesting by centrifugation. Cell pellets were suspended in PEB and the remaining purification steps were performed as previously described (6), except pure $(UreABC)_3$ was buffer exchanged into HT and stored similarly to UreB and $(UreAC)_3$.

The soluble, heterotrimeric, accessory protein complex MBP-UreD—UreF—UreG was purified from *E. coli* BL21-Gold(DE3) cells harboring plasmids pEC002 and pEC005 (6). The former plasmid encodes MBP-UreD and the latter encodes UreF and UreG. The cells were grown in LB supplemented with 300 μg ml^{-1} of ampicillin and 50 μg ml^{-1} of chloramphenicol with shaking at 37 °C until reaching $O.D._{600}$ of ~0.4. Protein production was induced with 0.5 mM IPTG, the cultures were incubated at 28 °C with shaking for 16 h, and cells were harvested by centrifugation. Cell pellets were resuspended in TEB [20 mM 2-amino-2-(hydroxymethyl)-1,3-propanediol (Tris)-HCl, pH 7.5, 1 mM EDTA, 1 mM β-ME] containing 25 mM NaCl and disrupted by sonication as described above. Soluble cell-free extracts were obtained by ultracentrifugation (under conditions identical to those for the purification of UreB) and loaded directly onto a 2.5 cm x 6.1 cm amylose resin column (New England Biolabs) equilibrated in resuspension buffer. The column was washed in the same buffer until the A_{280} reached baseline, and protein was eluted with two bed volumes of TEB containing 25 mM NaCl and 10 mM maltose. The eluted fractions were pooled and loaded directly onto a DEAE-Sepharose column

(2.5 cm x 13 cm) equilibrated in TEB. The column was washed with 1.5 bed volumes of TEB buffer before a linear gradient from 0 to 1 M NaCl was applied in the same buffer. Fractions containing MBP-UreD—UreF—UreG were identified by SDS-PAGE, pooled, and concentrated by using a 10,000 MWCO Amicon centrifugal filter device to a final volume of 1 ml. The sample was buffer exchanged into TEB containing 25 mM NaCl by dialysis and loaded onto a Superdex-200 column (1.5 cm x 68 cm) equilibrated in the same buffer. Elution fractions were analyzed by SDS-PAGE and those containing pure MBP-UreD—UreF—UreG were pooled and concentrated in the same manner as noted above.

MBP-UreD was purified from *E. coli* BL21-Gold(DE3) cells containing pEC002, as previously described (6).

Complex formation, analytical gel filtration, and Matrix-Assisted Laser Desorption Ionization Time of Flight Mass Spectrometry (MALDI-TOF MS). Complex formation between $(UreAC)_3$ and either UreB or UreBΔ1-19 was monitored by gel filtration chromatography. In 1 ml final volume of HT buffer, $(UreAC)_3$ (42 μM) was mixed with UreB or UreBΔ1-19 (208 μM). The mixture was incubated at room temperature for 15 min and chromatographed on a Superdex-200 column (1.5 cm x 68 cm) that was equilibrated in TBS (50 mM Tris-HCl, pH 7.4, 150 mM NaCl) using a BioLogic LP System (Bio-Rad, CA). The column eluant was monitored at 280 nm, fractions correlating to absorbance peaks were pooled and concentrated by using a 10,000 MWCO Amicon centrifugal filter device, and the fractions were analyzed by SDS-PAGE.

The native molecular masses of $(UreAC)_3$ and UreB were estimated by using gel filtration chromatography. Samples (40 μl) of $(UreAC)_3$ (10 mg ml^{-1}) and UreB (1.2 mg ml^{-1})

in 50 mM Na-phosphate, pH 7.0, were chromatographed on a Shodex KW-804 column (8 x 300 mm; Shodex, Japan) equilibrated in the same buffer by using a Waters Breeze chromatography system while monitoring the A_{280} of the elution buffer. Another approach included chromatography of $(UreAC)_3$ (200 µl, 12.9 mg ml^{-1}) on a Superdex-200 column (1.5 cm x 68 cm) equilibrated in 20 mM Tris-HCl, pH 7.4, 1 mM EDTA, 1 mM β-ME, and 25 mM NaCl using a BioLogic LP System while monitoring the A_{280} of the elution buffer. Columns were standardized with a set of molecular mass markers (Bio-Rad). The retention times of the standards were plotted versus the logarithm of their molecular masses; the slope derived from the linear regression of the data points was used to estimate the molecular mass of $(UreAC)_3$ or UreB based on their retention times.

To verify the protein content of gel filtration chromatography fractions, MALDI-TOF MS was utilized. Samples of authentic urease apoprotein $(UreABC)_3$, UreBΔ1-19, and selected gel filtration chromatography pools were buffer exchanged into deionized water and diluted to a final concentration of 1 µg $µl^{-1}$ in 40% acetonitrile containing 0.1% trifluoroacetic acid. Samples were diluted 1:1 with a solution of 20 mg ml^{-1} sinapic acid prepared in 40% acetonitrile plus 0.1% trifluoroacetic acid, and 2 µl samples of each preparation were spotted onto a Kratos Analytical MALDI MS plate and analyzed in a Shimadzu Axima CFR Plus MALDI-TOF MS. Spectra were standardized with human insulin (MH^+ = 5808.7 Da) and apomyoglobin (MH^+ = 16952.6).

Circular dichroism (CD). $(UreAC)_3$ (10 µM heterodimer), UreB (100 µM), the complex derived from these species denoted $(UreABC^*)_3$ (10 µM heterotrimer), and UreBΔ1-19 (100 µM) in HT buffer were diluted to the indicated concentrations in 50 mM Na-phosphate, pH 7.0. Parallel solutions containing the same mixtures of protein-free HT buffer plus 50 mM Na-phosphate, pH 7.0, were used for establishing baselines. Samples (300 µl) were placed in a Spectrosil 1 mm quartz cuvette (Starna Cells) equipped with a stopper and 3-4 scans were taken from 260-200 nm with 0.5 nm intervals and 20 sec reads per interval in a Chirascan CD Spectrometer (Applied Photophysics Limited; Leatherhead, U.K.) at ambient temperature. The baselines were subtracted, and the scans were averaged using Chirascan Pro-Data Viewer software.

In vitro *activation*. $(UreAC)_3$ (10 µM heterodimer), $(UreABC)_3$ (10 µM heterotrimer), and $(UreABC^*)_3$ (5 µM heterotrimer) were incubated for 1 h at 37 °C in standard activation buffer (100 mM HEPES, pH 8.3, 150 mM NaCl, 100 mM $NaHCO_3$, and 100 µM $NiCl_2$) unless otherwise indicated. The $(UreABC^*)_3$ sample was prepared by incubating $(UreAC)_3$ (100 µM) with UreB (500 µM) in 250 µl total volume of HT buffer at room temperature for 30 min, chromatographing on Superdex-200 as described above, and identifying appropriate fractions by SDS-PAGE. Aliquots of the reaction mixtures were assayed for urease activity as described above.

To assess the effect of UreB on activity following the *in vitro* activation process, 10 µM $(UreAC)_3$ was activated for 60 min at 37 °C under standard conditions in a total volume of 100 µl prior to addition of 10 µl of UreB (520 µM stock) with an additional incubation for 60 min at

37 °C before assaying aliquots for urease activity. Specific activities were calculated by using the concentration of the UreABC heterotrimer (i.e., 0.756 mg ml^{-1}) after the addition of UreB.

In addition, the effect of UreBΔ1-19 on the *in vitro* activation process was examined. $(UreAC)_3$ (100 µM) was mixed with UreBΔ1-19 (500 µM) in 20 µl total volume of HT and incubated for 30 min at ambient temperature. A portion (10 µl) of this mixture was transferred into 90 µl standard activation buffer, incubated at 37 °C for 60 min, and assayed for urease activity. Specific activities were calculated by using the concentration of UreAC heterodimer plus stoichiometric UreBΔ1-19 (i.e., 0.812 mg ml^{-1}), excluding the excess UreBΔ1-19.

Metal analysis of in vitro *activated species.* To assess the nickel content of activated $(UreABC^*)_3$, 120 µl $(UreAC)_3$ (370 µM heterodimer in HT buffer) was mixed with 120 µl of UreB (1450 µM in HT buffer) and incubated for 30 min at ambient temperature. The mixture was diluted to ~10 µM UreC protomer with 4.2 ml of standard activation buffer and incubated at 37 °C for 60 min. The sample was concentrated with a 10,000 MWCO Amicon centrifugal filter device (pre-washed with deionized water) to ~300 µl and either immediately chromatographed on a 1 cm x 43 cm Sephacryl S300 HR column (GE Healthcare) equilibrated in 100 mM HEPES, pH 8.3, or treated with 10 mM EDTA for 5 min at ambient temperature and chromatographed in the same buffer plus 1 mM EDTA. Fractions of interest were verified for protein content with SDS-PAGE, allowed to equilibrate at least 16 h at 4 ºC, concentrated by use of 10,000 MWCO Amicon centrifugal filter devices, and analyzed in parallel with protein-free buffer for metal content by inductively coupled plasma atomic emission spectroscopy (ICP-AES; Chemical Analysis Laboratory at the University of Georgia, Athens, GA).

For studies focusing on the nickel content of $(UreAC)_3$ after activation, similar methodology was employed as described above except that $(UreAC)_3$ (120 µl, 370 µM in HT buffer) was directly diluted to a final concentration of ~10 µM UreC protomer in activation buffer prior to concentration, ± EDTA treatment, and gel filtration chromatography. Lastly, 4.3 ml of $(UreAC)_3$ (~10 µM UreC protomer final concentration) was subjected to standard activation conditions at 37 °C for 60 min, mixed with 120 µl UreB (1450 µM in HT buffer), incubated at ambient temperature for 30 min, and analyzed for nickel content after concentration, ± EDTA treatment, and gel filtration chromatography as described above.

In vivo *amylose pull-down studies*. Competent *E. coli* BL21-Gold(DE3) cells were transformed with pCDF-MBP-UreD by following the manufacturer's instructions (Stratagene) and maintained on LB agar supplemented with spectinomycin at 66 µg ml^{-1}. The preceding strain was made competent by using $CaCl_2$ and co-transformed with either pEC004 (6), pUreAC, pUreB, or pUreBΔ1-19 by using a standard heat-shock transformation protocol (31). The resultant co-transformants were maintained on LB agar with spectinomycin at 66 µg ml^{-1} plus 50 µg ml^{-1} of chloramphenicol for the maintenance of pEC004, 100 µg ml^{-1} of ampicillin for pUreAC, or 50 µg ml^{-1} of kanamycin for pUreB. An overnight culture (5 ml) was used to inoculate 500 ml of LB that was supplemented with the same antibiotics as described for each strain (except that 300 µg ml^{-1} of ampicillin was used in liquid medium, rather than 100 µg ml^{-1}). The cells were grown with shaking at 37 °C to $O.D._{600}$ of ~0.5, at which point protein production was induced with 1 mM IPTG. The cultures were incubated under the same

conditions for an additional 3 h and harvested by centrifugation. Cell pellets were washed once with TBS, and suspended in 15 ml of TEB containing 25 mM NaCl. The slurries were disrupted by sonication using a Branson sonifier (see above). Soluble cell-free extracts were obtained by ultracentrifugation at 120,000 *g* for 1 h and loaded onto a 5 ml bed volume, 1.5 cm diameter, amylose resin column equilibrated in TEB containing 25 mM NaCl. The column was washed with the same buffer until the A_{280} reached the baseline at which point bound proteins were eluted in TEB containing 25 mM NaCl and 10 mM maltose. Elution fractions were pooled, concentrated with a 10,000 MWCO Amicon centrifugal filter device, and examined by SDS-PAGE analysis.

In vitro *amylose pull-down studies*. MBP-UreD—UreF—UreG, $(UreABC)_3$, $(UreAC)_3$, and UreB were dialyzed into TEB containing 25 mM NaCl. In a final volume of 250 µl, MBP-UreD—UreF—UreG (2 µM) was mixed with $(UreAC)_3$ (20 µM heterodimer), UreB (20 µM monomer), or $(UreABC)_3$ (10 µM heterotrimer) in the same buffer. The mixtures were incubated at 42 °C for 1 h (previously shown to be optimal for UreEF binding to MBP-UreD (6)) and aliquots were analyzed by SDS-PAGE. Amylose resin was equilibrated in TEB buffer containing 25 mM NaCl and added to each sample (at $1/4^{th}$ of the solution volume), and the slurries were gently rocked for 1 h at ambient temperature and centrifuged at 1000 *g*. The supernatant solutions were discarded, the resins washed 5 times with TEB buffer containing 25 mM NaCl (at volumes equivalent to the starting reaction volume, with the fifth wash reserved for SDS-PAGE analysis), and TEB buffer containing 25 mM NaCl and 10 mM maltose was added (again at a volume equivalent to the starting reaction volume). The slurries were vortexed, centrifuged at 4000 *g*, and the supernatant solutions containing the eluted proteins were

examined by SDS-PAGE. Prior studies with MBP alone had found no interaction with any urease-related protein (6).

Amylose pull-down studies using MBP-UreD were conducted in a similar manner as described above, except that $(UreABC)_3$, $(UreAC)_3$, and UreB (initially in HT buffer) were diluted to their working concentrations in TEB with 25 mM NaCl. Equilibrated amylose resin was added to the incubations (total volumes of 500 µl) at 1/5 of the mixture volumes.

Protease stability studies. Stock solutions of $(UreAC)_3$ and $(UreABC)_3$ in HT buffer were diluted to 2 µg $µl^{-1}$ in TBS. 10 µl mixtures consisted of 1 µl (2 µg) of either $(UreAC)_3$ or $(UreABC)_3$, 1 µl of 0.1 µg $µl^{-1}$ trypsin (sequencing grade, modified porcine trypsin, Promega; used at 1:20 ratio (w/w) of trypsin to protein sample), and 8 µl of TBS. These mixtures were incubated for 10 min, 30 min, or 60 min at 37 °C, and the reactions were stopped by the addition of SDS-PAGE loading buffer and boiling for 3 min. Control reactions lacking trypsin were incubated at 37 °C for 60 min in parallel. The digested samples were analyzed with SDS-PAGE.

RESULTS

Purification and properties of UreB, UreBΔ1-19, and $(UreAC)_3$. To evaluate the function of UreB and its N-terminal 19 residues (a potential tether and hinge region) during urease activation, the full-length and truncated proteins were purified free of the partner subunits, UreA and UreC. Wild-type *ureB* and a *ureB* fragment lacking the nucleotides coding for residues 1-19 were cloned into pET-42b, resulting in pUreB and pUreBΔ1-19, respectively. These plasmids were transformed into *E. coli* BL21-Gold(DE3) cells for protein overproduction, and UreB and UreBΔ1-19 were isolated from cell-free extracts by successive chromatography on

anion-exchange and gel filtration matrices (Figure 3.2, panel C, lanes 2 and 3, respectively). The native molecular mass of purified UreB was estimated by Shodex KW-804 gel filtration chromatography in comparison to the retention time of a set of molecular mass standards, yielding a mass of 9490 ± 60 kDa [average of triplicate determinations ± standard deviation (SD)]. This result indicates that UreB (calculated molecular mass of 11.7 kDa) is a monomer in solution.

To purify $(UreAC)_3$ free of UreB, *ureA* and *ureC* were cloned into pETDuet-1, an expression vector containing two T7 RNA polymerase-driven transcription units (composed of independent T7 promoters, *lac* operators, ribosomal binding sites, and multiple cloning sites) for the simultaneous production of two proteins in the cell. The resultant vector, pUreAC, was transformed into *E. coli* BL21-Gold(DE3) for protein production and $(UreAC)_3$ was isolated from cell-free extracts by successive chromatography on anion-exchange and hydrophobic-interaction matrices (Figure 3.2, panel C, lane 1). The native molecular mass of purified $(UreAC)_3$ was estimated to be 171,100 ± 680 kDa (average of triplicate determinations ± SD) by using a Shodex KW-804 gel filtration column, equivalent to 2.4 UreAC heterodimers in the quaternary structure. A similar analysis using Superdex-200 resin yielded a molecular mass of 219,000 kDa, or 3.1 UreAC heterodimers per complex. Taken together, these data suggest that $(UreAC)_3$ exists as a trimer of heterodimers in solution.

The purified UreB, UreBΔ1-19, and $(UreAC)_3$ proteins were examined by CD spectroscopy to assess their secondary structures. Spectra for the full-length and truncated UreB proteins were similar (Figure 3.3, panel A) and had the characteristic shape associated with a protein predominantly composed of β-sheets and random coils (11), as expected from the crystal

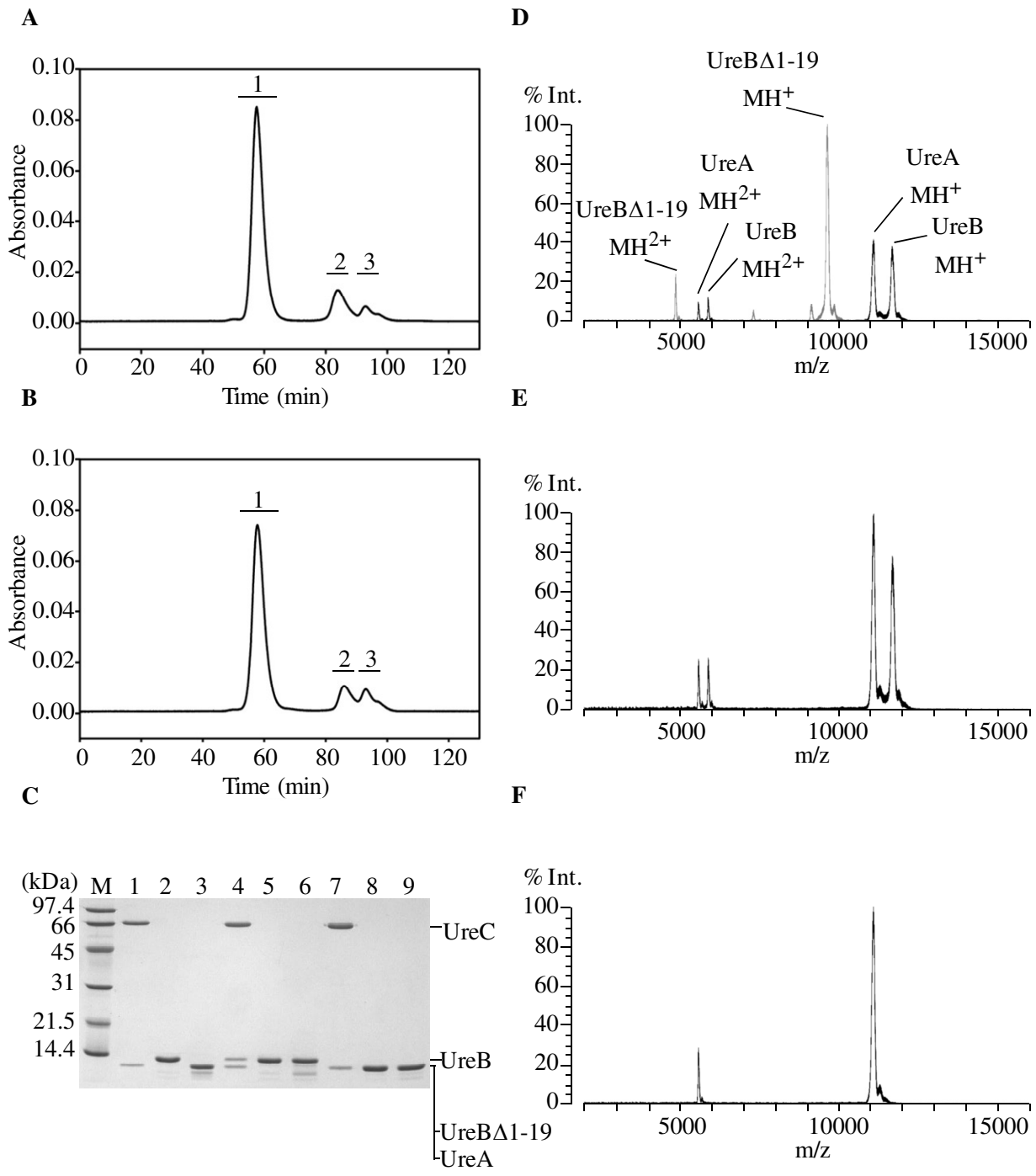

Figure 3.2: *In vitro* complex formation between $(UreAC)_3$ and UreB or UreBΔ1-19. (A) Superdex-200 chromatogram of a mixture containing $(UreAC)_3$ and excess UreB or (B) $(UreAC)_3$ and excess UreBΔ1-19. (C) SDS-PAGE analysis of pure proteins (2 µg) and individual peaks (denoted by horizontal black bars and numbering; 2 µg) from panels (A) and

Figure 3.2 legend continued:
(B). Lanes: M, molecular mass markers; 1, $(UreAC)_3$; 2, UreB; 3, UreBΔ1-19; 4, $(UreAC)_3$ plus UreB, peak 1; 5, same, peak 2; 6, same, peak 3; 7, $(UreAC)_3$ plus UreBΔ1-19, peak 1; 8, same, peak 2; 9, same, peak 3. MALDI-TOF MS spectra (depicting the *m/z* range of 2,000 – 16,000) of (D) authentic $(UreABC)_3$ (black) overlaid with UreBΔ1-19 (gray), (E) peak 1 of panel A, and (F) peak 1 of panel B.

structure of this subunit within intact urease (3% α-helix, 38% β-sheet, 59% random coil) (14). Attempts to predict the secondary structural elements of UreB by deconvolution programs were unsuccessful due to the low level of α-helix which is known to limit prediction analysis (39). By contrast, the CD spectrum of $(UreAC)_3$ (Figure 3.3, panel B) was readily deconvoluted by the K2D program of the Dichroweb server (38), revealing a composition of 32% α-helix, 13% β-sheet, and 55% random coil. The proportions of these elements agree well with those in the corresponding components of the urease crystal structure (34% α-helix, 23% β-sheet, and 43% random coil) (14).

Complex formation between $(UreAC)_3$ and UreB in vitro. The ability of $(UreAC)_3$ to form a complex with UreB or UreBΔ1-19 *in vitro* was monitored by gel filtration chromatography (Figure 3.2, panel A and B, respectively). The mixtures of $(UreAC)_3$ with excess UreB or UreBΔ1-19 chromatographed as three distinct peaks of 280 nm absorbing species. The first peak to elute from the mixture (peak 1) was a high molecular weight species containing UreA, UreB, and UreC (Figure 3.2, panel C, lane 4), demonstrating that UreB had formed a complex with $(UreAC)_3$. The $(UreABC^*)_3$ sample [i.e., the complex of $(UreAC)_3$ plus UreB] was examined by CD spectroscopy (Figure 3.3, panel B), and its spectrum was similar to that of $(UreAC)_3$ suggesting that the small UreB subunit had little influence on the overall

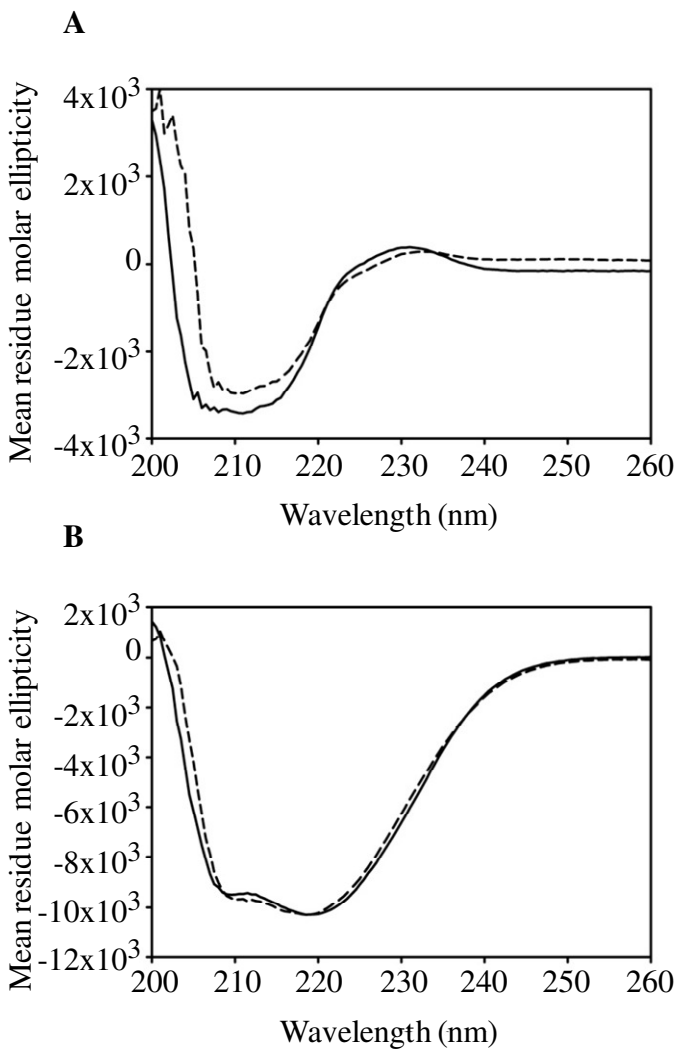

Figure 3.3: Secondary structure analysis of UreB, UreBΔ1-19, $(UreAC)_3$, and $(UreABC^*)_3$. (A) Raw averaged CD spectra for UreB (dashed line) and UreBΔ1-19 (solid line). (B) Raw averaged CD spectra for $(UreAC)_3$ (solid line) and $(UreABC^*)_3$ (dashed line).

α-helical content. Peaks 2 and 3 of the same mixture both contained excess UreB that had not bound to $(UreAC)_3$ (Figure 3.2, panel C, lanes 5 and 6); however, peak 3 also contained some low-molecular weight contamination likely arising from the UreB preparation. Comparison of the retention time of UreB in peak 2 with a set of molecular mass standards yielded a mass of

9,600 kDa, consistent with the monomeric form of the protein. The delayed elution position of UreB in peak 3 indicates this sample had interacted with the gel filtration matrix, thereby causing the appearance of two peaks containing UreB. Peak 1 of the $(UreAC)_3$ plus UreBΔ1-19 mixture appeared to contain only $(UreAC)_3$ (Figure 3.2, panel C, lane 7); however, UreBΔ1-19 overlaps with UreA during SDS-PAGE. Gel scanning and integration of the bands for $(UreAC)_3$ yielded an apparent UreA:UreC ratio of 0.5:1, while sample in peak 1 of the $(UreAC)_3$ plus UreBΔ1-19 sample yielded an apparent low-molecular-weight species:UreC ratio of 0.4:1. If UreBΔ1-19 had formed a complex with $(UreAC)_3$, the resultant ratio of protein bands would have increased compared to that for $(UreAC)_3$; therefore, UreBΔ1-19 does not form a complex with $(UreAC)_3$. For comparison, analysis of the protein bands derived from peak 1 of the $(UreAC)_3$ plus UreB sample provided an apparent UreA:UreB:UreC ratio of 0.5:0.5:1, similar to that found when native urease was subjected to this analysis, i.e. a UreA:UreB:UreC ratio of 0.7:0.6:1 (Figure 3.7, lane 1).

MALDI-TOF MS was used to further examine whether UreB and UreBΔ1-19 bound to $(UreAC)_3$. As illustrated in Figure 3.2, panel D, both small subunits were detected in authentic $(UreABC)_3$ with *m/z* of 11,119 and 11,718 for the singly-protonated species of UreA and UreB, respectively, and 5,610 and 5,916 for the doubly-protonated species. UreC also was detected near 60 kDa for this sample, but its intensity was greatly diminished in comparison to the small subunits. Also shown in this panel are species associated with singly- and doubly-protonated UreBΔ1-19, possessing *m/z* of 9,676 and 4,894, respectively. Similar analysis of peak 1 from

panel A provided the spectrum of panel E, demonstrating the presence of both UreA and UreB. By contrast, analysis of peak 1 of panel B revealed the clear presence of UreA and the absence of UreBΔ1-19.

In vitro *activation.* When activated under standard conditions with varying Ni^{2+} concentrations, $(UreABC)_3$ and $(UreABC^*)_3$ both exhibited sigmoid-like activation profiles (Figure 3.4) with respect to increasing [Ni^{2+}]. $(UreABC)_3$ yielded a specific activity of ~400 U (mg of protein)$^{-1}$, as previously reported (24, 25, 41), while $(UreABC^*)_3$ generated even greater activity reaching ~570 U (mg of protein)$^{-1}$ (Figure 3.4, Table 3.1). These results indicate that $(UreABC^*)_3$ represents a functional form of urease apoprotein with greater activation competence than the preformed apoprotein as isolated from the cells. By contrast, efforts to activate $(UreAC)_3$ under standard conditions led to negligible levels of activity [<0.2 U (mg of protein)$^{-1}$]. Treatment of $(UreAC)_3$ to activation conditions followed by the addition of UreB led to a specific activity of 34.0 ± 1.9 U (mg of protein)$^{-1}$ (average of triplicate experiments ± SD), consistent with the inability of UreB to trap and activate a pre-loaded UreC active site. By contrast, a mixture of $(UreAC)_3$ and excess UreBΔ1-19 subjected to activation conditions generated a specific activity of only 2.5 ± 0.1 U (mg protein)$^{-1}$ (average of triplicate experiments ± SD).

Metal analyses of in vitro *activated species*. To examine the effect of inclusion of UreB on Ni^{2+} incorporation into urease apoprotein, samples that had been subjected to the standard

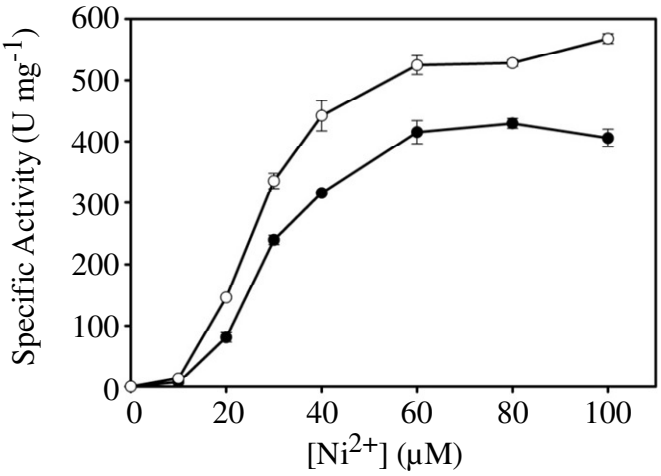

Figure 3.4: *In vitro* activation of $(UreABC)_3$ and $(UreABC^*)_3$ as a function of varying $[Ni^{2+}]$. $(UreABC)_3$ (closed circles) and $(UreABC^*)_3$ (open circles) were incubated for 1 h in standard activation buffer containing the indicated concentrations of $NiCl_2$, and aliquots were assayed for urease activity. Data points represent the average of triplicate experiments ± SD.

activation conditions were analyzed for metal content by ICP-AES (Table 3.1). For comparison, 0.53 equivalents of Ni per heterotrimer were associated with authentic $(UreABC)_3$ apoprotein that was activated by use of standard conditions and treated with EDTA (41); whereas, 1.74 or 1.83 equivalents of Ni were incorporated into sample that was not treated with chelator (24, 41). When using $(UreABC^*)_3$, obtained by mixing UreB with $(UreAC)_3$ before activation, the metal content of EDTA-treated sample was 1.00 Ni per heterodimer; whereas, samples not treated with chelator possessed 2.56 equivalents of metal. In contrast, $(UreAC)_3$ subjected to activation conditions bound only 0.10 equivalents of nickel if treated with chelator, but still bound 2.57 equivalents in the absence of EDTA. Finally, $(UreAC)_3$ that was activated and then mixed with UreB contained 0.18 equivalents of nickel with EDTA treatment and 2.78 equivalents of metal without the chelator.

Table 3.1: Properties of urease apoprotein samples subjected to activation conditions.

Apoprotein Sample[a]	**Specific Activity U (mg protein)$^{-1}$**	**Nickel Content**[b]
$(UreABC^*)_3$	568 ± 8	1.00 ± 0.04 (2.56 ± 0.27)
$(UreAC)_3$	<0.2	0.10 ± 0.03 (2.57 ± 0.36)
$(UreAC)_3$, then add UreB	34.0 ± 1.9	0.18 ± 0.04 (2.78 ± 0.17)
$(UreAC)_3$ plus UreBΔ1-19	2.5 ± 0.1	--[c]

Standard activation conditions involved incubation of the apoprotein sample (5-10 μM) for 1 h at 37 °C in 100 mM HEPES, pH 8.3, containing 100 mM $NaHCO_3$, 150 mM NaCl, and 100 μM $NiCl_2$. [a] $(UreABC^*)_3$ is the complex derived from mixing $(UreAC)_3$ with UreB prior to incubation in activation buffer. $(UreAC)_3$ was subjected to activation conditions followed by incubation with UreB, or a mixture of $(UreAC)_3$ and excess UreB Δ 1-19 was subjected to activation conditions. [b] Metal content is indicated per UreC protomer and was determined after removal of adventitious metal by sample treatment for 5 min with 10 mM EDTA followed by gel filtration chromatography. Numbers in parentheses are for samples not treated with EDTA, but subjected to gel-filtration chromatography. Specific activity and metal content values represent the average of triplicate experiments ± SD. [c] Metal content was not determined.

In vivo *interactions of MBP-UreD with $(UreABC)_3$, UreB, UreBΔ1-19, and $(UreAC)_3$.*

We investigated the *in vivo* interactions between a soluble form of UreD [i.e., the MBP-UreD

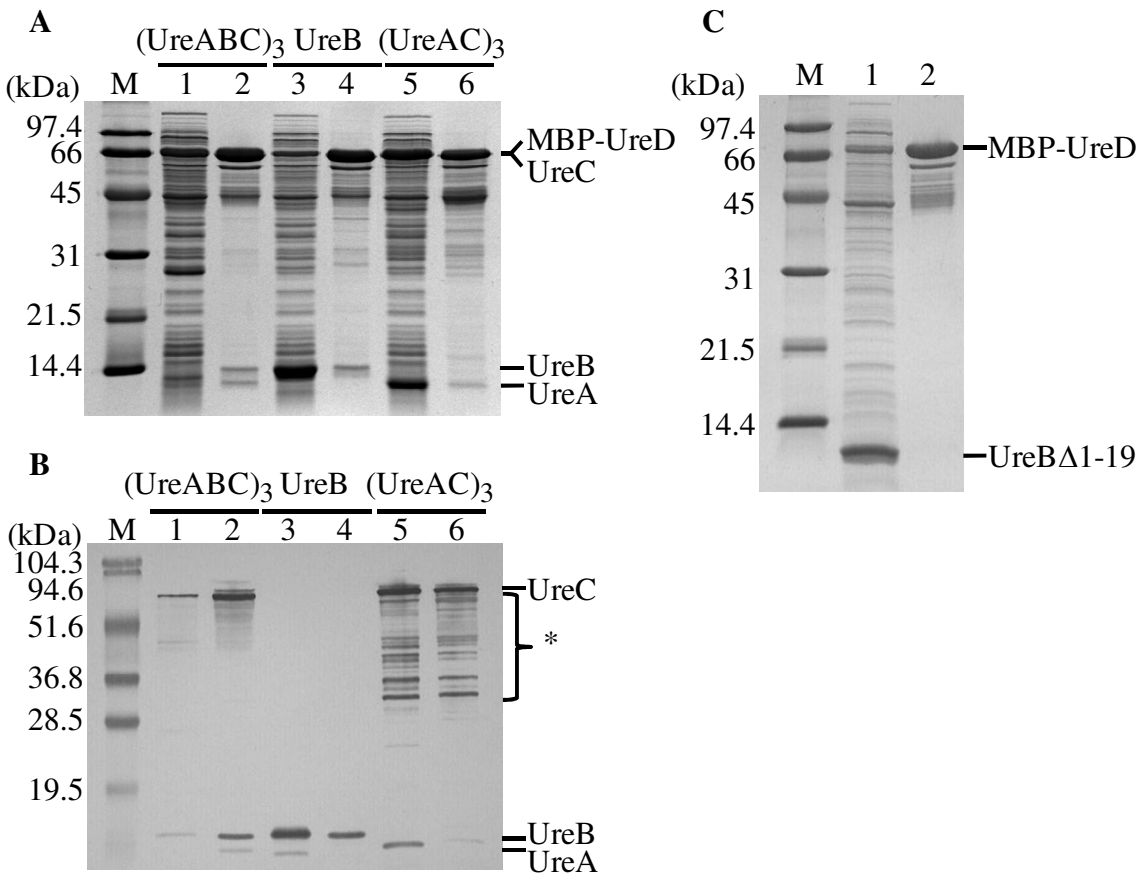

Figure 3.5: *In vivo* interactions of MBP-UreD with $(UreABC)_3$, UreB, $(UreAC)_3$, and UreBΔ1-19. (A) SDS-PAGE depicting the interactions of MBP-UreD with $(UreABC)_3$, UreB, and $(UreAC)_3$. *E. coli* BL21-Gold(DE3) cells were co-transformed with pCDF-MBP-UreD (encoding MBP-UreD) and either pEC004, pUreB, or pUreAC [encoding $(UreABC)_3$, UreB, and $(UreAC)_3$, respectively]. Soluble cell-free extracts of IPTG-induced cultures (10 µg, odd numbered lanes) and proteins eluted from amylose resin upon maltose addition (5 µg, even numbered lanes) were subjected to SDS-PAGE and stained with Coomassie brilliant blue. (B) Western blot of the same samples. Each sample (1 µg) was subjected to SDS-PAGE, electroblotted onto an Immobilon membrane, and blotted with anti-*K. aerogenes* urease antibodies. The asterisk (*) indicates the migration positions of cross-reactive bands that may represent UreC degradation products. (C) Interaction of MBP-UreD with UreBΔ1-19. Studies analogous to those shown in panel A were carried out, but using cells that produce MBP-UreD and UreBΔ1-19. In each panel, M indicates molecular mass markers.

fusion protein (6)] and $(UreABC)_3$, UreB, UreBΔ1-19, and $(UreAC)_3$ by using amylose resin affinity purification (i.e., amylose pull-down studies). *E .coli* BL21-Gold(DE3) cells were

transformed with pCDF-MBP-UreD, a vector producing MBP-UreD, and either pEC004 [encoding $(UreABC)_3$ (6)], pUreB, pUreBΔ1-19, or pUreAC. Soluble cell-free extracts from cultures induced with IPTG were subjected to amylose resin chromatography, and the samples were analyzed by SDS-PAGE and Western blotting using anti-*K. aerogenes* urease antibodies (Figure 3.5). Pull-down analysis of soluble extracts from cells co-transformed with pCDF-MBP-UreD and pEC004 revealed the co-purification of $(UreABC)_3$ with MBP-UreD (Figure 3.5, panel A, lane 2). This result was substantiated by the presence of urease cross-reactive bands in the cognate Western blot (Figure 3.5, panel B, lane 2). A similar analysis of extracts from cells co-transformed with pCDF-MBP-UreD and pUreB revealed that UreB co-purifies with MBP-UreD (Figure 3.5, panels A and B, lane 4). In contrast, UreBΔ1-19 did not interact with MBP-UreD (Figure 3.5, panel C, lane 2) when these proteins were co-produced in the cell. Finally, pull-down analysis of soluble extracts from cells co-transformed with pCDF-MBP-UreD and pUreAC indicate that $(UreAC)_3$ co-purifies with MBP-UreD (Figure 3.5, panels A and B, lane 6). In the latter sample, numerous cross-reactive protein bands were visible in the Western blot of the cell extracts and the amylose resin elution pool, consistent with partial degradation of UreC.

In vitro *interactions of MBP-UreD and MBP-UreD—UreF—UreG with* $(UreABC)_3$*, UreB, and* $(UreAC)_3$. The *in vivo* interaction results described above were extended by monitoring the *in vitro* formation of complexes between purified proteins. MBP-UreD and the soluble heterotrimer MBP-UreD—UreF—UreG were each mixed with $(UreABC)_3$, UreB, or $(UreAC)_3$ and monitored for complex formation by amylose resin chromatography followed by

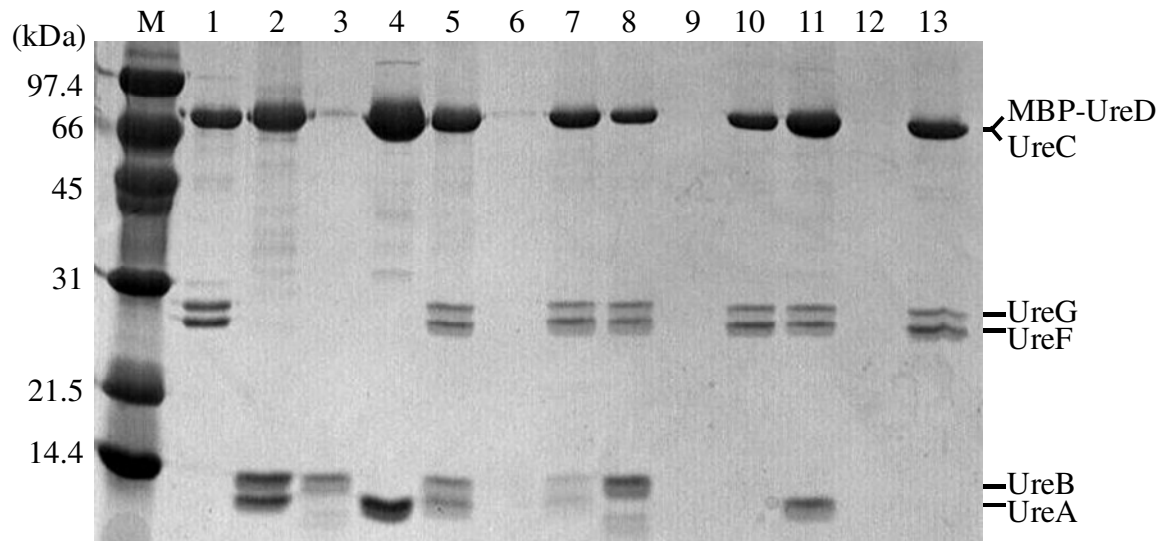

Figure 3.6: *In vitro* interactions of MBP-UreD—UreF—UreG with $(UreABC)_3$, $(UreAC)_3$, and UreB. MBP-UreD—UreF—UreG (2 μM) was mixed with $(UreABC)_3$ (10 μM heterotrimer), $(UreAC)_3$ (20 μM heterodimer), or UreB (20 μM), incubated at 42 °C, chromatographed on amylose resin, and bound protein complexes were eluted in buffer containing maltose. Samples analyzed by SDS-PAGE included the mixtures prior to chromatography, the final washes before elution, and the eluted complexes. Lanes: M, molecular mass markers; 1, MBP-UreD—UreF—UreG; 2, $(UreABC)_3$; 3, UreB; 4, $(UreAC)_3$; 5, MBP-UreD—UreF—UreG plus $(UreABC)_3$ prior to chromatography; 6, final wash prior to elution; 7, elution; 8, MBP-UreD—UreF—UreG plus UreB prior to chromatography; 9, final wash prior to elution; 10, elution; 11, MBP-UreD—UreF—UreG plus $(UreAC)_3$ prior to chromatography; 12, final wash prior to elution; 13, elution.

SDS-PAGE analysis. Despite its ability to interact with $(UreABC)_3$, UreB, and $(UreAC)_3$ *in vivo* (see above), MBP-UreD did not bind to these purified proteins *in vitro* (data not shown). In the same way, neither $(UreAC)_3$ (Figure 3.6, lane 4) nor UreB (lane 3) co-purified with MBP-UreD:UreF:UreG (lane 1) as shown by the absence of the small subunit bands [and by the unchanged ratio of the MBP-UreD versus UreG and UreF band intensities, negating the presence of UreC for the $(UreAC)_3$ sample] in the eluted fractions (Figure 3.6, lanes 10 and 13).

Conversely, $(UreABC)_3$ did bind to MBP-UreD:UreF:UreG as evident by the appearance of UreA and UreB bands (and by the increased relative intensity of the upper band compared to the UreG and UreF bands) in the elution fraction (Figure 3.6, lane 7). This result suggests that intact urease is required to interact *in vitro* with the preformed complex of the UreD, UreF, and UreG accessory proteins.

Protease susceptibility studies. To follow up on the observation that $(UreAC)_3$-derived UreC was degraded in soluble extracts from cells producing $(UreAC)_3$ and MBP-UreD, as revealed during the amylose resin pull-down studies (Figure 3.5, panels A and B, lane 6), we monitored the protease susceptibility of selected samples. As a representative protease, trypsin was incubated with purified $(UreAC)_3$ and $(UreABC)_3$ at 37 °C, and aliquots were examined by SDS-PAGE over time (Figure 3.7). Several UreC digestion fragments were observed within 10 min of subjecting $(UreABC)_3$ to proteolysis, with little further change noted over the next 50 min. Conversely, UreC in $(UreAC)_3$ was completely digested within 10 min and fewer fragments were visible at each subsequent time point, indicating an enhanced susceptibility of $(UreAC)_3$ in comparison with $(UreABC)_3$. The most prominent digestion fragment in the latter sample, which was also present in $(UreABC)_3$, has a molecular mass of ~30 kDa.

DISCUSSION

A wealth of literature details the urease catalytic mechanism and activation process, primarily related to the dinuclear nickel metallocenter in the large subunits of the enzyme. By contrast, there is scant information available related to the roles of the protein's small subunits

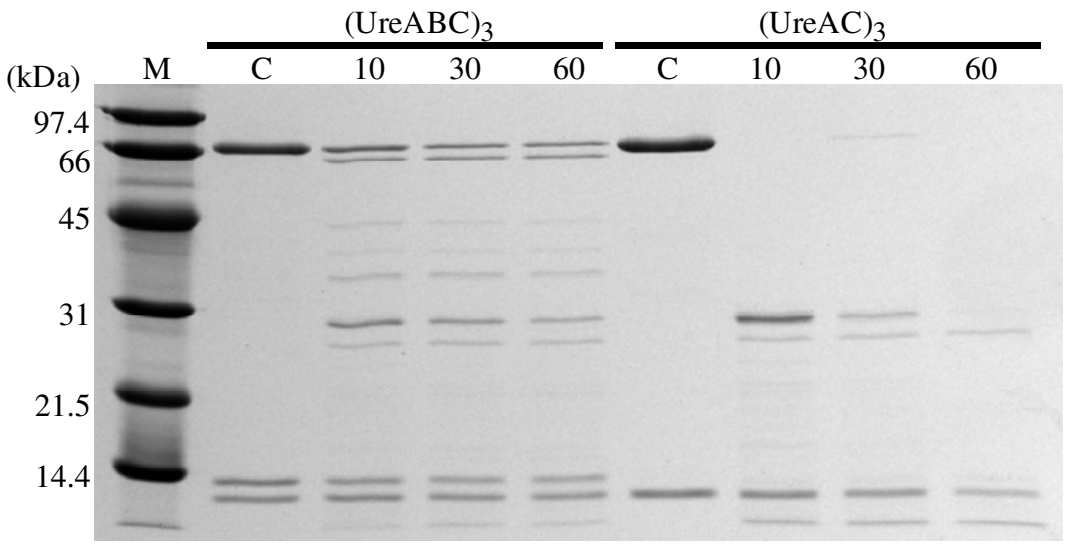

Figure 3.7: Trypsin proteolysis of $(UreABC)_3$ and $(UreAC)_3$. 2 µg of either $(UreABC)_3$ or $(UreAC)_3$ was incubated with 0.1 µg of trypsin at 37 °C for 10 min, 30 min, or 60 min as indicated above each lane, and samples were analyzed by SDS-PAGE. Non-digested control samples are indicated by C, and molecular mass markers are denoted by M.

found in most bacterial enzymes or the corresponding domains of the fused subunits in *Helicobacter* species, fungi, and plants. In this chapter, I have focused on the role of UreB during urease activation through several lines of investigation.

As a first step in my analysis, I engineered cells to separately produce UreB, UreBΔ1-19 (a truncated form of UreB missing a putative hinge and tether region), and $(UreAC)_3$. My subsequent purifications represent the first examples of isolated UreB subunits and UreB-free urease. UreB was demonstrated to be a soluble monomer composed solely of β-sheets and random coils according to gel filtration chromatography and CD spectroscopy. UreBΔ1-19 was purified in the same manner and shared a similar size and CD spectrum. By contrast, $(UreAC)_3$ was established as a trimer of the heterodimer and shown to contain substantial amounts of α-

helix (32%). The secondary structure estimations provided by CD spectroscopy are in good agreement with the appropriate components of the crystal structure of *K. aerogenes* urease (14) (note the α-helix-free structure of UreB and the α-helical-rich structure of UreA and UreC in Figure 3.1); thus, UreB, UreBΔ1-19, and $(UreAC)_3$ appear to adopt structures similar to that in the native protein, confirming their utility for functionality studies.

I next examined whether UreB or UreBΔ1-19 could bind spontaneously to $(UreAC)_3$ and thus generate a functional urease apoprotein. Incubation of UreB and $(UreAC)_3$ for only 15 min yielded the stable $(UreABC^*)_3$ species. The apparent non-integer ratio of UreA:UreB:UreC (~0.5:~0.5:1) found during SDS-PAGE analysis of this species and authentic urease apoprotein is attributed to differential binding of the anionic dye to the variably charged subunits. The MALDI-TOF MS results clearly demonstrate that UreBΔ1-19 does not spontaneously bind to $(UreAC)_3$. These results are attributed to the absence of residues 2-8 at the N-terminus of UreB which are known to form the terminal strand of a β-sheet that is primarily composed of β-strands from UreC (28), thus underscoring the importance of this tether region for UreB:UreC interaction. The main domain of UreB exhibits few polar and hydrophobic interactions with UreC, accounting for the inability of the truncated protein to bind to UreC.

The *in vitro* activation competence of $(UreABC)_3$ and its reconstituted version were compared to validate the functionality of $(UreABC^*)_3$. Both species exhibited a sigmoid-like activation behavior with respect to varied Ni^{2+} concentration, a previously unreported observation. I attribute the sigmoidicity to the need for incorporating two atoms of nickel per active site, a process that is promoted by greater metal ion concentration. $(UreABC)_3$ was

maximally activated to ~400 U (mg of protein)$^{-1}$, as was previously observed (25), equating to 16% of the nascent active sites gaining activity. Unexpectedly, $(UreABC^*)_3$ was activated to even greater levels, reaching a maximal specific activity of ~570 U (mg of protein)$^{-1}$ (Figure 3.4). On the basis of single metal content analyses of purified $(UreABC)_3$ (yielding 0.3 iron and 0.1 zinc) and $(UreAC)_3$, (providing undetectable levels of any metal), I hypothesize that the decreased activation competence of apoprotein purified from the cell compared to that formed by mixing UreB with $(UreAC)_3$ relates to non-nickel metal contamination of $(UreABC)_3$ compared to the metal-free $(UreAC)_3$. Regardless of the explanation, these results confirm the efficacy of $(UreABC^*)_3$ as functional urease apoprotein.

To gain insight into the role of UreB during *in vitro* activation, $(UreAC)_3$ was subjected to the standard activation conditions and negligible levels of activity were detected. All residues that coordinate the metallocenter or participate in catalysis are present in the UreB-free protein, yet a functional active site was not produced. It was conceivable that the activation conditions did lead to normal metallation of the protein, but the lack of UreB caused a conformational change in $(UreAC)_3$ that hindered substrate access, restricted movement of a flap containing a catalytic residue that covers the active site, or otherwise stifled activity. To test this possibility, UreB was added to a preparation of $(UreAC)_3$ that had been incubated in standard activation conditions. A small fraction of active enzyme was generated [i.e., yielding a specific activity of 34 U (mg of protein)$^{-1}$, or 6% of that for maximally activated $(UreABC^*)_3$], but this likely arises

from UreB associating with low levels of $(UreAC)_3$ apoprotein followed by partial activation. For comparison, a mixture of $(UreAC)_3$ and excess UreBΔ1-19 that had been treated to activation conditions yielded less than $1/10^{th}$ of the activity found when using UreB. In sum, full-length UreB must bind to $(UreAC)_3$ prior to exposure to Ni^{2+} and bicarbonate in order to exert its positive effect on the activation process.

In addition to measuring the urease activities of various samples following *in vitro* activation, it was of interest to quantify their nickel contents. After subjecting $(UreABC)_3$ to activation conditions, nearly two nickel per heterotrimer are present (24, 41). When this sample is subsequently incubated with EDTA, the metal content is reduced to 0.53 equivalents (41), but activity is unaffected. Activation of $(UreABC^*)_3$ leads to 2.56 equivalents of bound nickel, but this is reduced to 1.00 equivalents in the presence of EDTA. The increased level of tightly bound Ni^{2+} correlates well with the greater activity of this sample than for activated $(UreABC)_3$. Of great significance, when $(UreAC)_3$ is subjected to the same activation conditions (but yielding negligible levels of activity) it contains 2.57 equivalents of nickel without chelator that is reduced to only 0.10 equivalents when treated with EDTA, suggesting that UreB protects the metallocenter from chelation. When $(UreAC)_3$ is first treated to activation conditions, then incubated with UreB, and finally treated with EDTA, no additional metal is bound than when compared to $(UreAC)_3$ alone. This result demonstrates that UreB cannot trap a preformed metallocenter, but rather this subunit must be present to generate the properly bound metal complex.

The interaction of *K. aerogenes* UreD with urease was previously examined by using amylose resin pull-down studies with the MBP-UreD fusion protein (6) along with chemical cross-linking and small-angle X-ray scattering analyses of the $(UreABC)_3$—UreD protein complex (8, 28). Interactions among these proteins from other organisms also were investigated by using yeast two-hybrid and immunoprecipitation methods (13, 29, 36). These efforts provided evidence that UreD interacts with both UreB and UreC, consistent with UreD binding to the vertices of the urease triangular structure. To obtain further details on these UreD interactions, I extended the amylose resin pull-down approach, both *in vivo* and *in vitro*, to study MBP-UreD binding to UreB, UreBΔ1-19, $(UreAC)_3$, and control $(UreABC)_3$. Pull-down analyses of extracts from cells producing MBP-UreD along with UreB, $(UreAC)_3$ or $(UreABC)_3$ all demonstrated binding between the paired components, whereas cellular MBP- UreD and UreBΔ1-19 did not form a complex. These results suggest binding can occur between UreD and UreC, confirm a direct interaction between UreD and UreB, and underscore the importance of the N-terminal region of UreB for the latter interaction. Because the CD spectrum of UreBΔ1-19 is essentially identical to that of UreB and consistent with the fold of UreB in the crystal structure, the lack of interaction between UreBΔ1-19 and MBP-UreD specifically relates to the missing N-terminus, not to a mis-folded protein. When the interactions of MBP-UreD with the other proteins were examined *in vitro*, the results were quite different. Purified MBP-UreD and $(UreABC)_3$ proteins do not form a complex, as I previously described (6), nor does MBP-UreD bind UreB or $(UreAC)_3$. I attribute these results to a requirement for an unidentified cellular constituent (i.e., a protein chaperone or small molecule) that facilitates the interaction between these components. Alternatively, it is possible that purified MBP-UreD is structurally different

from the form (perhaps partially unfolded) that interacts with UreB, $(UreAC)_3$, and $(UreABC)_3$ *in vivo*.

I also examined the *in vitro* interactions of UreD with the urease subunits by making use of the MBP-UreD—UreF—UreG complex (6). Amylose pull-down studies with the heterotrimeric complex of accessory proteins demonstrated binding to $(UreABC)_3$, but not to $(UreAC)_3$ or UreB. This result suggests that the added presence of UreF and UreG in the complex containing MBP-UreD modifies its properties such as to allow binding to fully assembled urease. This result is similar to what was observed *in vivo* using cells that produce MBP-UreD and $(UreABC)_3$, hinting that a cellular protein mimicking UreF and/or UreG is involved in that interaction. In contrast, binding of MBP-UreD—UreF—UreG to urease apoprotein missing UreB or to the isolated UreB subunit is precluded, suggesting a greater specificity in this interaction than for the *in vivo* binding with MBP-UreD.

The anti-*K. aerogenes* urease Western blot analyzed as part of the *in vivo* interaction studies revealed numerous cross-reactive bands in extracts of cells producing $(UreAC)_3$, whereas the other samples were free of these contaminants. These bands are likely to be UreC degradation products, consistent with enhanced proteolysis of $(UreAC)_3$ compared to $(UreABC)_3$. Follow-up studies provided clear evidence that $(UreAC)_3$ is proteolyzed by trypsin at a faster rate than $(UreABC)_3$ suggesting that, in addition to its role in urease activation, UreB protects apoprotein from spurious proteolysis *in vivo*. Analysis of the *K. aerogenes* urease crystal structure (14) indicates that Arg339 of UreC is moderately exposed in the wild-type

protein, but the absence of UreB may lead to increased protease susceptibility involving this residue. Similarly, the loss of UreB could reasonably expose Arg52 to the protease.

In conclusion, my results demonstrate that UreB stimulates the productive binding of nickel to urease apoprotein and stabilizes it against chelation. Moreover, UreB acts as an important interface between the active site-containing UreC subunit and the accessory proteins, with residues 1-19 being critical for this interaction. Finally, UreB protects the urease apoprotein from proteolysis. This work, the first study focused on the function of UreB, establishes the central importance of this subunit to the enzyme. The important roles of UreB in *K. aerogenes* are likely to be replicated in other three-subunit bacterial ureases and by the corresponding domains in the *Helicobacter*, fungal, and plant enzymes.

BIBLIOGRAPHY

BIBLIOGRAPHY

1. **Balasubramanian, A., and K. Ponnuraj.** 2010. Crystal structure of the first plant urease from jack bean: 83 Years of journey from its first crystal to molecular structure. Journal of Molecular Biology **400:**274-283.

2. **Benini, S., W. R. Rypniewski, K. S. Wilson, S. Ciurli, and S. Mangani.** 1998. The complex of *Bacillus pasteurii* urease with ß-mercaptoethanol from X-ray data at 1.65-Å resolution. Journal of Biological Inorganic Chemistry **3:**268-273.

3. **Benini, S., W. R. Rypniewski, K. S. Wilson, S. Miletti, S. Ciurli, and S. Mangani.** 1999. A new proposal for urease mechanism based on the crystal structures of the native and inhibited enzyme from *Bacillus pasteurii*: Why urea hydrolysis costs two nickels. Structure **7:**205-216.

4. **Boer, J. L., S. Quiroz-Valenzuela, K. L. Anderson, and R. P. Hausinger.** 2010. Mutagenesis of *Klebsiella aerogenes* UreG to probe nickel binding and interactions with other urease-related proteins. Biochemistry **49:**5859-5869.

5. **Carter, E. L., N. Flugga, J. L. Boer, S. B. Mulrooney, and R. P. Hausinger.** 2009. Interplay of metal ions and urease. Metallomics **1:**207-221.

6. **Carter, E. L., and R. P. Hausinger.** 2010. Characterization of *Klebsiella aerogenes* urease accessory protein UreD in fusion with the maltose binding protein. Journal of Bacteriology **192:**2294-2304.

7. **Carter, E. L., D. E. Tronrud, S. R. Taber, P. A. Karplus, and R. P. Hausinger.** 2011. Iron-containing urease in a pathogenic bacterium. Proceedings of the National Academy of Sciences, United States of America **108:**13095-13099.

8. **Chang, Z., J. Kuchar, and R. P. Hausinger.** 2004. Chemical crosslinking and mass spectrometric identification of sites of interaction for UreD, UreF, and urease. Journal of Biological Chemistry **279:**15305-15313.

9. **Colpas, G. J., T. G. Brayman, L.-J. Ming, and R. P. Hausinger.** 1999. Identification of metal-binding residues in the *Klebsiella aerogenes* urease nickel metallochaperone, UreE. Biochemistry **38:**4078-4088.

10. **Dixon, N. E., C. Gazzola, R. L. Blakeley, and B. Zerner.** 1975. Jack bean urease (EC 3.5.1.5). A metalloenzyme. A simple biological role for nickel? Journal of the American Chemical Society **97:**4131-4133.

11. **Greenfield, N. J., and G. D. Fasman.** 1969. Computed circular dichroism spectra for the evaluation of protein conformation. Biochemistry **8:**4108-4116.

12. **Ha, N.-C., S.-T. Oh, J. Y. Sung, K.-A. Cha, M. H. Lee, and B.-H. Oh.** 2001. Supramolecular assembly and acid resistance of *Helicobacter pylori* urease. Nature Structural Biology **8:**505-509.

13. **Heimer, S. R., and H. L. Mobley.** 2001. Interaction of *Proteus mirabilis* urease apoprotein and accessory proteins identified with yeast two-hybrid technology. Journal of Bacteriology **183:**1423-1433.

14. **Jabri, E., M. B. Carr, R. P. Hausinger, and P. A. Karplus.** 1995. The crystal structure of urease from *Klebsiella aerogenes*. Science **268:**998-1004.

15. **Kim, J. K., and R. P. Hausinger.** 2006. The UreEF fusion protein provides a soluble and functional form of the UreF urease accessory protein. Journal of Bacteriology **188:**8413-8420.

16. **Laemmli, U. K.** 1970. Cleavage of structural proteins during the assembly of the head of bacteriophage T4. Nature (London) **227:**680-685.

17. **Lam, R., V. Romanov, K. Johns, K. Battaile, J. Wu-Brown, J. L. Guthrie, R. P. Hausinger, E. Pai, and N. Y. Chirgadze.** 2010. Structure of a truncated urease accessory protein UreF from *Helicobacter pylori*. Proteins **78:**2839-2848.

18. **Lee, M. H., H. S. Pankratz, S. Wang, R. A. Scott, M. G. Finnegan, M. K. Johnson, J. A. Ippolito, D. W. Christianson, and R. P. Hausinger.** 1993. Purification and characterization of *Klebsiella aerogenes* UreE protein: A nickel-binding protein that functions in urease metallocenter assembly. Protein Science **2:**1042-1052.

19. **Mobley, H. L. T., and R. P. Hausinger.** 1989. Microbial ureases: Significance, regulation, and molecular characterization. Microbiological Reviews **53:**85-108.

20. **Mobley, H. L. T., M. D. Island, and R. P. Hausinger.** 1995. Molecular biology of microbial ureases. Microbiological Reviews **59:**451-480.

21. **Moncrief, M. B. C., and R. P. Hausinger.** 1997. Characterization of UreG, identification of a UreD-UreF-UreG complex, and evidence suggesting that a nucleotide-binding site in UreG is required for in vivo metallocenter assembly of *Klebsiella aerogenes* urease. Journal of Bacteriology **179:**4081-4086.

22. **Moncrief, M. B. C., and R. P. Hausinger.** 1996. Purification and activation properties of UreD-UreF-urease apoprotein complexes. Journal of Bacteriology **178:**5417-5421.

23. **Park, I.-S., M. B. Carr, and R. P. Hausinger.** 1994. *In vitro* activation of urease apoprotein and role of UreD as a chaperone required for nickel metallocenter assembly. Proceedings of the National Academy of Sciences, United States of America **91:**3233-3237.

24. **Park, I.-S., and R. P. Hausinger.** 1996. Metal ion interactions with urease and UreD-urease apoproteins. Biochemistry **35:**5345-5352.

25. **Park, I.-S., and R. P. Hausinger.** 1995. Requirement of carbon dioxide for *in vitro* assembly of the urease nickel metallocenter. Science **267:**1156-1158.

26. **Pearson, M. A., L. O. Michel, R. P. Hausinger, and P. A. Karplus.** 1997. Structure of Cys319 variants and acetohydroxamate-inhibited *Klebsiella aerogenes* urease. Biochemistry **36:**8164-8172.

27. **Quiroz-Valenzuela, S.** 2008. New insights in the urease activation process obtained by characterization of apourease complexes and the UreG accessory protein of *Klebsiella aerogenes*. Michigan State University.

28. **Quiroz-Valenzuela, S., S. C. K. Sukuru, R. P. Hausinger, L. A. Kuhn, and W. T. Heller.** 2008. The structure of urease activation complexes examined by flexibility analysis, mutagenesis, and small-angle X-ray scattering. Archives of Biochemistry and Biophysics **480:**51-57.

29. **Rain, J.-C., L. Selig, H. de Reuse, V. Battaglia, C. Reverdy, S. Simon, G. Lenzen, F. Petel, J. Wojcik, V. Schächter, Y. Chemama, A. Labigne, and P. Legrain.** 2001. The protein-protein interaction map of *Helicobacter pylori*. Nature **409:**211--215.

30. **Salomone-Stagni, M., B. Zambelli, F. Musiani, and S. Ciurli.** 2007. A model-based proposal for the role of UreF as a GTPase-activating protein in the urease active site biosynthesis. Proteins **68:**749-761.

31. **Sambrook, J., E. F. Fritsch, and T. Maniatis.** 1989. Molecular cloning: A laboratory manual, 2nd ed, vol. Cold Spring Harbor Laboratory, Cold Spring Harbor, NY.

32. **Soriano, A., G. J. Colpas, and R. P. Hausinger.** 2000. UreE stimulation of GTP-dependent urease activation in the UreD-UreF-UreG-urease apoprotein complex. Biochemistry **39:**12435-12440.

33. **Soriano, A., and R. P. Hausinger.** 1999. GTP-dependent activation of urease apoprotein in complex with the UreD, UreF, and UreG accessory proteins. Proceedings of the National Academy of Sciences, United States of America **96:**11140-11144.

34. **Sumner, J. B.** 1926. The isolation and crystallization of the enzyme urease. Journal of Biological Chemistry **69:**435-441.

35. **Todd, M. J., and R. P. Hausinger.** 1987. Purification and characterization of the nickel-containing multicomponent urease from *Klebsiella aerogenes*. Journal of Biological Chemistry **262:**5963-5967.

36. **Voland, P., D. L. Weeks, E. A. Marcus, C. Prinz, G. Sachs, and D. Scott.** 2003. Interactions among the seven *Helicobacter pylori* proteins encoded by the urease gene cluster. Liver Physiology **284:**G96-G106.

37. **Weatherburn, M. W.** 1967. Phenol-hypochlorite reaction for determination of ammonia. Analytical Chemistry **39:**971-974.

38. **Whitmore, L., and B. A. Wallace.** 2004. DICHROWEB, an online server for protein secondary structure analyses from circular dichroism spectroscopic data. Nucleic Acids Research **32:**W668-W673.

39. **Whitmore, L., and B. A. Wallace.** 2008. Protein secondary structure analyses from circular dichroism spectroscopy: Methods and reference databases. Biopolymers **89:**392-400.

40. **Witte, C.-P.** 2011. Urea metabolism in plants. Plant Science **180:**431-438.

41. **Yamaguchi, K., N. J. Cosper, C. Stalhanske, R. A. Scott, M. A. Pearson, P. A. Karplus, and R. P. Hausinger.** 1999. Characterization of metal-substituted *Klebsiella aerogenes* urease. Journal of Biological Inorganic Chemistry **4:**468-477.

42. **Zambelli, B., F. Musiani, S. Benini, and S. Ciurli.** 2011. Chemistry of Ni^{2+} in urease: Sensing, trafficking, and catalysis. Accounts of Chemical Research **44:**520-530.

CHAPTER 4

Iron-Containing Urease in a Pathogenic Bacterium

This work was published in the *Proceedings of the National Academy of Science, United States of America*, 2011, 108 (32), pp 13095-13099 with authors listed as Eric L. Carter, Dale E. Tronrud, Scott R. Taber, P. Andrew Kaplus, and Robert P. Hausinger

E.L.C. designed and performed the molecular biological, biochemical, and spectroscopic research and wrote the initial draft of the paper; D.E.T. (in the P.A.K. laboratory) solved the structure of UreA2B2; and S.R.T. assisted in the research

ABSTRACT

Helicobacter mustelae, a gastric pathogen of ferrets, synthesizes a distinct iron-dependent urease in addition to its archetypical nickel-containing enzyme. The iron-urease is oxygen-labile, with the inactive protein exhibiting a methemerythrin-like electronic spectrum. Significantly, incubation of the oxidized protein with dithionite under anaerobic conditions leads to restoration of activity and bleaching of the spectrum. Structural analysis of the oxidized species reveals a dinuclear iron metallocenter bridged by a lysine carbamate, closely resembling the traditional nickel-urease active site. Although the iron-urease is less active than the nickel-enzyme, its activity allows *H. mustelae* to survive the carnivore's low-nickel gastric environment.

INTRODUCTION

Urease, a urea-hydrolyzing enzyme, is a virulence factor associated with gastric ulceration by *Helicobacter pylori*, infection-induced urinary stones, and other disease states (28). Furthermore, the plant enzyme is essential for seed germination and is toxic to some fungi and insects (45). Of historical interest, urease from jack bean (*Canavalia ensiformis*) seeds was the first enzyme to be crystallized (42) and the first protein shown to utilize nickel ions for its catalytic function (15). Crystal structures of ureases from *Klebsiella aerogenes* (22), *Bacillus pasteurii* (7), *Helicobacter pylori* (20), and jack bean (3) reveal a highly conserved active site architecture consisting of two nickel ions bridged by a lysine carbamate. Assembly of this metallocenter requires a complex maturation machinery involving several accessory proteins (12). In this study I describe the purification, properties, and structure of an oxygen-labile, iron-dependent urease from a pathogen of ferrets, the first report of a naturally-occurring nickel-

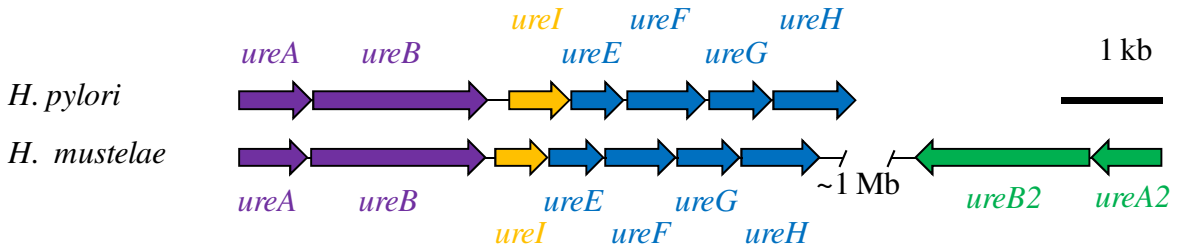

Figure 4.1: Urease gene clusters in *H. pylori* and *H. mustelae*. Structural genes coding for nickel-containing ureases are shown in purple while those coding for the iron urease are illustrated in green. Accessory genes are blue, and the genes encoding the proton-gated urea channel, *ureI*, are orange. Gene sizes are to scale according to genome coordinates obtained for *H. pylori* 26695 from The J. Craig Venter Institute website, and *H. mustelae* 12198 from GenBank.

independent form of this enzyme.

Helicobacter mustelae is a microaerophilic gastric pathogen of the ferret (*Mustela putorius furo*). This microbe and its mammalian host represent a useful model for *H. pylori* infection of humans (19, 37). The ferret-associated microorganism produces high levels of urease activity in order to neutralize the acidic gastric contents, much like the pathogen of humans (35, 41). *H. pylori* cells contain a single genetic cluster (*ureABIEFGH*) encoding two urease structural subunits, a proton-gated urea permease, and four urease accessory proteins (Figure 4.1), whereas *H. mustelae* contains both this cluster and a second set of urease structural genes (*ureA2B2*) located ~1 Mb downstream and not associated with any apparent maturation factors (29, 39). UreA2 and UreB2 share 57.4% and 69.5% identity to their UreA and UreB counterparts where the latter subunits are known to form an active nickel-containing enzyme (16). In contrast to *ureABIEFGH* which is induced by the addition of nickel ions, transcription of *ureA2B2* is up-regulated by iron and down-regulated by nickel ions due to repression via NikR, a nickel-responsive transcriptional regulator (39). *Helicobacter felis* and *Helicobacter acinonychis*, infectious agents of cats and big cats, also possess this genetic arrangement (39).

MATERIALS AND METHODS

Bacterial strains and growth. The *H. mustelae* strains used in this study were previously described (39) and include wild-type cells and *nikR ureB* (a constitutive producer of UreA2B2), *nikR ureB2* (a constitutive producer of UreAB), *nikR ureB ureB2* (a urease-negative control), and *ureB2* (a nickel-responsive producer of UreAB) mutants. Cells were grown on blood agar plates (Columbia blood agar base (Oxoid) with 7% defibrinated horse blood (HEMA Resources, Oregon, USA) and DENT selective supplement (Oxoid)) after inoculating with cells from frozen stock. Plates were incubated for ~72 h at 37 °C in Gas-Pak anaerobic systems (Becton, Dickinson and Company) using CampyGen (Oxoid) sachets to maintain a microaerobic environment. Studies involving the heterologous production of UreA2B2 in *Escherhichia coli* were carried out by using BL21-Gold (Stratagene) transformed with pEC015 or its site-directed variants (see below) and grown in Lennox broth (Fisher Scientific) (LB) at 37 °C with shaking.

Urease and protein assays. Urease activity was determined by quantifying the ammonia released during urea degradation by the formation of indophenol which was monitored at 625 nm (44). One unit of activity is defined as the amount of enzyme necessary to degrade 1 µmol of urea per min at 37 °C. Standard assay buffer consisted of 50 mM HEPES, pH 7.8, and 50 mM urea unless otherwise indicated. Kinetic constants were determined by fitting data with a standard Michaelis Menten equation using SigmaPlot software (Systat Software, Inc.). Protein concentrations were determined by using the Bio-Rad Protein Assay with bovine serum albumin as the standard. Molecular masses of 86,949 Da for UreA2B2, and 86,344 Da for UreAB were used to calculate protein concentrations.

Urease activities in whole cells, disrupted cells, and cell-free lysates of H. mustelae. The urease activities of *H. mustelae* strains were determined by scraping the whole cells into Tris-

buffered saline (TBS: 50 mM Tris-HCl, pH 7.4, containing 150 mM NaCl) from blood agar plates where they had grown for ~72 h at 37° C under microaerobic conditions. The resulting slurries were directly assayed or made anaerobic by several vacuum/argon purge cycles on a Schlenk line then assayed under anoxic conditions. Anaerobic disruption of the cells was carried out in sealed serum vials under argon by mixing the anaerobic whole cell slurry with degassed B-PER lysis reagent (Thermo Scientific) in a 1:1 (v/v) ratio. The mixture was incubated for 10 min on ice before assaying for urease activity under anoxic conditions. In some cases, the anaerobically disrupted cells were exposed to air for 2 h and then assayed under aerobic conditions, resulting in a complete loss of urease activity. For some experiments, aerobic whole cells were mixed with 12.5 mM sodium dithionite, incubated for 10 min on ice, and assayed. Aerobic soluble cell-free extracts were obtained by brief sonication of whole cells followed by centrifugation at ~16,000 *g* for 20 min in a microcentrifuge at 4 °C and subsequently assayed for urease activity. Protein concentrations for whole cells were assayed after sonication and centrifugation, as above. Protein assays were carried out directly on cell-free extracts and B-PER lysates.

Urease activity in whole cells of recombinant E. coli *cultures*. *E. coli* BL21-Gold cells harboring pEC015 were inoculated into LB medium containing 300 μg ml^{-1} ampicillin, grown overnight with shaking at 37 °C, and used to inoculate fresh medium containing 0, 0.1, 0.5, or 1.0 mM $FeSO_4$ (from a stock solution containing 10 mM ascorbate), $NiCl_2$, or $ZnCl_2$. Cultures were grown at 37 °C with shaking to an optical density at 600 nm of ~0.5, induced with 0.1 mM isopropyl β-D-1-thiogalactopyranoside (IPTG, Calbiochem), and incubated another 3 h before the cells were harvested by centrifugation. The cell pellets were twice resuspended and pelleted in 0.5 ml of TBS, and the resultant slurries were directly assayed for urease activity.

Cloning of ureA2B2 *for recombinant expression*. Genomic DNA from *nikR ureB H. mustelae* was isolated by using the DNeasy Blood and Tissue Kit (Qiagen) and following the manufacturer's instructions. This DNA served as template for PCR amplification of *ureA2B2* using forward primer (5'-TATA*GGATCC*AGGAGGTCACAGATGAAACTAACACC-TAAAGAACAAGAA-3') containing a BamHI restriction site (in italics) and an engineered ribosomal binding site (underlined), reverse primer (5'-TATA*CTGCAG*TTAGAAGAATG-TATAGCGGCTAGCCAAAGCTACTTCA-3') containing a PstI restriction site, and the Phusion High-Fidelity PCR kit following the manufacturer's instructions (New England BioLabs). The isolated BamHI-PstI *ureA2B2* fragment was digested and ligated into similarly digested pEXT20 (17) (a pBR322 derived expression vector) by using standard protocols (36), resulting in pEC015.

Site-directed mutagenesis. Site-directed mutations were introduced into pEC015 by using previously described methods (9) and the following overlapping primer sets: K218A, GGGTGC-GATTGGATTTGCGTTGCATGAAGACTGGG and CCCAGTCTTCATGCAACGCAAATCC-AATCGCACCC; K218R, CGGGTGCGATTGGATTTCGTTTGCATGAAGACTGGG and CC-CAGTCTTCATGCAAACGAAATCCAATCGCACCCG; K218E, GGTGCGATTGGATTT-GAATTGCATGAAGACTG and CAGTCTTCATGCAATTCAAATCCAATCGCACC; and C245A, GTATGATGTACAAGTTGCGATCCACACTGATACTG and CAGTATCAGTGTG-GATCGCAACTTGTACATCATAC. All plasmid constructs were verified by sequencing (Davis Sequencing).

Polyacrylamide gel electrophoresis and Western blot analysis. Samples were analyzed by sodium dodecyl sulfate-polyacrylamide gel electrophoresis (SDS-PAGE) using previously described buffers (25) with 12% running and 5% stacking polyacrylamide gels. After

electrophoresis, protein bands were visualized with Coomassie brilliant blue dye or the proteins were transferred to Immobilon-P polyvinylidene fluoride membranes (Millipore) and blotted with anti-*K. aerogenes* urease antibodies (33). The protein:antibody complexes were visualized with anti-rabbit alkaline phosphatase conjugated antibodies (Sigma) and BCIP®/NBT liquid reagent containing 5-bromo-4-chloro-3-indolyl phosphate and nitroblue tetrazolium (Sigma).

Aerobic purification of UreA2B2 from H. mustelae. The *nikR ureB* mutant of *H. mustelae* was grown on 48-60 blood agar plates for ~72 h under microaerobic conditions, harvested with a cell scraper, and collected into 0.15 M NaCl. The resultant slurry was centrifuged to pellet the cells, which were frozen at -80 °C or immediately resuspended in ice-cold 20 mM Tris-HCl, pH 7.0. Soluble cell-free extracts were prepared by sonication (Branson Sonifier, 3-5 cycles of 2 min each, power level 1-4, 50% duty cycle with cooling in an ice water/ethanol mixture) and pelleting the insoluble material by centrifugation at 120,000 *g* for 45 min or ~16,000 *g* for 10-20 min at 4 °C. Cell-free extracts were applied to DEAE-Sepharose resin (GE Healthcare) that had been equilibrated in resuspension buffer, the unbound species were allowed to flow through the column, and a linear gradient from 0 M to 1 M NaCl in 20 mM Tris-HCl, pH 7.0, was applied over ~6 column volumes. Fractions containing UreA2B2 (eluting at 0.1-0.2 M NaCl) were verified with SDS-PAGE, collected, pooled, and adjusted to 1.5 M NaCl. The pool was applied to phenyl-Sepharose CL-4B resin (GE Healthcare) that was equilibrated in 20 mM Tris-HCl, pH 7.0, containing 1.5 M NaCl, washed with the same buffer to elute the unbound species, and subjected to a linear gradient from 1.5 M NaCl to 0 M NaCl in the same buffer over ~6 column volumes followed by ~1-2 column volumes of buffer containing no salt. The UreA2B2 pool eluting in the latter half of the linear gradient and following the 0 M NaCl step was concentrated by using a 10,000 Da molecular weight cutoff Amicon Ultra centrifugal filter device or an

Amicon ultra-filtration stirred cell equipped with a 30,000 Da molecular weight cutoff membrane (Millipore). In some experiments the concentrated Phenyl-Sepharose pool was treated with 1 mM EDTA or 1 mM sodium dithionite plus 1 mM 2,2-bipyridyl overnight on ice before proceeding to the next aerobic purification step. The concentrated pool (at a volume <1% of the total bed volume of the column) was loaded onto a Sephacryl S300-HR column (GE Healthcare) that was equilibrated in 20 mM Tris-HCl, pH 7.0. Elution fractions containing UreA2B2 were verified by SDS-PAGE and concentrated as described above.

Anaerobic purification of UreA2B2 from H. mustelae. Similar to the above situation, *nikR ureB H. mustelae* cells were grown on 60 blood agar plates under microaerobic conditions and harvested into TBS. The slurry was thoroughly degassed by multiple vacuum and argon flush cycles on a Schlenk line and transferred into a Coy anaerobic chamber (Grass Lake, M.I., USA) with an atmosphere consisting of 1-3% H_2 with balance N_2. All further purification steps were carried out within the anaerobic chamber. The slurry was adjusted to contain 2.5 mM sodium dithionite, dispersed into 1 ml aliquots, and placed in a microcentrifuge tube cooler equilibrated at -20 °C. Each aliquot was disrupted with eight ~4 sec sonication bursts using a Fisher Scientific Sonic Dismembrator Model 100 at power level 4 and centrifuged at ~16,000 *g* at ambient temperature. Soluble cell-free extracts were adjusted with solid $(NH_4)_2SO_4$ to 40% saturation. The precipitate was removed by centrifugation, and the remaining soluble material was applied to Phenyl-Sepharose CL-4B resin equilibrated in 50 mM Tris-HCl, pH 7.4, containing 1.8 M $(NH_4)_2SO_4$ and 500 µM sodium dithionite. The unbound species were removed by washing with equilibration buffer for 3-4 column volumes, and the enzyme was eluted in the same buffer lacking $(NH_4)_2SO_4$. The pool was concentrated to 1-2 ml by using 10,000 Da molecular weight

cutoff Microcon centrifugal filter devices (Millipore) and the sample applied to a ~80 ml bed volume, 2.5 cm diameter Sephacryl S300-HR column equilibrated with 50 mM Tris-HCl, pH 7.4, containing 500 μM sodium dithionite. The fraction containing the largest amount of urease activity was collected and used in downstream studies. To test the effect of EDTA inclusion on the metal content of UreA2B2, 2.5 ml of the pool was treated with 1 mM EDTA for 60 min at ambient temperature before being applied to a PD-10 desalting column (8.3 ml Sephadex G-25 medium, GE Healthcare). The eluant was collected and concentrated via a 10,000 Da molecular weight cutoff Amicon Ultra centrifugal filter device before performing metal analysis by ICP-AES (see below for details). A similar sample left untreated by EDTA was analyzed in parallel as a control. Kinetic constants for the anaerobically purified UreA2B2 from *H. mustelae* reflect the value ± standard error generated by fitting data points averaged from two independent experiments with 10 concentrations of urea carried out with two different enzyme preparations.

Aerobic purification of UreA2B2 from E. coli. The *E. coli* BL21-Gold cells transformed with pEC015 were grown with shaking in LB supplemented with ampicillin at 300 μg ml^{-1} at 37 °C to an optical density at 600 nm of ~0.4, then induced with 0.1 mM IPTG and grown an additional 3 h. Cell pellets were resuspended in either 20 mM Tris-HCl, pH 7.4, or the same buffer plus 1 mM EDTA and 1 mM β-mercaptoethanol, and the slurry was sonicated as described for the aerobic purification from *H. mustelae*. Soluble cell-free extracts were obtained by centrifugation of cell lysates at 120,000 *g* for 45 min at 4 °C. Extracts were applied to DEAE-Sepharose resin equilibrated in cell resuspension buffer, unbound species allowed to flow through, and the sample eluted with a linear gradient from 0 M NaCl to 1 M NaCl in the same buffer over ~6 column volumes. Fractions containing UreA2B2 (eluting at ~0.2 M NaCl) were verified by SDS-PAGE, pooled, and adjusted to 1.8 M NaCl by direct addition of NaCl crystals

or dialysis. The resultant pool was filtered and applied to Phenyl-Sepharose CL-4B resin equilibrated in buffer containing 1.7 M NaCl, the unbound species were allowed to flow through, and a linear gradient from 1.7 M NaCl to 0 M NaCl was applied over ~6 column volumes followed by ~1-2 column volumes of buffer containing no salt. Fractions containing UreA2B2 (i.e., the latter portion of the linear gradient and wash step) were verified by SDS-PAGE, pooled, and concentrated using an Amicon ultra-filtration stirred cell equipped with a 30,000 Da molecular weight cutoff membrane or an Amicon Ultra 10,000 Da molecular weight cutoff centrifugal filter device. The pool (<1% of the total column volume) was applied to Sephacryl S300-HR resin equilibrated in buffer containing 300 mM NaCl. Fractions containing UreA2B2 were verified by SDS-PAGE.

Aerobic purification of UreAB from H. mustelae. UreAB was purified from wild-type and *nikR ureB2 H. mustelae* by making minor changes to the same purification technique as that described for the aerobically purified UreA2B2. Instead of Tris-based buffers, PEB (20 mM Na-phosphate, pH 7.4, containing 1 mM EDTA and 1 mM β-mercaptoethanol) buffers were used along with KCl rather than NaCl. Subsequent to the DEAE-Sepharose chromatography, fractions eluting during the gradient containing the highest amount of urease activity were collected, pooled, and dialyzed against PEB buffer containing 1.7 M KCl. The pool was chromatographed on Phenyl-Sepharose CL-4B resin equilibrated in the dialysate buffer, and bound proteins were eluted with a linear gradient from 1.7 M KCl to 0 M KCl in PEB buffer over ~6 column volumes, followed by 1 column volume of buffer with no salt. Fractions containing the greatest level of urease activity (eluting in the beginning of the linear gradient) were collected, pooled, and concentrated with an Amicon Ultra 10,000 Da molecular weight cutoff centrifugal filter device. The resultant pool (<1% of the total column bed volume) was loaded onto a Sephacryl

S300-HR column equilibrated in PEB buffer containing 100 mM KCl. Fractions containing UreAB were verified by SDS-PAGE. Kinetic constants for UreAB reflect the value ± standard error generated by fitting data points averaged from two independent experiments with 11-12 urea concentrations carried out with enzyme from a single preparation.

Metal analysis. Purified protein preparations and buffer blanks were analyzed for metal content by ICP-AES at the University of Georgia Center for Applied Isotope Studies. As a second approach to measure iron contents, the Fe-specific chromogenic chelator 1,10-phenanthroline (Sigma) was used. 196 µl of protein, in 20 mM Tris-HCl (pH 7.4) containing 25 mM NaCl for aerobically purified samples or 50 mM Tris-HCl (pH 7.4) with 500 µM dithionite for anaerobically purified samples, was mixed with 2 µl of 10% SDS prepared in water and 2 µl of 100 mM 1,10-phenanthroline dissolved in dimethyl sulfoxide. The mixtures were boiled for 5 min, sodium dithionite was added to 1 mM (to reduce oxidized iron), and the reaction incubated at ambient temperature for 5 min before measuring the absorbance at 512 nm. The results were compared to a standard curve developed using ferrous sulfate, diluted from a 10 mM ferrous sulfate stock prepared in 10 mM ascorbate.

In vitro *reactivation of aerobically-purified UreA2B2.* UreA2B2 purified aerobically from *H. mustelae* or *E. coli* was degassed and transferred into an anaerobic Coy chamber. Protein samples (~10 µM, 20 mM Tris-HCl, pH 7.4, 300 mM NaCl) were mixed with ~0.1 mM sodium dithionite and incubated at ambient temperature for the times indicated. Aliquots of the reaction mixtures were assayed for urease activity under anoxic conditions. To assess the effect of added metal ions on the reactivation, *E. coli*-derived protein (~10 µM in 20 mM Tris-HCl, pH 7.4, containing 300 mM NaCl) was mixed with 1 mM sodium dithionite and 10 µM $FeSO_4$, $NiCl_2$, or

$ZnCl_2$ for 90 min at ambient temperature before aliquots of the mixtures were assayed for urease activity.

Absorption spectroscopy. The electronic spectra of UreA2B2 samples were monitored by using a Shimadzu UV-2401PC spectrophotometer at room temperature. Samples in sealed serum vials were made anaerobic by repeated (> 10) vacuum/argon cycles on a Schlenk line before being transferred to anaerobic cuvettes using gas-tight syringes (Hamilton). Degassed sodium dithionite solution was anaerobically transferred into the anoxic protein solution, incubated at room temperature for up to 60 min, and spectra were recorded every 10 min. The protein concentration was diluted by less than 1% due to the addition of dithionite.

EPR spectroscopy. E. coli-derived UreA2B2 (100 µM) in 20 mM Tris-HCl, pH 7.4, with 300 mM NaCl was degassed by several vacuum/argon cycles and transferred into an anaerobic chamber (~2.5% H_2 and balance N_2). One aliquot was transferred directly into an EPR tube whereas a second sample (230 µl) was treated with sodium dithionite (2.3 µl of 50 mM, final concentration of ~0.5 mM) at ambient temperature. After 20 min the tubes were sealed with septa, removed from the chamber, and frozen in liquid N_2. The samples were examined by EPR spectroscopy at 4.3 K using a Bruker E300X spectrometer operating at X-band and equipped with an Oxford Instruments liquid helium flow system with a CF-935 cryostat and an ITC-503 temperature controller.

Crystallization and data collection of UreA2B2 urease. UreA2B2 purified aerobically from *E. coli* was tested for its ability to crystallize. In screens carried out using a Phoenix crystallization robot (Art Robbins Instruments), flat diamond-shaped crystals measuring 0.2 x 0.1

Table 4.1: Data collection and refinement statistics for *H. mustelae* UreA2B2.

Resolution	3.0 Å
Wavelength (Å)	0.97650 Å
Observations	1,281,593
Unique Observations	141,354
Multiplicity	8.8 (5.1)
R_{meas}	21.5% (90%)
R_{pim}	7.2% (37%)
$<I/\sigma_I>$	9.3 (1.8)
R (%)	17.0% (23.7%)
R_{free} (%)	18.9% (25.5%)
Rms bond lengths	0.009 Å
Rms bond angles	1.2°
Number waters	606
Ramachandran outliers	11*

* The 11 Ramachandran outliers are UreB2 residues 281, 365, and 464, which were flagged in one, four, and six of the ncs chains, respectively. All have conformations near the edge of the allowed regions.

x 0.02 mm^3 were grown in 1 week at 4 °C in 96 well trays in sitting drops with 0.5 µl protein stock (10 mg/ml in 10 mM Tris HCl, pH 7.4) mixed with 0.25 µl reservoir solution containing 30% (v/v) 2-methyl-2,4-pentanediol (MPD), 0.1 M sodium acetate, and 0.02 M $CaCl_2$ (condition #2 of Emerald Wizard III; Emerald BioSystems). The crystal was harvested by using a loop, pulled through oil, and flash-frozen by plunging into liquid nitrogen. Data were collected at beamline 5.0.3 at the Advanced Light Source (Lawrence Berkley National Laboratory). Three passes including a total of 463 frames were collected. The space group was I222, with a=166.98,

b=223.94, c=395.87 Å. The diffraction images were processed using iMOSFLM (26) leading to a complete data set at 3.0 Å resolution (Table 4.1). 5% of the reflections were randomly selected for an R_{free} test set.

Structure solution and refinement of UreA2B2 urease. The structure was solved by using molecular replacement with the program Phaser (27) in the Phenix package (2). The search structure was Protein Data Bank (8) entry 1EJX, a 1.6 Å resolution structure of *K. aerogenes* urease. This urease is 55% identical in sequence to UreA2B2, albeit with three chains instead of two. For molecular replacement, non-identical residues were truncated to Ala or Gly by phenix.sculptor, and solvent molecules, metals, and the metal coordinating side chains were removed. A clear solution was found placing six copies of this motif, arranged as two trimers. The initial R-factor was 44.3%. This model was passed to phenix.autoBuild (43) which performed a "rebuild in place," yielding a model that had an R/R_{free} (11) of 21.4%/23.5%.

All manual rebuilding was carried out with Coot (18). Initial changes included adding inserted (relative to the *K. aerogenes* urease) residues for the (now fused) UreA2 chain at positions 52, 101, 111, and the C terminal 19 residues; for the UreB2 chain two residues were inserted at position 108. Also, the loop in the C chain from 317 to 339 was substantially changed. This model was further refined in Buster (10) using tight non-crystallographic symmetry (ncs) restraints on the six copies of each chain and allowing waters to be added. The model, with 2085 waters, had R/R_{free} of 16.0%/20.8% with good geometry.

To keep the active site density unbiased through this stage in refinement the expected ligands to the iron atoms were modeled as Ala residues and no iron atoms were placed. The electron density in the active sites of each of the six copies in the asymmetric unit and in the ncs-

averaged map unambiguously shows a metallocenter with a structure very similar to that of the nickel center in the *K. aerogenes* urease. (Note: this also matches the metallocenter in the *H. pylori* urease structure with acetohydroxamic acid bound [PDB entry 1E9Y, (20)] but is different than the metallocenter seen in the unliganded *H. pylori* urease active site which has been incorrectly modeled (PDB entry 1E9Z, (20)) and by our analysis has significant apoenzyme present.) At this point, the iron atoms and ligating side chains were built into the active site and residues 321 thru 331 were removed from the model as their electron density was weak and difficult to interpret. Further refinement with Buster led to a model with 2435 water molecules and an R/R_{free} of 14.48%/19.09%.

Manual adjustments of details of the model, including partial rebuilding of the 321-330 loop, were guided by Molprobity (13) as well as comparison with the high resolution urease model 1EJX. In the end, residues 329-332 had insufficient density and were not modeled. Also, water molecules automatically placed by Buster were scrutinized because the philosophy behind the Buster placement of waters is to place many "water molecules" to be able to calculate better phases and correspondingly better maps rather than to represent a true model of the bound solvent. We deleted all water molecules further than 3.5 Å from a protein atom (limiting the solvent model to the first level hydration sphere), and furthermore developed a novel approach which utilized the ncs of this crystal form to predict the presence of water molecules in locations where the local density, alone, was of insufficient quality to justify placement. This procedure increased the number of water molecules to 3507 and, after additional refinement in Buster, the R values dropped to 15.4%/17.4%.

In the final round, water molecules were stringently filtered by requiring that each have $2F_o$-F_c density greater than 0.37 electrons/$Å^3$ in the $2F_o$-F_c ncs-averaged map as calculated by

COOT. A few water molecules were added to positions having ncs-averaged F_o-F_c density 0.30 electron/Å^3 and multiple hydrogen bonding partners. All water molecules continued to be restrained by the ncs unless the symmetry was locally broken. The final refined model contains 606 water molecules and an R/R_{free} of 17.0%/18.9%. Because at 3.0 Å resolution electron density peaks may not accurately reflect the positions of individual waters, a second model with no water sites included was refined, yielding R/R_{free} of 17.7%/19.5%. The two models have been deposited in the Protein Databank as entries 3QGA (3.0 Å, wild-type) and 3QGK (3.0 Å, wild-type, no solvent), respectively.

It is of interest to note that a formyl group was modeled onto Met-1 of the UreA2 chain. *H. pylori* urease (PDB entry 1E9Y) shows similar density, although the formyl group was not modeled. The N-terminus of jack bean urease (PDB code 3LA4; (3)) appears to be modified by CO_2 (an N-carboxy group), although this was modeled as waters. In three *B. pasteurii* urease structures (entries 2UBP (7), 3UBP (7), and 4UBP (6)) the density was modeled as an acetyl whereas it was modeled as a carboxyl group in two other structures (1UBP (5) and 1IE7 (4)). While an acetylated model and a carboxylated model are isostructural, the inferred hydrogen bond pattern in every case is consistent with carboxylation. In the urease from *K. aerogenes* urease the N-terminus is unmodified.

RESULTS

H. mustelae *UreA2B2 is an oxygen-labile urease*. A mutant strain of *H. mustelae* lacking *nikR* and *ureB* constitutively produces UreA2B2 and exhibits low levels of urease activity (39) (Figure 4.2 and Table 4.2). All strains producing UreAB yielded high levels of urease activity

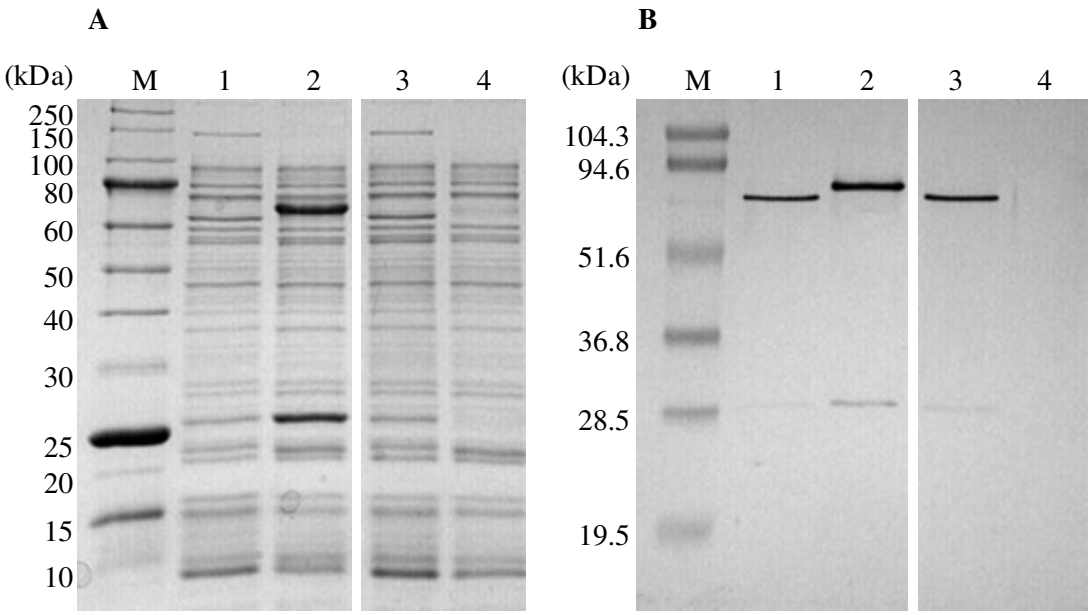

Figure 4.2: Denaturing gel electrophoretic analysis of *H. mustelae* strains. (**A**) Gel of soluble cell-free extracts of *H. mustelae* strains stained with Coomassie blue. Lanes: M, molecular mass markers; 1, wild-type; 2, *nikR*, *ureB*; 3, *ureB2*; 4, *nikR*, *ureB*, *ureB2*. (**B**) Western blot analysis of *H. mustelae* cell-free extracts. Lanes: M, molecular mass marker; lanes 1-4 correlate to lanes from (A) transferred to PVDF membranes and blotted with anti-*K. aerogenes* urease antibodies

that were stable to cell lysis, but the low urease activity of the *nikR ureB* mutant was lost upon aerobic cell disruption. Significantly, the urease activity of the *nikR ureB* cells increased under anaerobic conditions and the lysate activity was stable when kept anaerobic (Table 4.2). Although the mutant strain produces only about 10% of the urease activity of the wild type strain, it survives acidic shock conditions when provided with urea — consistent with UreA2B2 supporting *H. mustelae* growth in gastric tissue (39). Furthermore the UreA2B2 activity is independent of UreG or HypB, proteins known to be essential for maturation of the *Helicobacter* nickel-containing urease (30), suggesting a different activation mechanism (39). In sum, these results suggest that UreA2B2 is a novel oxygen-labile urease that does not require typical accessory proteins for maturation.

Table 4.2: Urease activities of whole cells, disrupted cells, or soluble cell-free extracts of *H. mustelae* strains.

***H. mustelae* strain**	**Assay conditions**	**Whole cell activity (U mg protein^{-1})**	**Activity (U mg^{-1})***
Wild-type	aerobic	17.2 ± 1.3	20.9 ± 0.1
ureB2	aerobic	23.2 ± 1.1	24.1 ± 0.4
nikR ureB2	aerobic	32.5 ±1.1	26.9 ±0.5
nikR ureB ureB2	aerobic	NA†	NA†
nikR ureB	aerobic	0.33 ± 0.01	NA†
nikR ureB	anaerobic	2.2 ± 0.2	2.9 ± 1.6‡
nikR ureB	aerobic, 12.5 mM dithionite	0.98 ± 0.02	ND§

*Activity in cell-free extracts unless stated otherwise. †No activity detected. ‡Activity in disrupted cells. §Not determined. Values represent the average ± standard deviation of 3-5 determinations. UreA2B2 is produced at elevated levels in *nikR* cells unless *ureB2* also is disrupted (Figure 4.2).

*Effects of medium supplementation with metal ions on UreA2B2 activity***.** To investigate the effects of various metal ions on UreA2B2 urease activity, we examined recombinant cells because *H. mustelae* cell growth was limited to blood agar plates. Thus, we cloned and expressed

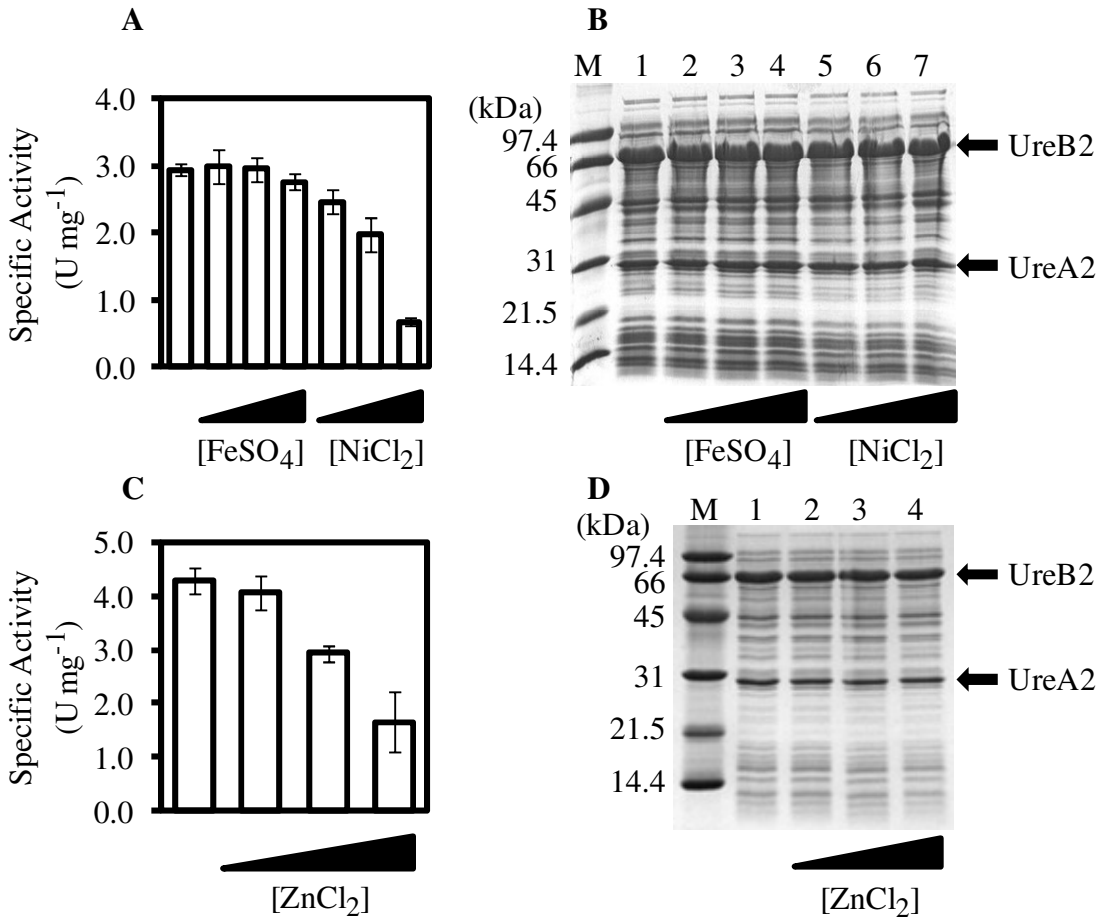

Figure 4.3: Effect of supplementing the growth medium with iron, nickel, and zinc ions on UreA2B2 urease activity and protein production in *E. coli* pEC015. (**A**) and (**C**) Urease specific activity of whole cells grown in medium supplemented with iron or nickel, and zinc, respectively. Black triangles indicate increasing concentrations of metal ions in the medium. Bars represent the average of three experiments with the standard deviation shown by error bars. (**B**) and (**D**) Denaturing gel electrophoresis of cell-free extracts corresponding to the whole cells from (**A**) and (**C**), respectively. M, molecular mass markers. Migration positions of UreA2 and UreB2 are shown to the right. 15 µg of each cell extract preparation were loaded onto the gel.

ureA2B2 in *E. coli*, grew the cells in LB, observed urease activity even in the absence of urease accessory proteins, demonstrated that supplementation with ferrous ions had negligible effects on activity, and found that addition of nickel or zinc led to diminutions of activity (Figure 4.3, panels A and C). The various perturbations to the medium did not affect UreA2B2 production

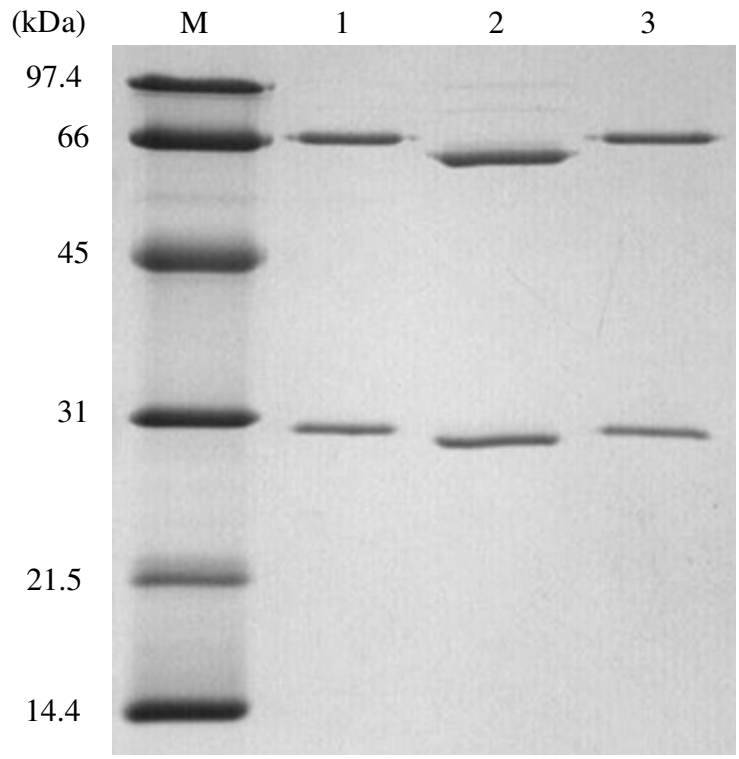

Figure 4.4: Homogeneity of aerobically-purified urease samples by denaturing gel electrophoresis. Lanes: M, molecular mass markers; 1, *H. mustelae*-derived UreA2B2; 2, *H. mustelae*-derived UreAB; 3, *E. coli*-derived UreA2B2.

levels in cell extracts (Figure 4.3, panels B and D). These results demonstrate that nickel or zinc additions to culture media do not increase UreA2B2 activity.

*UreA2B2 lacks nickel and contains iron***.** To directly assess the metal content of UreA2B2, the protein was purified both aerobically and anaerobically from *nikR ureB H. mustelae* cells collected off plates and also aerobically from recombinant *E. coli* cells grown in broth culture. The purified proteins (Figure 4.4) were examined for metal contents by inductively coupled plasma atomic emission spectroscopy and for iron by 1,10-phenanthroline assays (Table 4.3).

As purified aerobically from *H. mustelae*, UreA2B2 contains ~2 equivalents of iron per heterodimer, along with very small amounts of zinc and no detectable nickel. The iron content

Table 4.3: Kinetic properties and metal contents of purified *H. mustelae* ureases.

Protein	**Source**	**Purification conditions**	**V_{max} (U mg protein^{-1})**	**K_m (mM)**	**Metals per heterodimer ***
UreA2B2	*H. mustelae nikR ureB*	Aerobic (O_2)	NA† (10.7 ± 0.4)	NA†	ICP: 2.3 Fe, 0.2 Zn PA: 2.01 ± 0.05 Fe
UreA2B2	*H. mustelae nikR ureB*	EDTA, O_2	NA†	NA†	ICP: 2.3 Fe, 0.2 Zn
UreA2B2	*H. mustelae nikR ureB*	BP‡, O_2	NA†	NA†	ICP: 1.9 Fe, 0.1 Zn
UreA2B2	*H. mustelae nikR ureB*	Anaerobic	14.0 ± 0.2	1.6 ± 0.1	ICP: 1.1 Fe, 0.7 Zn PA: 1.05 ± 0.07 Fe
UreA2B2	*E. coli* pEC015	O_2	NA† (9.8 ± 0.5)	NA†	ICP: 1.0 Fe, <0.1 Zn PA: 1.13 ± 0.12 Fe
UreA2B2	*E. coli* pEC015	EDTA, βME, O_2	NA†	NA†	ICP: 0.8 Fe, <0.1 Zn PA: 0.89 ± 0.02 Fe
UreAB	*H. mustelae* wild type	EDTA, βME, O_2	390 ± 6	1.7 ± 0.1	ICP: 0.6 Ni, 0.2 Fe, <0.1 Zn
UreAB	*H. mustelae nikR ureB2*	EDTA, βME, O_2	840 ± 20	2.3 ± 0.2	ICP: 1.1 Ni

* Measured by ICP-AES (ICP) or based on reactivity with 1,10-phenanthroline (PA, average of triplicate experiments ± SD). † Not active; numbers in parentheses are specific activities of samples after reductive activation for 80 min. ‡ Treated with 2,2-bipyridyl and dithionite prior to aerobic purification.

was not greatly affected by treatment with EDTA or 2,2-bipyridyl (BP), indicating that the metal is tightly bound and chelator inaccessible—as is the case for nickel-containing ureases. When UreA2B2 was purified from *H. mustelae* under anaerobic conditions in the absence of chelator, both iron and zinc (1.1 and 0.7 equivalents, respectively) were found. A similar sample of anaerobically isolated enzyme (containing 1.3 equivalents of iron and 0.42 equivalents of zinc) treated with EDTA resulted in less zinc content (to 0.26 equivalents) while not affecting the iron content or the activity. Thus, zinc content does not correlate with enzyme activity. The anaerobic protein samples consistently bound less iron than aerobic samples, compatible with lower binding affinity for ferrous ions compared to the more highly charged ferric ions.

Aerobic purification of UreA2B2 from *E. coli* yielded sample with only ~1 equivalent of iron regardless of the presence or absence of EDTA and 2-mercaptoethanol (βME). Trace amounts of zinc and no nickel were detected. This result is consistent with UreA2B2 spontaneously acquiring some active site iron regardless of the host or with *E. coli* utilizing an endogenous iron incorporation system that partially compensates for unidentified maturation proteins in *H. mustelae*. In summary, these results demonstrate that regardless of the host UreA2B2 contains iron and small amounts of zinc while lacking nickel.

For comparison, the oxygen-stable UreAB was isolated from wild-type and *nikR ureB2 H. mustelae* (Figure 4.4). In contrast to the iron-dominated metal content of UreA2B2, UreAB purified from wild-type and *nikR ureB2 H. mustelae* contained 0.6 and 1.1 equivalents of nickel, respectively (Table 4.3). NikR represses transcription of genes encoding nickel import proteins in *H. mustelae* and *E. coli* (34, 40); thus, the *nikR ureB2* mutant likely contains higher cellular

levels of nickel compared to wild-type cells, thereby accounting for the ~2-fold increase in nickel content (and specific activity, see below) of UreAB in this strain.

Kinetic properties of UreA2B2. UreA2B2 purified anaerobically from *nikR ureB H. mustelae* was active (V_{max} of ~14 U mg protein^{-1}), whereas all samples of this protein purified aerobically lacked activity (Table 4.3). Progress curves generated using anaerobically-prepared UreA2B2 demonstrated inhibition by acetohydroxamic acid, a common inhibitor of nickel-containing ureases, and 2-fold enhancement of activity by 1 mM EDTA, consistent with tight binding of the active site iron and chelation of an inhibitory metal ion (Figure 4.5, panel A). Metal ion inhibition of ureases is well established (31), and the inclusion of $NiCl_2$ in the assay led to a time-dependent decrease of activity. Exposure to air (~20 min) abolished the activity of purified enzyme, confirming its oxygen lability. Of great importance, subjecting aerobic UreA2B2 (which contains only trace levels of zinc) to gas exchange and dithionite treatment led to its reactivation (Figure 4.5, panel B) and the reactivated *H. mustelae*- and *E. coli*-derived proteins possessed activities approaching that of the enzyme isolated using strictly anaerobic purification procedures (Table 4.3). The inclusion of one equivalent of nickel or zinc in the reductive reactivation buffer containing *E. coli*-derived protein did not have a marked effect on the resultant specific activity (Figure 4.5, panel C); iron may have stimulated modestly and nickel may have slightly inhibited the process. These results further establish that neither nickel nor zinc is required for UreA2B2 activity.

Anaerobic UreA2B2 exhibited a K_m (~2 mM) similar to that for UreAB; however, UreAB had much greater activity (V_{max} of ~387 and 836 U mg protein^{-1}, respectively, from the wild-type or *nikR ureB2* mutant *H. mustelae* cells). For comparison, urease from *H. mustelae*

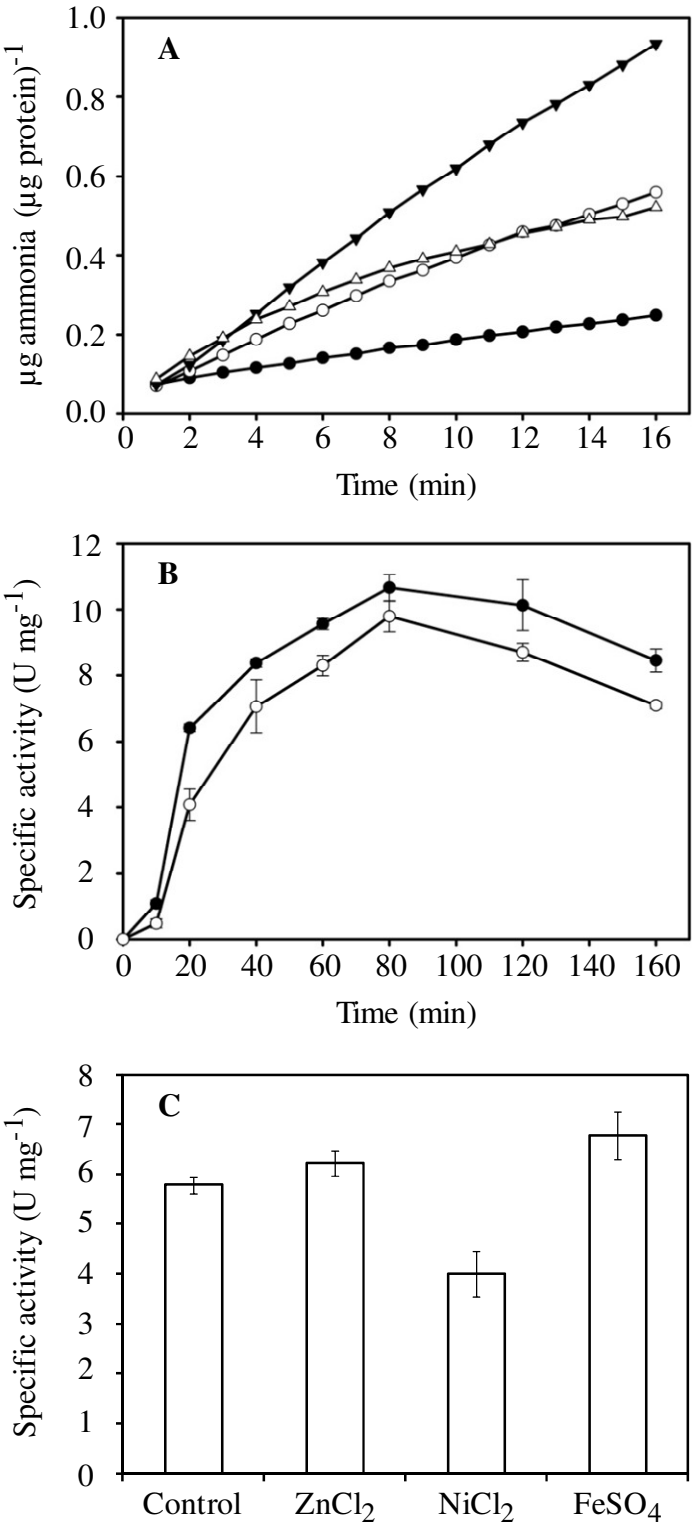

Figure 4.5: Activity of purified UreA2B2. (**A**) Progress curves for UreA2B2 purified anaerobically from *H. mustelae* when assayed in anaerobic buffer containing 50 mM urea (○) or

Figure 4.5 legend continued:
further supplemented with 3 mM acetohydroxamic acid (●), 1 mM EDTA (▼), or 100 μM $NiCl_2$ (Δ). Data points represent the average of duplicate experiments. (**B**) Activation kinetics of oxidized UreA2B2 by dithionite. Inactive samples (~10 μM heterodimer) purified aerobically from *H. mustelae* (●) and *E. coli* (○) were subjected to vacuum/argon cycling, supplemented with ~100 μM dithionite, and incubated at ambient temperature. At the indicated time points, samples were assayed anaerobically in buffer containing 50 mM urea. (**C**) Specific activity after reductive activation of *E. coli*-derived protein in the presence of metal ions. Protein (~10 μM) was incubated with 1 mM dithionite and one equivalent of $FeSO_4$, $NiCl_2$, or $ZnCl_2$ for 90 min before aliquots were assayed. Bars represent the average of triplicate experiments ± standard deviation.

cells grown on 5% sheep blood and Trypticase soy agar (a medium with more nickel (46)) exhibited a specific activity of 1,560 U mg^{-1} and a urea K_m of 0.45 mM (16).

Analysis of the UreA2B2 metallocenter. To probe the electronic properties of the UreA2B2 metallocenter, UV-visible spectroscopy was carried out on aerobic and anaerobic samples. Wavelength scans of the aerobically-purified protein indicated a small and broad absorption at ~500 nm, with more prominent shoulders at ~380 nm and ~320 nm (Figure 4.6, panel A). These features are reminiscent of the methemerythrin spectrum attributed to a μ-oxo bridged diferric metallocenter (24). Addition of sodium dithionite to oxidized UreA2B2 under anaerobic conditions caused bleaching of the spectrum, in parallel to the restoration of activity, consistent with direct reduction of the active site ferric ions (Figure 4.6, panel B). Exposure of the reduced sample to oxygen led to the redevelopment of the chromophore.

Additional evidence that the UreA2B2-associated iron is associated with a homodinuclear center was derived from electron paramagnetic resonance (EPR) studies. In particular, neither the oxidized nor the reduced sample exhibited an EPR spectrum in the standard perpendicular mode. For an oxidized dinuclear center [i.e., Fe(III)/Fe(III)], antiferromagnetic coupling yields an overall $S = 0$ accounting for lack of signal. For reduced [Fe(II)/Fe(II)] species, the ferrous ions

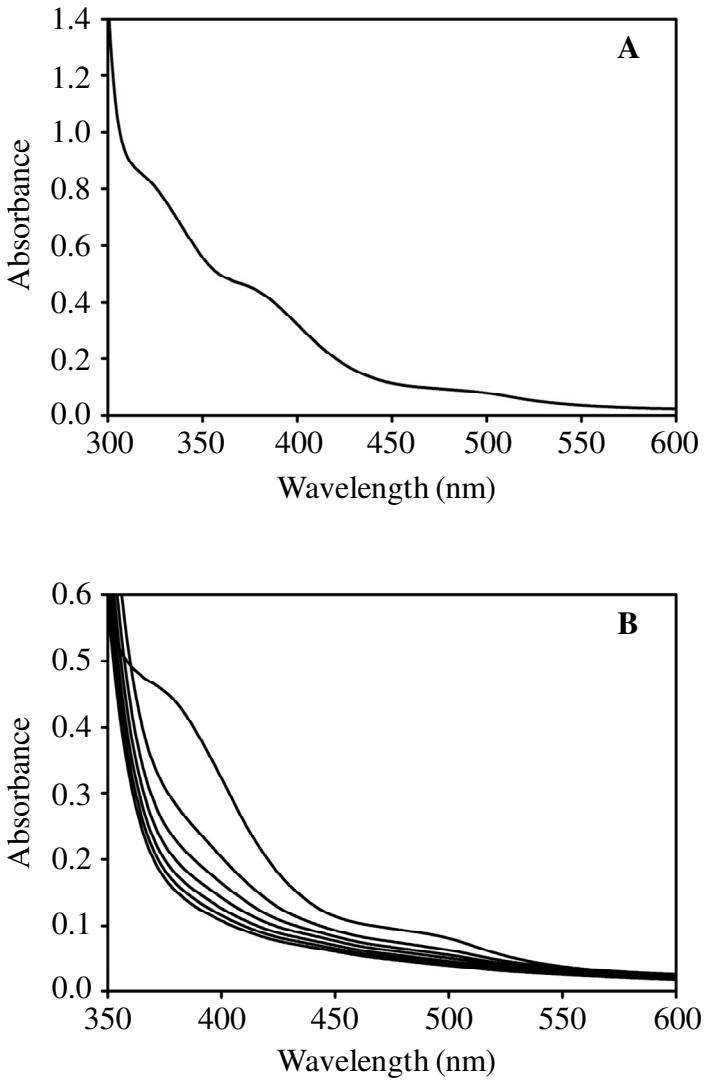

Figure 4.6: Electronic absorption spectra of UreA2B2. (**A**) Inactive UreA2B2 (100 µM) was purified aerobically from *E. coli* and its spectrum obtained in buffer containing 200 mM Tris-HCl, pH 7.4. (**B**) Dithionite reduction of UreA2B2 under anaerobic conditions. The protein sample shown in **A** was gas exchanged by vacuum/argon cycling, supplemented with degassed 0.5 mM dithionite, and incubated at ambient temperature for 60 min, with spectra recorded every 10 min. Only the 350-600 nm region is shown as dithionite yields intense absorption features below 350 nm.

often possess a signal with a high g-value in parallel mode that may not be visible in perpendicular mode. This would not be the situation for a mononuclear iron site or for an iron-zinc heterodinuclear site, thus ruling out significant levels of these species.

Alignment of UreA2B2 with other urease sequences indicated the presence of a Lys at position 218 in UreB2, comparable to the Lys that forms a carbamate which serves as a ligand bridging the two metal ions in nickel-containing ureases. Recombinant *E. coli* cells expressing mutated *ureA2B2*, where this residue was substituted with Ala, Arg, or Glu, lacked urease activity, consistent with Lys218 playing a critical role at the active site. A homology model of UreA2B2, created using the structure of *H. pylori* urease as a template, identified a unique Cys residue near the active site that initially was suspected of being important for metal ion specificity. Substitution of this residue by Ala, as found in *H. pylori* and most other urease sequences, had only modest effects (85% activity retained) in whole *E. coli* cells grown in LB when compared to recombinant cultures containing wild-type UreA2B2; hence, we conclude that Cys245 is not required for proper metallocenter assembly.

Crystal structure of UreA2B2. To identify potential functionally relevant differences between the active sites of the UreA2B2 iron-containing active site in comparison to that of nickel ureases, the aerobically-isolated protein was crystallized and the structure elucidated at 3.0 Å resolution (Table 4.1). As expected, the tertiary structure matches that of other ureases, and the quaternary structure matches that of *H. pylori* urease (20), being a superstructure of four UreA2B2 trimers arranged as a hollow ball with tetrahedral symmetry (Figure 4.7, panel A). The active sites open to the outer surface of the sphere, with access partially occluded by the 317 to 333 loop. This active site flap adopts a different conformation in various urease crystal forms, and has high flexibility in all cases (Figure 4.7, panel A).

At this resolution, the ligands to the iron atoms are arranged in an indistinguishable manner from their equivalents in the nickel ureases (Figure 4.7, panel B). Some additional electron density near the Fe1 atom is similar in placement and shape to the density seen for

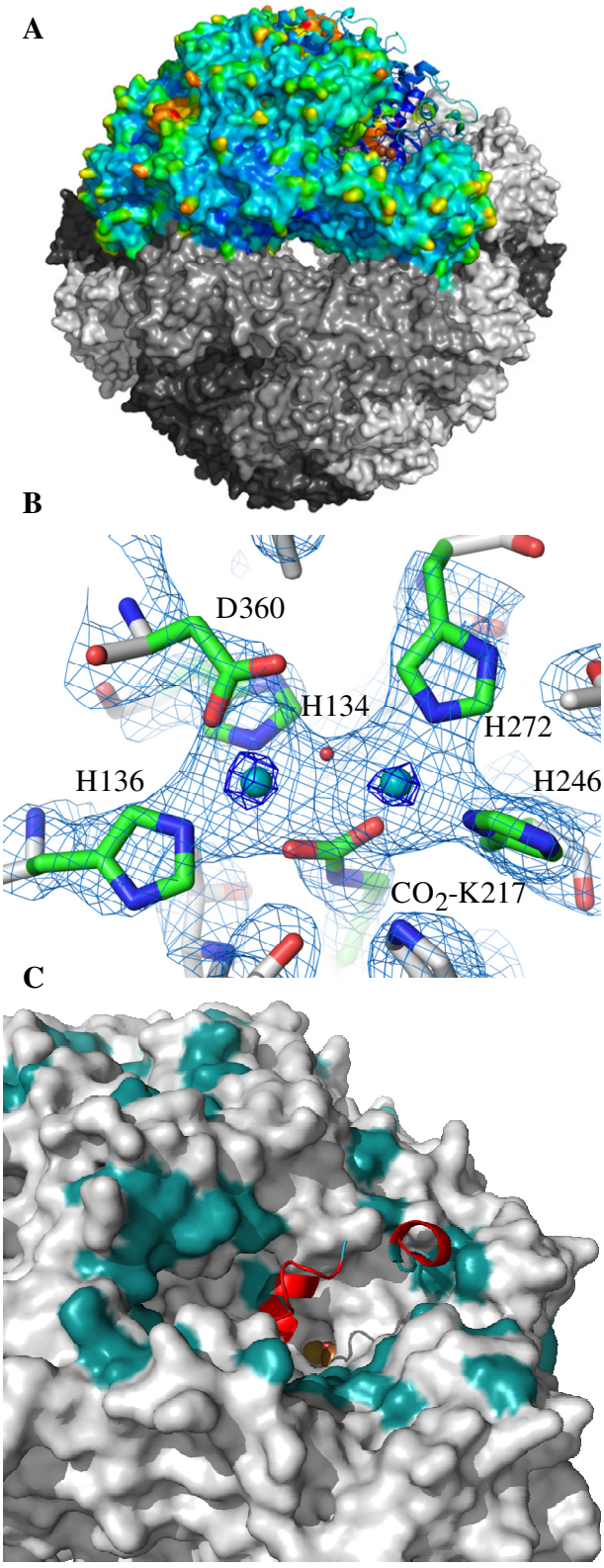

Figure 4.7: Structure and unique features of dinuclear Fe-containing *H. mustelae* UreA2B2. (**A**) Molecular surface of the UreA2B2 dodecameric super-structure. One $(UreA2B2)_3$ trimer is

Figure 4.7 legend continued:
rainbow-colored from blue to red, indicating increasing chain mobility as measured by B factors, with one UreA2B2 unit shown as a ribbon with the active site irons as brown spheres. The three active site flaps are visible as red-orange patches and, for the ribbon representation, a gap is due to disorder of four residues that were not modeled. (**B**) An unbiased $2F_o$-F_c electron density map of the metallocenter, generated from a model before the metals or metal ligands were built, is compared with the *K. aerogenes* urease structure. Nickels (teal spheres), side chains not included in the phasing model (green carbons and labeled) and other local protein atoms (white carbons) are shown, and the electron density is contoured at two levels (0.3 and 1.3 e/Å^3). (**C**) Active site region highlighting (in cyan) residues differing between UreA2B2-type ureases and other ureases. The molecular surface is shown except for the active site flap (red ribbon) and irons (brown spheres). The view is as for the molecule shown as a ribbon in panel A.

acetohydroxamic acid bound to *H. pylori* urease (PDB entry 1E9Y)(20). With acetate present in the mother liquor of our crystals, this density may represent acetate binding to the active site, but because an unambiguous identification cannot be made we have not modeled this density. Comparison of B factors of the metal ions with those of ligating residues indicates that the metal sites are fully occupied, consistent with preferential crystallization of the metallated form of the enzyme.

DISCUSSION

The biochemical and crystallographic data described here demonstrate that *H. mustelae* UreA2B2 is a dinuclear ferrous ion-dependent urease, the first nickel-independent urease reported. Oxidation by O_2 likely leads to a μ-oxo bridged diferric inactive species that can be chemically reduced to restore activity. The presence of two types of urease in *H. mustelae*, *H. felis* (32), and *H. acinonychis* may represent an evolutionary adaptation to their niches, as previously hypothesized on the basis of the differential regulation of their urease gene clusters (39). *Helicobacter* species require urease activity to colonize the host gastric tissue; however, carnivores have diets rich in iron and low in nickel content (38) so infection by these pathogens

would be hindered if they were limited to possessing only nickel ureases. The capacity to produce either nickel- or iron-urease allows these microbes to colonize their hosts regardless of their host's diets.

The basis of the distinct metal specificities for the two ureases in *H. mustelae* remains obscure. The immediate environment around the iron active site is nearly identical to that in nickel ureases, and so we considered the broader context of the whole protein chains, which reveals 92 residues that are conserved in UreA2B2 sequences and lacking in nickel ureases. Notably, mapping these UreA2B2-distinct residues onto the urease structure (Figure 4.8) revealed a prominent cluster that encircles the entrance to the active site (Figure 4.7, panel C). This finding leads us to the hypothesis that the difference in metal discrimination occurs during the metal loading process.

An interesting question is whether a conventional nickel-dependent urease could function with iron. The apoprotein from *K. aerogenes* can be produced in *E. coli* either by leaving out an accessory gene in the transformed operon or by growing the cells in the absence of nickel, and has been well studied (47). Roughly (~15%) of the *K. aerogenes* urease apoprotein is activated by incubation in bicarbonate-containing buffer with 100 μM nickel [yielding ~400 U (mg protein)$^{-1}$], less activity is obtained with manganese and cobalt [7 and 9 U (mg protein)$^{-1}$], and no activity is obtained for copper or zinc. Our efforts to activate the conventional *K. aerogenes* urease apoprotein in the same conditions with ferrous rather than nickel ions led to variable levels of highly oxygen-labile activity, with the maximum observed activity for the iron-substituted enzyme of 9.0 ± 1.4 U (mg protein)$^{-1}$. Thus, under artificial conditions low levels of iron-dependent urease activity can be obtained in a conventional urease.

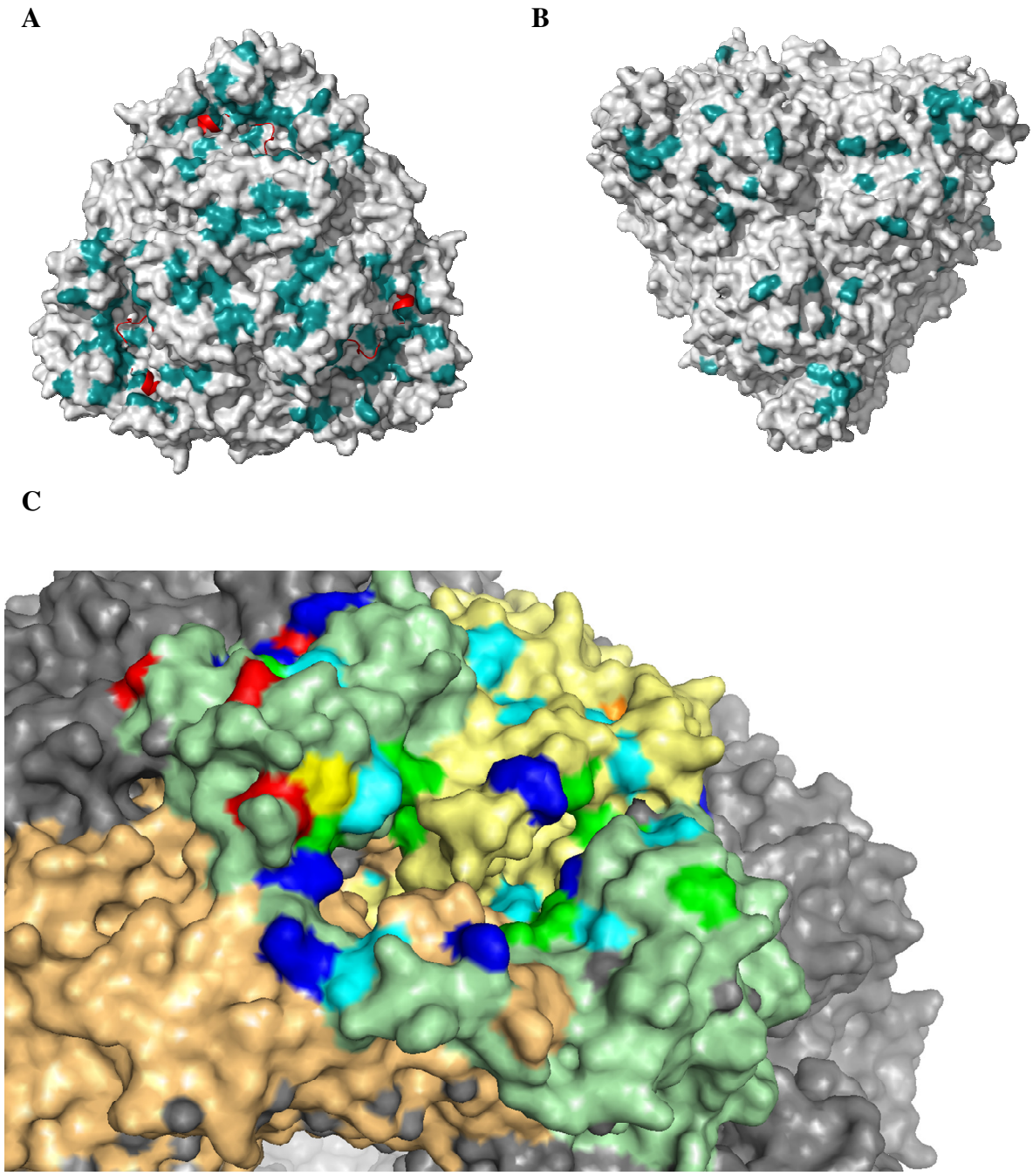

Figure 4.8: Surface residues which differ between UreA2B2 and other ureases. Three views of the surface of *H. mustelae* UreA2B2 are illustrated. (**A**) The outer surface of an individual trimeric unit with residues distinct to UreA2B2 sequences shown in cyan and the flexible flap covering the active site shown as a red cartoon, except for four residues that were not modeled. (**B**) The inner surface of the trimer, colored as for view A. (**C**) UreA2B2 amino acids located on the surface of the dodecamer directly surrounding the access to the active site. One UreB2 subunit is colored in beige with its corresponding small subunit, UreA2, colored in green,

Figure 4.8 legend continued:
while another UreB2 subunit is colored in yellow. The coloring of the residues is dark blue for R, K, and H; cyan for hydrophobic (F, W, L, A, V, G), yellow for P, green for hydroxyl or amide containing (Y, S, T, N, Q), orange for C, and red for D and E.

Urease thus joins a small group of enzymes for which homologous sequences are known to bind alternative metals for carrying out the same catalytic function. Examples of such enzymes include the Mo-, V-, and Fe-nitrogenases (23), Mn- and Fe-superoxide dismutases (1), di-Fe, Mn-Fe, and di-Mn class I ribonucleotide reductases (14), and Zn- versus Ni-glyoxylases (21). Whereas metallocenter assembly for the different nitrogenases makes use of distinct sets of accessory proteins, the basis of metal specificity in superoxide dismutases is less clear. Ribonucleotide reductases are of interest because formation of active enzyme occurs spontaneously with O_2 for the di-ferrous protein, whereas activation of the di-Mn protein requires hydroperoxyl anion from a reduced flavoprotein. A possible close parallel to urease is glyoxylase, for which high resolution structures of various metallated proteins indicate differences in coordination for active (octahedral) versus inactive (five-coordinate) sites. This finding demonstrates that very subtle changes in metallocenter structure can have profound effects on activity, a situation likely to be relevant to Fe- and Ni-ureases.

BIBILIOGRAPHY

BIBLIOGRAPHY

1. **Abreu, I. A., and D. E. Cabelli.** 2010. Superoxide dismutases--a review of the metal-associated mechanistic variations. Biochimica et Biophysica Acta **1804:**263-274.

2. **Adams, P. D., P. V. Afonine, G. Bunkóczi, V. B. Chen, I. W. Davis, N. Echols, J. J. Headd, L.-W. Hung, G. J. Kapral, R. W. Grosse-Kunstleve, A. J. McCoy, N. W. Moriarty, R. Oeffner, R. J. Read, D. C. Richardson, J. S. Richardson, T. C. Terwilliger, and P. H. Zwart.** 2010. *PHENIX*: a comprehensive Python-based system for macromolecular structure solution. Acta Crystallographica **D66:**213-221.

3. **Balasubramanian, A., and K. Ponnuraj.** 2010. Crystal structure of the first plant urease from jack bean: 83 years of journey from its first crystal to molecular structure. Journal of Molecular Biology **400:**274-283.

4. **Benini, S., W. R. Rypneiwski, K. S. Wilson, S. Ciurli, and S. Mangani.** 2001. Structure-based rationalization of urease inhibition by phosphate: Novel insights into the enzyme mechanism. Journal of Biological Inorganic Chemistry **6:**778-790.

5. **Benini, S., W. R. Rypniewski, K. S. Wilson, S. Ciurli, and S. Mangani.** 1998. The complex of *Bacillus pasteurii* urease with ß-mercaptoethanol from X-ray data at 1.65-Å resolution. Journal of Biological Inorganic Chemistry **3:**268-273.

6. **Benini, S., W. R. Rypniewski, K. S. Wilson, S. Miletti, S. Ciurli, and S. Mangani.** 2000. The complex of *Bacillus pasteurii* urease with acetohydroxamate anion from X-ray data at 1.55 Å resolution. Journal of Biological Inorganic Chemistry **5:**110-118.

7. **Benini, S., W. R. Rypniewski, K. S. Wilson, S. Miletti, S. Ciurli, and S. Mangani.** 1999. A new proposal for urease mechanism based on the crystal structures of the native and inhibited enzyme from *Bacillus pasteurii*: Why urea hydrolysis costs two nickels. Structure **7:**205-216.

8. **Berman, H. M., J. Westbrook, Z. Feng, G. Gilliland, T. N. Bhat, H. Weissig, I. N. Shindyalov, and P. E. Bourne.** 2000. The Protein Databank. Nucleic Acids Research **28:**235-242.

9. **Boer, J. L., S. Quiroz-Valenzuela, K. L. Anderson, and R. P. Hausinger.** 2010. Mutagenesis of *Klebsiella aerogenes* UreG to probe nickel binding and interactions with other urease-related proteins. Biochemistry **49:**5859-5869.

10. **Bricogne, G., E. Blanc, M. Brandl, C. Flensburg, P. Keller, W. Paciorek, P. Roversi, O. S. Smart, C. Vonrhein, and T. O. Womack.** 2009. Buster, version 2.8.0. Global Phasing Ltd., Cambridge, U.K.

11. **Brünger, A. T.** 1992. A novel statistical quantity for assessing the accuracy of crystal structures. Nature (London) **355:**472-475.

12. **Carter, E. L., N. Flugga, J. L. Boer, S. B. Mulrooney, and R. P. Hausinger.** 2009. Interplay of metal ions and urease. Metallomics **1:**207-221.

13. **Chen, V. B., B. Arendall, III, J. J. Headd, D. A. Keedy, R. M. Immormino, G. J. Kapral, L. W. Murray, J. S. Richardson, and D. C. Richardson.** 2010. MobProbity: all-atom structure validation for macromolecular crystallography. Acta Crystallographica **D66:**12-21.

14. **Cortuvo, J. A., Jr., and J. Stubbe.** 2011. Class I ribonucleotide reductases: metallocofactor assembly and repair in vitro and in vivo. Annual Review of Biochemistry **80:** in press.

15. **Dixon, N. E., C. Gazzola, R. L. Blakeley, and B. Zerner.** 1975. Jack bean urease (EC 3.5.1.5). A metalloenzyme. A simple biological role for nickel? Journal of the American Chemical Society **97:**4131-4133.

16. **Dunn, B. E., C.-C. Sung, N. S. Taylor, and J. G. Fox.** 1991. Purification and characterization of *Helicobacter mustelae* urease. Infection and Immunity **59:**3343-3345.

17. **Dykxhoorn, D. M., R. St. Pierre, and T. Linn.** 1996. A set of compatible *tac* promoter expression vectors. Gene **177:**133-136.

18. **Emsley, P., B. Lohkamp, W. G. Scott, and K. Cowtan.** 2010. Features and development of *Coot*. Acta Crystallographica **D66:**12-21.

19. **Fox, J. G., P. Correa, N. S. Taylor, A. Lee, G. Otto, J. C. Murphy, and R. Rose.** 1990. *Helicobacter mustelae*-associated gastritis in ferrets: An animal model of *Helicobacter pylori* gastritis in humans. Gastroenterology **99:**352-361.

20. **Ha, N.-C., S.-T. Oh, J. Y. Sung, K.-A. Cha, M. H. Lee, and B.-H. Oh.** 2001. Supramolecular assembly and acid resistance of *Helicobacter pylori* urease. Nature Structural Biology **8:**505-509.

21. **He, M. M., S. L. Clugston, J. F. Honek, and B. W. Matthews.** 2000. Determination of the structure of *Escherichia coli* glyoxylase I suggests a structural basis for differential metal activation. Biochemistry **39:**8719-8727.

22. **Jabri, E., M. B. Carr, R. P. Hausinger, and P. A. Karplus.** 1995. The crystal structure of urease from *Klebsiella aerogenes*. Science **268:**998-1004.

23. **Joerger, R. D., and P. E. Bishop.** 1988. Bacterial alternative nitrogen fixation systems. Critical Reviews in Microbiology **16:**1-14.

24. **Kao, W.-C., V. C. C. Wang, Y.-C. Huang, S. S. F. Yu, T.-C. Chang, and S. I. Chan.** 2008. Isolation, purification and characterization of hemerythrin from *Methylococcus capsulatus* (Bath). Journal of Inorganic Biochemistry **102:**1607-1614.

25. **Laemmli, U. K.** 1970. Cleavage of structural proteins during the assembly of the head of bacteriophage T4. Nature (London) **227:**680-685.

26. **Leslie, A. G. W.** 1992. Recent changes to the MOSFLM package for processing film and image plate data. Joint CCP4 + ESF/EACBM Newsletter on Protein Crystallography.

27. **McCoy, A. J., R. W. Grosse-Kunstleve, L. C. Storoni, and R. J. Read.** 2005. Likelihood-enhanced fast translation functions. Acta Crystallographica **D61:**458-464.

28. **Mobley, H. L. T., and R. P. Hausinger.** 1989. Microbial ureases: Significance, regulation, and molecular characterization. Microbiological Reviews **53:**85-108.

29. **O'Toole, P. W., W. J. Snelling, C. Canchaya, B. M. Forde, K. R. Hardie, C. Josenhans, R. L. J. Graham, G. McMullan, J. Parkhill, E. Belda, and S. D. Bentley.** 2010. Comparative genomics and proteomics of *Helicobacter mustelae*, an ulcerative and carcinogenic gastric pathogen. BMC Genomics **11:**164.

30. **Olson, J. W., N. S. Mehta, and R. J. Maier.** 2001. Requirement of nickel metabolism proteins HypA and HypB for full activity of both hydrogenase and urease in *Helicobacter pylori*. Molecular Microbiology **39:**176.

31. **Pearson, M. A., L. O. Michel, R. P. Hausinger, and P. A. Karplus.** 1997. Structure of Cys319 variants and acetohydroxamate-inhibited *Klebsiella aerogenes* urease. Biochemistry **36:**8164-8172.

32. **Pot, R. G. J., J. Stoof, P. J. M. Nuijten, L. A. M. de Haan, P. Loeffen, E. J. Kuipers, A. H. M. Van Vliet, and J. G. Kusters.** 2007. UreA2B2: A second urease system in the gastric pathogen *Helicobacter felis*. FEMS Immunology and Medical Microbiology **50:**273-279.

33. **Quiroz-Valenzuela, S.** 2008. New insights in the urease activation process obtained by characterization of apourease complexes and the UreG accessory protein of *Klebsiella aerogenes*. Thesis. Michigan State University.

34. **Rowe, J. L., G. L. Starnes, and P. T. Chivers.** 2005. Complex transcriptional control links NikABCDE-dependent nickel transport with hydrogenase expression in *Escherichia coli*. Journal of Bacteriology **187:**6317-6323.

35. **Sachs, G., D. L. Weeks, K. Melchers, and D. R. Scott.** 2003. The gastric biology of *Helicobacter pylori*. Annual Review of Physiology **65:**349-369.

36. **Sambrook, J., E. F. Fritsch, and T. Maniatis.** 1989. Molecular cloning: A laboratory manual, 2nd ed, vol. Cold Spring Harbor Laboratory, Cold Spring Harbor, NY.

37. **Solnick, J. V., and D. B. Schauer.** 2001. Emergence of diverse Helicobacter species in the pathogenesis of gastric and enterohepatic diseases. Clinical Microbiological Reviews **14:**59-97.

38. **Solomons, N. W., F. Viteri, T. R. Shuler, and F. H. Nielsen.** 1982. Bioavailability of nickel in man: Effects of foods and chemically-defined dietary constituents on the absorption of inorganic nickel. Journal of Nutrition **112:**39-50.

39. **Stoof, J., S. Breijer, R. G. J. Pot, D. van der Neut, E. J. Kuipers, and A. H. M. van Vliet.** 2008. Inverse nickel-responsive regulation of two urease enzymes in the gastric pathogen *Helicobacter mustelae*. Environmental Microbiology **10:**2586-2597.

40. **Stoof, J., E. Kuipers, and A. van Vliet.** 2009. Characterization of NikR-responsive promoters of urease and metal transport genes of *Helicobacter mustelae*. BioMetals **23:**145-159.

41. **Suerbaum, S., and P. Michetti.** 2002. *Helicobacter pylori* Infection. New England Journal of Medicine **347:**1175-1186.

42. **Sumner, J. B.** 1926. The isolation and crystallization of the enzyme urease. Journal of Biological Chemistry **69:**435-441.

43. **Terwilliger, T. C., R. W. Grosse-Kunstleve, P. V. Afonine, N. W. Moriarty, P. H. Zwart, L.-W. Hung, R. J. Read, and P. D. Adams.** 2008. Iterative model building, structure refinement and density modfication with PHENIX Autobuild wizard. Acta Crystallographica **D64:**61-69.

44. **Weatherburn, M. W.** 1967. Phenol-hypochlorite reaction for determination of ammonia. Analytical Chemistry **39:**971-974.

45. **Witte, C.-P.** 2011. Urea metabolism in plants. Plant Science **180:**431-438.

46. **Wolfram, L., and P. Bauerfiend.** 2009. Activities of urease and nickel uptake of *Helicobacter pylori* proteins are media- and host-dependent. Helicobacter **14:**264-270.

47. **Yamaguchi, K., N. J. Cosper, C. Stalhanske, R. A. Scott, M. A. Pearson, P. A. Karplus, and R. P. Hausinger.** 1999. Characterization of metal-substituted *Klebsiella aerogenes* urease. Journal of Biological Inorganic Chemistry **4:**468-477.

CHAPTER 5

Apoprotein Isolation and Activation, and Vibrational Structure of the *Helicobacter mustelae* Iron Urease

This work is adapted from work accepted for publication in the *Journal of Inorganic Biochemistry*, the authors are listed as Eric L. Carter, Denis A. Proshlyakov, and Robert P. Hausinger

D.A.P. assisted in collection and interpretation of the resonance Raman spectra

ABSTRACT

The micro-aerophilic pathogen *Helicobacter mustelae* synthesizes an oxygen-labile, iron-containing urease (UreA2B2) in addition to its standard nickel-containing enzyme (UreAB). An apoprotein form of the iron urease was prepared from *ureA2B2*-expressing recombinant *Escherichia coli* cells that were grown in minimal medium. Temperature-dependent circular dichroism measurements of holoprotein and apoprotein demonstrate an enhancement of thermal stability associated with the UreA2B2 metallocenter. In parallel to the situation reported for nickel activation of the standard urease apoprotein, incubation of UreA2B2 apoprotein with ferrous ions and bicarbonate generated urease activity in a portion of the nascent active sites. In addition, ferrous ions were shown to be capable of reductively activating the oxidized metallocenter. Resonance Raman spectra of the inactive, aerobically-purified UreA2B2 holoprotein exhibit vibrations at 495 cm^{-1} and 784 cm^{-1}, consistent with ν_s and ν_{as} modes of an Fe(III)-O-Fe(III) center; these modes undergo downshifts upon binding of urea and were unaffected by changes in pH . The low-frequency mode also exhibits an isotopic shift from 497 to 476 cm^{-1} upon $^{16}O/^{18}O$ bulk water isotope substitution. Expression of subunits of the conventional nickel-containing *Klebsiella aerogenes* urease in cells grown in rich medium without nickel resulted in iron incorporation into a portion of the protein. The inactive iron-loaded species exhibited a UV-visible spectrum similar to oxidized UreA2B2 and was capable of being reductively activated under anoxic conditions. Results from these studies more clearly define the formation and unique properties of the iron urease metallocenter.

INTRODUCTION

Urease catalyzes a deceptively simple reaction; i.e., the hydrolysis of urea to form

ammonia and carbamate which spontaneously decomposes into a second molecule of ammonia and carbonate. The enzyme is present in all plants, many fungi, some archaea, and a diversity of bacteria where it plays important roles in global nitrogen metabolism and virulence (6, 14, 21, 22, 32, 36). Jack bean urease was the first enzyme to be crystallized (29) as well as the premier nickel enzyme (9). The structure of this plant urease (2) and bacterial representatives from *Klebsiella aerogenes* (12, 25), *Bacillus pasteurii* (3), and *Helicobacter pylori* (11) reveal identical dinuclear nickel metallocenters in various quaternary arrangements of the closely related subunit sequences (6, 36). Each nickel is coordinated by two His side chains and terminal water molecules, one metal possesses an additional Asp ligand, and the two cations are bridged by a Lys-carbamate and a water molecule (Figure 5.1). This dinuclear center is uniquely poised to hydrolyze urea, a highly stable molecule (5, 14). The substrate carbonyl is thought to bind to and replace the terminal water on the five-coordinate metal, and one urea amide nitrogen may displace the terminal water from the six-coordinate site (3). The bridging water attacks the urea carbon to form a tetrahedral intermediate that decomposes with release of ammonia. This chemistry is facilitated by several protein side chains, including a critical His residue on a loop that must open to allow substrate entry into the buried site and then close for catalysis with each turnover.

Metal content analyses of many ureases led to a consensus view that all ureases contain nickel; however, that notion came into question in 2008 from work involving *Helicobacter mustelae* (28). This micro-aerophilic pathogen of ferrets synthesizes two distinct ureases: one involving the *ureABIEFGH* structural and accessory genes that are induced by nickel and a second encoded by the *ureA2B2* structural genes which are inversely regulated by this metal

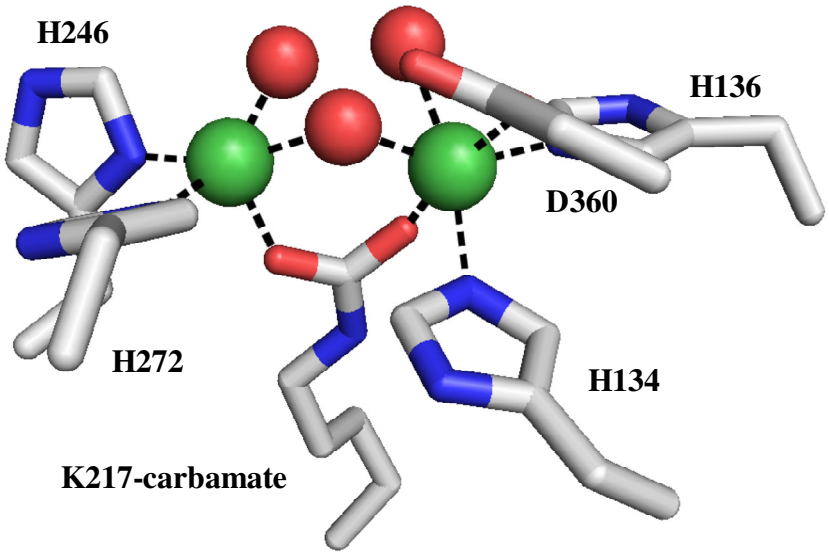

Figure 5.1: Urease active site. The dinuclear nickel active site is depicted for *K. aerogenes* urease (PDB access code 1FWJ), but essentially identical metallocenters are present in the enzymes from jack bean (PDB 3LA4), *B. pasteurii* (PDB 2UBP), and *H. pylori* (PDB 1E9Z). UreA2B2 from *H. mustelae* contains a dinuclear iron metallocenter with the same configuration of ligands (PDB 3QGA). The metal ions are show as green spheres, water molecules as red spheres, metal ligand carbon atoms as grey, oxygen atoms as red, and nitrogen atoms as blue.

(28). UreA2B2 subsequently was shown to be an oxygen-labile enzyme containing a dinuclear iron active site (8). The 3.0 Å resolution structure of the inactive, oxidized form of UreA2B2 revealed a metallocenter that recapitulates all features of the metallocenter shown in Figure 5.1, except for possessing iron rather than nickel (8). Such similarity is not entirely surprising given that UreA2 and UreB2 share 57.4% and 69.5% identity to their UreA and UreB counterparts in this microorganism. The oxidized UreA2B2 species exhibits an electronic spectrum resembling methemerythrin which contains μ-oxo bridged dinuclear ferric ions, and this spectrum was bleached as the protein was reactivated by reduction of the metallocenter under anaerobic conditions (8). Whereas activation of nickel urease requires multiple accessory proteins, the iron urease is activated without any *ure*-encoded auxiliary proteins (8, 28). Nevertheless, expression of *ureA2B2* in *Escherichia coli* yields enzyme with about half of its dinuclear active sites filled

with iron, suggesting a partial deficiency in the activation process. The maximum specific activity observed for the UreA2B2 iron urease was less than 1% of that for typical nickel ureases; however, this activity is suggested to be sufficient for allowing *H. mustelae* to colonize the ferret stomach (8, 28).

Here, I present novel features of the iron urease. In particular, I describe the purification of an apoprotein form of UreA2B2, demonstrate the ability to activate this species with iron (but not nickel), examine the resonance Raman spectra of the unique metallocenter, and report the *in vivo* formation of a dinuclear iron site in *K. aerogenes* urease when only the structural genes are expressed in *E. coli* cells growing on rich medium.

MATERIALS AND METHODS

Urease assays, protein analyses, and metal determination. Urease assays were carried out with the iron enzyme, UreA2B2, or the *K. aerogenes* protein, UreABC, in an anaerobic chamber with an atmosphere consisting of ~2.5% H_2 with N_2 balance (Coy Laboratory Products, Inc.) unless otherwise indicated. The standard urease assay buffer consisted of 50 mM 4-(2-hydroxyethyl)-1-piperazineethanesulfonic acid (HEPES), pH 7.8, with 50 mM urea, except as noted. Aliquots were removed at selected time points after enzyme addition and activity was quantified by reacting the released ammonia with phenol to form indophenol which was monitored at 625 nm (30). One unit of activity (U) is defined as the amount of enzyme necessary to degrade 1 µmol of urea per min at 37 °C. Values shown are average ± standard deviation for three experiments.

Protein concentrations were determined by using the Bio-Rad Protein Assay with bovine serum albumin as the standard and the following molecular masses: *H. mustelae* UreA2B2, 86,949 Da, and *K. aerogenes* UreABC, 83,086 Da.

Metal analyses were carried out by inductively coupled plasma-atomic emission spectroscopy (ICP-AES) at the University of Georgia Center for Applied Isotope Studies. An additional approach to measure iron content used the iron-specific chromophoric chelator 1,10-phenanthroline (Sigma). Samples (196 µl, <100 µM protein concentration, 20 mM tris(hydroxymethyl)aminomethane (Tris)-HCl, pH 7.4, containing 25 mM NaCl) were mixed with 2 µl of 10% sodium dodecylsulfate (SDS) prepared in water and 2 µl of 100 mM 1,10-phenanthroline dissolved in dimethyl sulfoxide. The mixtures were boiled for 5 min, sodium dithionite was added to 1 mM to reduce the oxidized iron, and the reaction incubated 5 min at ambient temperature before measuring the absorbance at 512 nm. The results were compared to a standard curve of ferrous sulfate, prepared by diluting a 10 mM ferrous sulfate stock solution containing 10 mM ascorbate. Results are presented as the average ± standard deviation for three replicates.

Purification of UreA2B2 apoprotein and UreA2B2 holoenzyme. The UreA2B2 apoprotein was generated in *E. coli* BL21-Gold (Stratagene) cells transformed with pEC015 (8) and grown in M9 minimal medium containing 100 µg ml^{-1} ampicillin and 0.4% mannitol. The culture was incubated at 37 °C with shaking to an optical density at 600 nm of 0.1-0.2, induced with 0.1 mM isopropyl β-D-1-thiogalactopyranoside (IPTG, Calbiochem) and grown overnight. Cell pellets were resuspended in 20 mM Tris-HCl, pH 7.4, containing 1 mM EDTA plus 1 mM β-mercaptoethanol and the slurry was sonicated (Branson Sonifier, 3-5 cycles of 2 min each, power level 1-4, 50% duty cycle with cooling in ice water/ethanol mixture). The disrupted cell

material was centrifuged at 120,000 *g* for 1 h and the apoprotein was purified by DEAE-Sepharose, phenyl-Sepharose CL-4B, and Sephacryl S300-HR chromatographic methods in 20 mM Tris-HCl buffer (pH 7.4) containing 1 mM EDTA and 1 mM β-mercaptoethanol, as previously described for the holoenzyme (8). Fractions were examined and pooled according to results from SDS-polyacrylamide gel electrophoresis (PAGE), using 12% running and 4% stacking gels (16), with the proteins visualized by Coomassie brilliant blue staining. Of note, the apoprotein was labile to freezing as judged by the loss of ability to activate the protein.

UreA2B2 holoprotein was purified from *E. coli* BL21-Gold [pEC015] cells grown in Lennox broth (LB, Fisher Scientific) containing 300 μg ml^{-1} ampicillin, as reported earlier (8), except in some cases Superdex-200 (GE Healthcare) gel filtration matrix was used instead of Sephacryl S300-HR. The 320 and 380 nm extinction coefficients for the oxidized enzyme were obtained with a Shimadzu UV-2401PC spectrophotometer at room temperature by subtracting the spectrum of apoprotein from that of holoprotein, each at 100 μM heterodimer in HT buffer [50 mM HEPES buffer (pH 7.8) containing 1 mM tris(2-carboxyethyl)phosphine (TCEP)], and correcting for the amount of iron present (where holoprotein contained 1.0 equivalent and apoprotein contained about 0.2 equivalents). The effect of pH on the UreA2B2 spectrum was analyzed by comparing spectra of the protein (100 μM heterodimer) that was equilibrated in either 200 mM Tris-HCl, pH 7.4, or 200 mM 2-(cyclohexylamino)ethanesulfonic acid (CHES), pH 9.4. The influence of urea was monitored by comparing the spectrum of UreA2B2 (100 μM) in 28 mM Tris-HCl, pH 7.4, versus protein in the same buffer plus 20 mM urea.

Circular dichroism (CD) spectroscopy for measurement of thermal stability. CD spectra were collected on UreA2B2 holoprotein and apoprotein (10 μM heterodimer, 50 mM Na-phosphate, pH 7.4) by using a 1 mm Spectrosil quartz cuvette (Starna Cells) and a Chirascan CD

Spectrometer (Applied Photophysics Limited; Leatherhead, U.K.) at 20 °C. Three scans were averaged by using Chirascan Pro-Data Viewer software. Thermal stability was examined by monitoring the changes in ellipticity at 220 nm as a function of temperature, which was controlled with a Melcor MTCA Series thermoelectric temperature controller (Laird Technologies) and a circulating water bath. Equipment parameters consisted of a 20.0-99.0 °C gradient with stepped ramping, 1 °C per step, with a 60 s equilibration time, and a 20 s read at each step subsequent to equilibration. Ellipticity profiles were fitted to a two-state model (26), using Igor Pro software (Wavemetrics).

Activation of UreA2B2 apoprotein. The *H. mustelae* UreA2B2 apoprotein was subjected to activation conditions analogous to those previously developed for the *K. aerogenes* urease apoprotein (23, 24), except that an anaerobic atmosphere was maintained during activation and assays. To test the effect of sodium bicarbonate on the *in vitro* activation process, UreA2B2 apoprotein (233 μM in HT buffer) was diluted to 10 μM in 100 mM HEPES, pH 8.3, containing 150 mM NaCl and 0, 10, or 100 mM $NaHCO_3$. The solutions were incubated at ambient temperature for 1 h before adding $FeSO_4$ to 100 μM, incubated an additional 1 h at 37 °C, and aliquots of the mixtures were assayed for urease activity. Alternatively, UreA2B2 (9.9-12.6 μM in 100 mM HEPES, pH 8.3, containing 150 mM NaCl) was incubated with 100 μM $FeSO_4$ with or without 100 mM $NaHCO_3$ for 1 h at 37 °C prior to activity assays. The effects of Ni^{2+} and Zn^{2+} ions on activation were tested by incubating 10 μM UreA2B2 apoprotein with 100 mM $NaHCO_3$ in 100 mM HEPES, pH 8.3, containing 150 mM NaCl for 4 h at ambient temperature,

adding 100 μM $NiCl_2$ or $ZnSO_4$ (diluted from stocks prepared in 1 mM HCl), and incubating at 37 °C for 1 h prior to urease assays.

UreA2B2 activation by ferrous ions was examined as a function of time and pH by incubating UreA2B2 apoprotein (9.7-17 μM) in 100 mM buffer [N-tris(hydroxymethyl)methyl-3-aminopropanesulfonic acid (TAPS), pH 8.6, HEPES, pH 7.6, or 2-(*N*-morpholino)ethane-sulfonic acid (MES), pH 6.6 and 5.6; each containing 150 mM NaCl] with 100 μM $FeSO_4$ at 37 °C. Aliquots of the mixtures were assayed for urease activity at various time points. The concentration dependence of UreA2B2 activation by ferrous ions was examined by mixing UreA2B2 apoprotein (71.4 μM heterodimer) in 100 mM HEPES buffer, pH 8.3, containing 150 mM NaCl with varying stoichiometric concentrations of $FeSO_4$ (diluted from a 1 mM stock prepared in 1 mM HCl). After incubating at 37 °C for 1 h, aliquots were assayed for urease activity. The addition of $FeSO_4$ led to a dilution of the buffered protein solution by no more than 22%.

UreA2B2 apoprotein activation by sodium dithionite was investigated by incubating apoprotein (10 μM final concentration) with 1 mM sodium dithionite in 100 mM HEPES, pH 8.3, containing 150 mM NaCl at 37 °C for 1 hr prior to assaying the mixtures for urease activity. For all urease assays, the lower detection limit was ~0.05 U (mg protein)$^{-1}$.

Resonance Raman spectroscopy. UreA2B2 was subjected to resonance Raman analysis with excitation using the 363.8 nm line (100 mW) of an Ar^+ ion laser (model I-300, Coherent Inc., CA) or the 413.1 nm line (5 mW) of a Kr^+ ion laser (model I-90, Coherent Inc., CA). Several different samples were analyzed for Raman scattering by using 363.8-nm excitation. To

test the effect of pH and urea on the UreA2B2 spectrum, protein (~0.6 mM) was equilibrated in either 28 mM Tris-HCl (pH 7.4), containing 20 mM urea, 28 mM TAPS (pH 8.4), or 28 mM CHES (pH 9.4). Oxygen isotope substitution was carried out by diluting 60 µl of UreA2B2 (2.7 mM in 200 mM Tris-HCl, pH 7.4) with 100 µl of either $H_2{}^{16}O$ or $H_2{}^{18}O$ followed by concentration to ~60 µl by 10,000 Da molecular weight cut-off Microcon centrifugal filter devices (Millipore; pre-washed with deionized water), second dilution with 100 µl of the respective water isotope leading to a final concentration of ~1 mM protein in 28 mM Tris-HCl, pH 7.4. Isotope enrichment of ^{18}O sample was ~80%. These samples were incubated on ice for 4 d prior to Raman measurement.

To facilitate isotopic exchange of metal ligands, UreA2B2 was subjected to sequential reduction and reoxidation (where indicated). The protein samples were degassed with at least 20 vacuum/argon purge cycles on a Schlenk line apparatus, reduced by addition of a degassed sodium dithionite solution (100 mM prepared in 200 mM Tris-HCl, pH 7.4) to a final concentration of 5 mM, and incubated at ambient temperature for at least 100 min. For experiments involving oxidation of reduced UreA2B2 in the presence of isotopic water, samples (~1 mM protein in 28 mM Tris-HCl, pH 7.4, in either $H_2{}^{16}O$ or ~80% enriched $H_2{}^{18}O$) were exposed to air for 1 h prior to analysis. For experiments involving oxidation of reduced UreA2B2 in the presence of $^{16}O_2$ or $^{18}O_2$, reduced anaerobic samples (100 µl of 0.5 mM UreA2B2 in 37 mM Tris-HCl, pH 7.4) in ~3 ml vials were oxidized by injecting 1 ml of pure gas into the vessel and incubating at room temperature for 10 min prior to Raman measurement. For the 413.1-nm excitation studies, the protein (1.9 mM in 200 mM Tris-HCl, pH 7.4; 100 µl final

sample volume) was diluted 4-fold with $H_2{}^{16}O$ or $H_2{}^{18}O$ ($H_2{}^{18}O$ obtained from Isotec, 99% enrichment).

Aliquots of samples (80-100 µl) were subjected to Raman spectroscopy by using a spinning cell. Scattered light was collected at right angle geometry and analyzed with a single polychromator (model Triax 550, Jobin Yvon, NJ) equipped with a liquid N_2-cooled CCD detector (model Spectrum One, Jobin Yvon, NJ). Holographic notch filters (Kaiser Optical Systems, MI) were used to reject Rayleigh scattering. Spectra were acquired in 30 s intervals over 10-40 min and subsequently integrated in post-processing over the time period where the spectra demonstrated minimal changes due to laser illumination. A 2400 ln/mm grating (spectral slit width 5.9 cm^{-1}) and 3600 ln/mm grating (spectral slit width 7.1 cm^{-1}) were used with 413.1 nm and 363.8 nm excitation, respectively.

Purification of iron-containing K. aerogenes *urease.* BL21-Gold(DE3) cells harboring pEC004 (7), containing *K. aerogenes ureABC* with no urease accessory genes, were grown in LB containing chloramphenicol at 50 µg ml^{-1} with shaking at 37 °C to $O.D._{600}$ ~0.5, adjusted to 0.5 mM IPTG, and grown under the same conditions overnight. Cells were harvested, suspended in 20 mM Na-phosphate buffer, pH 7.4, containing 1 mM EDTA and 1 mM β-mercaptoethanol (PEB), sonicated, and the lysate cleared by ultra-centrifugation as described above. Soluble cell-free extracts were loaded onto DEAE-Sepharose (2.5 cm x 13 cm) equilibrated in PEB, unbound species were removed by washing with PEB, and a linear gradient from 0-1 M KCl over ~6 column volumes was applied. Fractions containing urease apoprotein were identified by SDS-PAGE, pooled, and dialyzed against PEB containing 1.5 M KCl. The resultant pool was filtered (0.22 micron) and applied to phenyl-Sepharose CL-4B resin (2.5 cm x 13 cm) equilibrated in

PEB with 1.5 M KCl. The column was washed with PEB plus 1.5 M KCl to eliminate unbound species, and urease apoprotein was eluted by using PEB with no salt. Fractions containing urease apoprotein were concentrated with a 10,000 molecular weight cut-off (MWCO) Amicon centrifugal filter device (Millipore) to 1 ml before being loaded onto Superdex-200 resin (1.5 cm x 68 cm) equilibrated in 50 mM HEPES, pH 7.8, containing 1 mM TCEP. Fractions containing pure urease apoprotein were verified with SDS-PAGE, the protein was concentrated with a 10,000 MWCO Amicon, and aliquots were snap-frozen in liquid N_2 prior to storage at -80 °C.

The isolated protein was reddish-yellow, unlike the colorless preparations of apoprotein purified from cells expressing the entire urease operon and grown in the absence of nickel. The electronic spectrum of the iron-containing *K. aerogenes* urease (131 µM in 50 mM HEPES, pH 7.8, containing 1 mM TCEP) was used to determine the extinction coefficients at 320 and 380 nm after subtracting the spectrum of apoprotein (obtained from pKAU22Δ*ureD-1* (18) at the same concentration) and correcting for iron content (where holoprotein contained 1.0 equivalents and apoprotein contained 0.3 equivalents).

Urease activity of recombinant E. coli cells. To determine whether *E. coli* BL21-Gold(DE3) cells harboring pEC004 were ureolytic, cells were grown overnight in LB containing chloramphenicol at 50 µg ml^{-1} with shaking at 37 °C. The culture was diluted 1:100 into 25 ml of fresh LB medium containing the same concentration of antibiotic and either 0.5 mM of $FeCl_3$ dicitrate (diluted from a 500 mM $FeCl_3$ stock prepared in 1 M citrate) or $NiCl_2$, grown with shaking at 37 °C until the cells reached an $O.D._{600}$ of ~0.4, adjusted to 0.1 mM IPTG, and continued incubating overnight. Subsequently, the cells were harvested by centrifugation, the supernatant was discarded, and the cell pellets were suspended in 0.5 ml 50 mM Tris-HCl, pH

7.4, containing 150 mM NaCl and directly assayed for urease activity. Specific activities were calculated using the protein concentration in soluble cell-free extracts prepared by briefly sonicating cell slurries and clearing the lysate for 20 min at 16,000 *g*.

Reductive activation of iron-containing K. aerogenes *urease.* The reductive activation competence of the iron-containing *K. aerogenes* urease was ascertained by degassing a protein solution (263 µM heterotrimer in 50 mM HEPES, pH 7.8, containing 1 mM TCEP) and transferring into an anaerobic chamber. The protein (25 µM final concentration) was mixed with sodium dithionite (2.5 mM final concentration diluted from a 100 mM stock solution prepared in degassed 20 mM Tris-HCl, pH 7.4, containing 300 mM NaCl), and 20 mM Tris-HCl, pH 7.4, containing 300 mM NaCl in 50 µl total volume. The reaction was incubated for 80 min at ambient temperature before assaying an aliquot for urease activity under anoxic conditions.

RESULTS AND DISCUSSION

The UreA2B2 apoprotein and holoprotein possess the same secondary structures, and the iron metallocenter confers thermostability. The apoprotein form of UreA2B2 cannot be generated by methods used with the conventional nickel urease. For example, *K. aerogenes* urease apoprotein is produced when *E. coli* cells containing the complete heterologous operon are grown in the absence of nickel (17) or when recombinant cells lacking *ureD* are grown in LB (23, 35). These approaches do not work for UreA2B2 because iron is required for many essential cellular proteins and the iron urease is synthesized without the aid of accessory proteins. Due to these complications we could only approach a true apoprotein form of UreA2B2.

H. mustelae UreA2B2 was isolated from recombinant *E. coli* cells grown in minimal medium and shown to contain only 0.22-0.24 equivalents each of iron and 0.00-0.18 equivalents of zinc per UreA2B2 unit by ICP-AES. For simplicity, we refer to this sample as apoprotein. By contrast, protein isolated from *E. coli* cells grown in LB, where iron is more abundant, contained ~1.0 equivalent of iron and less than 0.1 equivalent of zinc (8). Although only half of the dinuclear sites were filled in this sample, we term this holoprotein. The apoprotein sample behaved like the metal-loaded enzyme during purification, consistent with their possessing similar quaternary structures as expected for changes associated with a deeply buried metallocenter.

The CD spectra of UreA2B2 apoprotein and holoprotein are very similar (Figure 5.2, panel A), and deconvolution by the K2D method on the Dichroweb server (31) led to a secondary structure prediction of 31% α-helix, 11% β-sheet, and 58% random coil for the apoprotein and 32% α-helix, 12% β-sheet, and 56% random coil for the holoprotein. These estimated percentages of secondary structural elements closely match the assignments in the structure (8). In both cases, the negative ellipticity at 220 nm was lost when the sample temperature was increased (Figure 5.2, panel B), leading to the irreversible denaturation of the protein. Fitting of the data to a two-state model yielded a melting temperature of 345.7 ± 0.1 K for the apoprotein, and 349.8 ± 0.1 K for the holoprotein. Whereas the fit to the holoprotein data agreed very well to a two-state model, the apoprotein data showed a slight non-coincidence to this model at the inflection points and at the highest temperature, consistent with some heterogeneity of the sample. Notably, the melting temperature of the holoprotein represents a lower limit as this species contains ~1 equivalent of iron per heterodimer; i.e., if all of the iron is in the dinuclear state the preparation would contain a mixture of 50% holoprotein and 50%

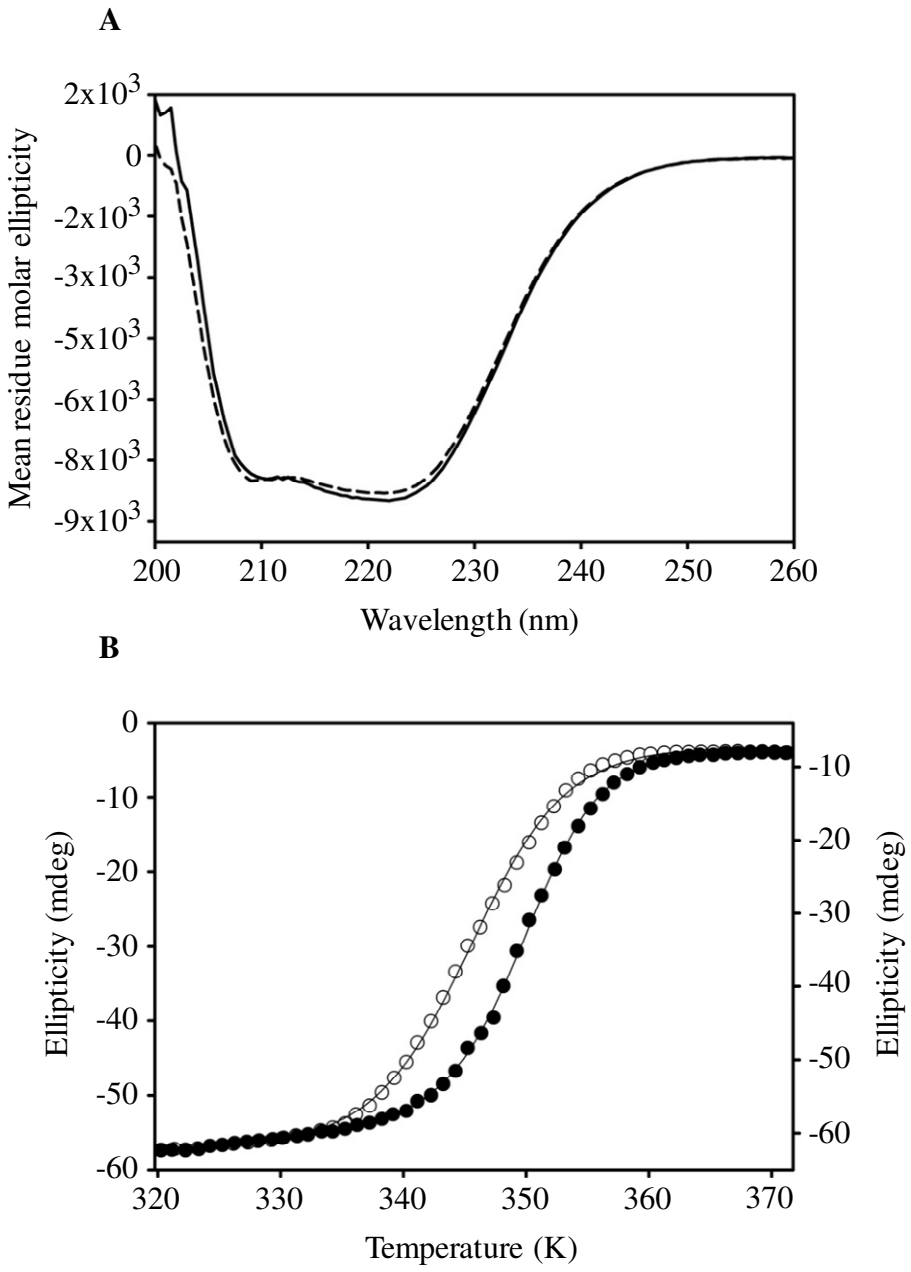

Figure 5.2: CD comparison of UreA2B2 apoprotein and holoprotein. (A) Raw CD spectra of UreA2B2 (10 μM) apoprotein (dashed line) and holoprotein (solid line) at 20 °C. Data are normalized as ellipticity per residue and are representative of three scans with baseline subtracted. (B) Changes in ellipticity at 220 nm are shown for holoprotein (filled circles, right y-axis) and apoprotein (open circles, left y-axis) as a function of temperature. Solid lines represent the nonlinear fits of experimental data to a two-state model.

apoprotein. Thus, a solution containing 100% holoprotein would likely have a higher melting temperature. These results demonstrate both that the apoprotein and holoprotein have essentially identical secondary structures and that the buried metallocenter contributes to the thermostability of the protein. This finding is similar to that reported for the enzyme from *K. aerogenes* where differential scanning calorimetry revealed increased stability of the nickel-loaded urease compared to the apoprotein species (17).

UreA2B2 apoprotein can be activated with ferrous ions, but not with nickel ions. Prior investigations had demonstrated the ability to partially convert the *K. aerogenes* urease apoprotein into active enzyme by incubation with bicarbonate and nickel ions (23, 24). Bicarbonate (optimal concentration of 100 mM) is in equilibrium with carbon dioxide, the component identified as being needed to form a Lys-carbamate which serves as a bridging ligand for the two metal ions. Apoprotein activation was maximized when using 100 μM nickel ions, a buffer at pH 8.3, and with NaCl added to 150 mM. Furthermore, this slow activation process required 60 min of incubation at 37 °C. By using radio-labeled bicarbonate to monitor Lys-carbamate formation and ICP-AES to measure nickel content in sample incubated with these optimal conditions, it was found that about half of the nascent active sites bound carbon dioxide while all sites were fully loaded with nickel. Nevertheless, the activated apoprotein [~400 U (mg protein)$^{-1}$] exhibited only ~16% of the activity observed with as-purified holoenzyme [2,500 U (mg protein)$^{-1}$]. This low extent of activation was attributed to subtle, and still undefined, structural perturbations at the metallocenter. Substitution of nickel by zinc or copper ions failed to yield any activity. By contrast, slight activity [7 and 9 U (mg protein)$^{-1}$] was observed with manganese and cobalt (for the C319A variant protein), respectively (35). Iron substitution for

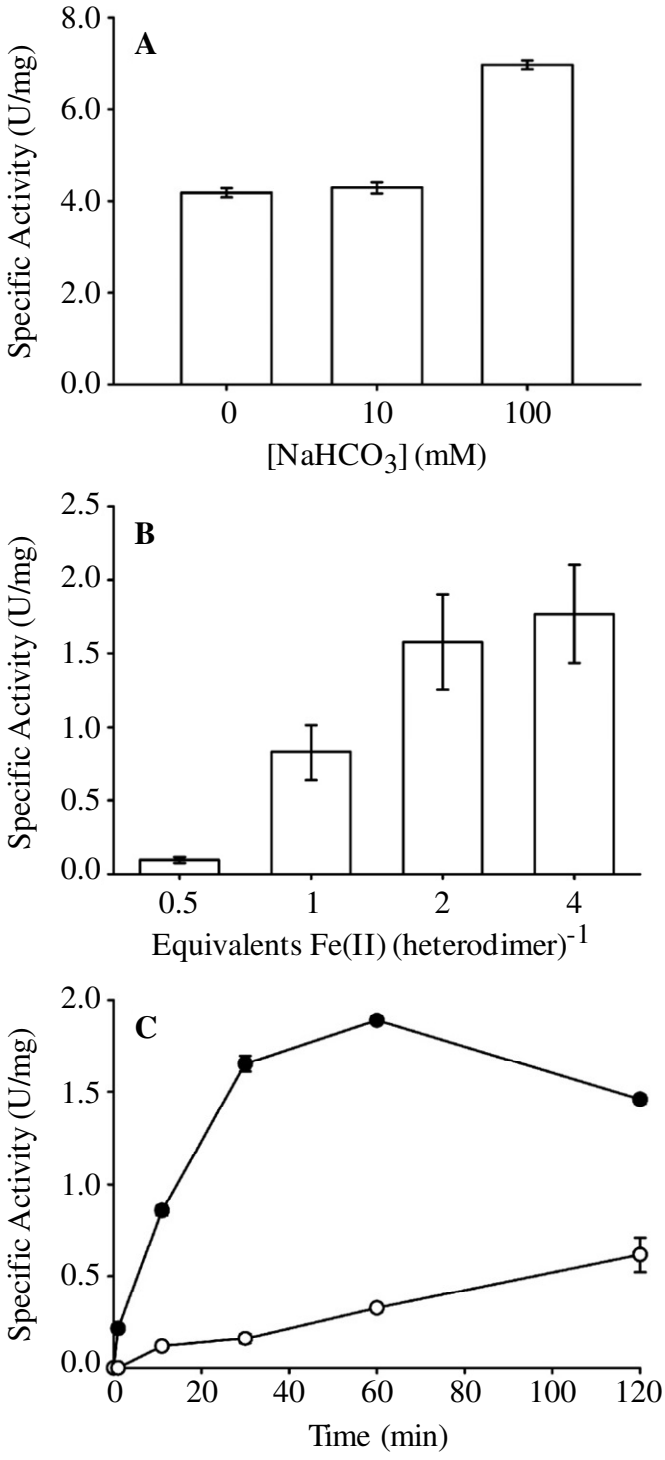

Figure 5.3: *In vitro* activation of UreA2B2 apoprotein. All incubations and assays were carried out under anaerobic conditions. (A) Bicarbonate dependence of UreA2B2 apoprotein activation. Apoprotein (10 μM heterodimer) was incubated with 0, 10, or 100 mM bicarbonate for 1 h at

Figure 5.3 legend continued:
ambient temperature, ferrous ions were added to 100 μM, and the mixtures were incubated at 37 °C for an additional 1 h prior to urease assays. (B) Ferrous ion concentration dependence of activation. Varying concentrations of UreA2B2 were incubated for 1 h at 37 °C in 100 mM HEPES buffer, pH 8.3, containing 150 mM NaCl and the indicated number of equivalents of $FeSO_4$ prior to activity assays. (C) Time and pH dependence of urease activation. UreA2B2 apoprotein was incubated at 37 °C in 100 mM HEPES, pH 7.6 (9.7 μM heterodimer; open circles), or 100 mM TAPS, pH 8.6 (17.0 μM heterodimer; closed circles), with both solutions also containing 100 μM $FeSO_4$ and 150 mM NaCl. Aliquots were removed at the indicated times and assayed for urease activity using standard conditions.

the native nickel ion in *K. aerogenes* urease yielded an oxygen-sensitive and very labile form of the protein exhibiting a maximum activity of ~9 U (mg protein)$^{-1}$ (8).

H. mustelae UreA2B2 apoprotein was incubated anaerobically using several conditions to examine its activation properties. Surprisingly, when the protein was subjected to activation conditions lacking added bicarbonate, 2-4 U (mg protein)$^{-1}$ of urease activity was observed, depending on the experiment/enzyme preparation. Inclusion of bicarbonate during these activations led to no further enhancement of activity. In contrast, mixing apoprotein with high levels of bicarbonate for 1 h prior to the addition of ferrous ions and incubation for an additional 1 h yielded ~2- fold increased specific activity for samples with bicarbonate (Figure 5.3, panel A). This enhanced activity is proposed to result from the slow incorporation of bicarbonate into the apoprotein to form new metallocenters. We propose that the background level of activity formed in the absence of bicarbonate is due to a distinct process. On the basis of results showing that sodium dithionite reductively activated apoprotein to near this basal level, we attribute the activity generated without added bicarbonate to reductive activation of the small amount of pre-existing metallocenter in the near apoprotein (0.24 Fe per heterodimer for the sample shown).

Significantly, nearly full reductive activation is generated in the presence of only two equivalents of added iron (Figure 5.3, panel B).

The ferrous ion-dependent activation of the UreA2B2 apoprotein in the absence of added bicarbonate was a slow process that required 60 min to achieve maximal activity (Figure 5.3, panel C) in TAPS buffer at pH 8.6. The loss in activity after this time might relate to the exquisite oxygen sensitivity of this enzyme. The rate of activation was greatly reduced when using HEPES buffer at pH 7.6, and activation was not detectable when using buffers at pH 6.6 or pH 5.6. In sum, these results are consistent with the UreA2B2 metallocenter having a reduction potential significantly greater than that of ferrous ions in these activation conditions. Whereas the aqueous ferrous/ferric reduction potential is 0.771 V, this value can shift dramatically for a cation that is complexed to buffer components or to protein (e.g., three His coordination environments for iron in designed metalloproteins resulted in reduction potentials ranging from 0.43 V to 0.01 V (4)) or for different ligand protonation states. While the reduction potential of the UreA2B2 metallocenter is unknown, the met/semi-met and semi-met/deoxy states of *Thermiste zostericola* hemerythrin were measured as 0.11 V and 0.31 V, respectively (1). The activity formed in the bicarbonate-containing incubation mixtures at pH 8.3 under standard activation conditions represents both partial reductive activation and true apoprotein activation. The maximal level of true apoprotein activation was estimated to be ~2.8 U (mg protein)$^{-1}$ or 20% of the activity for enzyme directly isolated from the native host when using anaerobic conditions (8). The incomplete activation of UreA2B2 closely coincides with the partial activation of *K. aerogenes* urease apoprotein (23, 24). Significantly, no activity was formed when UreA2B2 was incubated with zinc or nickel ions. Given the close structural similarity

between the *K. aerogenes* and *H. mustelae* active sites, the reason for the lack of activation by nickel is unclear.

Raman spectroscopy reveals oxygen vibrations in the dinuclear center. The UV-visible absorbance spectrum of UreA2B2 (8) resembles that of methemerythrin or metmyohemerythrin (Table 5.1), which contain a μ-oxo bridge between two Fe(III) atoms (10, 13, 34). The UreA2B2 absorbance spectrum did not change when shifting the pH from 7.4 to 9.4, or when 20 mM urea was present. A number of anionic ligands are known to perturb the absorption spectrum of methemerythrin (15), raising the question of whether similar perturbations would occur in UreA2B2. The addition of 50 mM azide or thiocyanate had no effect of the spectrum of oxidized UreA2B2 (100 μM) (data not shown), indicating distinct metallocenter differences from methemerythrin. To further probe the unique iron urease metallocenter, the protein was examined by resonance Raman spectroscopy.

The resonance Raman spectrum of oxidized UreA2B2 holoprotein (pH 7.4) obtained with 363.8 nm excitation revealed several protein vibrations with the strongest band appearing at ~495 cm^{-1} and several prominent vibrations appearing at higher frequencies (Figure 5.4). Raman spectra remained invariant between pH 7.4 and pH 9.4. Excitation at 413.1 nm revealed noticeably different spectra strongly dominated by a single vibration at 500 cm^{-1} (~4-5 cm^{-1} upshifted from the frequency observed with 383.8 nm excitation) and no clear vibrations observed at higher frequencies. The addition of urea to UreA2B2 upon excitation at 363.8 nm led to a downshift of the 495 cm^{-1} band to 486 cm^{-1} along with spectra changes around 784 cm^{-1}. The difference between the Raman spectra of UreA2B2 with and without urea revealed a

Table 5.1: Absorption spectral properties of diferric μ-oxo core-containing proteins

Protein	Wavelength (nm)	Extinction coefficient (M^{-1} cm^{-1})	Wavelength (nm)	Extinction coefficient (M^{-1} cm^{-1})
H. mustelae UreA2B2	320	4129[a] (8258)[b]	380	1994[a] (3988)[b]
K. aerogenes UreABC	320	2856[a] (5712)[b]	380	1589[a] (3178)[b]
Phascolopsis gouldii myohemerythrin[c]	324	6600	366	6400
Desulfovibrio vulgaris (Hildenborough) DcrH hemerythrin domain[d]	322	6500	380	4700
Methylococcus capsulatus (Bath) hemerythrin[e]	327	4431	376	3715

[a] Calculated from experimental data on the basis of protein concentration; extinction coefficients represent protein containing 1.0 equivalent of iron heterodimer^{-1}. [b] Calculated assuming full diferric center occupancy; i.e., 2.0 iron heterodimer^{-1} . [c] From (19). [d] From (33). [e] From (13).

downshift of two vibrations due to urea binding at 497/484 cm^{-1} (visible in the absolute spectra) and 790/763 cm^{-1}. The latter, weaker band is not seen in the absolute spectra due to overlap with modes at 784 cm^{-1} and 754 cm^{-1}, neither of which shows sensitivity to urea. Significantly urea-sensitive bands coincide well with the symmetric and asymmetric vibrational modes of Fe(III)-O-Fe(III) sites. For example, methemerythrin from *Phascolopsis gouldii* exhibits a vibration at 511 cm^{-1} (20), metmyohemerythrin from the same organism shows a vibration at 505 cm^{-1}, and a variant of the protein reveals a feature at 492 cm^{-1} (34). Extensive comparisons of ν_s and ν_{as}

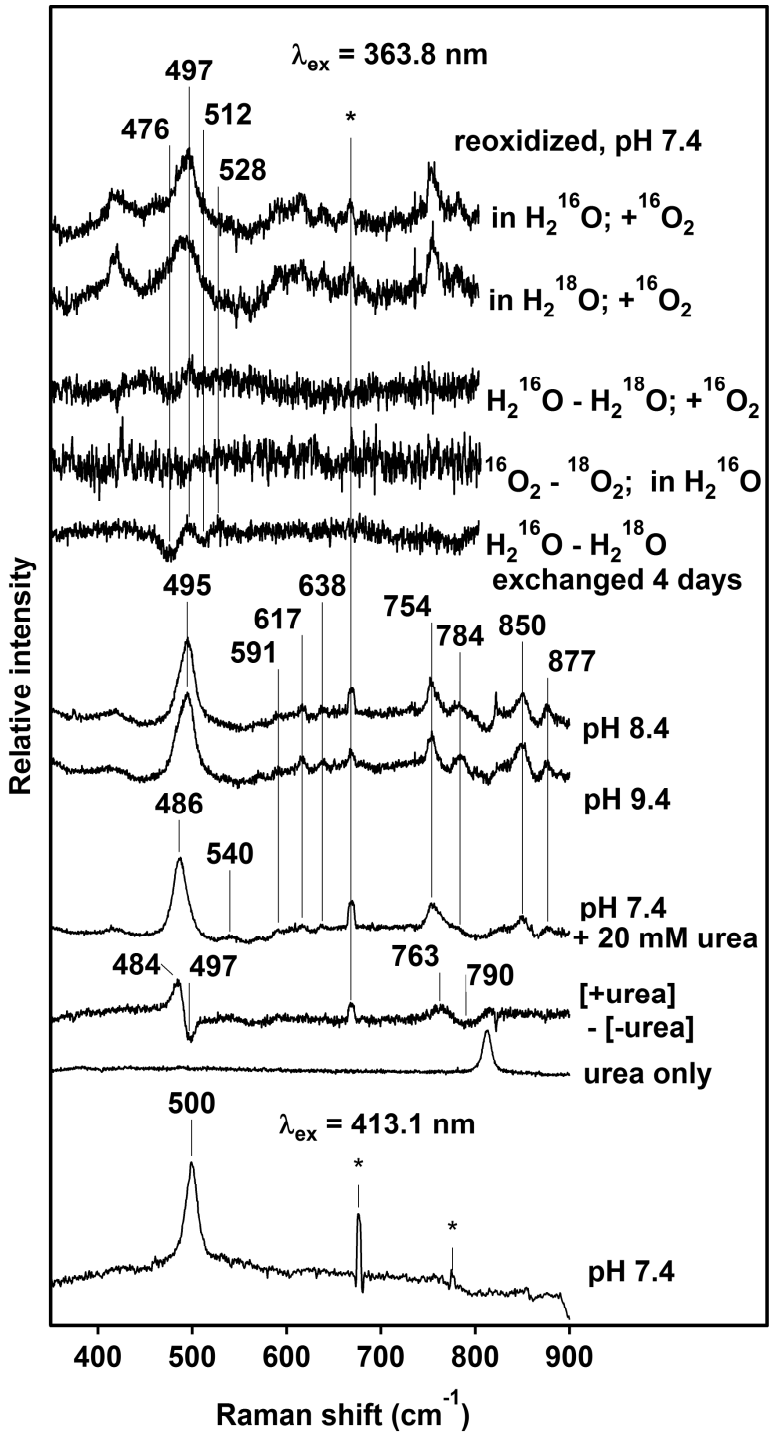

Figure 5.4: Resonance Raman spectra of oxidized UreA2B2. Top: Absolute and oxygen isotope difference spectra of UreA2B2 at pH 7.4. UreA2B2 was sequentially reduced and reoxidized with $^{16}O_2$ or $^{18}O_2$ in $H_2{}^{16}O$ or $H_2{}^{18}O$, as indicated. $H_2{}^{16}O - H_2{}^{18}O$ isotope difference spectrum obtained without reoxidation for samples in the corresponding medium for four d at 4 °C also is shown. Isotope difference spectra ($H_2{}^{16}O - H_2{}^{18}O$ and $^{16}O_2 - {}^{18}O_2$) were calculated by subtracting the corresponding absolute spectra, which cancels all vibrations that are not

Figure 5.4 legend continued:
sensitive to the oxygen mass. Middle: Absolute spectra of UreA2B2 samples at pH 8.4, pH 9.4, and pH 7.4 (with added urea). The urea-induced difference spectrum of UreA2B2 is shown in comparison with the absolute spectrum of urea in buffer. Middle and top spectra were obtained with 363.8 nm excitation. Bottom: Absolute spectrum of oxidized UreA2B2 upon excitation at 413.1 nm. Asterisks indicate the positions of major plasma lines.

versus Fe-O-Fe angles for structurally characterized proteins and model complexes (27, 37) suggest that the Fe-O-Fe angle in oxidized UreA2B2 is ~130°. The low resolution of the UreA2B2 crystal precludes accurate estimation of the Fe-O-Fe angle, but for comparison the Ni-OH-Ni angle is 119° for *B. pasteurii* urease or 121° for *K. aerogenes* urease (3).

The 500 cm^{-1} vibration detected when exciting at 413.1 nm showed no evidence of rapid exchange with bulk water as indicated by the lack of sensitivity to $H_2{}^{16}O$/ $H_2{}^{18}O$ isotope substitution (not shown). Using 363.8 cm^{-1} excitation, prolonged incubation of UreA2B2 in isotopically labeled water revealed the presence of an oxygen isotope-sensitive vibration at 497/476 cm^{-1} for $^{16}O/^{18}O$, respectively. An isotopic shift of 21 cm^{-1} is consistent with either the $\nu_{Fe\text{-}O}$ of terminal solvent bound to iron or the symmetrical stretching mode ν_s of a μ-oxo bridge. Another weak feature in the $H_2{}^{16}O - H_2{}^{18}O$ difference spectrum was detected at 528 cm^{-1} for ^{16}O and an apparent trough at 512 cm^{-1}, although the trough position may be significantly affected by overlap with the ^{16}O mode at 497 cm^{-1}. No isotopic shifts were detected for the second urea sensitive mode at 790 cm^{-1}, possibly due to its significant lower intensity. It was noticed that isotopic exchange did not cause a quantitative shift of the 495 cm^{-1} band in the absolute spectrum suggesting that either the yield of exchange is small or, more

likely considering vibrational differences between 363.8-nm and 413.1-nm spectra and band shape of the 495 cm^{-1} mode, that the 495 cm^{-1} band consists of several individual vibrations with varying oxygen sensitivity or exchangeability. The UreA2B2 spectra can be compared to the high pH spectra of *P. gouldii* and *Themiste dyscritum* methemerythrins which contain an extra terminal hydroxide on one iron atom, providing hydroxomethemerythrin (20). The hydroxide ligand causes a shift of the 511 cm^{-1} vibration to 506 cm^{-1}, while introducing a new vibration at 490 cm^{-1} attributed to coupled Fe(III)-OH stretching and O-H bending. This precedent points to a possible explanation for the multiple vibrations near 500 cm^{-1} in UreA2B2 as arising from vibrations of the μ-oxo and Fe(III)-OH components of its metallocenter. Another possibility that we cannot exclude is that some of the observed vibrations are associated with the Lys-carbamate bridging ligand. $D_2{}^{16}O/H_2{}^{16}O$ substitution suggests that the 495 cm^{-1} band is hydrogen isotope sensitive and that such sensitivity may be significantly higher than the corresponding $^{16}O/^{18}O$ sensitivity, although further studies are necessary for unambiguous resolution and assignment of the 495 cm^{-1} band. Reduction and oxidation of UreA2B2 is expected to facilitate exchange of metal ligands with bulk solvent; however, such treatment of the sample with $^{16}O_2$ in $H_2{}^{16}O$ or $H_2{}^{18}O$ immediately prior to Raman measurement did not reveal any additional oxygen isotope-sensitive modes or significant enhancement of the mode(s) observed with long exchange without reduction. In contrast, the feature at 528 cm^{-1} appears to have lost intensity. The difference spectrum between the oxidation products obtained with $^{16}O_2$ and $^{18}O_2$ (both in $H_2{}^{16}O$, Fig. 5.4) indicated no oxygen isotope-sensitive bands, suggesting that

either ligand exchange is fast (min) or neither of the vibrations observed with this excitation wavelength originate from the products of O_2 reduction.

A dinuclear iron metallocenter can form in vivo *in* K. aerogenes *urease. E. coli* whole cells expressing *K. aerogenes ureABC* (but lacking the accessory genes) and grown in LB supplemented with excess iron were non-ureolytic while cells grown in the presence of nickel demonstrated low levels of urease activity, ~0.1 U (mg protein)$^{-1}$. Urease purified from the cells grown in non-supplemented LB was reddish-yellow and its spectrum closely resembled that of oxidized UreA2B2 (8) (Table 5.1), in contrast to the colorless apoprotein formed when *E. coli* cells containing the entire *K. aerogenes* urease gene cluster are grown in minimal medium lacking nickel (17) or when *E. coli* cells containing *K. aerogenes ureABCEFG* (i.e., missing *ureD*) are grown in LB (24, 35). The spectrum closely resembled that of oxidized UreA2B2 (8), and both of these spectra are similar to that of methemerythrin (13); however, methemerythrin has distinct peaks at 320 and 380 nm, whereas the urease features were less defined. On the basis of the resonance Raman results, this distinction may arise from terminal solvent-Fe(III) electronic transitions superimposed on the Fe(III)-O-Fe(III) spectrum. The *K. aerogenes* urease possessed 1.025 ± 0.005 equivalents of iron per UreABC unit as measured by using 1,10-phenanthroline. The protein was inactive as purified, however anaerobic reduction with dithionite led to a specific activity of 8.1 ± 0.3 U (mg protein)$^{-1}$. For comparison, the same sample was subjected to the standard *in vitro* activation conditions and resulted in 356 ± 9 U (mg protein)$^{-1}$ of oxygen-stable nickel-dependent activity when assayed in standard buffer containing 0.5 mM EDTA [or ~16% of the fully active enzyme exhibiting 2,500 U (mg protein)$^{-1}$].

CONCLUSIONS

I have demonstrated that UreA2B2 apoprotein exhibits the same properties during its purification and possesses the same secondary structure as the holoprotein, except that the metal-containing sample has greater thermal stability. UreA2B2 apoprotein was slowly and partially activated by ferrous ions and bicarbonate, but not with nickel or zinc ions. Surprisingly, activation also was observed without added bicarbonate, consistent with reductive activation of the small amount of oxidized dinuclear iron site found in this protein by ferrous ions. The level of activity catalyzed by UreA2B2 is quite low, so an alternative reaction cannot be excluded; however, ureolytic activity by this enzyme is sufficient to allow *H. mustelae* to survive acid shock if urea is provided (28). The oxidized metallocenter exhibited a resonance Raman spectrum consistent with ν_s and ν_{as} vibrations expected for a Fe(III)-O-Fe(III) metallocenter, and these modes were downshifted by added urea. Considering the inability of oxidized UreA2B2 to turn over substrate, this system provides a unique probe for monitoring the structural nature of urea binding at the urease metallocenter. The spectrum contained additional vibrations around 500 cm^{-1} with variable susceptibility to exchange with bulk solvent, likely corresponding to several oxygenic metal ligands. Finally, we demonstrated the *in vivo* formation of a dinuclear iron center in *K. aerogenes* urease when recombinant cells containing the structural subunit genes, but lacking the set of urease accessory genes, were grown in LB. This result suggests that iron can serve as the default metal in urease when the maturation proteins are not present, consistent with one of the roles for these auxiliary components being to prevent mis-incorporation of metal in the nickel enzyme.

In *H. mustelae*, the lack of UreA2B2-associated accessory proteins may be used as a mechanism to impart the desired metal specificity for this protein. The UreA2B2 proteins of

gastric pathogens possess a cohort of conserved residues that are unique when compared to the sequences of their nickel-containing UreAB counterparts (8). Many of these unique residues are on the outer surface of the dodecameric assembly, possibly rendering UreA2B2 incapable of interacting with the endogenous maturation proteins encoded by the UreAB urease cluster. Under these conditions, UreA2B2 would spontaneously acquire ferrous ions as the default metal, similar to what we observed for *K. aerogenes* urease when it is produced without accessory proteins. Whereas cells producing UreA2B2 are ureolytic (8), the *E. coli* cells producing Fe-containing *K. aerogenes* urease lacked urease activity. This exclusive aspect of UreA2B2 is consistent with the *H. mustelae* protein possessing the unique ability to utilize iron rather than nickel as the catalytic cofactor despite containing a highly conserved active site structure that is nearly identical to that of nickel ureases.

BIBLIOGRAPHY

BIBLIOGRAPHY

1. **Armstrong, F. A., P. C. Harrington, and R. G. Wilkins.** 1983. Reduction potentials of various hemerythrin oxidation states. Journal of Inorganic Biochemistry **18:**83-91.

2. **Balasubramanian, A., and K. Ponnuraj.** 2010. Crystal structure of the first plant urease from jack bean: 83 Years of journey from its first crystal to molecular structure. Journal of Molecular Biology **400:**274-283.

3. **Benini, S., W. R. Rypniewski, K. S. Wilson, S. Miletti, S. Ciurli, and S. Mangani.** 1999. A new proposal for urease mechanism based on the crystal structures of the native and inhibited enzyme from *Bacillus pasteurii*: Why urea hydrolysis costs two nickels. Structure **7:**205-216.

4. **Benson, D. E., M. S. Wisz, and H. W. Hellinga.** 2000. Rational design of nascent metalloenzymes. Proceedings of the National Academy of Sciences, United States of America **97:**6292-6297.

5. **Callahan, B. P., Y. Yuan, and R. Wolfenden.** 2005. The burden borne by urease. Journal of the American Chemical Society **127:**10828-10829.

6. **Carter, E. L., N. Flugga, J. L. Boer, S. B. Mulrooney, and R. P. Hausinger.** 2009. Interplay of metal ions and urease. Metallomics **1:**207-221.

7. **Carter, E. L., and R. P. Hausinger.** 2010. Characterization of *Klebsiella aerogenes* urease accessory protein UreD in fusion with the maltose binding protein. Journal of Bacteriology **192:**2294-2304.

8. **Carter, E. L., D. E. Tronrud, S. R. Taber, P. A. Karplus, and R. P. Hausinger.** 2011. Iron-containing urease in a pathogenic bacterium. Proceedings of the National Academy of Sciences, United States of America **108:**13095-13099.

9. **Dixon, N. E., C. Gazzola, R. L. Blakeley, and B. Zerner.** 1975. Jack bean urease (EC 3.5.1.5). A metalloenzyme. A simple biological role for nickel? Journal of the American Chemical Society **97:**4131-4133.

10. **Freier, S. M., L. L. Duff, D. F. Shriver, and I. M. Klotz.** 1980. Resonance Raman spectroscopy of iron-oxygen vibrations in hemerythrin. Archives of Biochemistry and Biophysics **205:**449-463.

11. **Ha, N.-C., S.-T. Oh, J. Y. Sung, K.-A. Cha, M. H. Lee, and B.-H. Oh.** 2001. Supramolecular assembly and acid resistance of *Helicobacter pylori* urease. Nature Structural Biology **8:**505-509.

12. **Jabri, E., M. B. Carr, R. P. Hausinger, and P. A. Karplus.** 1995. The crystal structure of urease from *Klebsiella aerogenes*. Science **268:**998-1004.

13. **Kao, W.-C., V. C.-C. Wang, Y.-C. Huang, S. S.-F. Yu, T.-C. Chang, and S. I. Chan.** 2008. Isolation, purification and characterization of hemerythrin from *Methylococcus capsulatus* (Bath). Journal of Inorganic Biochemistry **102:**1607-1614.

14. **Karplus, P. A., M. A. Pearson, and R. P. Hausinger.** 1997. 70 years of crystalline urease: What have we learned? Accounts of Chemical Research **30:**330-337.

15. **Kurtz, D. M., Jr., D. F. Shriver, and I. M. Klotz.** 1977. Structural chemistry of hemerythrin. Coordination Chemistry Reviews **24:**145-178.

16. **Laemmli, U. K.** 1970. Cleavage of structural proteins during the assembly of the head of bacteriophage T4. Nature (London) **227:**680-685.

17. **Lee, M. H., S. B. Mulrooney, and R. P. Hausinger.** 1990. Purification, characterization, and *in vivo* reconstitution of *Klebsiella aerogenes* urease apoenzyme. Journal of Bacteriology **172:**4427-4431.

18. **Lee, M. H., S. B. Mulrooney, M. J. Renner, Y. Markowicz, and R. P. Hausinger.** 1992. *Klebsiella aerogenes* urease gene cluster: Sequence of *ureD* and demonstration that four accessory genes (*ureD*, *ureE*, *ureF*, and *ureG*) are involved in nickel metallocenter biosynthesis. Journal of Bacteriology **174:**4324-4330.

19. **Long, R. C., J.-H. Zhang, D. M. Kurtz, Jr., A. Negri, G. Tedeschi, and F. Bonomi.** 1992. Myohemerythrin from the sipunclulid, *Phascolopsis gouldii*: Purification, properties and amino acid sequence. Biochimica et Biophysica Acta **1122:**136-142.

20. **McCallum, J. D., A. K. Shiemke, and J. Sanders-Loehr.** 1984. Hydroxide ion binding to methemerythrin. An investigation by resonance Raman and difference spectroscopy. Biochemistry **23:**2819-2825.

21. **Mobley, H. L. T., and R. P. Hausinger.** 1989. Microbial ureases: Significance, regulation, and molecular characterization. Microbiological Reviews **53:**85-108.

22. **Mobley, H. L. T., M. D. Island, and R. P. Hausinger.** 1995. Molecular biology of microbial ureases. Microbiological Reviews **59:**451-480.

23. **Park, I.-S., and R. P. Hausinger.** 1996. Metal ion interactions with urease and UreD-urease apoproteins. Biochemistry **35:**5345-5352.

24. **Park, I.-S., and R. P. Hausinger.** 1995. Requirement of carbon dioxide for *in vitro* assembly of the urease nickel metallocenter. Science **267:**1156-1158.

25. **Pearson, M. A., L. O. Michel, R. P. Hausinger, and P. A. Karplus.** 1997. Structure of Cys319 variants and acetohydroxamate-inhibited *Klebsiella aerogenes* urease. Biochemistry **36:**8164-8172.

26. **Ramsay, G. D., and M. R. Eftink.** 1994. Analysis of multidimensional spectroscopic data to monitor unfolding of proteins. Methods in Enzymology **240:**615-645.

27. **Sanders-Loehr, J., W. D. Wheeler, A. K. Shiemke, B. A. Averill, and T. M. Loehr.** 1989. Electronic and Raman spectroscopic properties of oxo-bridged dinuclear iron centers in proteins and model compounds. Journal of the American Chemical Society **111:**8084-8093.

28. **Stoof, J., S. Breijer, R. G. J. Pot, D. van der Neut, E. J. Kuipers, and A. H. M. van Vliet.** 2008. Inverse nickel-responsive regulation of two urease enzymes in the gastric pathogen *Helicobacter mustelae*. Environmental Microbiology **10:**2586-2597.

29. **Sumner, J. B.** 1926. The isolation and crystallization of the enzyme urease. Journal of Biological Chemistry **69:**435-441.

30. **Weatherburn, M. W.** 1967. Phenol-hypochlorite reaction for determination of ammonia. Analytical Chemistry **39:**971-974.

31. **Whitmore, L., and B. A. Wallace.** 2004. DICHROWEB, an online server for protein secondary structure analyses from circular dichroism spectroscopic data. Nucleic Acids Research **32:**W668-W673.

32. **Witte, C.-P.** 2011. Urea metabolism in plants. Plant Science **180:**431-438.

33. **Xiong, J., D. M. Kurtz, Jr., J. Ai, and J. Sanders-Loehr.** 2000. A hemerythrin-like domain in a bacterial chemotaxis protein. Biochemistry **39:**5117-5125.

34. **Xiong, J., R. S. Phillips, D. M. Kurtz, Jr., S. Jin, J. Ai, and J. Sanders-Loehr.** 2000. The O_2 binding pocket of myohemerythrin: Role of a conserved leucine. Biochemistry **39:**8526-8536.

35. **Yamaguchi, K., N. J. Cosper, C. Stalhanske, R. A. Scott, M. A. Pearson, P. A. Karplus, and R. P. Hausinger.** 1999. Characterization of metal-substituted *Klebsiella aerogenes* urease. Journal of Biological Inorganic Chemistry **4:**468-477.

36. **Zambelli, B., F. Musiani, S. Benini, and S. Ciurli.** 2011. Chemistry of Ni^{2+} in urease: Sensing, trafficking, and catalysis. Accounts of Chemical Research **44:**520-530.

37. **Zheng, H., Y. Zang, Y. Dong, V. G. Young, Jr., and L. Que, Jr.** 1999. Complexes with $Fe^{III2}(\mu\text{-}O)(\mu\text{-}OH)$, $Fe^{III2}(\mu\text{-}O)_2$, and $[Fe^{III3}(\mu_2\text{-}O)_3]$. Journal of the American Chemical Society **121:**2226-2235.

CHAPTER 6

Additional Studies and Concluding Remarks

ADDITIONAL MBP-UreD CHARACTERIZATION STUDIES

Influence of Tween-20 on the in vitro *interaction between MBP-UreD and UreEF.* In addition to the temperature dependence observed for the *in vitro* interaction between MBP-UreD and UreEF (Chapter 2), the addition of 0.1% Tween-20 detergent to the standard *in vitro* amylose resin pull-down assay at 37 °C increased the ratio of UreEF to MBP-UreD from 0.24:1 to 1.11:1 (taking into account the molecular masses of the proteins in the calculation of ratios; Figure 6.1, lanes 2 and 4). Although speculative, I hypothesize this phenomenon arises from Tween-20 (or higher temperatures) leading to some disaggregation of MBP-UreD and exposure of previously obstructed UreF binding surfaces (as a reminder, MBP-UreD exists as multimers > 670 kDa in solution (2)).

.

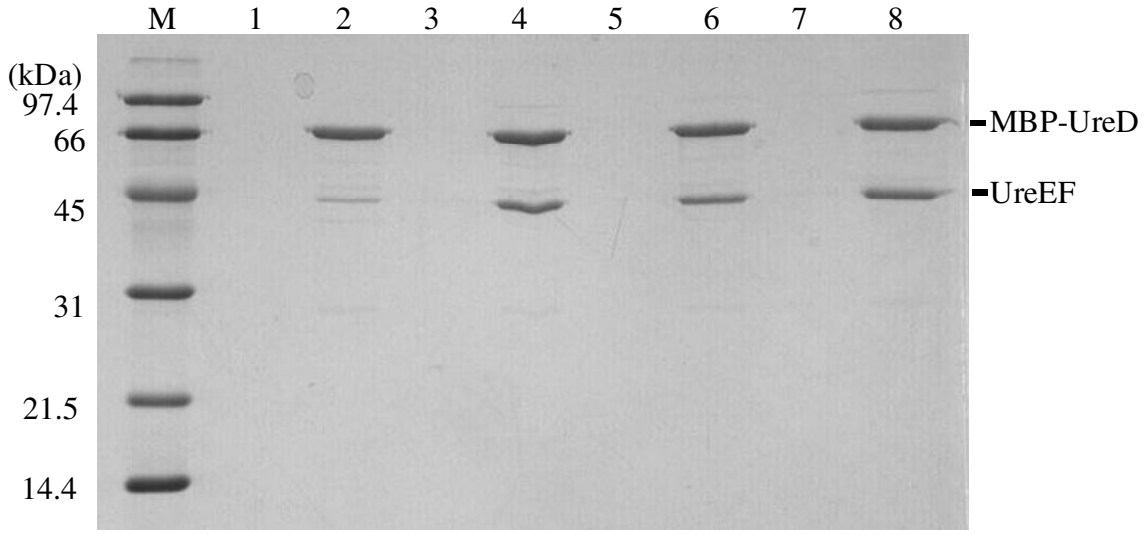

Figure 6.1: Influence of Tween-20 on the *in vitro* interaction between MBP-UreD and UreEF. Lanes: M, molecular mass markers; 1, empty lane; 2, MBP-UreD plus UreEF incubated at 37 °C; 3, empty lane; 4, MBP-UreD plus UreEF incubated at 37 °C with 0.1% Tween-20; 5, empty lane; 6, MBP-UreD plus UreEF incubated at 42 °C; 7, empty lane; 8, MBP-UreD plus UreEF incubated at 42 °C with 0.1% Tween-20.

In vitro *interactions of MBP-UreD with UreG*$_{Str}$*, UreEF, and urease in combination.*

Besides monitoring the *in vitro* interaction of MBP-UreD with individual purified proteins it was of interest to perform pull-down assays with multiple urease components in an attempt to form higher order complexes. In one representative assay, MBP-UreD (2 μM) was mixed with UreG$_{Str}$, UreEF, and urease apoprotein or holoprotein (each at 10 μM). I added amylose resin to the mixtures and incubated them at 42 °C (optimal temperature for the interaction between MBP-UreD and UreEF); all pull-down steps followed the standard protocol outlined in Chapter 2 (Figure 6.2).

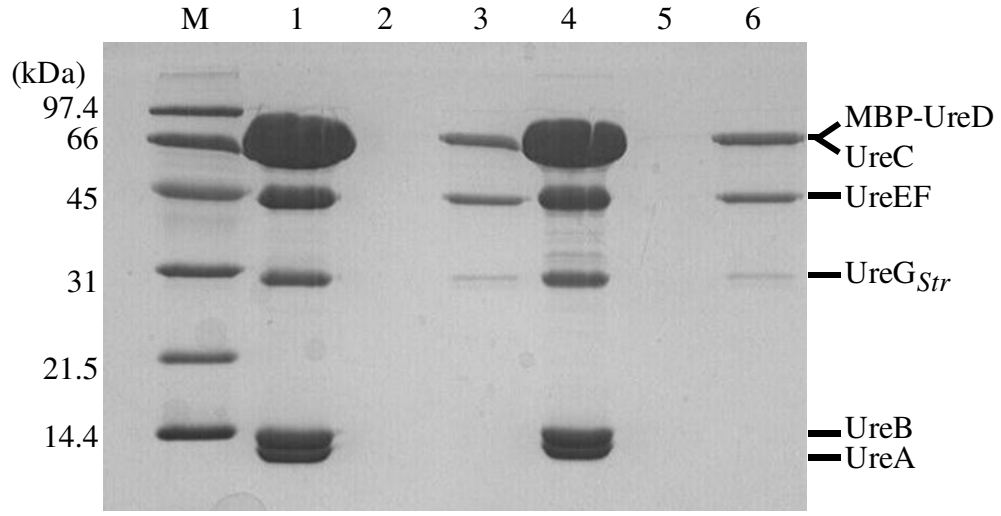

Figure 6.2: *In vitro* interaction of MBP-UreD with multiple urease components. Lanes: M, molecular mass markers; 1, unbound proteins recovered after the 1st wash of MBP-UreD plus UreEF, UreG$_{Str}$, and urease holoprotein applied to amylose resin; 2, 5th wash prior to elution; 3, eluted proteins; 4, unbound proteins recovered after the 1st wash of MBP-UreD plus UreEF, UreG$_{Str}$, and urease apoprotein applied to amylose resin; 5, 5th wash prior to elution; 6, eluted proteins.

The elution fractions (Figure 6.2, lanes 3 and 6) clearly demonstrate that urease apoprotein (or holoprotein) does not form a complex with MBP-UreD even in the presence of accessory proteins *in vitro*. However, MBP-UreD still bound UreEF and $UreG_{Str}$ in similar ratios (Figure 6.2, lane 6, UreEF:MBP-UreD, 1.37:1; $UreG_{Str}$:MBP-UreD, 0.54:1; ratios take into account the molecular masses of the individual proteins) as when these species were mixed individually (refer to Figure 2.6).

Site-directed mutagenesis of putative metal-binding residues in the UreD domain of MBP-UreD and preliminary studies with select variants. Subsequent to the discovery that the UreD domain of MBP-UreD bound nickel and zinc, it was of great interest to identify the amino acid residues responsible for metal ligation. On the basis of a sequence alignment of UreD from 15 randomly selected bacteria (not including *Helicobacter* species), I chose five conserved residues (C48, H49, H54, D63, and E176 using the *K. aerogenes* numbering) for alanine replacement. In addition, I constructed a H49A/D63A double variant. I performed site-directed mutagenesis as described (1), with pEC002 as a template and overlapping primer sets: C48A forward, 5'-CGGAAGAAGAGACCGCTCACCTCTATCTGC-3'; C48 reverse, 5'-GCAGA-TAGAGGTGAGCGGTCTCTTCTTCCG-3'; H49A forward, 5'-GAAGAAGAGACC-TGTGCCCTCTATCTGCTTC-3'; H49A reverse, 5'-GAAGCAGATAGAGGGCACAGGTCTC-TTCTTC-3'; H54A forward, 5'-CACCTCTATCTGCTTGCACCGCCCGGCGGCATC-3'; H54A reverse, 5'-GATGCCGCCGGGCGGTGCAAGCAGATAGAGGTG-3'; D63A forward, 5'-CAT-CGTCGGCGGTGCAGAGCTGACAATTAG-3'; D63A reverse, 5'-CTAATTGTCAGCTCTGC-ACCGCCGACGATG-3'; E176A forward, 5'-GCTGCTGGTCGCACGCCTGCACCTG-3'; E176A reverse, 5'-CAGGTGCAGGCGTGCGACCAGCAGC-3'. I verified all constructs by sequencing (Davis Sequencing).

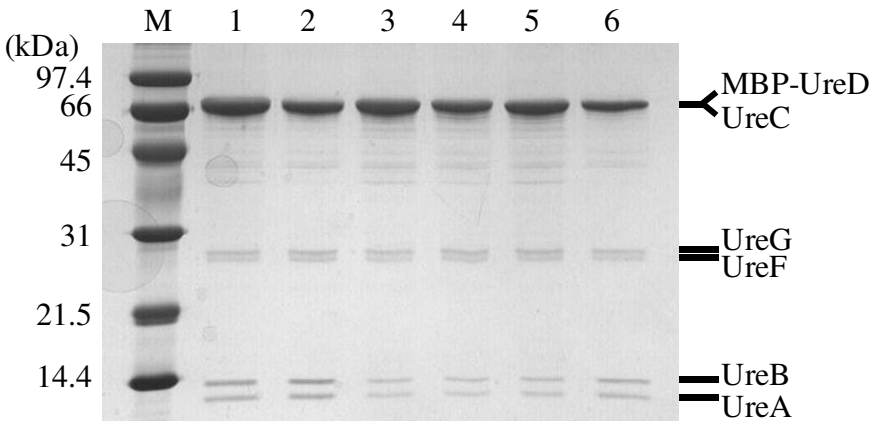

Figure 6.3: Wild-type and variant MBP-UreD interactions with UreABC, UreF, and UreG *in vivo*. Soluble cell-free extracts from cultures co-transformed with pEC006 (encoding a Δ*ureD* urease cluster) and versions of pEC002, encoding wild-type or variant MBP-UreD (as indicated below), were subjected to amylose resin chromatography and the eluted proteins were subjected to SDS-PAGE analysis. Lanes: M, molecular mass markers; 1, pEC002; 2, pEC002-C48A; 3, pEC002-H49A; 4, pEC002-H54A; 5, pEC002-D63A; 6, pEC002-E176A.

To assess the effect of site-directed mutants on the ability of UreD to interact with urease and accessory proteins *in vivo*, I co-transformed *E. coli* BL21-Gold(DE3) cells with pEC006 (encoding a Δ*ureD* urease cluster) and pEC002 harboring wild-type *malE-ureD* or the variants described above (See Appendix A for a complete list of plasmids). Overnight cultures were used to inoculate 25 ml of LB broth supplemented with 300 µg ml^{-1} ampicillin (for maintenance of pEC002 and its variants), 50 µg ml^{-1} chloramphenicol (for pEC006 maintenance), and 1 mM $NiCl_2$. I grew cells with shaking at 37 °C to $O.D._{600}$ of 0.4, supplemented with 0.1 mM IPTG, and grew for another 16 h prior to harvesting by centrifugation. I washed cell pellets twice with 1 ml of 50 mM HEPES, pH 7.8, before suspending the pellets in 1 ml of the same buffer and supplementing with 1 mM phenylmethanesulfonyl fluoride. The cell slurries were briefly sonicated and a soluble extract was prepared by centrifugation at 14,000 *g* for 20 min at 4 °C. I subjected the extracts to amylose resin pull-down analysis as described in Chapter 2. As depicted

in Figure 6.3, all of the MBP-UreD variants formed a complex with UreABC, UreF, and UreG. This situation was similar to the wild-type MBP-UreD, indicating that the selected mutations do not greatly affect the interactions of UreD with other urease components.

I assessed the influence of UreD variants on urease maturation *in vivo* by determining the urease activity of soluble cell-free extracts from the double transformants described above and *E. coli* BL21-Gold(DE3) transformed with pKK17 as a positive control (encoding the wild-type *K. aerogenes* urease cluster) (Figure 6.4). Preparation of cultures and cell-free extracts was identical to that described above for the pull-down assays.

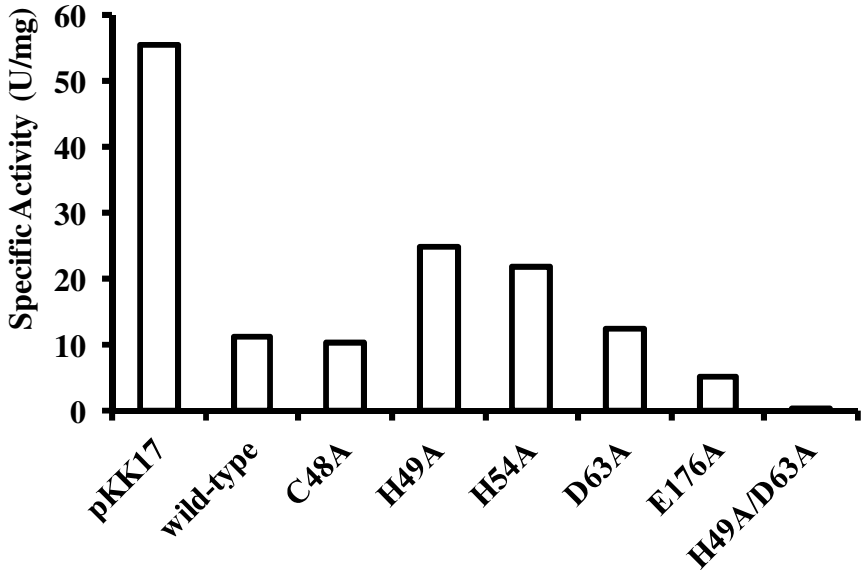

Figure 6.4: Urease activity in soluble cell-free extracts of *E. coli* BL21-Gold(DE3) transformed with pKK17, containing the complete urease gene cluster, or co-transformed with pEC006 (encoding a Δ*ureD* urease cluster) and pEC002 encoding wild-type or variant MBP-UreD.

Unfortunately the activity of the positive control was abnormally low in this assay compared to the typical specific activity for extracts from cells harboring pKK17 of ~200 U mg^{-1} (5, 12), thus it is difficult to compare activities of double transformants with wild-type levels. Of note, over a year after this experiment I found that the addition of EDTA to the urease assay

buffer had a profoundly positive and consistent effect on the urease activity of *in vitro* activated urease apoprotein, possibly accounting for some of the laboratory's issues with low urease activity in cell-free extracts. In addition to the anomalous control value, the results of Figure 6.4 are tentative because they represent a single replicate, so these experiments should be repeated to generate reliable error ranges. Nonetheless, comparing activities in cell extracts from double transformants harboring wild-type or variant MBP-UreD still offers some interesting data. Both the C48A and D63A substitutions seem to have little effect on the maturation process, H49A and H54A variants led to an increase in specific activity, and the double mutant, H49A/D63A generated negligible levels of activity. A replicate experiment demonstrated the same increase in activity for extracts from cells containing a Δ*ureD* urease cluster and producing H49A or H54A MBP-UreD versus wild-type MBP-UreD, however there was some variability in the activities of the other mutants in this assay.

I analyzed the solubility of MBP-UreD variants in cell extracts with SDS-PAGE. *E. coli* BL21-Gold(DE3) cells harboring pEC002 encoding wild-type or variant MBP-UreD (5 ml cultures, LB broth) were grown at 30 °C with shaking for 2 h prior to supplementing cultures with 0.5 mM IPTG and continuing to incubate overnight under the same conditions. I harvested 1 ml of culture by centrifugation and suspended the cell pellets in a small volume of B-PER lysis reagent (100 µl), vortexed for 30 sec, and separated the lysate by centrifugation at 14,000 *g* for 5 min. The soluble cell-free extract was removed and placed on ice, while the insoluble material was suspended in 100 µl 20 mM Tris, pH 7.4, 100 mM NaCl. 1 µl of 1:10 diluted benzonase (DNase enzyme, Sigma) was added and the slurry was incubated at room temperature for 5 min before adding 1 µl Tween-20 to each reaction. Samples were vortexed for 30 s prior to the preparation of SDS-PAGE samples. As shown in Figure 6.5, I always found a significant level

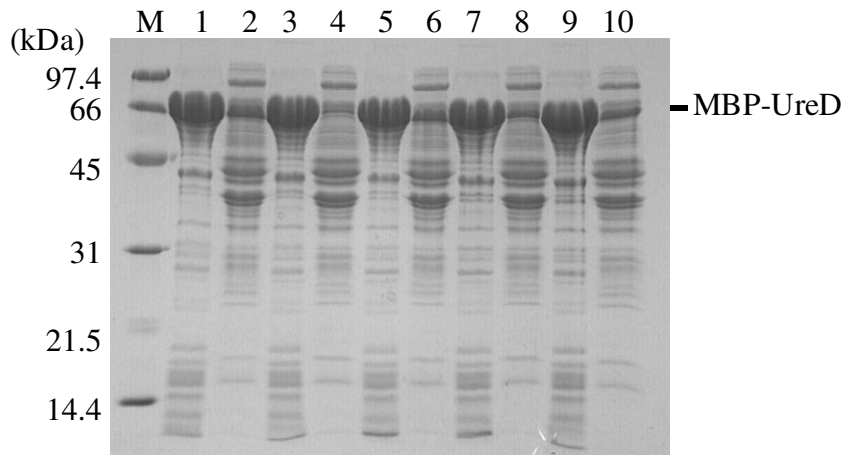

Figure 6.5: Solubility of MBP-UreD in cell-free extracts prepared from *E. coli* BL21-Gold(DE3) transformed with pEC002 encoding wild-type or variant MBP-UreD. Lanes: M, molecular mass markers; odd lanes, insoluble fractions; even lanes, soluble fractions; cells producing 1,2, wild-type MBP-UreD; 3,4, C48A MBP-UreD; 5,6, H49A MBP-UreD; 7,8, H54A MBP-UreD; 9, 10, D63A MBP-UreD.

of MBP-UreD in the insoluble fraction; however, appreciable levels of wild-type, H49A, H54A, and D63A variants were observed in the soluble fraction except for the C48A variant which was almost completely insoluble. E176A and H49A/H54A variants were also predominantly insoluble (data not shown). One shortcoming of this particular assay was the use of B-PER lysis reagent for the preparation of soluble cell-free extracts. Incomplete lysis by the detergent may lead to the appearance of higher levels of MBP-UreD in the insoluble fraction than actually exist. Nonetheless, these results demonstrate that solubility is a major concern that must be taken into account when characterizing MBP-UreD variants in the future.

I assessed the nickel-binding capability of the H49A and D63A MBP-UreD variants by using a microvolume equilibrium dialyzer (Hoefer Scientific Products). These studies were carried out in a manner similar to the previously described dialysis experiments (2), except that the incubation proceeded for 6 h at room temperature prior to analysis for nickel content using

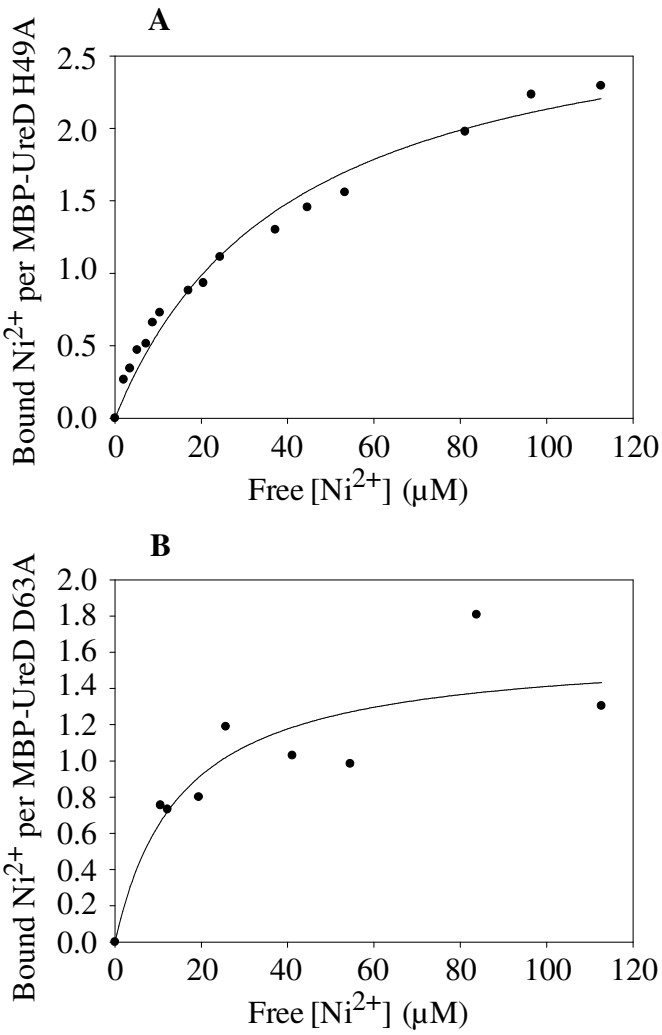

Figure 6.6: Equilibrium dialysis measurement of Ni^{2+} binding to (**A**) H49A and (**B**) D63A MBP-UreD variants.

PAR. As depicted in Figure 6.6, the H49A MBP-UreD variant bound a maximum (B_{max}) of 3.0 ± 0.2 Ni^{2+} per protomer with a dissociation constant (K_d) of 41.1 ± 5.6 µM while MBP-UreD D63A exhibited a B_{max} of 1.6 ± 0.2 Ni^{2+} per protomer with a K_d of 15.3 ± 7.8 µM. The fact that both variants bind nickel at levels fairly close to wild-type MBP-UreD (Chapter 2) suggests that these residues are not integral to the nickel binding function of UreD. Of note, experiments using

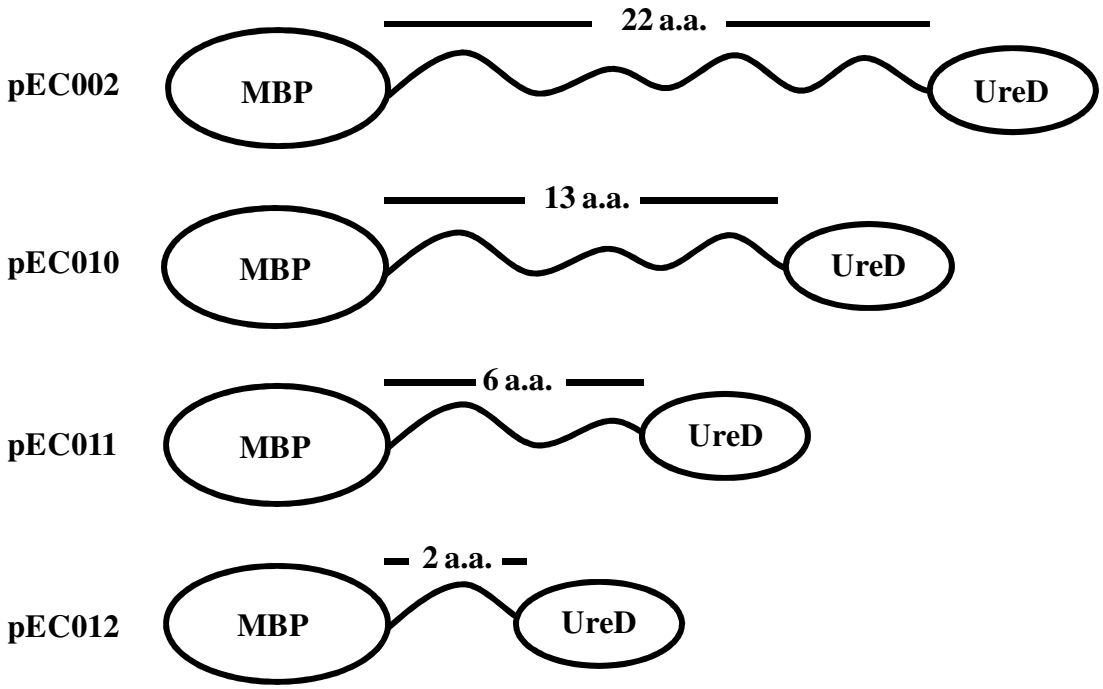

Figure 6.7: Cartoon depiction of MBP-UreD linker arm variants (a.a., amino acid).

$^{63}NiCl_2$ to ascertain binding constants for wild-type MBP-UreD yielded more reliable results than when PAR was used as the nickel detector; thus, the results described here could be repeated with the radionuclide to generate more reliable data.

MBP-UreD linker variant construction and preliminary characterization. Considering the lack of structural information available for *K. aerogenes* UreD [a structure of the *H. pylori* analogue, known as UreH, in complex with UreF was just published (7)], the soluble MBP-UreD fusion became an attractive target for crystallization screens. As a preliminary step, several linker variants were constructed in which the number of amino acid residues between MBP and UreD were varied (Figure 6.7). In all, four linker variants were constructed including (1) the original pEC002 vector, a 5'-BamHI-*ureD*-HindIII-3' fragment cloned into pMal-c2x with a linker region of 22 amino acids from the end of the SacI site within *malE* to the beginning of *ureD*; (2) pEC010, a 5'-EcoRI-*ureD*-HindIII-3' fragment cloned into pMal-c that yields a linker

arm of 13 amino acids; (3) pEC011, a 5'-BamHI-*ureD*-HindIII-3' fragment cloned into pMal-c that yields a linker arm of 6 amino acids; and (4) pEC012, a 5'-KpnI-*ureD*-HindIII-3' fragment cloned into pMal-c which gives a linker arm of 2 amino acids and replaces the GTG start codon of *ureD* with ATG. Examination of soluble cell-free extracts from *E. coli* BL21-Gold(DE3) transformed with pEC010, pEC011, or pEC012 revealed MBP-UreD in both the soluble and insoluble fractions, similar to the situation that is produced when using pEC002. In addition, gel filtration chromatography of amylose resin-purified linker variants (produced from cells containing pEC010, pEC011, and pEC012) indicated that each species exists as a soluble aggregate >670 kDa as was shown for MBP-UreD produced by pEC002 (2).

Factor Xa digestion of MBP-UreD. One attractive feature of using MBP fusion technology is the ability to liberate fused proteins from the purification/solubilization tag by using the Factor Xa protease cleavage site. Factor Xa cleaves the peptide backbone at a recognition sequence between the C-terminal portion of MBP and the beginning of the target protein. I assessed the ability of Factor Xa to digest MBP-UreD and tested the stability of UreD post-digestion. MBP-UreD (2 mg) was digested overnight at 4 °C with Factor Xa (1% (w/w) with respect to MBP-UreD) in 1 ml total volume of 20 mM Tris-HCl buffer, pH 8.0, containing 100 mM NaCl and 2 mM $CaCl_2$, with analysis by SDS-PAGE. As depicted in Figure 6.8, lane 2, MBP-UreD was almost completely digested by Factor Xa using these conditions. The digestion was specific for MBP-UreD as the band intensity of a high molecular mass contaminant found in all MBP-UreD preparations (observed on SDS-PAGE as a band positioned directly below MBP-UreD, indicated by an asterisk in Figure 6.8) remained unchanged. Unfortunately, liberated UreD was unstable as shown by the development of a visible precipitation in Factor Xa digests over prolonged incubation periods at room temperature. Additionally, my attempts to purify UreD

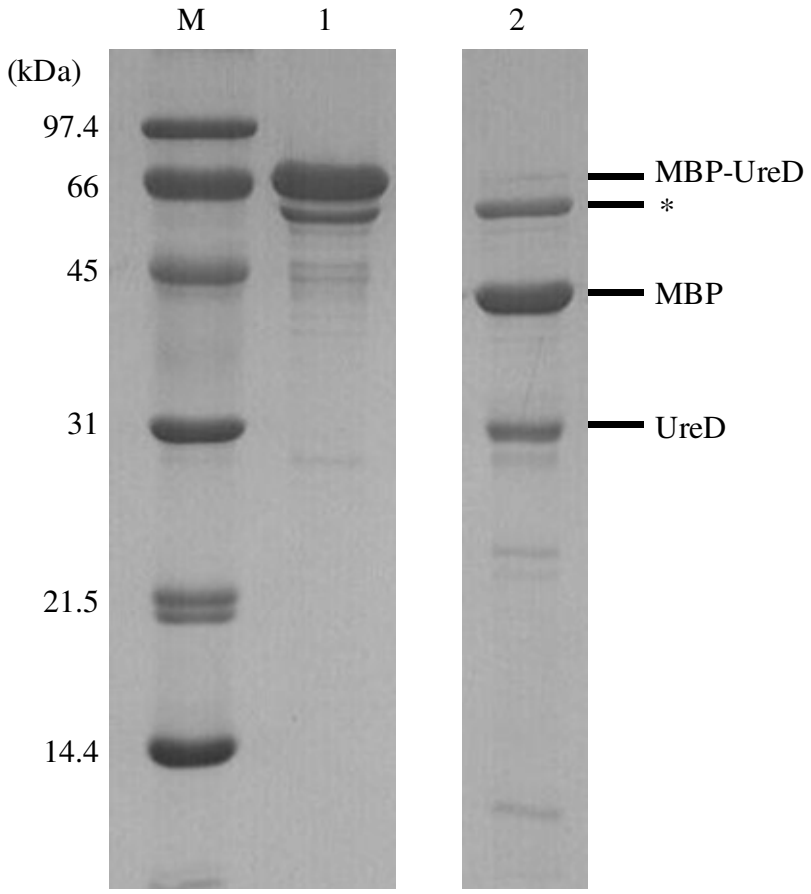

Figure 6.8: Factor Xa digestion of MBP-UreD. Lanes: M, molecular mass markers; 1, 5 µg of undigested MBP-UreD; 2, 5 µg Factor Xa-digested MBP-UreD. * = common MBP-UreD preparation contaminant.

post-digestion over anion-exchange resin were unsuccessful; the protein was unrecovered after application to the column matrix, likely due to protein denaturation and irreversible binding.

ADDITIONAL $(UreAC)_3$ PLUS UreB STUDIES

Blue-native polyacrylamide gel electrophoretic (BN-PAGE) analysis of $(UreAC)_3$ plus UreB complex formation. In addition to the gel filtration and MALDI-MS analysis of $(UreAC)_3$ plus UreB complex formation (described in Chapter 3, Figure 3.2), I utilized BN-PAGE to

monitor UreB and UreBΔ1-19 binding to $(UreAC)_3$ (Figure 6.9). Complex formation reactions consisted of mixing 1.5 µg $(UreAC)_3$ with 1.5 µg of either UreB or UreBΔ1-19 in 10 µl total volume 50 mM HEPES, pH 7.8, with 1 mM TCEP base buffer. The reactions were incubated for 10 min at ambient temperature prior to adding NativePage sample buffer (Invitrogen). Samples (including 1.5 µg of each, $(UreABC)_3$, $(UreAC)_3$, UreB, and UreBΔ1-19) were loaded onto an Invitrogen NativePAGE Bis-Tris 3-12% gradient gel and electrophoresed for 90 min at 150 V using dark blue cathode buffer. As depicted in Figure 6.9, panel A, lanes 1 and 2, $(UreABC)_3$ and $(UreAC)_3$ migrate as single bands at nearly equivalent migration positions, plus some additional banding in the $(UreAC)_3$ sample at a larger molecular mass. Close examination suggests that the main $(UreAC)_3$ band migrates slightly further than the $(UreABC)_3$ band, as is expected considering a ~30 kDa difference between $(UreABC)_3$ and $(UreAC)_3$. Unfortunately, both UreB and UreBΔ1-19 (lanes 3 and 4, respectively) migrated with the dye front, thereby preventing the visualization of these species on the gel. The major band of the mixture of $(UreAC)_3$ plus UreB (lane 5) migrated more slowly than that of $(UreAC)_3$ plus UreBΔ1-19 (lane 6), and it closely resembled $(UreABC)_3$ in terms of migration position, indicating that UreB formed a stable complex with $(UreAC)_3$. Of note, these data did not conclusively rule out the possibility that UreBΔ1-19 was bound to $(UreAC)_3$. To validate that the band visualized in lane 5 consisted of UreB complexed with $(UreAC)_3$, I excised it from a similar gel, ground it into smaller pieces, and incubated with 50 µl 1 X SDS-PAGE loading buffer for 1 h at 80 °C. I

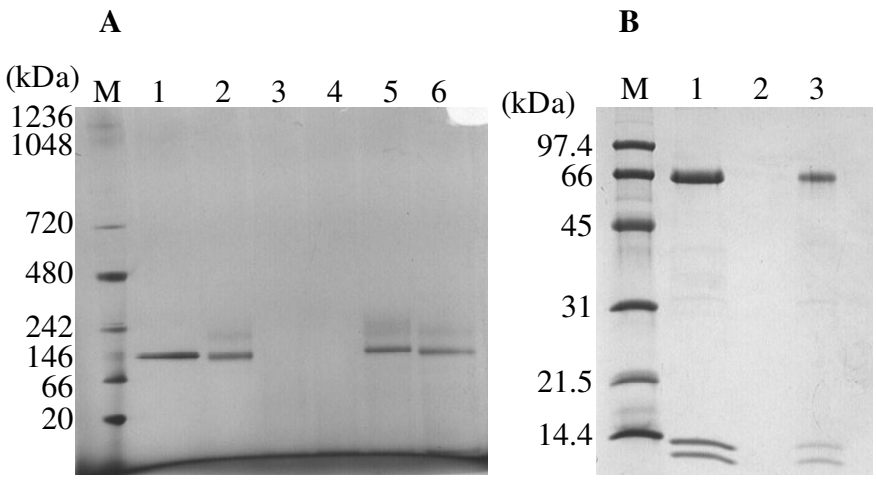

Figure 6.9: BN-PAGE and second-dimensional SDS-PAGE analysis of urease-related samples. (**A**) BN-PAGE lanes: M, molecular mass markers; 1, $(UreABC)_3$; 2, $(UreAC)_3$; 3, UreB; 4, UreBΔ1-19; 5, $(UreAC)_3$ plus UreB; 6, $(UreAC)_3$ plus UreBΔ1-19. (**B**) SDS-PAGE lanes: M, molecular mass markers; 1, $(UreABC)_3$; 2, empty lane; 3, band excised from lane 5 of panel A.

extracted the liquid from the gelatinous slurry and analyzed it by SDS-PAGE with intact $(UreABC)_3$ as a control (Figure 6.9, panel B, lanes 1 and 3). This result clearly demonstrated the presence of UreB in the extracted sample.

ADDITIONAL *H. mustelae* UreA2B2 STUDIES

Site-directed mutagenesis of K. aerogenes *UreABC to mimic amino acid substitutions in* H. mustelae *UreA2B2.* Alignment of UreA2B2 sequences from carnivorous mammal inhabiting *Helicobacter* species (*H. mustelae*, *H. felis*, and *H. acinonychis*) versus their UreAB counterparts revealed 92 conserved amino acid residues that were generally localized to the surface of the dodecameric assembly (3). Residues Y272, I136, and C245 are close to the active site and I hypothesized that they could possibly play a role in the unique metal ion selectivity of UreA2B2. Thus, I substituted the corresponding amino acids in the large subunit (UreC) of the *K.*

aerogenes nickel urease to mimic those substitutions found in UreA2B2 sequences. In all, I generated four variants including F271Y, A244C, F271-I135T double, and F271Y-I135T-A244C triple mutants using previously described techniques (1), with pEC004 as the starting template and overlapping primer sets (*K. aerogenes* numbering is used to distinguish mutations): F271Y forward, 5'-CCATCCACACCTACCATACCGAAGGG-3'; F271Y reverse, 5'-CCCTTCGGT-ATGGTAGGTGTGGATGG-3'; I135T forward, 5'-GATCGATACCCATACCCACTGG-ATCTGTCCG-3'; I135T reverse, 5'-CGGACAGATCCAGTGGGTATGGGTATCGATC-3'; A244C forward, 5'-GAAATGGACATCCAGGTCTGCCTGCACAGCGACACCC-3'; A244C reverse, 5'-GGGTGTCGCTGTGCAGGCAGACCTGGATGTCCATTTC-3'.

Several preliminary experiments were conducted to ascertain the effect of the various mutations on UreABC activity in whole cells. Plasmids producing wild-type or variant UreABC were transformed into *E. coli* BL21-Gold(DE3), DH5α, or BL21-Gold cells, and the cells were grown in LB broth supplemented with 50 μg ml^{-1} chloramphenicol and 0.5-1.0 mM $NiCl_2$, $MnCl_2$, or $FeCl_3$ with shaking at 37 °C until reaching an $O.D._{600}$ of ~0.5. Protein production was induced with 0.1-0.5 mM IPTG and the cells were grown overnight, harvested, washed, and directly assayed for urease activity under aerobic conditions; alternatively, soluble cell-free extracts were prepared and similarly assayed aerobically. I detected negligible activity for all strains grown in LB supplemented with $FeCl_3$. Cultures grown in medium supplemented with $NiCl_2$ or $MnCl_2$ had <0.5 U mg^{-1} of activity and there was not a marked difference in the activity levels between the wild-type and variants for any particular condition. Because the overall activity was low for all samples, I concluded that the unique metal ion selectivity of

UreA2B2 likely arises from amino acid substitutions outside the direct active site, perhaps related to more global changes of the protein.

Construction, expression, purification, and preliminary characterization of Strep-*tagged UreA2B2.* In order simplify the anaerobic purification of UreA2B2, I devised a method to introduce a *Strep*-tag onto the N-terminus of UreB2 thereby allowing for a single-step purification of the protein. A mini-gene construct, purchased from IDT-DNA, consisted of the *Strep*-tag DNA sequence (including linker amino acid codons on each end) flanked by wild-type sequence of *ureA2* and *ureB2* (Figure 6.10) and cloned into pIDT-SMART (this vector is referred to as pEC017, see Appendix A). I was able to use fortuitous, unique restriction sites in *ureA2* (an XbaI site towards the 3' end of the gene) and *ureB2* (a SapI site close to the 5' end of the gene) for engineering the 5' and 3' ends of the mini-gene to accommodate cloning of the XbaI—mini-gene—SapI fragment into similarly digested pEC015, leading to pEC018. The sequence of the linkers and the *Strep*-tag were derived from the IBA *Strep*-tag manual, specifically from the pASK-IBA5 vector sequence.

AACAAAAAGC<u>TCTAGA</u>AAAAGCAAAACATCACGGATTTATCAAGTAAGGAGAT
TCCC**atggctagc**tggagccacccgcagttcgaaaaa**ggcgccgagaccgcggtcATGAAAATGAAAAGAC
AAGAATATGTTAATACTTATGGCCCCACAACTGGCGATAAAGTACGCCTTGGT
GATACGGACCTTTGGGCAGAGGTGGAGCATGATTACACCGTCT<u>a</u>TGGT<u>GAAG
AGC</u>TCAAATTTGGTGCGGGTAAA**

Figure 6.10: DNA sequence of the mini-gene found on pEC017. Subsequent to digestion with XbaI and SapI, the mini-gene fragment was isolated and ligated into similarly digested pEC015, leading to pEC018. Restriction sites are upper case bold and underlined, the SapI cleavage site is lower case bold and underlined, Met start and linker amino acid codons for the *Strep*-tag are lower case bold, *Strep*-tag sequence is lower case, *ureA2*/*ureB2* sequence is upper case bold, and the intergenic space between *ureA2* and *ureB2* is upper case.

I transformed *E. coli* BL21-Gold with pEC018 and grew the cells in LB broth supplemented with 300 µg ml^{-1} at 37 °C with shaking until they reached an $O.D._{600}$ of 0.35. Protein production was induced with 0.1 mM IPTG and the cultures were incubated for an additional 3 hours prior to harvesting by centrifugation. Cell pellets were suspended in 100 mM Tris-HCl buffer, pH 8.0, with 1 mM EDTA and 150 mM NaCl, and the slurries were directly assayed for urease activity in buffer containing 50 mM urea. The specific activity of the whole cells was 2.9 U mg^{-1}, similar to the level found in whole cells producing UreA2B2 lacking the *Strep*-tag (3). In order to purify the protein, cells were prepared as described above and the slurries were sonicated. The lysate was cleared by centrifugation at ~14,000 *g* for 20 min at 4 °C. Soluble cell-free extracts were loaded onto a 5 ml bed volume *Strep*-tactin column that was equilibrated in cell resuspension buffer. Unbound proteins were eliminated by washing the column with the same buffer until the A_{280} of the column eluant reached baseline. I used the same buffer containing 2.5 mM desthiobiotin to elute the bound protein, which consisted of highly purified *Strep*-tagged UreA2B2 ($UreA2B2_{Str}$)(Figure 6.11, panel A, lane 4). I assessed the iron content of $UreA2B2_{Str}$ by using the 1,10-phenanthroline method, as previously described (3), which yielded 0.79 ± 0.03 iron $heterodimer^{-1}$, again similar to the levels found in the untagged species purified under similar conditions without βME [i.e., 1.13 ± 0.12 iron $heterodimer^{-1}$ (3)]. The circular dichroism spectrum of $UreA2B2_{Str}$ also resembled that of untagged UreA2B2 purified from cells grown in rich medium (Figure 6.11, panel B) indicating the *Strep*-tag had little or no effect on the overall secondary structure of the protein. Lastly, I estimated the native molecular mass of $UreA2B2_{Str}$ to be 502 kDa by using gel filtration

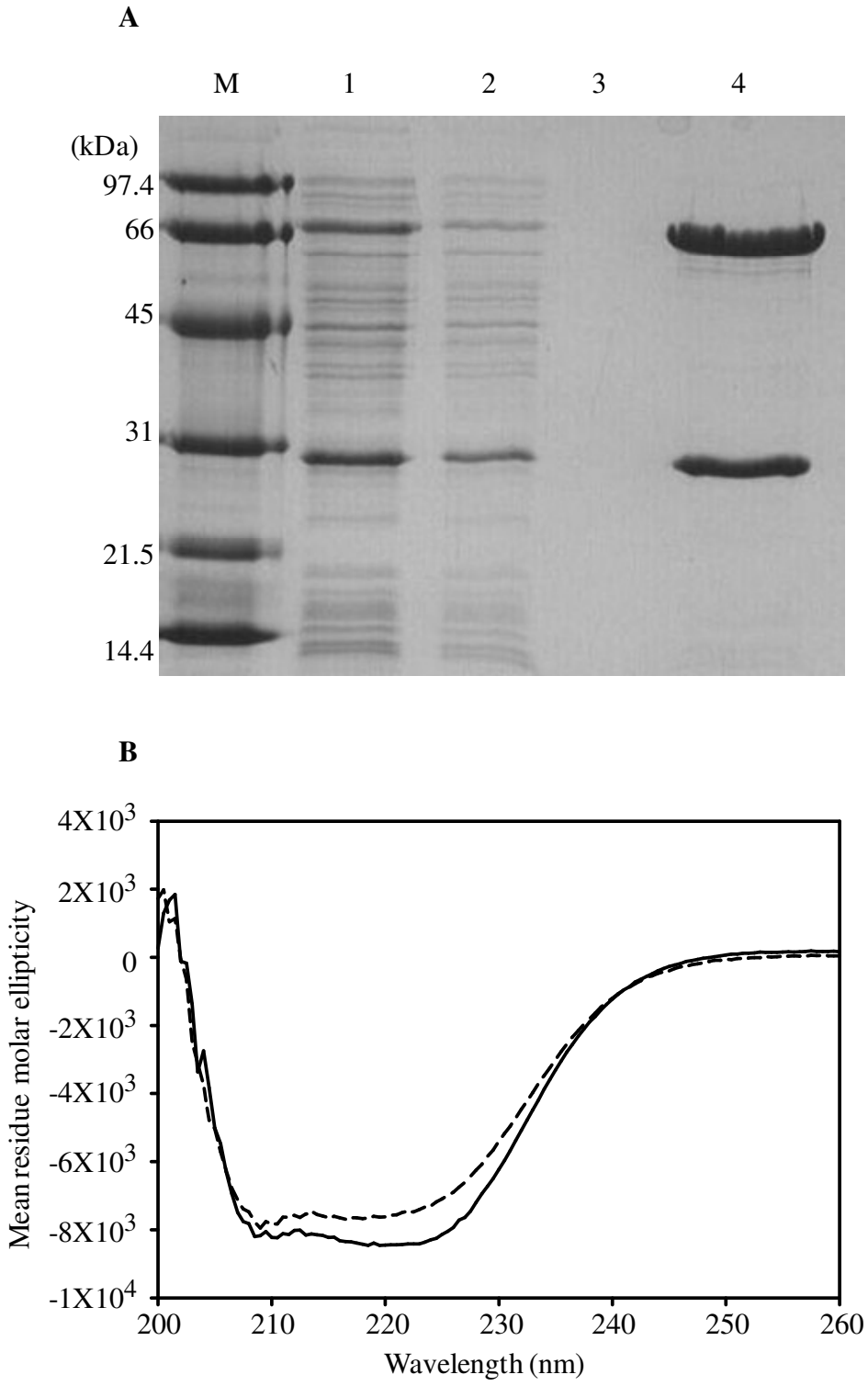

Figure 6.11: Expression, purification, and CD spectrum of UreA2B2$_{Str}$. (**A**) SDS-PAGE analysis of soluble cell-free extracts and *Strep*-tactin purification steps. Lanes: M, molecular mass markers; 1, soluble cell-free extracts of *E. coli* BL21-Gold transformed with pEC018 and

Figure 6.11 legend continued:
induced with IPTG; 2, column flow-through; 3, empty lane; 4, eluted protein. (**B**) Raw CD spectra of UreA2B2$_{Str}$ (dashed line) and untagged UreA2B2 (solid line).

chromatography with Superdex-200 resin (1.5 cm X 68 cm) equilibrated in 20 mM Tris-HCl buffer, pH 7.5, containing 1 mM EDTA, 1 mM βME, and 25 mM NaCl. This is similar to the estimated molecular mass of the untagged protein, 550 kDa, ascertained by using Sephacryl S300HR gel filtration matrix (1.5 cm X 68 cm) equilibrated in 20 mM Tris-HCl, pH 7.4, containing 1 mM EDTA, 1 mM βME, and 300 mM NaCl, and both values agree with the molecular mass of 535 kDa determined for *H. mustelae* UreAB (6). Since the crystal structure of UreA2B2 revealed a dodecameric superassembly, as was seen for UreAB from *H. pylori* (9), these gel filtration results suggest that UreA2B2$_{Str}$ assumes the same quaternary structure.

I purified UreA2B2$_{Str}$ from *E. coli* under anaerobic conditions in an attempt to describe the urea degradation kinetics of the enzyme. I prepared cell slurries as described above and degassed by several vacuum/argon-purge cycles. The degassed slurry was brought into an anaerobic chamber (~2.5% H_2 with N_2 balance) and supplemented with 2.5 mM dithionite. The slurry was sonicated and the lysate cleared as previously described for the anaerobic purification of UreA2B2 from *H. mustelae* (3). From this point onwards, all purification steps were identical to those described above for the aerobic purification of UreA2B2$_{Str}$, except that they were performed under anaerobic conditions and all buffers were supplemented with 0.5 mM dithionite. Purified UreA2B2$_{Str}$ was assayed for urease activity under anaerobic conditions in 50 mM HEPES buffer, pH 7.8, containing varying concentrations of urea (Figure 6.12). The specific activity of the enzyme was not saturated even at 50 mM urea, suggesting the K_m for urea may be

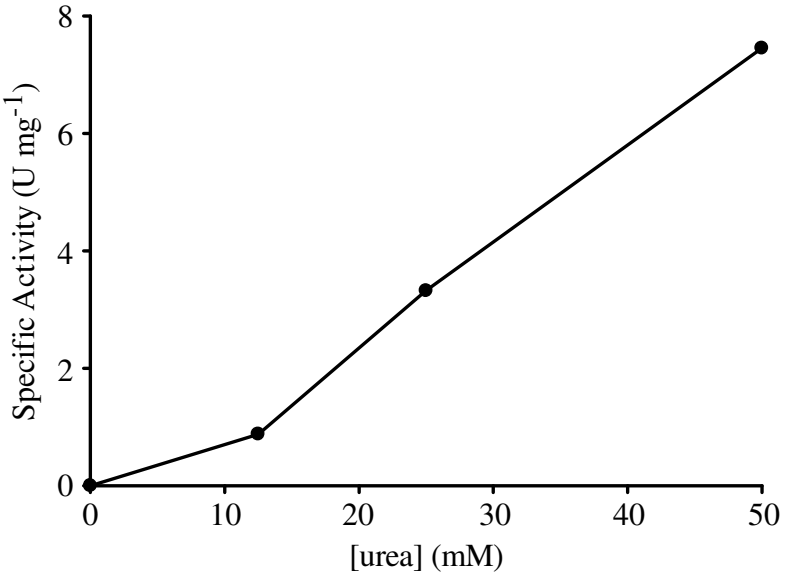

Figure 6.12: Specific activity of anaerobically purified UreA2B2$_{Str}$ as a function of urea concentration

much higher than for untagged UreA2B2. This experiment requires reproduction with more urea concentrations to definitively establish kinetic constants for UreA2B2$_{Str}$.

UreA2B2 activity in *H. mustelae* was previously shown to be independent of UreG (19), an accessory protein known to be essential for activation of the conventional nickel urease, suggesting the possibility of an alternative maturation pathway for the iron urease. Several experiments were performed in order to identify putative maturation factors. My first study utilized the convenient *Strep*-tag of UreA2B2$_{Str}$ to facilitate the single-step purification of the protein (originating from *E. coli*) that had been mixed with *H. mustelae* soluble cell-free extracts to monitor potential binding partners that co-elute with UreA2B2$_{Str}$. For these studies, I grew to confluence *H. mustelae nikR ureB* from ~6 Columbia blood agar plates, harvested into 0.15 M NaCl, pelleted cells by centrifugation, and suspended the pellet in 500 µl of 50 mM Tris-HCl, pH

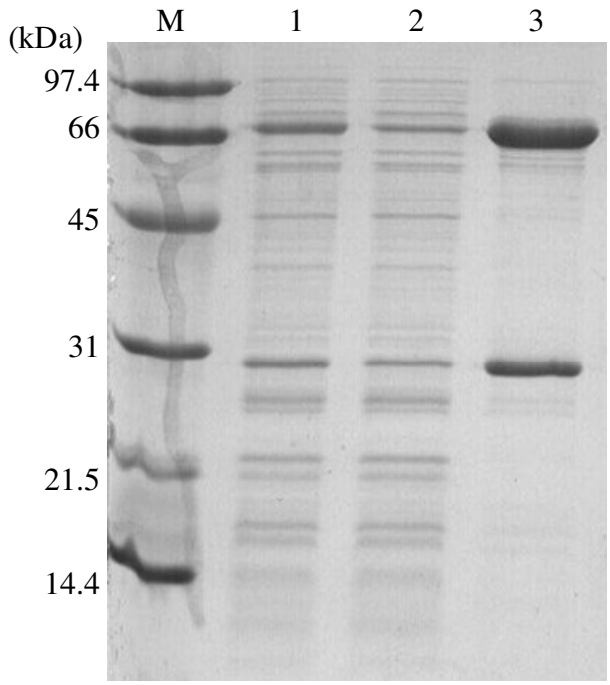

Figure 6.13: SDS-PAGE analysis of the purification of UreA2B2$_{Str}$ in the presence of *H. mustelae nikR ureB* soluble cell-free extracts. Lanes: M, molecular mass markers; 1, mixture of *H. mustelae nikR ureB* soluble cell-free extracts and UreA2B2$_{Str}$ purified from *E. coli* prior to chromatography; 2, column flow-through; 3, elution fraction.

8.0. I sonicated the slurry, cleared the lysate at 14,000 *g* for 20 min at 4 °C, and mixed ~500 µl of soluble cell-free extract with 500 µl 15.5 µM UreA2B2$_{Str}$ in 50 mM Tris-HCl, pH 8.0. I incubated the mixture on ice for 1 h, loaded onto a 500 µl bed volume Strep-tactin column, allowed 10 min for binding, washed the column with ~10 bed volumes of 50 mM Tris-HCl, pH 8.0, before eluting bound proteins with 100 mM Tris-HCl buffer, pH 8.0, containing 1 mM EDTA, 150 mM NaCl, and 2.5 mM desthiobiotin. I analyzed fractions by SDS-PAGE (Figure 6.13). Unfortunately the elution fraction did not contain any co-eluting proteins that were stoichiometric with UreA2B2$_{Str}$. Several faint bands were present below UreA2, the small subunit, however, these proteins were not analyzed further.

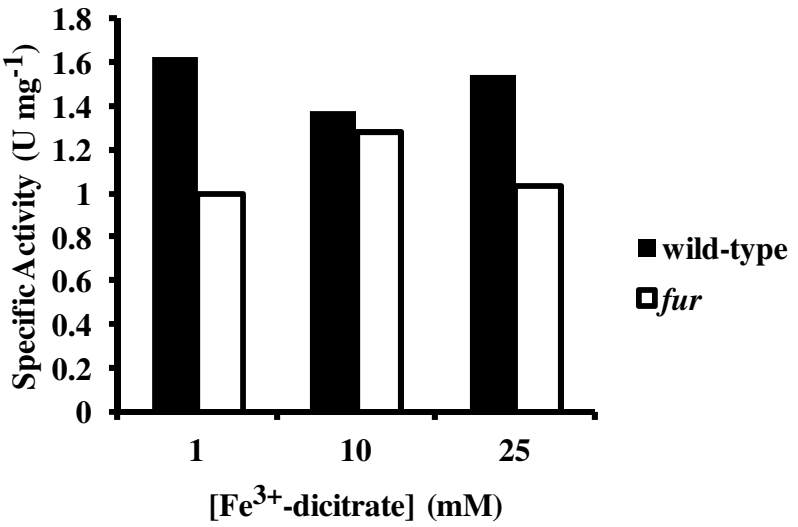

Figure 6.14: Urease activity of *E. coli* BW25113 wild-type or a *fur* mutant transformed with pEC018 and grown in LB broth with varying concentrations of Fe^{3+}-dicitrate.

Attempts to boost the iron content of UreA2B2 purified from E. coli. In *E. coli,* iron homeostasis is partially controlled by the global transcriptional regulator, Fur, which represses the synthesis of iron-storage and transport proteins in response to increasing intracellular iron concentrations (16). In an attempt to boost the iron content of UreA2B2 purified from *E. coli*, I produced $UreA2B2_{Str}$ in a *fur* mutant of *E. coli* BW25113 and wild-type BW25113 as a control. My assumption was that deletion of *fur* would lead to higher intracellular levels of iron. I grew cells transformed with pEC018 at 37 °C with shaking in LB supplemented with 100 µg ml^{-1} ampicillin and 1, 10, or 25 mM ferric dicitrate until they reached an $O.D._{600}$ of ~0.4 at which point protein production was induced with 0.1 mM IPTG. Cultures were grown for an additional 3 h prior to harvesting the cells by centrifugation and suspending the cell pellets in 50 mM Tris-HCl, pH 7.4, with 150 mM NaCl. I assayed cell slurries for urease activity, prepared soluble cell-free extracts, and assayed them for protein content (Figure 6.14). In short, there were

negligible differences in activity levels between wild-type and *fur* mutant cells producing UreA2B2$_{Str}$.

Another effort to raise the iron content of purified UreA2B2 consisted of growing *E. coli* BL21-Gold cells transformed with pEC015 in the highly rich medium, terrific broth, supplemented with 300 μg ml^{-1} ampicillin at 37 °C with shaking until the cells reached an O.D.$_{600}$ of ~0.5. Protein production was induced with 0.5 mM IPTG and the culture was incubated under the same conditions overnight prior to harvesting the cells by centrifugation and purifying UreA2B2 as described (3) in buffer containing EDTA and βME. The purified protein contained 1.011 ± 0.006 Fe atoms heterodimer^{-1} (average of triplicate determinations on one preparation) by the phenanthroline method (3), similar to the iron content (0.9 Fe atoms heterodimer^{-1}) of UreA2B2 purified from cells grown in a less rich medium, LB.

The effect of E. coli cyaY *and* iscA *mutations on UreA2B2 activity.* In a quest to uncover maturation factors responsible for iron delivery to UreA2B2, I used *E. coli* BW25113 strains with deletion mutations in *iscA* and *cyaY*, encoding iron-binding proteins proposed to donate iron atoms to the iron-sulfur cluster biosynthesis machinery (13, 17). I transformed the cells with pEC015 and assayed for urease activity in tandem with the wild-type strain. Cells were grown, prepared, and assayed as described (3) resulting in the whole-cell activities shown (Figure 6.15). There was not a marked difference in the specific activity between strains indicating that CyaY and IscA do not play a critical role in UreA2B2 maturation in *E. coli*.

Purification of UreA2B2 from E. coli *cells grown in nickel-supplemented medium.* Following up on the observation that UreA2B2 activity in *E. coli* whole cells was diminished when the growth medium was supplemented with nickel ions (3), I transformed *E. coli* BL21-

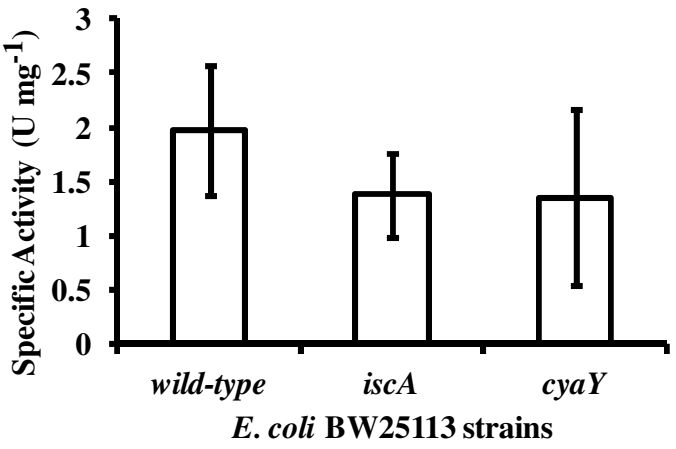

Figure 6.15: Urease activity of *E. coli* BW25113 wild-type and *iscA* or *cyaY* mutant strains transformed with pEC015.

Gold cells with pEC015, grew them in LB medium containing 300 μg ml^{-1} ampicillin and 1 mM $NiCl_2$ with shaking at 37 °C until they reached an $O.D._{600}$ of ~0.5, induced them with 0.1 mM IPTG, and incubated the cultures under the same conditions for 3 h prior to harvesting the cells by centrifugation. I purified UreA2B2 as described (3) using buffers containing EDTA and βME. The purified protein contained 0.25 ± 0.01 Fe atoms $heterodimer^{-1}$ (average of triplicate determinations on one preparation) by the phenanthroline method (3), and 0.3 Fe, 0.1 Ni, and <0.1 Zn $heterodimer^{-1}$ by ICP-AES. These data indicate that nickel ions inhibit iron incorporation into UreA2B2 by an unknown mechanism.

Electron paramagnetic resonance (EPR) analysis of nitric oxide (NO) treated UreA2B2. The profound oxygen-lability of UreA2B2 led me to question how the dinuclear ferrous metallocenter reacted with oxygen to form the inactive diferric species. One approach to answer this question was to treat the reduced, or diferrous, UreA2B2 with NO and then characterize the iron-nitrosyl species that form at the active site by using EPR spectroscopy. NO is commonly

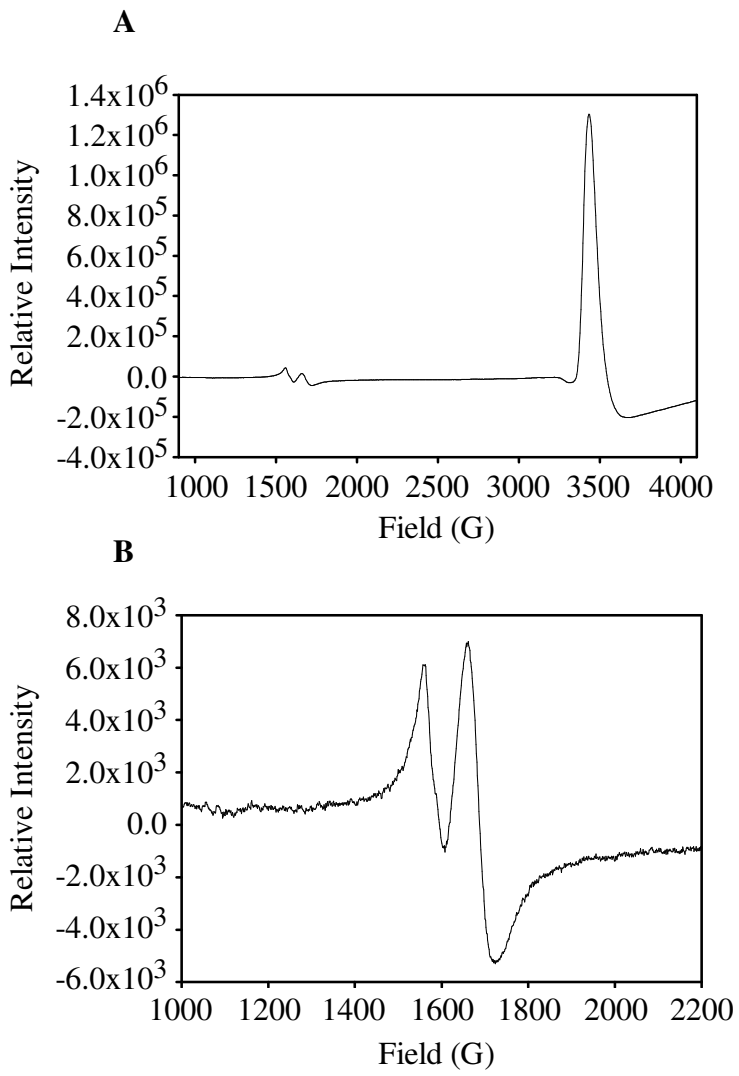

Figure 6.16: EPR spectrum of reduced UreA2B2 treated with NO. (**A**) Whole spectrum from 900-4100 Gauss. (**B**) Close-up of the spectrum from 1000-2200 Gauss.

used as an O_2 analog in studies focusing on the transient binding or activation of oxygen at protein metallocenters since it forms stable iron-nitrosyl complexes that have unique UV-visible spectra and are paramagnetic, thus observable by EPR (15). I reduced UreA2B2 (200 µl, 100 µM, with 1.0 Fe atom heterodimer^{-1}, purified from cells grown in terrific broth) with ~1 mM dithionite for 80 min under anaerobic conditions (NO reacts with oxygen) prior to flooding the vial with pure NO gas that had been bubbled through a saturated KOH solution (to remove

NO_2). I allowed the NO to react for 2.5 min before the sample was transferred to a degassed EPR tube by using gas-tight syringes, frozen in liquid N_2, and analyzed as described for reduced UreA2B2 samples (3) (Figure 6.16). Of note, immediately after I exposed solutions of reduced UreA2B2 to NO a white-colored precipitation developed. The precipitate was likely of protein origin and may result from the formation of thiolate-NO species that disrupt the protein structure. I did not test the effect of dithionite on NO stability, but this may also contribute to the phenomenon. Nevertheless, NO-treated sample containing the precipitate yielded an intense EPR signal (Figure 6.16, panel A) with features at ~3400 Gauss (g = ~2), arising in part from free NO in solution, and at ~1600 Gauss (g = ~4; see close-up view in Figure 6.16, panel B) which likely represents a mononuclear iron-nitrosyl species (14). Similar experiments by others with another diiron protein, ribonucleotide reductase subunit R2, demonstrated that each iron atom at the active site interacts with NO yielding an EPR silent product, however that sample also contained a small amount of mononuclear Fe-NO yielding a spectrum similar to that seen with UreA2B2 (14).

MALDI-MS analysis of UreA2 and UreB2 tryptic peptides. Prior to my discovery that oxygen inactivates UreA2B2 by forming a diferric μ-oxo core, I had hypothesized that oxygen may interact with the reduced diferrous metallocenter to form a high-valent Fe(IV)=O species capable of hydroxylating essential active site residue(s), thus leading to inactivity. To test this hypothesis I used MALDI-MS to analyze peptides from in-gel tryptic digests of UreA2 or UreB2. Peptides with a mass increase corresponding to the addition of an oxygen atom would indicate that an amino acid residue in that peptide may be hydroxylated. I was particularly interested in the modification of active site amino acids that could explain enzyme inactivation. I analyzed a sample of purified UreA2B2 by SDS-PAGE, stained the gel with Coomassie brilliant

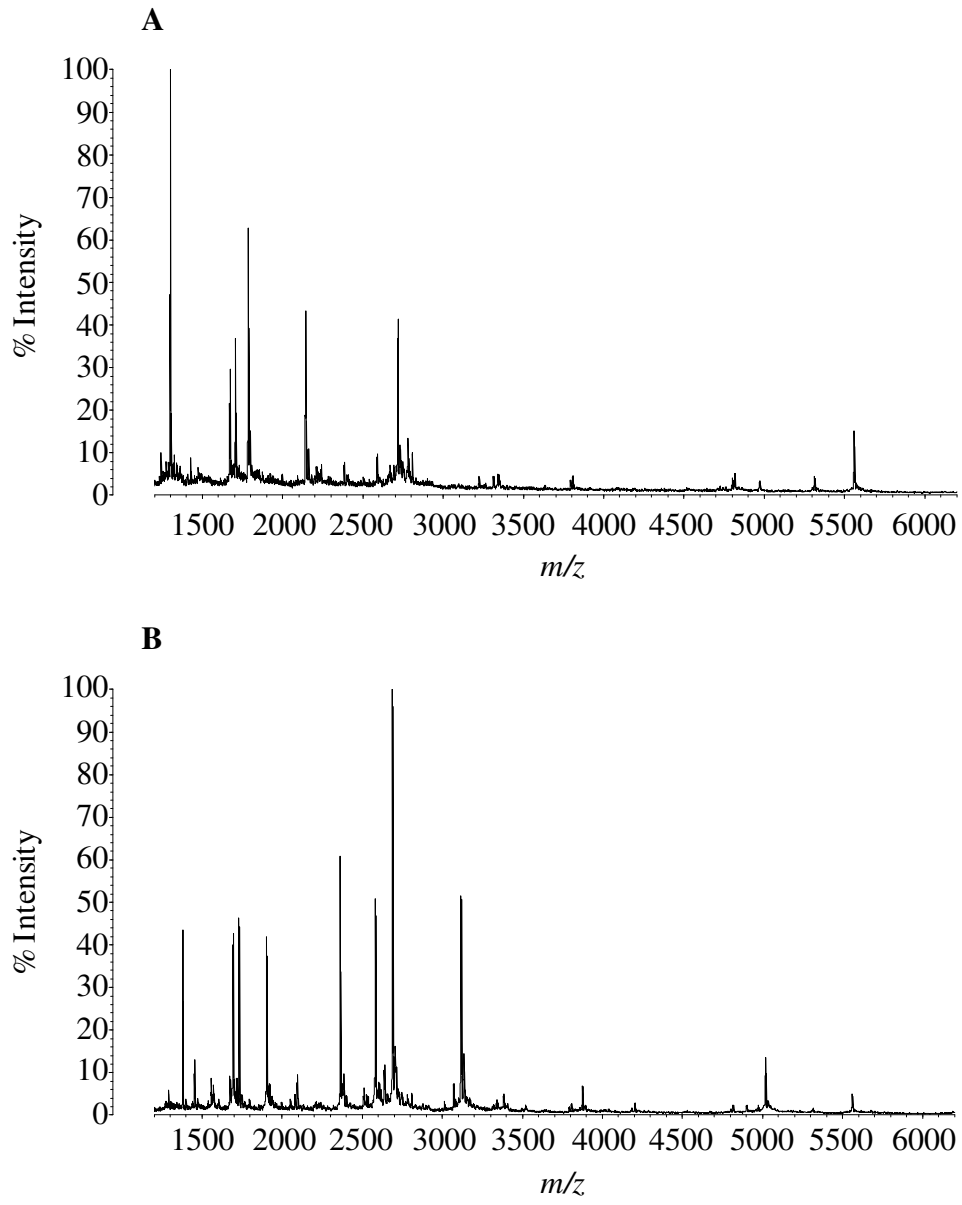

Figure 6.17: MALDI-MS spectra of UreA2B2 tryptic peptides. Peptides derived from trypsin digestion of gel excised (**A**) UreA2 or (**B**) UreB2.

blue for 15 min, and excised the UreA2 and UreB2 bands from the gel. I cut each band into small pieces (<1 mm^3), washed with 100 mM ammonium bicarbonate (100 µl) for 5 min, centrifuged, decanted the supernatant, added 50 µl of 100% acetonitrile, and dehydrated the gel pieces at ambient temperature. I repeated this step three times until the gel pieces were chalky white,

rehydrated them with 50 µl of 100 mM ammonium bicarbonate containing 10 mM DTT, and heated at 56 °C for 1 hr. The mixture was briefly centrifuged and the supernatant decanted by pipetting. The gel pieces were then dehydrated with 100% acetonitrile as described above (three rounds total), prior to hydration with 50 µl of 100 mM ammonium bicarbonate containing 55 mM iodoacetamide (for cysteine modification). I incubated the mixture for 1 h in the dark, discarded the supernatant, and washed the gel pieces with 50 µl 100 mM ammonium bicarbonate. I replaced the wash buffer with fresh 100 mM ammonium bicarbonate for 15 min before again replacing the buffer with 50 mM ammonium bicarbonate containing 50% acetonitrile and incubating at 37 °C for 30 min (the last step was required to eliminate trace levels of Coomassie stain remaining in the gel pieces). The gel cubes were dehydrated and then suspended in 50 µl of 50 mM ammonium bicarbonate containing 15 ng μl^{-1} sequencing grade trypsin (Promega) prior to incubating overnight at 37 °C. I briefly centrifuged the

Table 6.1: MALDI-MS analysis of tryptic peptides derived from UreA2 or UreB2.

Sample [a]	**Observed *m/z*** [b]	**Calculated *m/z*** [c]	**Δ Mass**	**Peptide assignment** [d]
UreA2	5561.3	N/A		
	2809.8	N/A		
	2782.1	N/A		
	2734.6	2734.1	0.5	67-92 (1 m.c.; Met71 or 77-OX (1))

Table 6.1 (cont'd)

	2718.5	2718.1	0.4	67-92 (1 m.c.)
	2160.2	2159.4	0.8	30-48 (Met44-OX)
	2143.9	2143.4	0.5	30-48
	1797.2	1795.1	2.1	195-211
	1786.8	1786.0	0.8	138-152
	1706.8	1706.0	0.8	53-66 (Cys61-CAM)
	1674.3	1673.9	0.4	93-106
	1303.2	1302.5	0.7	11-21
UreB2	5020.5	5020.4	0.1	219-262 (Cys233, 245-CAM)
	3135.9	3135.5	0.4	338-367 (Met352, 357, or 365-OX (1))
	3120.0	3119.5	0.5	338-367
	2707.2	2706.0	1.2	451-475 (Met453 or 459-OX (1))
	2690.6	2690.0	0.6	451-475
	2643.1	N/A		

Table 6.1 (cont'd)

	2584.1	2583.8	0.3	22-43
	2366.0	2365.6	0.4	408-429
	1902.7	1902.3	0.4	430-446
	1730.5	1729.8	0.7	5-19 (1 m.c.)
	1696.3	1694.9	1.4	535-549
	1453.3	1452.7	0.6	184-197
	1380.1	1379.5	0.6	327-337 (1 m.c.)

a Samples were derived from in-gel trypsin digested SDS-PAGE bands corresponding to UreA2 and UreB2. ***b*** Focusing on peaks with intensities that were >10% of that for the maximum feature and in a range from 1200-6000 *m/z* (note; acrylamide adducts dominated MALDI-MS spectra below 1200 *m/z* precluding analysis of peptides in that range). ***c*** Theoretical digests of UreA2 and UreB2 were conducted on the ExPASy server (PeptideMass function) taking into account the peptides with no greater than 1 missed cleavage, iodoacetamide modified cysteines, and oxidized methionines. ***d*** The amino acid residues are denoted for each peptide assignment; m.c., missed cleavage; modified cysteines are denoted as the specific Cys–CAM; oxidized methionines are denoted as the specific Met–OX (if more than one Met residue is oxidized, those residues are listed with the last residue followed by –OX; when a peptide contains fewer oxidized methionines than the total number of Met residues in the peptide, the possible Met-OX residues are listed followed by the number of Met-OX residues calculated in parentheses. N/A, unassigned peptide.

mixtures, saved the supernatant separately on ice, suspended the gel pieces in 50 µl of 60% acetonitrile containing 1% trifluoroacetic acid, and used a water-bath sonicator (with an ice-

water mix for cooling) for 5 min. The sample was centrifuged, the supernatant was combined with the solution saved earlier, and this process of sonication and extraction was repeated two more times. I dried the extraction pool in a heated Speedvac until ~1-2 µl remained, added 18 µl of 2% acetonitrile containing 0.1% trifluoroacetic acid, sonicated the tubes for 5 min as before, and then briefly centrifuged the sample before storing at -20 °C prior to use. I mixed 1 µl of thawed sample with 1 µl of 10 mg ml^{-1} α-cyano-4-hydroxycinnamic acid and analyzed with a Shimadzu Axima CFR Plus MALDI-TOF MS. The spectra were calibrated with insulin β-chain (MH^+ = 3497.0), angiotensin-II (MH^+ = 1047.2), and bovine insulin (MH^+ = 5734.6). The spectra of UreA2 (Figure 6.17, panel A) and UreB2 (Figure 6.17, panel B) tryptic peptides contain distinct peaks; the *m/z* values of these peaks were compared to the MH^+ values of peptides from a theoretical digest of each subunit allowing for a maximum of one missed cleavage for any identification and taking into account the modified cysteines from iodoacetamide treatment and the oxidized methionine residues (methionine sulfoxide) (Table 6.1). In summary, I obtained 51.6% amino acid coverage of UreA2 and 37.9% coverage for UreB2. I was unable to assign any *m/z* values to theoretical cleavage products with masses increased by multiples of 16 (indicating a putative hydroxylation).

CONCLUDING REMARKS

My dissertation has made significant advances in our understanding of urease maturation and metal selectivity. Significant contributions are detailed below along with suggested future studies.

Chapter 2 elaborates on the construction, purification, and characterization of the first soluble form of the UreD accessory protein. The unexpected discovery that the UreD domain of MBP-UreD bound nickel and zinc ions provides another layer of complexity to the urease maturation pathway *in vivo.* I suggest that UreD may directly participate in the sequential transfer of nickel from UreE, to UreG, to UreD, and finally to the appropriate ligands in the urease apoprotein. To confirm this hypothesis, the metal-binding ligands of UreD must be described. Future studies should include X-ray absorption spectroscopy of nickel-bound MBP-UreD to provide the identification of metal-binding ligands. One shortcoming of this technique is the ambiguity of ligand identification; i.e., XAS can only provide the atomic composition of ligands, for example, the detection of oxygen could be derived from Glu or Asp residues. Nonetheless, XAS can serve to eliminate some potential ligands, focusing site-directed mutagenesis efforts. Once putative metal-binding residues are identified, plasmids should be constructed to produce the MBP-UreD variants, and the effect of these variants on the generation of urease activity *in vivo* ascertained to determine whether the selected residues play a role during maturation. Another potentially important set of experiments is the cloning and purification of UreD from other bacteria in an attempt to isolate a soluble, native form of the protein for use in metal-binding studies. Demonstration that UreD proteins from other organisms bind nickel, similar to the *K. aerogenes* UreD described here, would support the hypothesis that this accessory protein is critical during the nickel transfer event.

Chapter 3 describes several key functions for the *K. aerogenes* urease UreB structural subunit during urease maturation *in vivo*. Unfortunately, these studies did not address the UreD—UreF induced UreB-shift hypothesis outlined in Chapter 1 and Chapter 3. Future work should include more detailed analysis of the UreABC—UreDF complex in order to confirm

previous cross-linking and computational observations (4, 18). Experiments may include fluorescence resonance energy transfer studies where UreB and UreC are site-specifically labeled with fluorophores (11) such that the UreB shift in the UreABC—UreDF complex would cause a change in resonance energy transfer that would not be observed in similarly labeled UreABC—UreD. These studies will require careful planning on the location of fluorophore labeling, which is complicated by the large size and complex quaternary structure of urease. Another option is X-ray crystallography of the UreABC—UreDF complex. Structural information could provide proof of a conformational change; unfortunately, a highly uniform version of this complex is not available, condition screening for crystal formation is time consuming, and success is not guaranteed. Lastly, iron-EDTA protein footprinting techniques (8) could be useful if the UreB shift exposes new sites that are susceptible to oxidative cleavage by iron-EDTA chelate. This could be assessed by comparing the footprints of UreABC—UreD and UreABC—UreDF; i.e., analyzing digestion fragments on Western blots using urease-specific antibodies or examining fragments on MS. This approach would allow for the isolation and identification of new fragments that arise in the UreABC—UreDF complex as a result of major conformational changes. One concern is that UreF may affect the footprint of UreABC producing false positives and complicating the analysis.

My characterization of the UreA2B2 iron-containing urease in Chapters 4, 5, and 6 lays the groundwork for future biophysical studies aimed at determining intermediates during urea degradation. One such technique is Mössbauer spectroscopy, a powerful tool that generates detailed information about iron metallocenters including the coordination state(s) and magnetic interactions. The apoprotein activation assays described in Chapter 5 suggest that new metallocenters are synthesized during the process. Utilizing similar methodologies, a sample of

UreA2B2 apoprotein could be loaded with ^{57}Fe, the isotope required for Mössbauer spectroscopy.

To extend the EPR studies involving NO described in this chapter, one could treat ^{57}Fe loaded UreA2B2 with NO, and analyze the sample with Mössbauer spectroscopy to definitively establish whether NO binds to one or both iron atoms in the UreA2B2 active site. Furthermore, the UV-visible spectrum of the NO treated diferrous UreA2B2 should also be obtained to compare extinction coefficients with other diiron proteins (10). One concern is the precipitation issue observed during sample preparation, which precluded UV-visible spectroscopy experiments. Future studies should include developing a preparation protocol that limits precipitation. Several avenues can be explored including modification of free thiols in UreA2B2 by iodoacetamide to avoid formation of thiolate-NO species. More care could be taken in delivering NO to the anaerobic sample vial by titrating with a solution of known % saturation of NO so that minimal excess NO is present in relationship to the iron stoichiometry of the protein. Along these lines, NONOate compounds that liberate NO in neutral pH solutions could also be used to fine tune the concentration of NO.

Additional work I performed in the laboratory involved several active collaborations with experts in XAS, MCD, and X-ray crystallography. EXAFS data for oxidized UreA2B2 (containing ~1 equivalent of Fe heterodimer^{-1}) obtained by Van Vu of the Lawrence Que lab at the University of Minnesota indicate an Fe-Fe distance of ~3.6 Å. XANES analysis suggests the metallocenter more closely resembles the μ-hydroxo bridged diferric core of oxidized methane monooxygenase rather than a μ-oxo bridged diferric core-containing protein. Preliminary MCD spectra (obtained by Kenneth Light of the Edward Solomon laboratory, Stanford University) of

dithionite-reduced UreA2B2 suggest the presence of 5- and 6-coordinate Fe sites; furthermore, strong MCD features present at low temperatures decrease in intensity as the temperature is raised which doesn't fit well to a μ-oxo-bridged core. Curiously, if the active diferrous metallocenter of UreA2B2 is μ-hydroxy bridged (as found in nickel-containing ureases) the species would be coupled and unobservable by MCD; thus, the strong MCD signals indicate the reduced UreA2B2 metallocenter may exist in a different state, perhaps μ-aqua bridged. Another possibility is that dithionite or a dithionite degradation product interacts with the active site and leads to artifactual MCD signals. In addition to these studies, follow-up X-ray crystallographic analysis of UreA2B2 is being conducted by the P. Andrew Karplus lab at Oregon State University. I have supplied the Karplus lab with a sample of oxidized UreA2B2 which will be used to reproduce crystals (3) to be used for studies of the urea-bound state, as shown by resonance Raman spectroscopy in Chapter 5. UreA2B2 crystals will be soaked in urea prior to diffraction analysis in an attempt to reveal structural information for the urea-bound metallocenter. In conclusion, more detailed XAS and MCD analyses are required to fully understand the nature of the reduced versus oxidized metallocenter. Additionally, the unique ability of the inactive, oxidized UreA2B2 to bind substrate without turnover provides an attractive target for analysis of this structural state.

BIBLIOGRAPHY

BIBLIOGRAPHY

1. **Boer, J. L., S. Quiroz-Valenzuela, K. L. Anderson, and R. P. Hausinger.** 2010. Mutagenesis of *Klebsiella aerogenes* UreG to probe nickel binding and interactions with other urease-related proteins. Biochemistry **49:**5859-5869.

2. **Carter, E. L., and R. P. Hausinger.** 2010. Characterization of *Klebsiella aerogenes* urease accessory protein UreD in fusion with the maltose binding protein. Journal of Bacteriology **192:**2294-2304.

3. **Carter, E. L., D. E. Tronrud, S. R. Taber, P. A. Karplus, and R. P. Hausinger.** 2011. Iron-containing urease in a pathogenic bacterium. Proceedings of the National Academy of Sciences, United States of America **108:**13095-13099.

4. **Chang, Z., J. Kuchar, and R. P. Hausinger.** 2004. Chemical crosslinking and mass spectrometric identification of sites of interaction for UreD, UreF, and urease. Journal of Biological Chemistry **279:**15305-15313.

5. **Colpas, G. J., T. G. Brayman, L.-J. Ming, and R. P. Hausinger.** 1999. Identification of metal-binding residues in the *Klebsiella aerogenes* urease nickel metallochaperone, UreE. Biochemistry **38:**4078-4088.

6. **Dunn, B. E., C.-C. Sung, N. S. Taylor, and J. G. Fox.** 1991. Purification and characterization of *Helicobacter mustelae* urease. Infection and Immunity **59:**3343-3345.

7. **Fong, Y. H., H. C. Wong, C. P. Chuck, Y. W. Chen, H. Sun, and K.-B. Wong.** Assembly of the preactivation complex for urease maturation in Helicobacter pylori: Crystal Structure of the UreF/UreH complex. Journal of Biological Chemistry.

8. **Greiner, D. P., K. A. Hughes, A. H. Gunasekera, and C. F. Meares.** 1996. Binding of the sigma 70 protein to the core subunits of Escherichia coli RNA polymerase, studied by iron-EDTA protein footprinting. Proceedings of the National Academy of Sciences, United States of America **93:**71-75.

9. **Ha, N.-C., S.-T. Oh, J. Y. Sung, K.-A. Cha, M. H. Lee, and B.-H. Oh.** 2001. Supramolecular assembly and acid resistance of *Helicobacter pylori* urease. Nature Structural Biology **8:**505-509.

10. **Haskin, C. J., N. Ravi, J. B. Lynch, E. Munck, and L. Que.** 1995. Reaction of NO with the Reduced R2 Protein of Ribonucleotide Reductase from *Escherichia coli*. Biochemistry **34:**11090-11098.

11. **Kapanidis, A. N., Y. W. Ebright, and R. H. Ebright.** 2001. Site-Specific Incorporation of Fluorescent Probes into Protein: Hexahistidine-Tag-Mediated Fluorescent Labeling with $(Ni^{2+}$:Nitrilotriacetic Acid$)_n$-Fluorochrome Conjugates. Journal of the American Chemical Society **123:**12123-12125.

12. **Kim, J. K., and R. P. Hausinger.** 2006. The UreEF fusion protein provides a soluble and functional form of the UreF urease accessory protein. Journal of Bacteriology **188:**8413-8420.

13. **Layer, G., S. Ollagnier-de Choudens, Y. Sanakis, and M. Fontecave.** 2006. Iron-Sulfur Cluster Biosynthesis. Journal of Biological Chemistry **281:**16256-16263.

14. **Lu, S., E. Libby, L. Saleh, G. Xing, J. M. Bollinger, and P. Moënne-Loccoz.** 2004. Characterization of NO adducts of the diiron center in protein R2 of *Escherichia coli* ribonucleotide reductase and site-directed variants; implications for the O_2 activation mechanism*. Journal of Biological Inorganic Chemistry **9:**818-827.

15. **McCleverty, J. A.** 2004. Chemistry of Nitric Oxide Relevant to Biology. Chemical Reviews **104:**403-418.

16. **McHugh, J. P., F. Rodríguez-Quiñones, H. Abdul-Tehrani, D. A. Svistunenko, R. K. Poole, C. E. Cooper, and S. C. Andrews.** 2003. Global iron-dependent gene regulation in *Escherichia coli*. A new mechanism for iron homeostasis. Journal of Biological Chemistry **278:**29478-29486.

17. **Py, B., and F. Barras.** Building Fe-S proteins: bacterial strategies. Nature Reviews Microbiology **8:**436-446.

18. **Quiroz-Valenzuela, S., S. C. K. Sukuru, R. P. Hausinger, L. A. Kuhn, and W. T. Heller.** 2008. The structure of urease activation complexes examined by flexibility analysis, mutagenesis, and small-angle X-ray scattering. Archives of Biochemistry and Biophysics **480:**51-57.

19. **Stoof, J., S. Breijer, R. G. J. Pot, D. van der Neut, E. J. Kuipers, and A. H. M. van Vliet.** 2008. Inverse nickel-responsive regulation of two urease enzymes in the gastric pathogen *Helicobacter mustelae*. Environmental Microbiology **10:**2586-2597.

APPENDIX A

Table A.1: Plasmids used in this work

Plasmid	Description	Reference
pKK17	Wild-type *K. aerogenes* urease cluster (*ureDABCEFG)* inserted into pKK223-3	(2)
pET-EF	Translationally fused *ureEF* genes inserted into pET21 for production of the UreEF fusion protein	(4)
pIBA3+G	SacII-PstI *ureG* fragment cloned into similarly digested pASK-IBA3 (IBA, Göttingen) resulting in a plasmid that encodes an in-frame C-terminal fusion of the plasmid-encoded *Strep*-tag with UreG	(1)
pKAU22Δ*ureD-1*	*K. aerogenes ureDABCEFG* harboring the Δ*ureD-1* deletion mutation cloned into pUC18	(5)
pACT3	pACYC184-based *tac* promoter expression vector	(3)
pEXT20	pBR322-based *tac* promoter expression vector	(3)
pEXT21	IncW-based *tac* promoter expression vector	(3)
pETDuet-1	Expression vector with two multiple cloning sites and independent T7 RNA polymerase-driven transcription units for the simultaneous production of two proteins in the cell	Merck
pET42-b	T7 RNA polymerase-driven expression vector with a pBR322 origin of replication	Merck
pCDF-1b	T7 RNA polymerase-driven expression vector with a CloDF13 origin of replication	Merck
pMal-c2x	Commercially available expression vector for construction and production of maltose binding protein fusions; encodes MBP-LacZα.	New England Biolabs
pMal-c	1st generation pMal vector lacking the 10 Asn linker found in pMal-c2x	New England Biolabs
pEC001	BamHI-HindIII *ureD* fragment cloned into similarly digested pEGAB1 resulting in production of a C-terminal fusion to SUMO protein	This work
pEC002	BamHI-HindIII *ureD* fragment cloned into similarly digested pMal-c2x resulting in production of a C-terminal fusion to maltose binding protein (encodes a linker region of 22 amino acids from the end of the SacI site to the beginning of *ureD*)	This work
pEC002-C48A	pEC002 containing a *ureD* mutation resulting in a C48A variant protein	This work
pEC002-H49A	pEC002 containing a *ureD* mutation resulting in a H49A variant protein	This work

Table A.1 (cont'd)

pEC002-H54A	pEC002 containing a *ureD* mutation resulting in a H54A variant protein	This work
pEC002-D63A	pEC002 containing a *ureD* mutation resulting in a D63A variant protein	This work
pEC002-E176A	pEC002 containing a *ureD* mutation resulting in a E176A variant protein	This work
pEC002-H49A-D63A	pEC002 containing *ureD* mutations resulting in a H49A and D63A variant protein	This work
pEC003	EcoRI-HindIII Δ*ureD2*-urease cluster subcloned from pKAUΔD2 into pEXT21	This work
pEC004	KpnI-XbaI *ureABC* fragment cloned into similarly digested pACT3	This work
pEC004-F271Y	pEC004 containing a *ureC* mutation encoding the F271Y variant protein	This work
pEC004-F271Y-I135T	pEC004 containing *ureC* mutations encoding the F271Y and I135Y variant protein	This work
pEC004-A244C	pEC004 containing a *ureC* mutation giving the A244C variant protein	This work
pEC004-F271Y-I135T-A244C	pEC004 containing *ureC* mutations giving the F271Y, I135T, and A244C variant protein	This work
pEC005	KpnI-XbaI *ureFG* fragment cloned into similarly digested pACT3	This work
pEC006	Δ*ureD K. aerogenes* urease cluster (*ureABCEFG*) cloned into pACT3	This work
pEC007	KpnI-XbaI *ureE* fragment cloned into similarly digested pACT3	This work
pEC008	KpnI-XbaI *ureF* fragment cloned into similarly digested pACT3	This work
pEC009	KpnI-XbaI *ureG* fragment cloned into similarly digested pACT3	This work
pEC010	EcoRI-HindIII *ureD* fragment cloned into similarly digested pMal-c resulting in a C-terminal fusion to maltose binding protein (encodes a linker region of 13 amino acids from the end of the SacI site to the beginning of *ureD*)	This work
pEC011	BamHI-HindIII *ureD* fragment cloned into similarly digested pMal-c resulting in a C-terminal fusion to maltose binding protein (encodes a linker region of 6 amino acids from the end of the SacI site to the beginning of *ureD*)	This work

Table A.1 (cont'd)

pEC012	KpnI-HindIII *ureD* fragment cloned into similarly digested pMal-c resulting in a C-terminal fusion to maltose binding protein (encodes a linker region of 2 amino acids from the end of the SacI site to the beginning of *ureD*)	This work
pEC013	EcoRI-SbfI *malE-ureD* fragment PCR amplified from pEC002 cloned into similarly digested pKK17	This work
pEC014	EcoRI-SbfI *malE-ureD* fragment PCR amplified from pEC011 cloned into similarly digested pKK17	This work
pEC015	BamHI-PstI *ureA2B2* fragment cloned into similarly digested pEXT20	This work
pEC015-K218A	pEC015 containing a *ureB2* mutation encoding a K218A variant protein	This work
pEC015-K218R	pEC015 containing a *ureB2* mutation encoding a K218R variant protein	This work
pEC015-K218E	pEC015 containing a *ureB2* mutation encoding a K218E variant protein	This work
pEC015-C245A	pEC015 containing a *ureB2* mutation encoding a C245A variant protein	This work
pEC016	KpnI-XbaI *ureAB* fragment cloned into similarly digested pEXT20	This work
pEC017	pIDT-SMART (pUC-derived vector, ampicillin resistance) containing a mini-gene construct encoding the C-terminal portion of UreA2 followed by a N-terminal *Strep* tag of UreB2	This work
pEC018	pEC015 that encodes a N-terminal *Strep*-tag of UreB2	This work
pEC019	BamHI-PstI *ureB2* fragment cloned into similarly digested pEXT20	This work
pEC020	BamHI-PstI *ureA2* fragment cloned into similarly digested pACT3	This work
pEC021	BamHI-PstI *H. mustelae ureA* fragment cloned into similarly digested pACT3	This work
pMBP2*	pMal-c2x with a stop codon inserted in the Factor-Xa cleavage site after the C-terminal Arg residue; used for overproduction of MBP	This work
pCDF-MBP-UreD	*malE-ureD* cloned into pCDF-1b to produce MBP-UreD with an N-terminal His_6 tag	This work
pUreAC	pETDuet-1 with *ureA* and *ureC* inserted into the two multiple cloning sites	This work
pUreB	pET-42b containing full-length *ureB*	This work

Table A.1 (cont'd)

pUreBΔ1-19	pET-42b containing 5'-truncated *ureB* that encodes Met plus UreB residues 20-106	This work

BIBLIOGRAPHY

BIBLIOGRAPHY

1. **Boer, J. L., S. Quiroz-Valenzuela, K. L. Anderson, and R. P. Hausinger.** 2010. Mutagenesis of *Klebsiella aerogenes* UreG to probe nickel binding and interactions with other urease-related proteins. Biochemistry **49:**5859-5869.

2. **Colpas, G. J., T. G. Brayman, L.-J. Ming, and R. P. Hausinger.** 1999. Identification of metal-binding residues in the *Klebsiella aerogenes* urease nickel metallochaperone, UreE. Biochemistry **38:**4078-4088.

3. **Dykxhoorn, D. M., R. St. Pierre, and T. Linn.** 1996. A set of compatible *tac* promoter expression vectors. Gene **177:**133-136.

4. **Kim, J. K., and R. P. Hausinger.** 2006. The UreEF fusion protein provides a soluble and functional form of the UreF urease accessory protein. Journal of Bacteriology **188:**8413-8420.

5. **Lee, M. H., S. B. Mulrooney, M. J. Renner, Y. Markowicz, and R. P. Hausinger.** 1992. *Klebsiella aerogenes* urease gene cluster: Sequence of *ureD* and demonstration that four accessory genes (*ureD*, *ureE*, *ureF*, and *ureG*) are involved in nickel metallocenter biosynthesis. Journal of Bacteriology **174:**4324-4330.